

# Conformations of single polymer chains on surfaces

non-equilibrium, equilibrium and manipulation

## DISSERTATION

zur Erlangung des akademischen Grades  
doctor rerum naturalium  
(Dr. rer. nat.)  
im Fach Physik

eingereicht an der  
Mathematisch-Naturwissenschaftlichen Fakultät I  
Humboldt-Universität zu Berlin

von

Herr Dipl.-Phys. Christof Ecker  
geboren am 10.7.1972 in Rheinberg

Präsident der Humboldt-Universität zu Berlin:  
Prof. Dr. Jürgen Mlynek

Dekan der Mathematisch-Naturwissenschaftlichen Fakultät I:  
Prof. Thomas Buckhout, PhD

Gutachter:

1. Prof. Dr. J. P. Rabe
2. Prof. Dr. I. M. Sokolov
3. Prof. Dr. R. v. Klitzing

eingereicht am: 20. 9. 2004  
Tag der mündlichen Prüfung: 20. 12. 2004

## Abstract

Frontali et al. [137] showed in 1979 that it is possible to characterize the structure of polymers by analyzing high resolution microscopy images. The authors adsorbed DNA molecules onto mica and imaged them using electron microscopy. From the vectorized contours of single chains, they were able to determine both contour and persistence lengths so that the polymers were fully described in the framework of the wormlike-chain (WLC) model. In contrast to the conventional characterization methods for polymer solutions this approach has two important advantages: 1) single molecules instead of an ensemble are investigated, and 2) the results can be compared to the model in a much more direct way. As a disadvantage, high resolution microscopy such as transmission electron microscopy (TEM) or scanning force microscopy (SFM) require the polymers to be adsorbed onto a solid substrate surface which influences the chain conformations.

Until now, the method is not well established. In particular, basic knowledge about single molecule conformations on surfaces is missing. Investigations in literature are mainly concerned with adsorption under equilibrium conditions. Often however, the interaction between molecule and substrate is strong so that the equilibration is inhibited and chains remain trapped in the initial conformation determined by the kinetics of the adsorption process.

The goal of this thesis was to develop and establish methods for the characterization of single chains of polymers using scanning force microscopy. Therefore, methods for the analysis and procession of SFM-images were developed. This includes a method for the determination of the persistence length which is very efficient and features an analytic expression for the statistical error. Furthermore, a new algorithm for background removal was found which replaces the commonly used *flattening*. It avoids the misleading “shadows” characteristic for SFM-images and therefore enables elaborate quantitative analysis of height values, e.g. along the contour of an adsorbed polymer molecule. In addition an automated vectorization method has been developed which avoids errors due to the discreteness of the image pixels.

Models were developed which allow for the first time a detailed prediction of conformational characteristics in the non-equilibrium. It is shown that two

kinds of very regular conformations can appear on strong interacting substrates: sine-like undulations and spiral shaped “tron”-conformations. Undulations have been observed by other groups before but were probably misinterpreted, e.g. as helices.

Strongly physisorbed polymers were investigated experimentally for two model systems: charged dendronized polymers on mica and DNA on poly-ornithine layers. For the dendronized polymers conformations were found to be undulated with a period of  $13\pm 3$  nm. The adsorbed DNA molecules showed “tron” features with a dependence on the ion concentration in agreement to the proposed model.

The persistence length of poly(isocyanodipeptides) (PIC) has been determined for the first time. The obtained value of  $76\pm 6$  nm shows that these polymer molecules are extraordinarily rigid, more rigid than double stranded DNA and probably the most rigid synthetic polymers yet. This behavior is attributed to the helical backbone which is additionally reinforced by a network of side groups connected by hydrogen bonds. The persistence length has also been determined for PICs where the polymerization was catalyzed using acid instead of Ni, leading to a contour length of up to  $5.3 \mu\text{m}$ . Those long chains were not able to equilibrate on the surface, nevertheless the same value for the persistence length was obtained confirming the idea that chains can equilibrate on the local scale of up to 100 nm.

The method of single chain nanomanipulation has been developed in our group during the last years. It allows to move molecules in a precise way on the substrate surface. The resulting lateral forces have been used in this work to investigate the mechanical properties of adsorbed molecules. Of special interest was the investigation of dendronized polymers because special mechanical properties can be expected for this new class of molecules. Dendronized polymers carry a regularly branched side group (dendron) at each of the repeat units. The mass of a dendron grows exponentially with the number of branching generations. For high generation numbers it can be expected, that the mechanical bending behavior of the chain is strongly influenced by the dendrons and therefore deviates from the usual chain flexibility. Our experiments indicate that a glassy state exists for molecules of generation 3 and 4, in which the molecule no longer behaves as a flexible chain but instead plastically keeps the shape in which it is frozen-in, similar to a macroscopic body. Further experiments show that also a liquid state exists for elevated temperatures and good solvents in which molecules are flexible. The glassy state of a single molecule is a new and unusual property

for polymers. It might be useful in nanotechnology as it enables e.g. the creation of single molecular components with a selectable rigid shape. For future research, it would be interesting to investigate the influence of the glassy state on macroscopic material properties. This question has to remain unanswered for now as the amount of available dendronized polymers is not sufficient yet.

**Keywords:**

single molecules, polymer conformation, manipulation, scanning force microscopy

## Zusammenfassung

In ihrer Arbeit von 1979 haben Frontali et al. [137] gezeigt, daß es prinzipiell möglich ist, die Struktur von Polymeren durch die Analyse hochaufgelöster Mikroskopiebilder zu charakterisieren. Die Autoren haben DNS-Moleküle auf Glimmer adsorbiert und mit dem Elektronenmikroskop abgebildet. Aus den vektorisierten Konturen einzelner Moleküle konnten sie sowohl die Kontur- als auch die Persistenzlänge bestimmen und damit die Polymere im Rahmen des Wormlike-Chain-Modells vollständig beschreiben. Gegenüber gebräuchlichen Methoden zur Polymeruntersuchung hat der mikroskopische Ansatz einige Vorteile: es werden einzelne Moleküle statt eines Ensembles untersucht und die Meßergebnisse können viel direkter mit dem Modell verglichen werden. Allerdings müssen Moleküle, um sie mit dem Rasterkraftmikroskop (RKM) oder dem Elektronenmikroskop zu untersuchen, auf einer Substratoberfläche adsorbiert werden, was die Interpretation der Konformationen erschwert.

Die Methode ist bisher wenig etabliert und insbesondere fehlt grundsätzliches Wissen über die Konformationen von vereinzelt Molekülen an Oberflächen. So befassen sich die bisher in der Literatur beschriebenen Untersuchungen hauptsächlich mit Konformationen unter Gleichgewichtsbedingungen. Häufig besteht aber eine starke Wechselwirkung zwischen Molekül und Unterlage, sodaß eine Äquilibration nicht möglich ist und die durch die Kinetik des Adsorptionsprozesses bestimmte Anfangskonformation eingefroren wird.

Das Ziel der vorliegenden Arbeit war es, Methoden der Charakterisierung einzelner Polymere mit dem Rasterkraftmikroskop zu erforschen und zu etablieren. Es wurden zunächst Methoden der Auswertung von RKM-Bildern und zur Bildbearbeitung entwickelt. So wurde eine Methode zur Bestimmung der Persistenzlänge hergeleitet, die besonders effizient ist und es erlaubt, den statistischen Fehler analytisch zu berechnen. Außerdem wurde ein einfacher Algorithmus zur Korrektur des Untergrunds gefunden, der das übliche *Flat-ten* ersetzt. Es werden damit die für RKM-Bilder typischen irreführenden "Schatten" vermieden und so eine quantitative Analyse der Höhenwerte, z.B. entlang der Kontur einer Polymerkette, ermöglicht. Weiter wurde eine Methode der automatisierten Vektorisierung entwickelt, die das Problem der Fehler durch diskrete Pixel vermeidet.

Es wurden Modelle entwickelt, die erstmals detaillierte Vorhersagen über Konformationen im Nichtgleichgewicht zulassen. Sie basieren auf der Annahme, daß sich die Konformationen bei dem Adsorptionsprozeß bilden und nicht mehr verändern. Es wurde gezeigt, daß zwei Arten von besonders regelmäßigen Konformationen auftreten können: sinusartige Undulationen und spiralartige “Tron“-Konformationen. Erstere wurden in der Literatur verschiedentlich beschrieben, aber nach dem Resultat dieser Arbeit fragwürdig (z.B. als Helizes) interpretiert.

Konformationen stark physisorbierter Polymere wurden für zwei Modellsysteme experimentell untersucht: geladene dendronisierte Polymere auf Glimmer und DNS auf Polyornithin-Schichten. Für dendronisierte Polymere wurden Undulationen mit einer Periode von  $13\pm 3$  nm gefunden. Die steiferen DNS Moleküle dagegen bildeten Tron-Konformationen, wobei die Abhängigkeit von der Salzkonzentration in der Lösung der Modellvorstellung entspricht.

Es wurde erstmalig die Persistenzlänge von Poly(Isocyanodipeptiden) (PIC) bestimmt. Der gefundene Wert von  $76\pm 6$  nm zeigt, daß die Moleküle zu den steifsten synthetischen Makromolekülen überhaupt gehören und damit sogar noch steifer als doppelsträngige DNS sind. Diese Eigenschaft wird auf das helikale Rückgrat zurückgeführt, das zusätzlich durch ein Netzwerk von durch Wasserstoffbrücken verbundenen Seitengruppen verstärkt wird. Außerdem wurden durch Säurekatalyse hergestellte PIC-Moleküle mit Konturlängen von bis zu  $5.3 \mu\text{m}$  untersucht. Obwohl diese langen Ketten keine Gleichgewichtskonformationen bilden, wurde der gleiche Wert für die Persistenzlänge gefunden, was die Vermutung bestätigt, daß die Moleküle zumindest auf der lokalen Längenskala um bis 100 nm äquilibrieren können.

Die Methode der Nanomanipulation von Polymerketten, die innerhalb der letzten Jahre in der Arbeitsgruppe entwickelt wurde, erlaubt es, Moleküle gezielt auf der Substratoberfläche zu verschieben. Die dabei auftretenden lateralen Kräfte wurden in der vorliegenden Arbeit dazu benutzt, um das mechanische Verhalten adsorbierter Moleküle zu untersuchen. Von besonderem Interesse war die Untersuchung von dendronisierten Polymeren, da diese eine neue Klasse von Molekülen bilden, von denen besondere mechanische Eigenschaften erwartet werden können. Dendronisierte Polymere tragen an jeder Monomereinheit des Rückgrats eine regelmäßig verzweigte Seitengruppe (Dendron). Die Masse eines Dendrons wächst exponentiell mit der Zahl der Verzweigungsgenerationen. Für hohe Generationen ist daher zu erwarten, daß das mechanische Biegeverhalten der Kette wesentlich durch die Dendronen bestimmt wird und daher erheblich von dem üblichen Polymerverhalten

abweicht. Die Experimente zeigen, daß für Moleküle der Generation 3 und 4 ein “glasartiger” Zustand existiert, in dem sich das Polymermolekül nicht mehr wie eine flexible Kette verhält, sondern plastisch seine Form behält, ähnlich einem makroskopischen festen Körper. Erst bei Anwendung höherer Temperaturen und in guten Lösungsmitteln konnte ein “flüssiger” Zustand, in dem sich die Moleküle flexibel verhalten, erreicht werden. Dieser erstmalig beobachtete Glaszustand eines einzelnen Polymermoleküls ist eine völlig neue und ungewöhnliche Eigenschaft. Er könnte beispielsweise in der Nanotechnologie dazu benutzt werden, einzelne molekulare Bausteine mit einer wählbaren Form herzustellen. Für die Zukunft wäre es interessant zu untersuchen, wie sich der Glaszustand auf die makroskopischen Materialeigenschaften auswirkt. Diese Frage mußte vorerst unbeantwortet bleiben, da dendronisierte Polymere erst allmählich in ausreichender Menge zur Verfügung stehen.

**Schlagwörter:**

Einzelmolekül, Polymerkonformation, Manipulation,  
Rasterkraftmikroskopie

# Contents

<b>1</b>	<b>Introduction</b>	<b>1</b>
<b>2</b>	<b>Basic polymerphysics</b>	<b>4</b>
2.1	Flexible chains . . . . .	4
2.2	Semiflexible chains . . . . .	5
2.3	Excluded volume . . . . .	8
2.4	Ions in solution . . . . .	10
2.5	Polyelectrolytes . . . . .	12
2.6	Persistence length . . . . .	14
<b>3</b>	<b>Experimental methods</b>	<b>18</b>
3.1	Scanning force microscopy . . . . .	18
3.1.1	Tip-Sample forces . . . . .	20
3.1.2	Modes of operation . . . . .	22
3.1.3	Image artifacts . . . . .	26
3.2	Equipment . . . . .	33



3.3	Sample preparation . . . . .	34
<b>4</b>	<b>Data analysis</b>	<b>35</b>
4.1	Image processing . . . . .	35
4.1.1	Background correction . . . . .	36
4.1.2	Automated vectorization . . . . .	38
4.1.3	Sections along the contour . . . . .	41
4.1.4	Implementation . . . . .	42
4.2	Statistical characterization of conformations . . . . .	45
4.2.1	Determination of the persistence length . . . . .	45
4.2.2	Radius of gyration . . . . .	47
4.2.3	Orientation correlation function . . . . .	48
4.2.4	Mean segment-segment distance . . . . .	49
4.3	Monte Carlo simulation of self avoiding worm-like chains . . . . .	49
4.4	Simulation of the “undulation” model . . . . .	50
4.5	Simulation of the “tron” model . . . . .	52
<b>5</b>	<b>Materials</b>	<b>53</b>
5.1	Substrates . . . . .	53
5.2	Dendronized polymers . . . . .	55
5.3	Poly(isocyanodipeptides) . . . . .	59
5.4	DNA . . . . .	60

<b>6</b>	<b>Non-equilibrium: characteristic conformations upon strong adsorption</b>	<b>62</b>
6.1	Introduction . . . . .	62
6.2	Related work . . . . .	64
6.3	Modeling . . . . .	66
6.3.1	Projection model . . . . .	66
6.3.2	Different regimes of zipping . . . . .	67
6.3.3	Free zipping: undulation model . . . . .	69
6.3.4	Self avoiding zip: “tron process” . . . . .	74
6.4	Experiment . . . . .	75
6.4.1	Experimental procedures . . . . .	76
6.4.2	Conformations of self avoiding worm-like chains . . . . .	76
6.4.3	Test of lateral mobility of adsorbed chains . . . . .	80
6.4.4	Conformations of charged dendronized polymers . . . . .	81
6.4.5	Trapped conformations of DNA . . . . .	90
6.5	Discussion . . . . .	96
6.5.1	Overall conformations . . . . .	96
6.5.2	Undulations . . . . .	97
6.5.3	Lateral self avoidance . . . . .	97
6.5.4	Alternative explanations . . . . .	98
6.6	Conclusions . . . . .	99

6.7	Appendix . . . . .	100
<b>7</b>	<b>Equilibrium: Persistence of poly(isocyanodipeptides)</b>	<b>103</b>
7.1	Introduction . . . . .	103
7.2	Experimental procedures . . . . .	106
7.3	Results and discussion . . . . .	107
7.3.1	Single chains visualization with SFM . . . . .	107
7.3.2	Contour length . . . . .	108
7.3.3	Persistence length . . . . .	109
7.3.4	Conclusions . . . . .	110
<b>8</b>	<b>Manipulation: Glassy state of single dendronized polymer chains</b>	<b>115</b>
8.1	Introduction . . . . .	115
8.2	Experimental procedures . . . . .	117
8.3	Results and discussion . . . . .	118
8.4	Summary and Conclusion . . . . .	130

# Chapter 1

## Introduction

Polymer molecules are large, often threadlike molecules made up of a linked series of repeated simple monomers. The modeling of their thermodynamic properties is part of the field of polymer physics and goes back to the middle of last century. Basis of the physical description is the modeling of the molecules' shape in solution or melt. The shape is usually simplified to the line formed by the backbone and will be denoted in the following as conformation. An important polymer model is the worm-like chain (WLC) model by Kratky and Porod [247] which describes a chain by two parameters: the contour length and the persistence length. The WLC model allows the calculation of properties such as the size of the random coil formed in solution, which can be measured experimentally by, e.g., light scattering. A fundamentally different experimental way is provided by single molecule microscopy, where chains are adsorbed onto a substrate surface and imaged using Scanning Force Microscopy (SFM) or Electron Microscopy (EM). Vectorizing the chain contours not only gives access to macroscopic properties as the coil size, but allows the direct comparison to the model and, e.g., to fit model parameters such as persistence and contour lengths. This approach was first followed by Frontali et al. [137] who investigated DNA molecules adsorbed onto mica. In recent works also synthetic molecules are investigated [17, 67, 237, 428, 243]. Despite the great potential, this approach of polymer experiments is still not well established. This might be due to the difficulties of single molecule experiments, and also the lack of theoretical knowledge about conformations of adsorbed chains which are not investigated systematically thus far. Especially it is not known under which conditions chains are in a thermal equilibrium state which can be described statistically, and

what are the characteristics of chains not in equilibrium. In all the mentioned works deviations from the expected worm-like chain statistics were found and various reasons are speculated about.

The goal of the present thesis was to investigate and establish methods to characterize single polymers using scanning force microscopy. This includes the building of models for the non-equilibrium, the development of tools and methods for analysis, and experimental studies of model cases.

The thesis is divided into eight chapters: after this introduction, chapter 2 will introduce the relevant basic polymer physics. Chapter 3 describes the experimental methods such as scanning probe microscopy and sample preparation. In chapter 4 data analysis techniques developed for this thesis are presented, including the methods for image processing and determining the persistence length. Chapter 5 introduces the investigated polymer systems.

The main part of this thesis consists of three chapters, corresponding to the classification of experiments to non-equilibrium conformations, equilibrium conformations and the change of conformation. In the non-equilibrium section (chapter 6), these conformations are investigated experimentally, theoretically and with simulations. A framework is proposed which allows the prediction of conformations.

In chapter 7 conformations of poly(isocyanodipeptides) (PIC) are investigated on mica surfaces. PICs are very stiff helical polymers first synthesized in the group of R. Nolte [90]. It will be shown that these molecules at least locally can be equilibrated and their persistence length is determined for the first time.

In the last part, chapter 8, external forces are used to change the conformation of adsorbed chains. This was done using the method of single chain nanomanipulation which has been developed in our group during the last years. It allows to move molecules in a precise way on the substrate surface. Lateral forces result from the friction on the surface. By comparing the conformations before and after manipulation, information on the mechanical behavior can be gathered. Of special interest was the investigation of so-called dendronized polymers because special mechanical properties can be expected for this new class of molecules. Dendronized polymers carry a regularly branched side group (dendron) at each of the repeat units. The mass of a dendron grows exponentially with the number of branching generations. For high generation numbers it can be expected, that the mechanical bending

behavior of the chain is strongly influenced by the dendrons and therefore deviates from the usual chain flexibility.

# Chapter 2

## Basic polymerphysics

This chapter shall give a short and consistent introduction to the polymer theory needed later. More complete treatments can be found in the text book of Doi [107] and the book of Grosberg and Khoklov [168]. Unlike the standard texts, in the following also formulae for polymer chains confined to two dimensions are derived. They are needed for the description of adsorbed chains.

### 2.1 Flexible chains

Chains considered in this thesis are either flexible or semi-flexible. A simple model for flexible chains is the *freely jointed chain*. According to this, a chain consists of a series of  $N$  stiff segments, which are freely connected by hinges. The segments are described by vectors  $\mathbf{r}_i$ , where  $i = 0, \dots, N - 1$  and the length is fixed by  $|\mathbf{r}_i| = a$ . The end-to-end vector is consequently  $\mathbf{R} = \sum_{i=0}^{N-1} \mathbf{r}_i$ .

Chains are assumed to be *ideal* if only neighboring segments can interact, while long range interaction is ignored. In particular it is allowed for different segments to be in the same volume of space. The mean quadratic end-to-end distance  $R^2$  for the freely jointed chain can be calculated by averaging all possible conformations. It is

$$R^2 = a^2 N, \tag{2.1}$$

as  $\langle \mathbf{r}_i \mathbf{r}_j \rangle = 0$  for  $i \neq j$  and  $\langle \mathbf{r}_j^2 \rangle = a^2$  otherwise. Thus the mean size of a flexible chain,  $R = aN^{1/2}$ , is considerably smaller than the contour length  $L_c = aN$ .

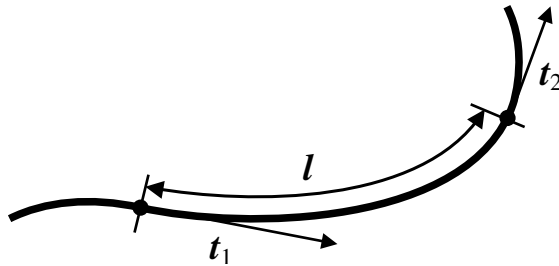
## 2.2 Semiflexible chains

Real polymers are not fully flexible, especially not on short length scales. They possess an intrinsic stiffness, leading to locally straight sections of several monomer lengths. For such chains, tangent vectors along the contour are no longer uncorrelated as for flexible chains.

Semi-flexibility is described by the *Worm-Like Chain* (WLC) model introduced by Kratky and Porod [247]. For simplicity the molecule is modeled as a continuous chain. The correlation of tangent vectors  $\mathbf{t}_1$  and  $\mathbf{t}_2$  is by definition

$$\langle \mathbf{t}_1 \mathbf{t}_2 \rangle = \exp(-\ell/\ell_P), \quad (2.2)$$

where  $\ell$  is the distance between the tangent foot-points along the contour (see sketch below).



The chain property  $\ell_P$  is a measure of the stiffness. It can be interpreted as the length, over which the polymer is approximately straight. For larger  $\ell$  fluctuations are relevant and the information of the chain orientation is lost. For a chain confined to two dimensions the formula corresponding to 2.2 is

$$\langle \mathbf{t}_1 \mathbf{t}_2 \rangle = \exp\left(-\frac{\ell}{2\ell_P}\right), \quad (2.3)$$

as will be shown later.

The mean squared end-to-end distance of a chain can be calculated by  $\int_0^{L_c} \int_0^{L_c} \mathbf{t}(\ell) \mathbf{t}(\ell') d\ell' d\ell$ . Therefore, for worm-like chains the mean square end-to-end distance  $R^2$  can be obtained by inserting equation 2.2. For a 3D-chain it is



$$R^2 = \int_0^{L_c} \int_0^{L_c} \langle \mathbf{t}(\ell) \mathbf{t}(\ell') \rangle d\ell' d\ell \quad (2.4)$$

$$= \int_0^{L_c} \int_0^{L_c} \exp\left(-\frac{|\ell - \ell'|}{\ell_P}\right) d\ell' d\ell \quad (2.5)$$

$$= 2 \int_{\ell=0}^{L_c} \int_{\ell'=0}^{\ell} \exp\left(-\frac{\ell - \ell'}{\ell_P}\right) d\ell' d\ell \quad (2.6)$$

$$= 2\ell_P L_c + 2\ell_P^2 \left( \exp\left(-\frac{L_c}{\ell_P}\right) - 1 \right). \quad (2.7)$$

For a chain in 2D the mean squared end-to-end distance can be calculated in a similar way using equation 2.3 instead of 2.2 and amounts to

$$R^2 = 4\ell_P L_c + 8\ell_P^2 \left( \exp\left(-\frac{L_c}{2\ell_P}\right) - 1 \right). \quad (2.8)$$

Two marginal cases can be distinguished: for short chains ( $L_c \ll \ell_P$ ) equation 2.7 can be approximated by the Taylor expansion

$$R^2 = L_c^2 - \frac{L_c^3}{3\ell_P} + \dots \quad (2.9)$$

$$\simeq L_c^2. \quad (2.10)$$

and short chains therefore behave as stiff rods ( $R \simeq L_c$ ); for long chains ( $L_c \gg \ell_P$ ) on the other hand

$$R^2 \simeq 2\ell_P L_c, \quad (2.11)$$

i.e. they do behave as freely jointed chains (equation 2.1) having an effective segment length (Kuhn-length) of

$$b = 2\ell_P \quad (2.12)$$

and the effective number of segments

$$N_{\text{eff}} = \frac{L_c}{2\ell_P}. \quad (2.13)$$

The radius of gyration  $r_g$  is another measure for the coil size.  $r_g^2$  is the mean squared distance of a monomer from the coil's center of mass [168]

$$r_g^2 = \frac{1}{L_c} \int_0^{L_c} \langle (\mathbf{r}(\ell) - \mathbf{r}_{\text{CM}})^2 \rangle d\ell \quad (2.14)$$

$$= \frac{1}{2L_c^2} \int_0^{L_c} \int_0^{L_c} \langle (\mathbf{r}(\ell) - \mathbf{r}(\ell'))^2 \rangle d\ell' d\ell, \quad (2.15)$$

where  $\mathbf{r}_{\text{CM}}$  is the center of mass. Using the mean squared end-to-end distance of a WLC in 3D (equation 2.7) it is

$$r_g^2 = \frac{1}{2L_c^2} \int_0^{L_c} \int_0^{L_c} R(|\ell - \ell'|) d\ell' d\ell \quad (2.16)$$

$$= 4 \frac{\ell_P^3}{L_c} + \frac{L_c \ell_P}{3} + 2 \frac{\ell_P^4}{L_c^2} \left( \exp\left(-\frac{L_c}{\ell_P}\right) - 1 \right). \quad (2.17)$$

Similar, for 2D chains  $r_g$  can be derived and reads

$$r_g^2 = 32 \frac{\ell_P^3}{L_c} + \frac{2}{3} L_c \ell_P + 64 \frac{\ell_P^4}{L_c^2} \left( \exp\left(-\frac{L_c}{2\ell_P}\right) - 1 \right). \quad (2.18)$$

## 2.3 Excluded volume

In the models presented so far only interactions between neighboring segments were allowed. All other interactions are commonly called “excluded volume” interactions. They include interactions between different polymers, different monomers of the same polymer and between the monomer and solvent molecules.

Fig. 2.1 gives the typical interaction potential between two monomers as a function of the spatial distance. The characteristic energy of the attractive interaction  $\varepsilon$  is typically on the order of the thermal energy  $k_B T$ .

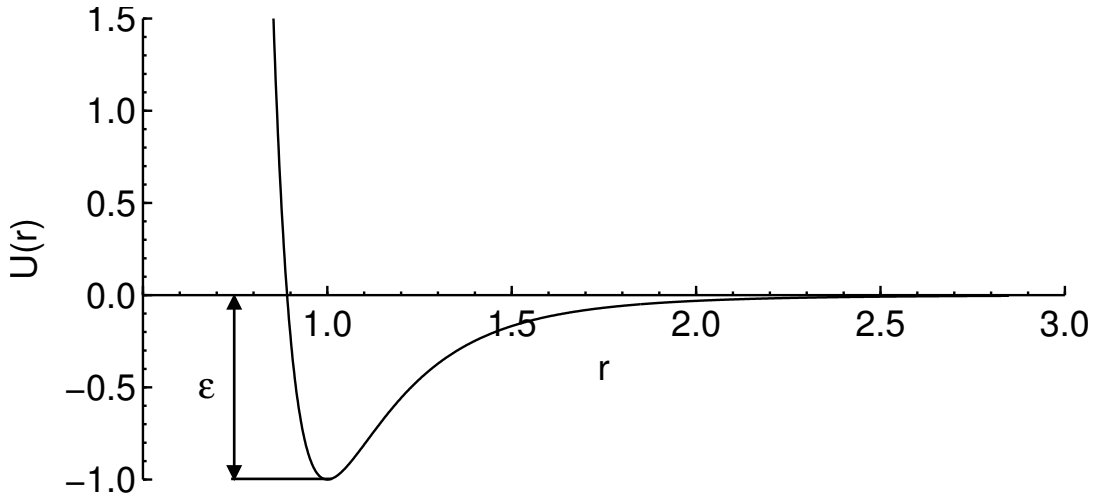


Figure 2.1: Typical interaction potential between two monomers as a function of their distance (arbitrary units).

For  $\varepsilon \gg k_B T$  the attractive part of the potential is dominating the interaction and the chain will obtain a conformation which is more compact compared to the ideal chain. For high  $T$  or in good solvents it is  $\varepsilon \ll k_B T$  so that the repulsive part is dominating, leading to a swelling of the coil. The effect can be described by the swelling coefficient  $\alpha$ :

$$\alpha := \frac{R}{R_0}, \quad (2.19)$$

where  $R_0 = aN^{1/2}$  is the size of the ideal chain.

An example of the swelling of the polymer coil is displayed in Fig. 2.2 where a WLC is compared to a self avoiding WLC in two dimensions.

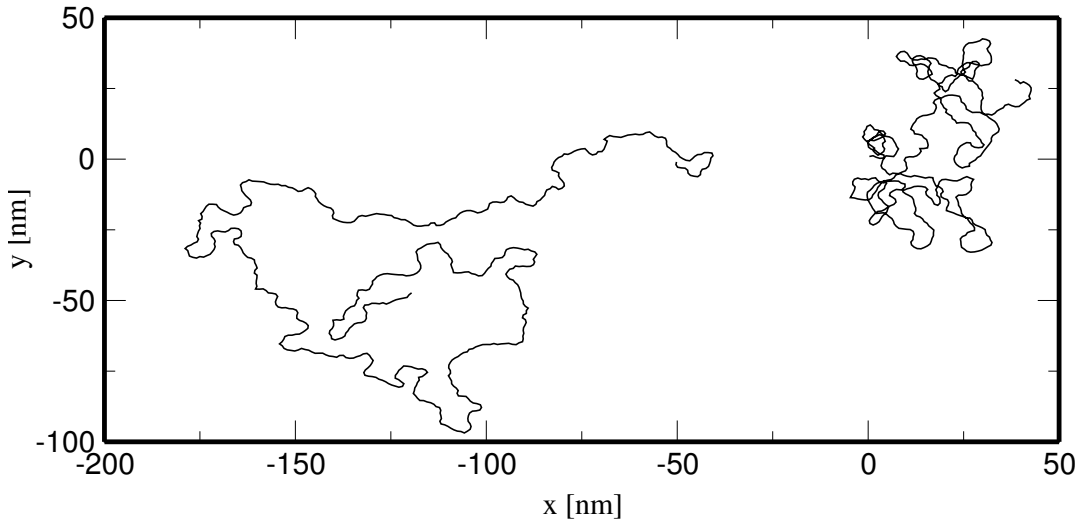


Figure 2.2: Simulated chains in two dimensions. Left: self avoiding WLC. Right: worm-like chain. For the simulation of both chains the intrinsic persistence length was chosen as 3 nm. The simulation method is described in section 4.3.

### Chain with volume interactions

In the simplest model excluded volume interactions are reduced to self avoidance, i.e. each monomer occupies a certain volume of space such that no other monomer can be in the same volume. The freely jointed chain model with this addition is denoted as *Self Avoiding Walk* (SAW) model.

According to Flory, the size of a SAW is given by  $\langle R^2 \rangle \propto N^{6/5}$  in three dimensional space and  $\langle R^2 \rangle \propto N^{3/2}$  in a two dimensional space [168].

### Virial expansion

For ideal and swollen chains the monomer density is very small. Thus the virial expansion of the inner energy  $U = V k_B T (n^2 B + n^3 C + \dots)$  can be truncated after a few terms. The second virial coefficient  $B$  gives the contribution

of two-particle interactions and  $C$  the contribution of three-particle contributions. Here it is assumed, that  $C$  and all higher coefficients are negligible, so that

$$U = k_{\text{B}}TBVn^2. \quad (2.20)$$

According to the sign of  $B$  the temperature range can be divided into two regions: for low temperatures the attractive part of  $U(r)$  is dominating and  $B$  is negative. On the other hand, a positive value of  $B$  is assigned to high temperatures. At the so-called  $\Theta$ -temperature  $B$  vanishes and the chains behave as ideal chains. Correspondingly, a solvent is denoted as  $\Theta$ -solvent when the  $\Theta$  condition is fulfilled at a certain temperature.

## 2.4 Ions in solution

Mobile ions surround charged objects by a diffusive layer and effectively shield the coulombic interactions between them, having substantial influence on e.g. polyelectrolyte conformation or adsorption on charged surfaces.

A characteristic length scale of ionic solutions is the *Bjerrum length*  $\ell_{\text{B}}$  which denotes the distance at which the coulombic interaction between two elementary charges equals the thermal energy  $k_{\text{B}}T$ :

$$\ell_{\text{B}} = \frac{e_0^2}{4\pi\epsilon_0\epsilon k_{\text{B}}T}, \quad (2.21)$$

with  $\epsilon$  being the dielectric constant of the solution and  $e_0$  the elementary charge. In water and at room temperature the Bjerrum length is  $\ell_{\text{B}} \simeq 0.7$  nm.

### Poisson-Boltzmann equation

The electric field around charges is determined by the Poisson equation:

$$\Delta\psi = -\frac{\rho(\mathbf{r})}{\epsilon\epsilon_0}, \quad (2.22)$$

where  $\psi$  is the electrostatic potential and  $\rho(\mathbf{r})$  the total charge density at the point  $\mathbf{r}$ . In a salt solution the charge density consists of the contribution

of mobile cations and anions of the salt and possibly also a contribution of immobile charges  $\rho_b(\mathbf{r})$  at the boundaries.

In the *self-consistent field* approximation the local charge density of ions is assumed to be given by the Boltzmann distribution

$$\rho_i(\mathbf{r}) = c_i z_i e_0 \exp\left(\frac{-z_i e_0 \psi(\mathbf{r})}{k_B T}\right), \quad (2.23)$$

with index  $i$  numbering the different types of ions,  $z_i$  being the ion valence and  $c_i$  the concentration in solution. Then the total charge density is  $\rho(\mathbf{r}) = \sum_i \rho_i(\mathbf{r})$ . For an electrolyte solution with 1:1 positive and negative monovalent salt ions it follows  $z_1 = 1$ ,  $z_2 = -1$  and  $c_1 = c_2 =: c$ . Using equation 2.23 the local ionic charge density is

$$\rho(\mathbf{r}) = ce_0 \left( -\exp\left(\frac{e_0 \psi}{k_B T}\right) + \exp\left(-\frac{e_0 \psi}{k_B T}\right) \right) \quad (2.24)$$

$$= 2ce_0 \sinh\left(\frac{e_0 \psi}{k_B T}\right), \quad (2.25)$$

Using equation 2.22 and the abbreviations  $\tilde{\psi} := \frac{e_0 \psi}{k_B T}$  and  $\tilde{\rho} := \frac{e_0 \rho}{4\pi\epsilon_0\epsilon k_B T} = \frac{\ell_B}{e_0} \rho$ , the *Poisson-Boltzmann* equation follows as

$$\Delta \tilde{\psi} = r_D^{-2} \sinh \tilde{\psi} - \tilde{\rho}_b, \quad (2.26)$$

with  $r_D$  being the *Debye length* which is defined as

$$r_D^{-2} = 8\pi z^2 \ell_B c. \quad (2.27)$$

Due to the non-linearity in  $\tilde{\psi}$  equation 2.26 can only be solved exactly for the case of a planar charged surface [194]. For other geometries solutions of the Poisson-Boltzmann equation must be obtained either numerically or by approximation. For small charge concentrations also  $\tilde{\psi}$  is small and  $\sinh$  can be linearized leading to

$$\Delta \tilde{\psi} = r_D^{-2} \tilde{\psi} - \tilde{\rho}_b. \quad (2.28)$$

This is the so-called *Debye-Hückel* (DH) approximation. The solution for an immobile point charge  $\rho_b(\mathbf{r}) = e_0 \delta(\mathbf{r})$  is

$$\tilde{\psi}^0(\mathbf{r}) := \tilde{\psi}(\mathbf{r}) = \frac{\ell_B \exp\left(-\frac{|\mathbf{r}|}{r_D}\right)}{|\mathbf{r}|}. \quad (2.29)$$

For salt-free solutions the exponential becomes 1 and equation 2.29 reduces to the common coulomb potential of a point charge.

As a consequence of the linearity of equation 2.28 the potential of complicated distributions of immobile charges can be calculated by the superposition

$$\tilde{\psi}(\mathbf{r}) = \int dv' \tilde{\psi}^0(\mathbf{r} - \mathbf{r}') e_0^{-1} \rho_b(\mathbf{r}). \quad (2.30)$$

In this way the potential of a wall with surface charge density  $\sigma$  is

$$\tilde{\psi}(z) = 2\pi\ell_B r_D \sigma e_0^{-1} \exp\left(-\frac{z}{r_D}\right). \quad (2.31)$$

Analogously, for the infinite line which is uniformly charged with charge density  $e_0\lambda^{-1}$  the Debye-Hückel potential reads

$$\tilde{\psi}(x, y) = 2\ell_B \lambda^{-1} K_0 \left[ r_D^{-1} \sqrt{x^2 + y^2} \right], \quad (2.32)$$

with the Bessel function  $K_0$ .

Often, the linearized Poisson-Boltzmann equation is a rather rough approximation [168]. Particularly in the close vicinity of a polyelectrolyte chain the assumption  $\tilde{\psi} \ll 1$  is not fulfilled. This results in the effect of counterion condensation [295], leading to a renormalization of the polyelectrolyte charge.

## 2.5 Polyelectrolytes

Polyelectrolytes (PE) are polymers which carry charges in solutions. Along the chain backbone there are ionizable groups, which can dissociate ions in solution. Most biopolymers, in particular DNA and proteins are polyelectrolytes.

Compared to neutral polymers the physical modeling of polyelectrolytes is considerably more difficult. Their conformational properties, although of fundamental importance for many topics in chemistry and biology, are still not well understood. The complexity arises due to the simultaneous appearance

of the short ranged van der Waals interactions and the long ranged coulombic interactions. Additionally, the counterions have a large entropic contribution and can have a substantial influence on the chain conformation.

### Electrostatic stretching

In the simplest approximation, the coulombic interaction of charges along the backbone is screened by many homogeneously distributed charged particles and the interaction with the polyelectrolyte chain can be described by the Debye-Hückel potential (equation 2.32). The debye length  $r_D$  therefore describes a relevant length scale for polyelectrolytes. Since  $r_D$  can easily be on the order of the chain length, a simple estimation of the exponent  $\nu$  of the scaling relation  $R \propto N^\nu$  is no longer possible.

The screening of charges is increasing with increasing ion concentration. If the charges are fully screened the limiting case of the SAW is reached. The opposite case of a low screening leads to a stretching of the chain [168]:

$$R \simeq N f^{2/3} (\ell_B a^2)^{1/3}. \quad (2.33)$$

where  $f$  is the relative charge fraction per monomer  $f = a\lambda^{-1}$ .

From equation 2.33 follows that the chain extension is proportional to  $N$ . This does not necessarily imply a full stretching of the chain, as shown in the next section.

### Blob model

The *blob-model* introduced by deGennes [100], gives a detailed picture of polyelectrolyte conformations. It is assumed that the chain is weakly charged, i.e.  $\lambda \gg a$  and the chain is in a  $\Theta$ -solvent. Then there is a characteristic length  $D$ , the *electrostatic blob size*, describing the monomer-monomer correlations. For lengths  $\ell < D$  the conformation is mainly determined by the solvent quality and the chain can be described as semiflexible chain. The larger scale is dominated by the electrostatic repulsion, leading to an overall chain stretching. The combined picture is a chain conformation which resembles a pearl necklace, where each pearl is a blob consisting of  $g \simeq D^2/a^2$



The blob size is given by

$$D \simeq a \left( \frac{f^2 l_B}{a} \right)^{1/3} \quad (2.34)$$

for flexible chains [100].

### Electrostatic persistence length

If the electrostatic blob size  $D$  is on the same order of magnitude than the persistence length  $\ell_P$ , the electrostatic stretching is already relevant on length scales comparable to  $\ell_P$ . Hence the chain has an increased local stiffness preventing the formation of blobs. Conformations can then be characterized by an effective persistence length  $\ell_{\text{eff}}$  which is larger than  $\ell_P$ ,

$$\ell_{\text{eff}} = \ell_P + \ell_{\text{OSF}}. \quad (2.35)$$

The electrostatic persistence length was derived by Odijk [339] and independently by Skolnick and Fixmann [444] and reads

$$\ell_{\text{OSF}} = \frac{\ell_B r_D^2}{4\lambda^2} \propto \frac{r_D^2}{\lambda^2}. \quad (2.36)$$

It is derived under the assumption of the Debye-Hückel theory and is only valid for conformations which do not deviate too much from straight rods.

## 2.6 Persistence length

The persistence length was introduced in section 2.2 in the framework of the WLC-model. It is a key quantity to characterize polymer molecules. Unfortunately there is more than one definition of the persistence length. They are equivalent for the wormlike chain model, but not for a charged polymer, as was shown theoretically and by MC-studies [484]. The cause of difference is that the stiffening of a wormlike chain is only transmitted along the contour, while electrostatic interactions act directly through space. Following Ullner und Woodward [485] four common classes of definitions can be distinguished: (1) projection length, which is the mean projection of the end-to-end distance on the direction of the first segment; (2) orientation correlation length, which is the decay length of an exponential function; (3)

bending coefficient, which is a length representing a bending force constant; and (4) crossover distance, which is the monomer-monomer distance at the boundary between a rodlike and a swollen behavior.

In the following the definitions (2) and (3) are explained since they are used in this work. We will denote (3) as the *intrinsic* persistence length, and use it unless stated otherwise.

## Definition of the orientation correlation length

Commonly, chains are described as series of straight segments, which makes sense since real polymers also consist of discrete atoms. For many polymer models the so-called multiplicativity relation [168]  $\langle \cos \sum_{i=j\dots j+n} \theta_j \rangle = \langle \cos \theta_i \rangle^n$  is fulfilled, where  $\theta_i$  is the angle between consecutive segments of length  $a$ . For those models the correlation of tangent vectors along the contour is decreasing exponentially [168]. The persistence length  $\ell_{\text{OC}}$  of a chain in 2D is defined by

$$\langle \cos \theta_i \rangle^n = \exp\left(-\frac{an}{2\ell_{\text{OC}}}\right). \quad (2.37)$$

*Worm-like Chains* are the continuous analog of these chains. Per definition, for a WLC (in 2D) it is

$$\langle \cos \theta(\ell) \rangle = \exp\left(-\frac{\ell}{2\ell_{\text{OC}}}\right). \quad (2.38)$$

## Definition of the intrinsic persistence length

The work of bending a macromolecular rod of length  $a$  by the angle  $\theta$  is

$$U = \frac{k_{\text{bending}}}{2a} \theta^2, \quad (2.39)$$

where  $k_{\text{bending}}$  is the flexural rigidity [258].

To calculate the statistical bending of a worm-like chain we imagine the chain to be broken in segments of length  $a$ , with  $a$  being sufficiently short ( $a \ll$

$\ell_P$ ). Segments will be bent by thermal fluctuations so that the equilibrium distribution of  $\theta_i$  is given by the Boltzmann distribution

$$P(\theta_i) \propto \exp\left(-\frac{U(\theta_i)}{k_B T}\right). \quad (2.40)$$

The angles  $\theta_i$  are therefore normal distributed around zero with variance  $\frac{a k_B T}{k_{\text{bending}}}$ . In 2D, the bending of a chain section consisting of several segments can be calculated by summing up successive segment bending angles. The distribution of  $\theta := \sum_{i=0}^{n-1} \theta_i$  follows from the central limit theorem [51] to be a normal distribution with zero mean and variance  $n \langle \theta_i^2 \rangle$  and therefore

$$P(\theta) \propto \exp\left(-\frac{k_{\text{bending}} \theta^2}{2a n k_B T}\right). \quad (2.41)$$

Defining the persistence length as

$$\ell_P := \frac{k_{\text{bending}}}{k_B T}. \quad (2.42)$$

and using  $\ell := a n$  we get

$$P(\theta) \propto \exp\left(-\frac{\ell \theta^2}{2\ell_P}\right). \quad (2.43)$$

The average value of  $\cos \theta$  is then

$$\langle \cos \theta(\ell) \rangle = \int_{-\infty}^{\infty} \cos(\theta) P(\theta) d\theta \quad (2.44)$$

$$= \exp\left(-\frac{\ell}{2\ell_P}\right), \quad (2.45)$$

i.e. the orientation correlation function of a WLC in 2D.

The definition of  $\ell_P$  by equation 2.42 corresponds to number (3) in the scheme of Ullner et al.: the persistence length as bending coefficient. It is a material property but does also depend on the temperature. In this work, we denote this variant of the persistence length as *intrinsic* persistence length  $\ell_{\text{int}}$  to distinguish it from the orientation correlation length  $\ell_{\text{OC}}$  which is a property describing the *geometry*. For ideal worm-like chains both values are the same, but they can also deviate e.g. due to the interaction of the chain to surface atoms or when chains are not in equilibrium.

Mean and variance of a random variable are generally given by the first two moments of the distribution. For the value  $\theta(\ell)$  this is from the above discussion

$$\langle \theta(\ell) \rangle = \int_{-\infty}^{\infty} \theta P(\theta) d\theta = 0 \quad (2.46)$$

$$\langle \theta(\ell)^2 \rangle = \int_{-\infty}^{\infty} \theta^2 P(\theta) d\theta = \frac{\ell}{\ell_P}. \quad (2.47)$$

# Chapter 3

## Experimental methods

This section contains the description of the scanning force microscope and the sample preparation procedures. Emphasis is placed on the discussion of image artifacts, including the problem of the height of single molecules, which is still under discussion in the literature. Recommendable further reading includes the review articles [148], [459], the DI-manual [102] and [502]. For topics such as the tip sample interaction, sample deformation and tapping the book of Sarid [395] is invaluable. The classic book about surface forces is [194].

### 3.1 Scanning force microscopy

The history of microscopy begins with the optical microscope which was developed at the end of the 16th century and was greatly improved in the following. As was shown by Abbe a principle resolution limitation is given by the wavelength of the used light (about 600 nm). A consequent improvement is therefore the electron microscope in which photons are replaced by electrons and the theoretical resolution limit is given by the de Broglie wavelength of the electron. Good electron microscopes reach a resolution which is about one angstrom for 100 keV electrons. A fundamentally different way of microscopy started with the development of the scanning tunneling microscope (STM) by Binnig and Rohrer [50] (honored with the physics Nobel prize in 1986) and has led to the family of scanning probe microscopes (SPM),

including the scanning force microscope (SFM) developed by Binnig, Gerber and Quate in 1986 [49].

The principle of the scanning probe microscopes is surprisingly simple. As shown schematically in Fig. 3.1 a sensor traces the contour of a sample surface. It is moved in  $x$ ,  $y$  and  $z$ -direction with a piezoelectric scanner. The distance between sensor and surface is controlled by a feedback circuit which sets the voltage at the  $z$ -piezo. While the sensor is scanned over the surface, the feedback circuit compares the control parameter to a given set point value and raises or lowers the tip to match the set point. In this way a relief image of the sample topography is obtained.

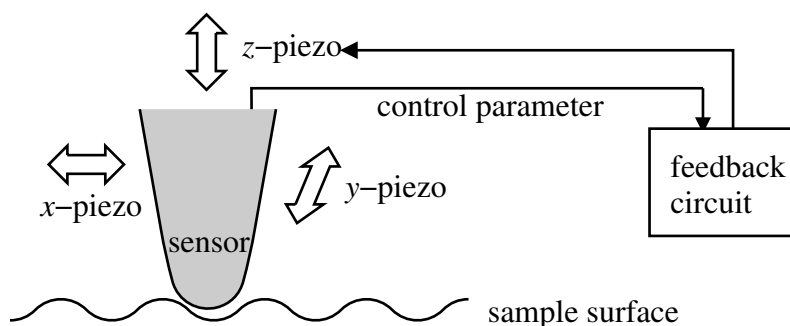


Figure 3.1: Schematic diagram of a scanning probe microscope.

In the case of the STM the control parameter is the current of electrons tunneling across the gap between tip and sample, under the influence of a voltage applied to the tip. Since the tunneling current decays strongly with the separation between tip and surface the  $z$ -resolution can be as good as a picometer. Compared to the electron microscope the STM has the advantage of a high contrast for molecules. To image single molecules on a flat substrate surface electron microscopy usually requires the sample to be stained, i.e. coated with a layer of contrast enhancing material which has the drawback of reducing the resolution.

The scanning force microscope produces images that are much closer to the sample topography than STM and is able to image also non-conducting samples. Instead of the tunneling current the force exerted by the surface on a probe is used as  $z$ -dependant control parameter. Measuring forces of single atoms using a macroscopic detection device might appear amazing. Typical force constants of atomic bonds are several 100 N/m, but the force constant of a strip of household aluminum foil, 1 mm long and 3 mm wide is only 1

N/m and can therefore be used as force sensor to detect atoms. Nowadays, force sensors are usually etched from silicon and consist of a very sharp tip, located at the free end of a silicon cantilever 100 to 500  $\mu\text{m}$  long. Brought close to a sample surface, the cantilever bends due to the surface forces and the deflection is detected by a laser beam reflected from the back of the cantilever. The schematic view of a SFM force detector is shown in Fig. 3.2.

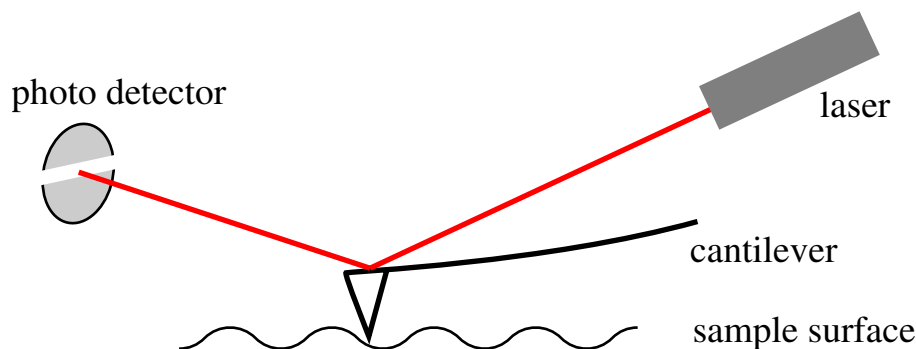


Figure 3.2: Force detection in a scanning force microscope.

Scanning force microscopes can be operated in two basically different ways of operation: in the static and the dynamic modes. In the former, the tip is scanned over the surface while tip sample forces are detected through the cantilever deflection. In the dynamic modes, the cantilever is excited to oscillate at the resonance frequency  $f_0$ . As  $f_0$  is strongly dependent on the separation between tip and surface, it can be used as  $z$ -dependant control parameter.

The advantage of the dynamic modes is the lower lateral friction forces exerted on the sample, enabling imaging of fragile samples as single molecules or biological samples.

The maximum resolution obtained in SFM can be similar to STM. A recent highlight is the resolution of sub atomic features, showing atomic orbitals of the (111)-(7x7) surface of a silicon crystal [151].

### 3.1.1 Tip-Sample forces

Depending on the SFM operation mode, the tip detects different surface forces effecting both resolution and sample deformation. The forces can be

classified as either long- or short ranged. The so-called *non-contact regime* far from the surface is dominated by the long ranged van der Waals forces and possibly also electrostatic and magnetic forces. In the *contact regime*, which is in the angstrom range close to the surface, relevant forces are the surface repulsion and adhesion. In ambient air capillary forces arise due to water condensation between tip and sample.

Unlike the commonly used term “atomic force microscope” suggests, the detected forces are not necessarily between one single atom from the sample and one single atom on the tip. In fact the tip apex typically has a curvature radius of 10 nm and therefore many tip atoms interact with many atoms of the sample.

The interaction potential between two charge neutral atoms can be described by the Lennard-Jones (LJ) potential

$$U(r) \propto (Ar^{-12} - Br^{-6}) \quad (3.1)$$

with the empiric parameters  $A$  and  $B$ . It is composed of the long ranged van der Waals attraction term and a hard-core repulsion term. The attraction is a sum of

- dipole-dipole interactions (Keesom force)
- induced dipole interactions (Debye force)
- interactions of fluctuating dipoles (dispersion force)

These contributions show a  $r^{-6}$  dependence and are commonly referred to as van der Waals forces.

The hard-core repulsion is of much shorter range and has two physical reasons:

- the Pauli exclusion principle leading to a repulsion of the electron shell and
- the repulsion of the charged atom cores.

The repulsion is usually approximated as  $r^{-n}$  where  $n > 8$ .



The LJ-potential is only a valid approximation of the tip-sample forces in the non-contact regime. In contact, the surface behaves elastic, allowing deformations.

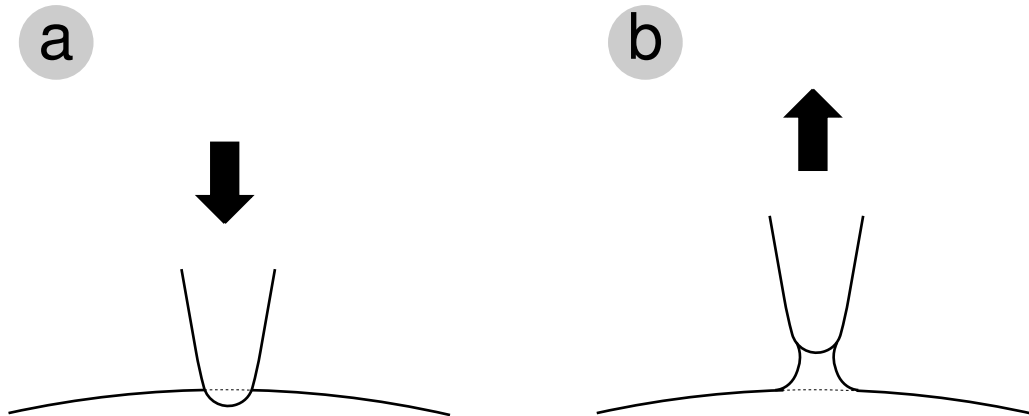


Figure 3.3: Schematic diagram of the tip adhesion for (a) push-in and (b) pull-out.

Figure 3.3 shows a sketch of tip and sample. Applying a downward external force to the tip will push it into the sample. When the external force is pointing up, the tip will be pulled out of the sample and for a limited range of forces a neck connecting both is formed. Indentation and adhesion are described by the JKR-model [194]. The combined force of JKR in the contact region and LJ in non-contact region is shown in Fig. 3.4 for a silicon tip of radius 10 nm and a silicon surface. The irreversibility between tip approach and retraction is due to the neck-formation. The area between both curves equals the dissipated energy during the approach and retract cycle. This tip-surface interaction model is described in detail in [395].

The deflection  $d$  of an elastic cantilever ( $k = 0.5$  N/m) due to this force field is shown in Fig. 3.5.

### 3.1.2 Modes of operation

#### Static mode

In the static mode, the elastic bending of the cantilever is used for the prime measurement. Depending on the settings of the feedback loop, two different

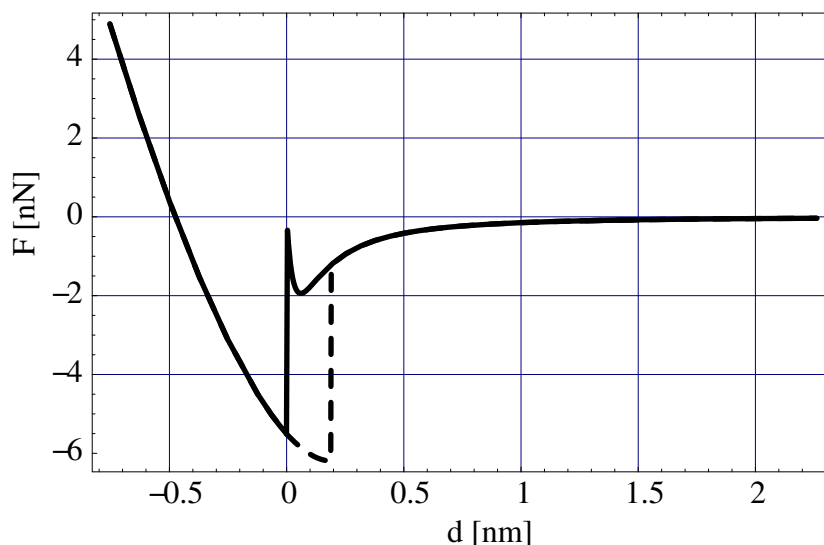


Figure 3.4: Force between tip and surface as a function of distance [395]. The hysteresis curve describes the pushing in (solid line) and pulling out (dashed line) of the tip from the sample.

operation modes can be distinguished: the height mode and the deflection mode.

In the deflection mode, the feedback is disabled and the  $z$ -piezo extension is kept fixed. When the tip is moved over the surface, the cantilever bends according to the topography. Recording the deflection as a function of the position therefore gives a topographic image. A major disadvantage of the deflection mode is the appearance of high lateral forces.

In the height mode the  $z$ -position is adjusted by the feedback-loop to keep the cantilever deflection at a constant set-point value. The recorded measurement signal is the voltage of the  $z$ -piezo.

The tip-sample distance can be chosen to be either in the contact or the non-contact regime (see Fig. 3.6). In the latter, the tip detects the attractive van der Waals forces. In the non-contact regime the sample abrasion is low but due to the long ranged nature of the van der Waals forces also the lateral resolution is low.

In contact mode the tip is moved in the sample's contact region and detects the short-ranged repulsive surface forces. Due to the strong distance

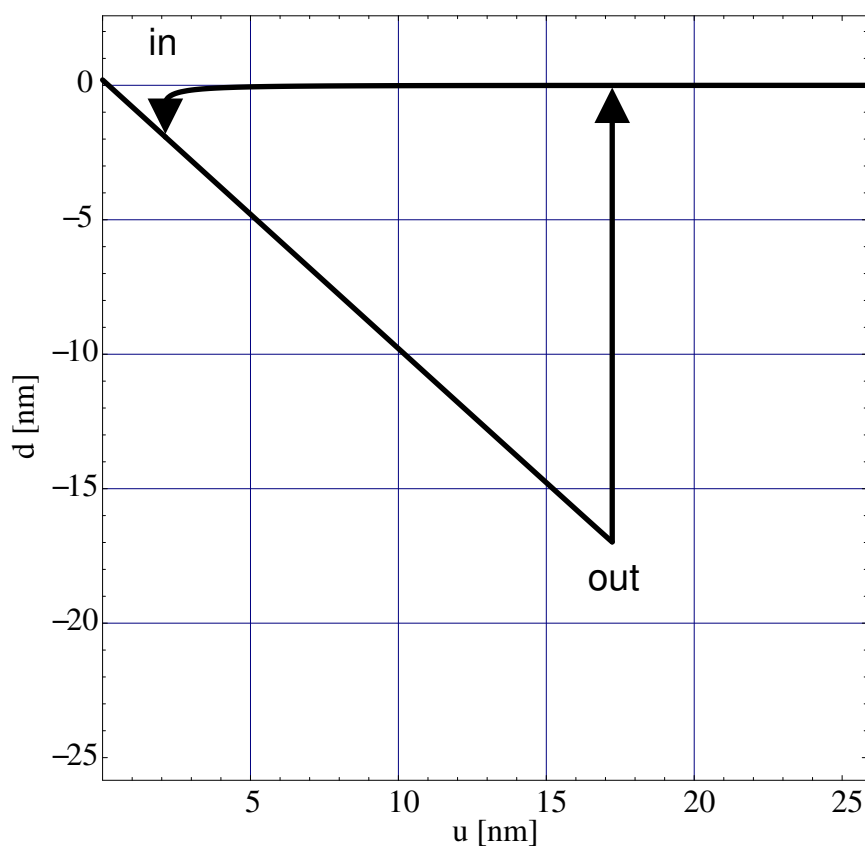


Figure 3.5: Cantilever deflection as a function of distance [395].

dependence of the forces, this mode has the highest vertical resolution (sub-angstrom). Moreover only a small spot contributes to the interaction, thus also the lateral resolution is high (about one angstrom). When scanning laterally across the sample, applied forces are kept as small as possible while still maintaining a stable tip-sample contact to avoid any damage of the specimen. Cantilevers used for contact SFM are usually very soft, with spring constants smaller than 1 N/m. By functionalizing the probing tip with selected molecules specific interactions and molecular recognition processes can be studied [459].

A main disadvantage of the contact mode is the appearance of large lateral forces between tip and sample. The contact mode is therefore not suitable for investigations of fragile samples like weakly adsorbed single molecules. On the other hand, flat and stable samples (i.g. crystal surfaces) can be imaged with high, often atomic resolution [148].

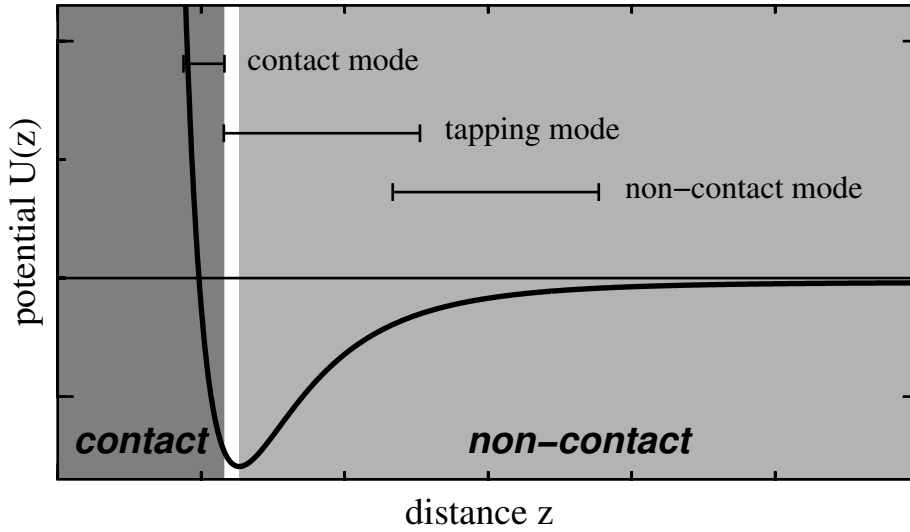


Figure 3.6: Tip sample potential curve showing the different regimes of measurement modes.

In addition, contact SFM can yield information on micro- and nanomechanical properties, e.g. friction (LFM: Lateral Force Microscopy), elasticity and viscosity (FMM: Force Modulation Microscopy) or adhesion forces [102].

By using a special technique called *force distance curves* or *force spectroscopy* forces acting between the probe tip and the sample surface can be investigated [102]. For this the tip is moved vertically (in  $z$ -direction), slowly approaching and retracting from the sample (and actually being pulled off the surface in most cases). Simultaneously the cantilever deflection is recorded, therefore giving the force acting on the tip as a function of  $z$ -position. Forces as small as 100 pN can be detected (e.g. [269]).

### Dynamic modes

In the dynamic mode, the cantilever is excited by a piezo transducer to oscillate at or near the resonance frequency. In an external force field  $F$  the cantilever force constant is modified to an effective force constant  $k_{\text{eff}} = k + \nabla F$ . A change of the external forces therefore leads to a change of the cantilever's resonance frequency  $f_0 = \frac{1}{2\pi} \sqrt{\frac{k_{\text{eff}}}{m}}$ , where  $m$  is the mass of the cantilever. In the frequency-modulation-SFM (FM-SFM)  $f_0$  is used as  $z$ -dependant feedback parameter [5]. Alternatively, the RMS value of the

amplitude can be used as feedback signal, while exciting the cantilever with a constant frequency.

Similar as above, the measurement modes can be categorized by the distance of the tip from the sample. The so-called true non-contact mode where the tip is oscillating in the purely attractive regime is not common. Usually, the tip sample distance is chosen in such a way that the tip is slightly touching the sample in the minimum  $z$ -position of the oscillation. This mode is referred to as tapping mode or intermittent contact mode (IC-mode).

In addition to the topography, in the dynamic mode, the phase difference  $\phi$  between transducer and cantilever can be recorded. The phase difference is related to the energy dissipation by the cantilever as  $\sin \phi \propto P_{\text{diss}}$  [142]. This contains the familiar result that the maximum power is delivered to an oscillator when the response is  $90^\circ$  out of phase with the drive. As the dissipation depends on sample properties like viscosity and elasticity, measuring the phase difference allows to distinguish different materials.

Assigning the phase difference directly to physical properties is rather complex and has yielded a controversial discussion in the literature. Especially the fact that more than one parameter contributes to the dissipation (surface energy, elasticity, amplitude) aggravate phase interpretation.

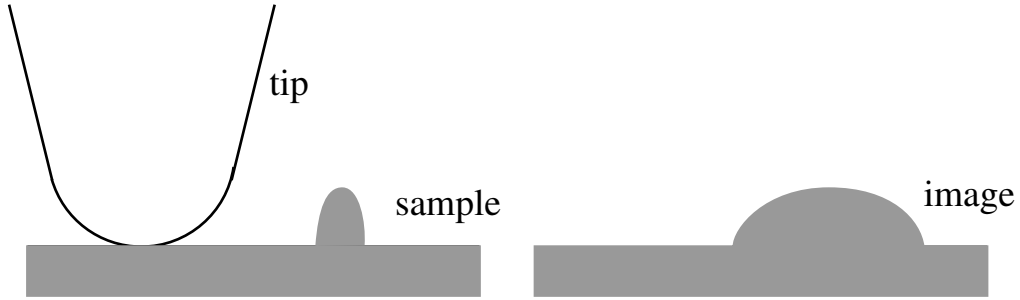
The advantage of the dynamic modi over the static ones is the small lateral interaction force between tip and sample. A certain disadvantage is the limited scanning speed. Due to the long setting time of the cantilever oscillation after a sudden change of external forces, the scan speed is considerably slower than in the static modes. The number of transient oscillations depends on the  $Q$ -factor of the cantilever by the empirical formula  $n \simeq 2Q$  [395]. For a typical  $Q$ -value of 200 and a resonance frequency of 350 kHz the maximum line frequency is 3.4 Hz, assuming 512 pixels per line.

### 3.1.3 Image artifacts

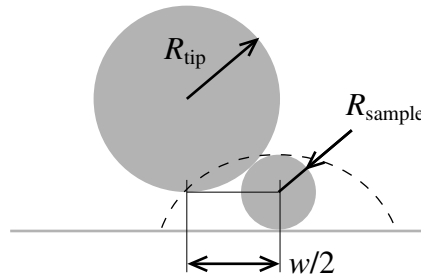
#### Tip broadening

The most obvious artifact when imaging single molecules is the broadened width of objects. As an example, measuring DNA usually yields a width

(FWHM) of about 20 nm instead of the true diameter of 2 nm. The reason is the finite size of the tip which leads to a convolution of tip and sample topography. Typically tips have a radius of curvature of about 10 nm. Objects which have the same size or even smaller will be drastically broadened as sketched below.

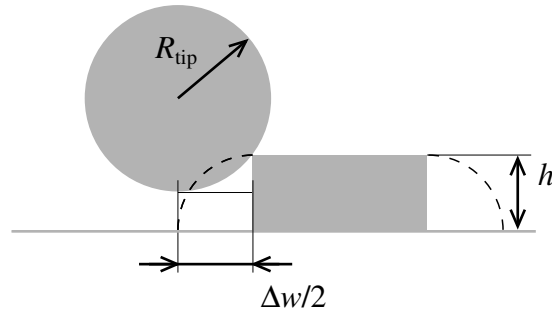


Knowing the tip geometry allows to calculate the broadening and therefore to determine the true width. For objects which are approximately spherical the following formula can be easily derived from the sketch below and gives the apparent width  $w$  (full width half maximum):



$$w = 2\sqrt{(R_{\text{tip}} + R_{\text{sample}})^2 - R_{\text{tip}}^2} \quad (3.2)$$

For objects having a flat geometry, the broadening can be estimated by approximating the cross section by a rectangular. The broadening  $\Delta w$  (again full width half maximum) can be derived from the sketch and reads:



$$\Delta w = 2\sqrt{h(2R_{\text{tip}} - h)} \quad (3.3)$$

Usually the tip geometry is only roughly known, since the manufacturer value only gives the statistical mean from which single tips can deviate considerably. Furthermore, tips can change during the measurement, e.g. by contamination or abrasion. Tips can be characterized by measuring samples of known geometry. An ideal but hypothetical tip characterizer would be a thin needle which has zero width. The resulting image would show the exact topography of the tip. Practically, objects having sharp orthogonal edges (e.g. nano-crystals) can be used.

A variation of the above idea of tip characterization is called blind tip estimation [492], where the shape of the tip is estimated just from the measured image.

### Tip instability in the tapping mode

Ideally the oscillation amplitude is increasing monotonically with the tip sample separation. As shown by experiment [159] and numerical simulation [333], surface attraction can lead to non-monotonic dependence. As a result there can be several stable  $z$ -positions for a given amplitude set point. Jumps of several nanometers can occur during a measurement, disturbing the image as shown in Fig. 3.1.3.

An often observed effect leading to systematically wrong height values is the so-called *contrast inversion* [333]. Imagine a bistable tip approaching an adsorbed molecule on a flat surface. Once the tip feels the molecule, the feed-back loop causes the tip to retract. Due to the feed-back's finite

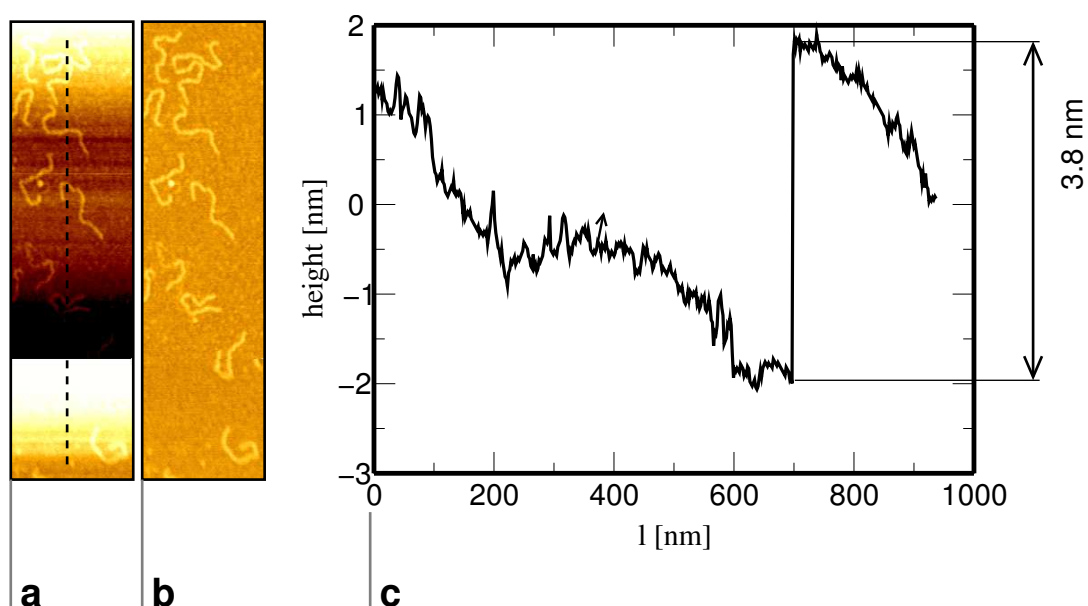


Figure 3.7: Jump observed while recording an image of DNA. The image (a) was scanned line wise from top to bottom. Image (b) shows the same region where the background is removed using the first order quantile filter. The diagram (c) gives the height along the dashed line in (a), showing a jump of 3.8 nm.

response time, the height of the tip over the object is for a short moment smaller than the set point value. This might trigger a jump to another stable position closer to the surface. When the tip is leaving the sample, the opposite happens and the oscillation jumps back to the starting position. This effect can cause objects to appear lower, or even inverted. Another inversion mechanism is described by [329] and results from the inhomogeneity of the tip sample interaction. When the tip instability is limited to certain regions of the sample surface, these regions can appear reduced in height.

### Sample deformation

The vertical forces applied by the tip to the sample can cause a relevant deformation of the sample and thereby a fault mapping of the sample topography. The depth to which the tip indents into the sample depends besides



the loading force mainly on the stiffness of tip and sample given by the corresponding Young's moduli and also on the size of the tip. The tentativeness of the tip geometry therefore leads to a general uncertainty of height values in SFM images.

Further, the geometry dependence can have a drastic influence on the height values measured for single molecules. Consider a spherical molecule of a radius smaller than the tip radius which is imaged on a flat surface. This molecule will be pushed by the tip into the substrate. The molecules height as it appears in the SFM image is the difference between the tips  $z$ -position on the substrate and the  $z$ -position atop the molecule (see Fig. 3.8). Depending on the diameter of tip and sample the apparent height can be much smaller than it is possible by compressing the molecule.

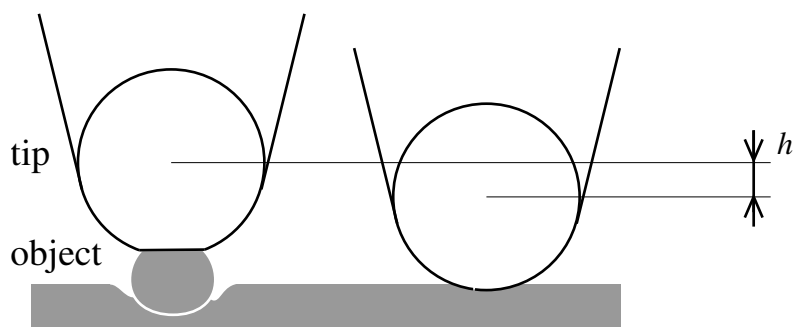


Figure 3.8: The apparent height  $h$  is the difference of the  $z$ -positions atop the object (left) and on the sample (right).

In the case of a rod like molecule geometry (i.e. a polymer chain), there is a similar effect. Above the flat substrate surface the pressure exerted to the sample is distributed over a circular disc of 1.9 nm diameter (for a 10 nm Si-tip pressed on graphite with a force  $F = 100$  nN, calculated using the JKR model). With the indentation depth  $d$  the disc area is increasing quadratically (this is only approximately true since also the tip is deformed). By pressing the tip on a flexible rod, the area is increasing approximately linear, as sketched in Fig. 3.9. Thus the indentation will be larger on the rod and the apparent height will underestimate the true value.

Reviewing the literature about height values of single molecules gives a diverse picture. Some authors report about finding the correct value, others find heights which are considerably too small. A possible explanation is the

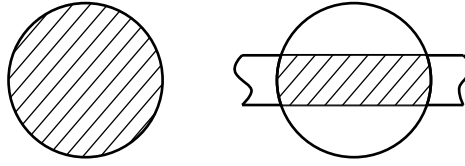


Figure 3.9: The area under the tip on a flat surface (left) and on a rodlike object (right).

dependence on the size of the molecule, which (to the authors knowledge) is not taken into account thus far.

### Tip indentation in the tapping mode

The average vertical force exerted on the sample during one oscillation is typically between 1 nN to 20 nN [121]. It gives no information about the sample deformation which is related to the much larger peak force during the short time of tip impact. The peak force can be obtained by numerically integrating the tip equation of motion (see [395, 461, 61, 41]).

Simulation results taken from [461] are displayed in Fig. 3.10. Shown is the tip indentation on several substrates as a function of the amplitude set-point. The tip sample forces were modeled as combination of JKR in the contact and LJ in the non-contact region. Additionally sample viscosity is introduced by a dissipation force term. Simulation parameters are force constant  $k = 20$  N/m, resonance frequency  $f_0 = 200$  kHz, quality factor  $Q = 500$ , free amplitude  $A = 100$  nm. Peak forces and sample deformation are similar to typical values in the contact mode. Further, there is a strong dependence on the amplitude set-point value. For set-point values close to the free amplitude, the deformation is the smallest. This important result has been verified with simulations based on different models [395, 461, 61, 41] and experiments [22].

To obtain results for the tip and sample combinations used in this thesis, simulations were performed using the model described by Sarid [395]. Results are shown below for a 10 nm tip.

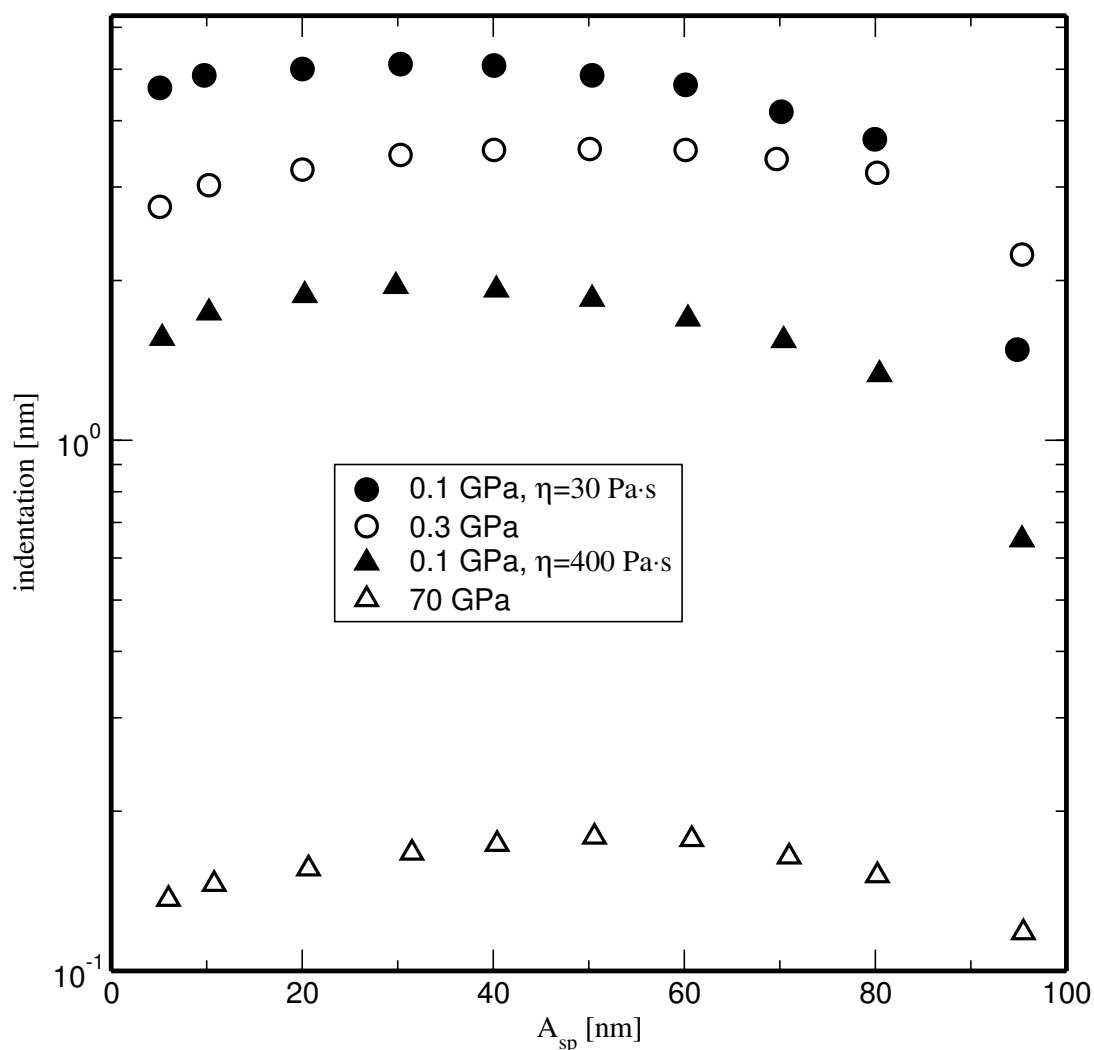


Figure 3.10: Tip indentation in the tapping mode after [461] for different substrates as characterized by the young moduli  $E$ . Viscoelastic substrates (filled markers) are additionally described by their viscosity  $\eta$ .

	Young modulus $E$	indentation $d$	peak force $F$
mica	0.14 ... 0.21 TPa	0.66 ... 0.78 nm	249 ... 274 nN
polymer	0.001 TPa	6.6 nm	78 nN
HOPG	0.2 TPa	0.7 nm	269 nN

The indentation dependence on the tip size is shown in Fig. 3.11. It is largest for very sharp tips and is decreasing with the radius. The corresponding peak forces increase from 199 nN at  $R = 1$  nm to 297 nN at  $R = 20$  nm. As

discussed before, the size dependant indentation leads to strong height errors since small molecules are pushed into the substrate.

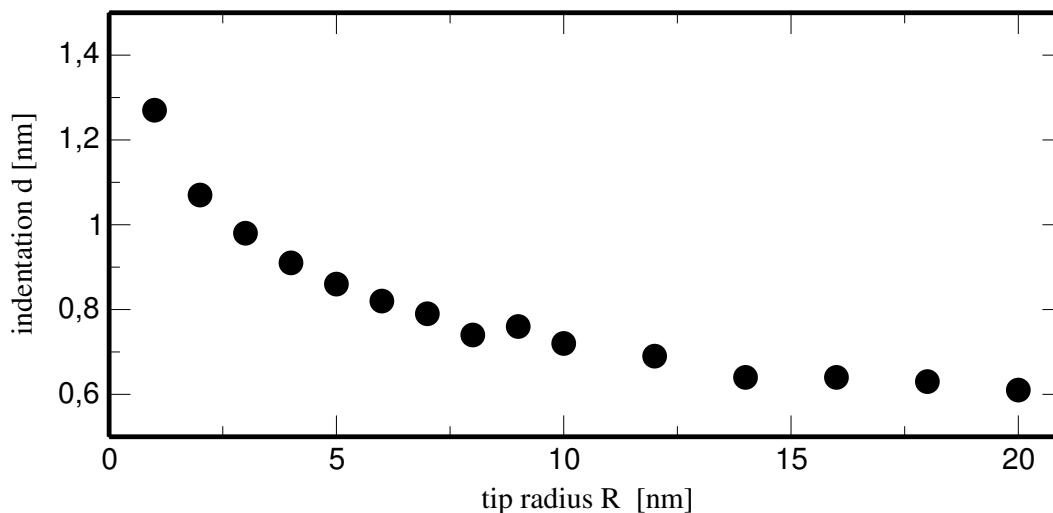


Figure 3.11: Tip indentation as a function of the tip radius.

## Conclusions

The apparent heights and widths in SFM images deviate considerably from the true topography. The distorting effects can be estimated in principle but realistically they exhibit a large error. In this thesis the interpretation of directly measured widths and heights is avoided and alternative information is used when possible, e.g. from the width in a lamellar packing.

## 3.2 Equipment

All measurements have been performed using a commercial SFM (Nanoscope, Digital Instruments, Santa Barbara, CA) with a Multimode IIIa controller. For noise reduction, the Nanoscope was operated on a massive granite table hanging at bungee chords. For cantilever and sample adjustment it can be placed under an optical microscope (Olympus). The SFM is equipped with three scanners with different scan ranges: A-scanner ( $1 \mu\text{m}$ ), E-scanner ( $13 \mu\text{m}$ ) and J-scanner ( $130 \mu\text{m}$ ).

Measurements in liquid were done using a fluid cell with acoustic cantilever excitation (Digital Instruments).

### 3.3 Sample preparation

Samples for SFM imaging consist of a metal puck on which the substrate is glued. For the deposition of molecules onto the substrate two methods proved useful: spin coating and solution casting. Substrates used in this thesis are muscovite mica and highly oriented pyrolytic graphite (HOPG). Immediately before deposition of molecules, the substrates are cleaved using adhesive tape to obtain clean surfaces.

#### Solution casting

Solution casting is useful for very dilute solutions of DNA. Typical concentrations are 1 ng/ $\mu\text{l}$ . A drop of solution is placed on the substrate surface allowing adsorption for a well defined time (e.g. 2 min). Adsorption is aborted by blotting off the solution and washing the sample by placing it on a drop of distilled water, and subsequent blotting.

#### Spin coating

A drop of the solution (5 to 10  $\mu\text{L}$ ) is pipetted onto the substrate which is rotating at 40 rotations/s. The centrifugal forces immediately tear off the drop from the surface, aborting the adsorption.

Spin coating might be preferred over solution casting when the length distribution of the adsorbed molecules should be representative for the molecules in solution. Due to the length dependence of the diffusion constant<sup>2</sup> a long adsorption time can lead to segregation of the short chains at the surface.

---

<sup>2</sup>In the  $\Theta$ -solvent it is  $D_{coil} \propto N^{-1/2}$  [168].

# Chapter 4

## Data analysis

### 4.1 Image processing

The term image processing means two things here, firstly improving the image and secondly extracting information by e.g. vectorization. A good source for image processing in general and not related to SFM is the book [503].

A height image as delivered by the Nanoscope SFM consists usually of a 512x512 matrix ( $z_{ij}$ ) of height values. For visualizing the 3D data usually a color coding is performed, i.e. a color scale is assigned to the height range, and the color coded data is plotted in a  $x, y$ -diagram. The minimum image enhancement usually performed is background removal, which is the subtraction of a background matrix from ( $z_{ij}$ ). Standard methods for background removal are *flattening* and *plane fitting*. Background correction is necessary because images usually exhibit a height gradient resulting from an imperfect alignment of the microscope's head with respect to the sample surface. Furthermore, in the tapping mode scan lines are usually shifted against each other so that a line-wise correction is necessary. For the evaluations done in this thesis it was necessary to have a better background correction than this standard methods can deliver. Therefore improved methods were developed. They are discussed in section 4.1.1.

For the statistical analysis of chain contours, SFM-images have to be vectorized. This can be done manually or by an automated procedure. The manual

vectorization can be more precise but bears the potential risk of introducing subjective vectorization errors. An automated vectorization procedure has the advantage of objectivity but introduces correlations on the short scale. For the experiments in this thesis both methods are used.

An automated procedure for chain vectorization was developed and is described in section 4.1.2. There has been at least one attempt before to write a program for the automated vectorization of SFM images, see [378]. The method described here was developed independently. It has the advantage that the delivered coordinates are continuous values, so that the discretization problem described in [378] is avoided.

### 4.1.1 Background correction

In this section two newly developed methods for background correction, the zero and first order quantile methods, are discussed. The name is chosen because it indicates the use of quantiles. In statistics, a quantile denotes a specific element in the range of a variate, e.g. the median.

In Fig. 4.1 flattening is compared to the newly developed *quantile*-method. The SFM image in (a) is the raw tapping mode image of **a-g2** adsorbed onto HOPG. For presentation reasons the background gradient is removed by subtracting a fitted plane (*plane fit*). In (b) the background is removed by flattening, i.e. least square fitting and subtraction of first order polynomials to each scan line. Characteristic for flattened images is the shadow accompanying all higher objects. When the image only contains a few such objects, they can in principle be masked out manually, however good results can be reached automatically by the quantile method. Shown in image (c) is the same image after applying the first order quantile method 3 times.

#### Quantile method of zero order

The basic idea of the quantile methods is not to use all data points of the scan line for fitting, but only values around the minimum. This way high objects are suppressed automatically. In the zero order method, a zero order polynomial is subtracted from each scan line, i.e. the lines are corrected for their bias. The method is sketched in Fig. 4.2. Sorting the  $z$  values of

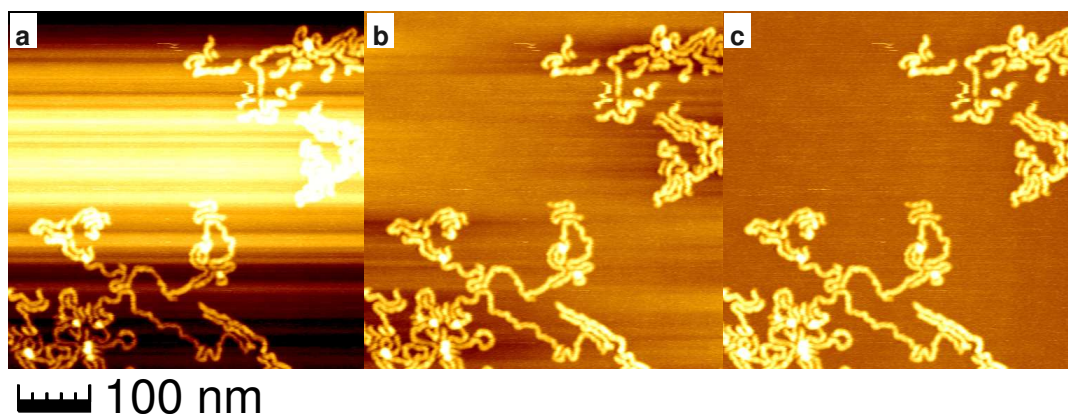


Figure 4.1: Comparison of image processing methods. a: raw SFM image of **a-g2** onto HOPG. b: image after flattening and c: image after applying the 1st order quantile method. The  $z$ -range is always 3 nm.

the scan line in the left gives the distribution shown in the right diagram.

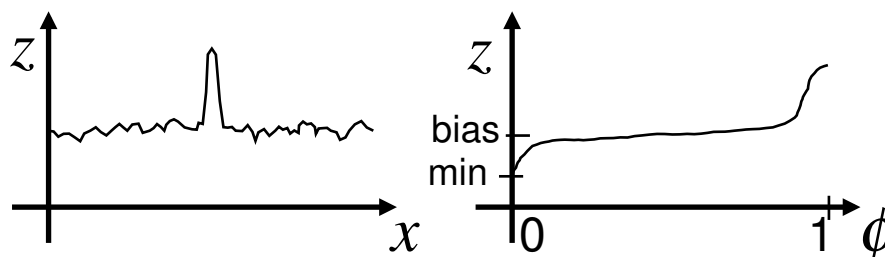


Figure 4.2: The zero order quantile method. Left: a trace of a typically scan line. Right: sorting the values gives the distribution function, ranging from 0 (smallest) to 1 (highest value). The minimum is at  $z[0]$ , a better estimate of the bias however is  $z[\phi]$ , where  $\phi$  is in 0.02 .. 0.2.

The abscissa is normalized from 0 (smallest value) to 1 (largest value). For hypothetical perfect images without any noise the minimum value  $z[0]$  could be used as bias. For real SFM images however, it is better to use  $z[\phi]$ , where  $\phi$  is chosen between 0.02 and 0.2, depending on the image quality.

This simple method can only be applied if the imaged surface is parallel to the  $xy$ -plane. The method described next can also remove image gradients.



### Quantile method of first order

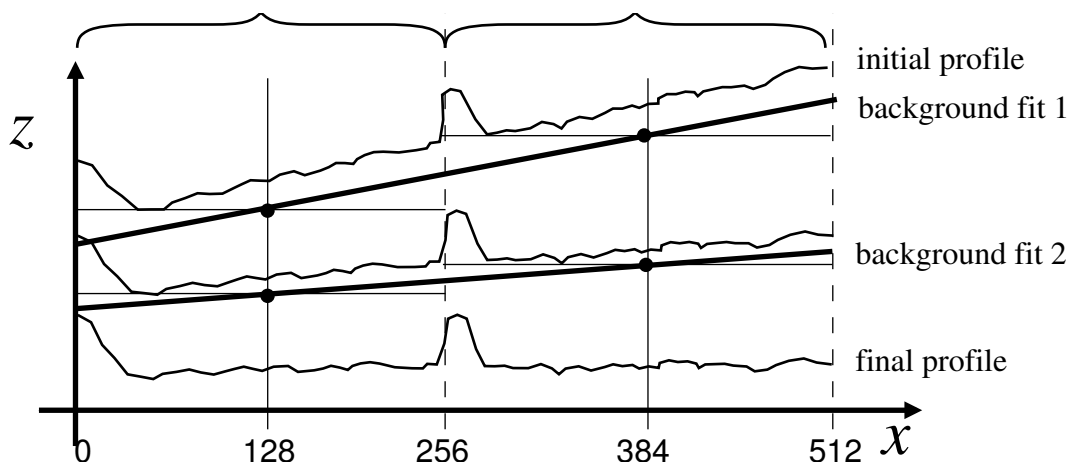


Figure 4.3: The first order quantile method.

Each scan line is divided into a region  $a$ , from pixel 0 to pixel 255 and a region  $b$  from 256 to 511. For both regions a certain  $z$ -value is chosen as background value in the same way as for the zero order method. The line defined by the points  $(128, z_a)$  and  $(384, z_b)$  is a fit to the background and is subtracted from the scan line. This procedure is sketched in 4.3. It is applied repeatedly and yields already good results after 2 to 4 passes.

### 4.1.2 Automated vectorization

#### The method

The contour line of an imaged chain can be defined as the 2D path which maximizes the value  $W = \int_{\mathbf{p}_1}^{\mathbf{p}_2} z(\mathbf{r}) d\mathbf{r}$ , where  $\mathbf{p}_1$ ,  $\mathbf{p}_2$  and  $\mathbf{r}$  are vectors in the  $xy$ -plane with  $\mathbf{p}_1$  and  $\mathbf{p}_2$  pointing to the ends of the chain and  $z(\mathbf{r})$  being a function which gives the  $z$ -value of the pixel containing  $\mathbf{r}$ .

Experimental SFM images contain a certain noise. Therefore instead of  $z(\mathbf{r})$ , also height values in the neighborhood of  $\mathbf{r}$  should be considered. Since SFM images consist of discrete pixels, the measured angles between three data points are discrete and the resulting contour lengths are too small. Both problems are avoided by using a “test-function”  $f(\mathbf{r})$  instead of  $z(\mathbf{r})$ , as discussed later in detail.

The remaining task is then to find the vectorization for which  $W$  has a maximum, at least locally. Due to the large number of possible vectorizations and the limited processing time, a deep search under all possible vectorizations is out of question.

On the other hand, the following method is fast and proved to be useful. The method consists of two different steps which are applied alternately (see Fig. 4.4): 1. A given vectorization is optimized, i.e. the vertices  $\mathbf{p}_i$  are shifted in order to optimize  $f(\mathbf{p}_i)$ . 2. The vectorization is refined by introduction of new vertices. These new vertices  $\tilde{\mathbf{p}}_i$  are chosen in such a way that they are in a local maximum of the test function. Optimization and refinement are repeated until all segments in the vectorization are shorter than a given segment length.

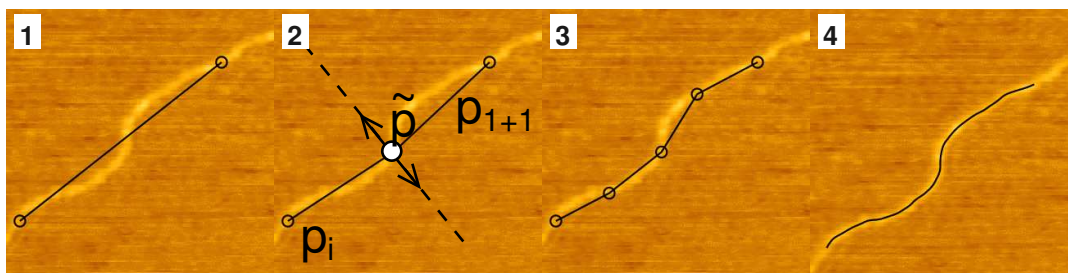


Figure 4.4: The vectorization is stepwise refined from 1 to 4 by insertion of vertices. Positions of new vertices are selected as shown in 2 and explained in the text. Image 4 shows the final vectorization.

### The test-function

The test-function is a function which notes whether a point  $\mathbf{r}$  is on the contour or not. It should fulfill the following requirements:

1. noise tolerance
2. delivering continuous values
3. not requiring a fixed cross section shape

By requirement 2 it is ensured that  $f(\mathbf{r})$  does not exhibit any jumps, even though the underlying SFM image consists of discrete pixels. The position

of the cross section maximum can be determined with a resolution which is better than the pixel resolution (4.5). The coordinates of points  $\mathbf{p}_i$  are therefore not restricted to positions of the pixel lattice. This way the problem of discrete values for angles and distances mentioned in Ref. [378] is avoided.

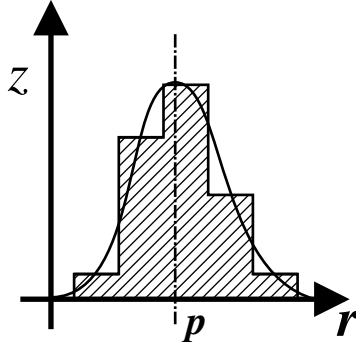


Figure 4.5: Finding the maximum of an adsorbate cross section. By fitting the height data  $z(\mathbf{r})$  (shaded) to an analytic cross section function  $f(\mathbf{r})$  the maximum position  $\mathbf{r} = \mathbf{p}$  can be determined with sub-pixel resolution.

Requirement 3 is needed because the cross section shape for some molecules is strongly varying (e.g. in meanders). Therefore using a simple least square fit of a given section to find the optimal  $\mathbf{p}_i$  is not possible.

A test-function which fulfills 1 to 3 is

$$f(\mathbf{r}) = \sum_{ij} z_{ij} \cdot \left[ \exp\left(-\frac{(\mathbf{r}_{ij} - \mathbf{r})^2}{w^2}\right) - \exp\left(-\frac{r_{\text{cutoff}}^2}{w^2}\right) \right]. \quad (4.1)$$

Indices  $i$  and  $j$  run through all integer values for which the center of the corresponding pixel,  $\mathbf{r}_{ij}$  is inside the cutoff region, i.e.  $|\mathbf{r}_{ij} - \mathbf{r}| < r_{\text{cutoff}}$ .  $z_{ij}$  is the image matrix. The parameter  $w$  describes the weighting of neighboring pixels and can be chosen according to the image quality. It should be selected as small as possible because large  $w$  will induce a lateral correlation of vertices  $\mathbf{p}_i$ . Typical values are between 2 to 6 pixels. The cutoff radius  $r_{\text{cutoff}}$  should be chosen larger than  $w$ . The common value is  $r_{\text{cutoff}} = 2w$ . Equation 4.1 is basically a convolution of the discrete SFM image with a continuous Gaussian as can be seen from the first exponential term. The second exponential term circumvents jumps at the cutoff.

## The optimization step

The vectorization is optimized by successively moving the vertices into local maxima of the test-function. To maintain the chain structure, vertices are only be moved perpendicular to the contour. For the very first and the very last vertex, optimal positions are searched on a line perpendicular to the first or last segment, respectively. For all other vertices the bisection line between the two adjacent segments is used. The search is implemented using the efficient algorithm of the golden section [362]. The searched interval must be restricted to the vicinity of the chain, since otherwise points on neighboring chains could be selected. We chose the mean segment length of the adjacent segments as limitation.

## The refinement algorithm

The algorithm refines a given vectorization by inserting new vertices. A segment given by the endpoints  $\mathbf{p}_i$  and  $\mathbf{p}_{i+1}$  is divided by inserting a vertex  $\tilde{\mathbf{p}}_i$  on the center line between both points. The position on the centerline is chosen such that  $f(\tilde{\mathbf{p}}_i)$  is maximized (see Fig. 4.4). The search is implemented as described above. By applying the refinement several times, from the initial rough vectorization (image 1) a detailed vectorization is obtained (images 2 to 4 of Fig. 4.4).

### 4.1.3 Sections along the contour

In this work, the height variations along the contour of adsorbed polymers are investigated. For that purpose  $z$ -values along a given path in the  $xy$ -plane are recorded. Often it is difficult to resolve the detailed contour in the images. As a result the path can be deviating from the contour and the height values recorded along the path are smaller than those wanted values along the contour. To avoid this problem a method is chosen which resembles the cutting of a salami: perpendicular to the molecular contour cross section slices are computed with a distance of one pixel. The maximum point from each slice gives the height value.

### 4.1.4 Implementation

For the implementation of image processing and analysis methods the drawing program *Sketch* was used. The program is free software and can be obtained as source code. The implementation into an already existing drawing program has the advantage that many functions, as zooming, drawing of lines saving and loading do not have to be written completely new.

SFM images are represented by a new graphic object “SFMimage”, similar to conventional pixel images. Basic image processing operations can be directly accessed by clicking on the objects. Others can be accessed through a scripting window. Fig. 4.6 shows the main window with opened image processing menu and section plot.

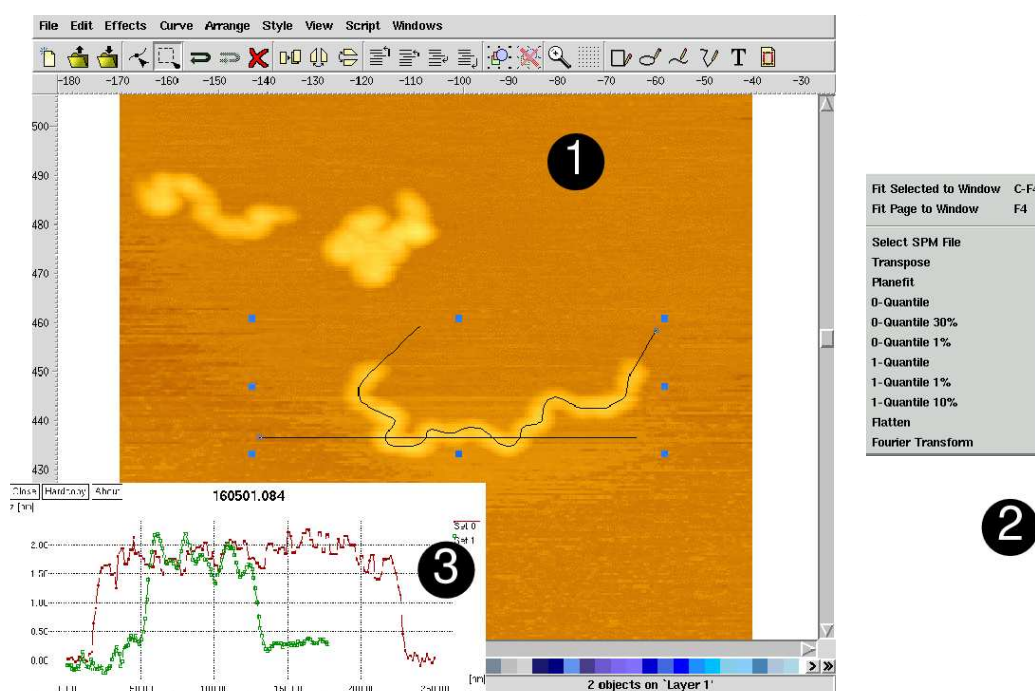


Figure 4.6: Main window of Sketch showing the analysis of a SFM image (1). By right-clicking on the SFM image, the context menu (2) opens, giving access to image processing functions. Cross sections (3) can be measured along all line objects.

Contours are represented by lines consisting of straight segments (poly-lines). The vectorization tool is another extension to Sketch. It allows to fit poly-lines to the underlying SFM image. As described in section 4.1.2 the vector-

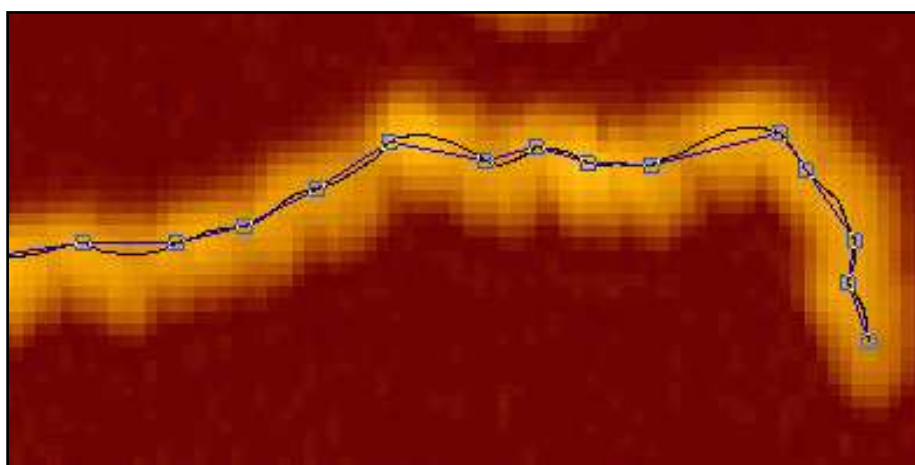


Figure 4.7: Vectorization of a **g3** molecule adsorbed onto mica. The blue line marks a rough vectorization before the refinement step. The black line is the final vectorization into segments of length  $\ell_i \leq 2$  pixel.

ization tool has two functions: optimization of given contours by moving the vertices into maxima and the refinement by division of segments. In Fig. 4.7 the vectorization of a **g3** polymer adsorbed onto mica is shown. The blue line marks a rough vectorization before the refinement step. The black line is the final vectorization into segments of length  $\ell_i \leq 2$  pixel.

## 4.2 Statistical characterization of conformations

### 4.2.1 Determination of the persistence length

#### Model assumption

In general, the shape of an adsorbed molecule is influenced by the process of adsorption, intrinsic molecular properties and the interaction with the surroundings (substrate, solvent). In order to determine the intrinsic persistence length from SFM images, a couple of assumptions have to be made. These assumptions can be checked experimentally and only if they are fulfilled, the method described below can be applied.

The assumptions are:

1. the chains can be modeled as worm-like chains
2. the molecules in the image are in thermal equilibrium, at least on a local length scale
3. there is no influence of the substrate on the 2D chain conformation

#### Method

A simple way to vectorize polymer chains manually from SFM images is to draw a consecutive series of connected straight line segments with a length of approximately 5 pixels each using a drawing program. From the angles between the tangents in vertices  $i$  and  $i + 1$  angles  $\theta_i$  can be constructed. If the segment lengths  $a_i$  are chosen sufficiently small,  $a_i \ll \ell_P$ , the length of the vectorization will approximate the contour length of the underlying chain. From equation 2.47 the variance of the thermal bending of a segment of length  $a$  is

$$V[\theta_i] = \frac{a}{\ell_P} \quad (4.2)$$

Since the segment lengths  $a_i$  are not constant, the angles  $\theta_i$  have to be normalized. Because of the proportionality  $\langle \theta_i^2 \rangle \propto a_i$  which is reflected in



equation 4.2, this normalization is carried out by the setting  $\tilde{\theta}_i := \theta_i/\sqrt{a_i}$  and consequently  $\tilde{a}_i = \tilde{a} \equiv 1$ . Assuming that the deviations  $a_i - a$  are small compared to the  $a$ , equation 4.2 can be replaced by

$$V[\tilde{\theta}_i] = \frac{1}{\ell_P}. \quad (4.3)$$

Since the set of measured data  $\theta_i^m$  was determined with a manual vectorization procedure, it possesses a random error:  $\theta_i^m = \theta_i + \phi_i$ . Thus,  $V[\tilde{\theta}_i^m]$  will differ from the variance of the exact  $\tilde{\theta}_i$ . Assuming the errors to have a normal distribution, the measured variance of the normalized data is

$$V[\tilde{\theta}_i^m] = V[\tilde{\theta}_i] + V[\tilde{\phi}_i]. \quad (4.4)$$

Since equation 4.3 is independent of the vectorization, a second equation of the form 4.4 can be obtained for a new chain which is built from different  $\tilde{a}$ . Constructing a set of  $\tilde{\theta}_i$  values corresponding to a segment length  $\tilde{a}_2 = 3\tilde{a} = 3$  yields a second equation 4.4. Since both chains are constructed from the same data points, the vectorization error term  $V[\tilde{\phi}_i]$  is the same and the two equations can be solved to give the true variance  $V[\tilde{\theta}_i]$ . It follows

$$V[\tilde{\theta}_i] = \frac{1}{2} \left( V[\tilde{\theta}_i^{m2}] - V[\tilde{\theta}_i^m] \right). \quad (4.5)$$

For an ensemble of several molecules, the values of  $V[\tilde{\theta}_i^m]$  and  $V[\tilde{\theta}_i^{m2}]$  are averaged, weighting the values by the contour length of the molecule. The weighting step is necessary as the molecules can differ in length. By combining 4.3 and 4.5 the expression of the persistence length is:

$$\ell_P = \frac{2}{V[\tilde{\theta}_i^{m2}] - V[\tilde{\theta}_i^m]}. \quad (4.6)$$

Due to the normal distribution of  $\tilde{\theta}_i^m$  and  $\tilde{\theta}_i^{m2}$  the distribution of the variances  $\tilde{\theta}_i^m$  and  $\tilde{\theta}_i^{m2}$  can be described by the  $\chi^2$ -statistics [51]. Using the standard deviation as confidence interval the errors of the variances are  $\Delta V[\tilde{\theta}_i^m] = V[\tilde{\theta}_i^m]\sqrt{3/N}$  and  $\Delta V[\tilde{\theta}_i^{m2}] = V[\tilde{\theta}_i^{m2}]\sqrt{6/N}$ , where  $N$  is the number of data points. Applying the formalism of Gaussian error propagation the error of  $\ell_P$  follows as

$$\Delta\ell_P = \sqrt{\frac{3(V[\tilde{\theta}_i^m])^2 + 2V[\tilde{\theta}_i^{m2}]^2}{(V[\tilde{\theta}_i^m] - V[\tilde{\theta}_i^{m2}])^2}}. \quad (4.7)$$

An alternative way for the measurement of  $\ell_P$  is to determine the orientation correlation function as described below and fit it to equation 2.37. An advantage of the above approach is that it is very efficient, i.e. the data of only a few chains already gives good results. Further there is an analytic expression for the statistical error (equation 4.7) allowing to estimate the experimental effort needed. An important difference is that the persistence length is obtained from local data and therefore no large scale equilibrium is needed. Local means here a few times segment length  $a$ . Large scale equilibrium would take a longer time and therefore might not be reached in experiments. A certain disadvantage is that WLC behavior is assumed in the derivation of equation 4.6 and therefore values can be wrong in a systematic way when it is not fulfilled. It is further important to assure that chains do not orient due to the interaction with substrate atoms.

## 4.2.2 Radius of gyration

The radius of gyration  $r_g$  is defined by equation 2.14. For chains consisting of discrete monomers it reads

$$r_g^2 = \frac{1}{N} \sum_{i=0}^{N-1} \langle (\mathbf{r}_i - \mathbf{r}_c)^2 \rangle \quad (4.8)$$

$$= \frac{1}{2N^2} \sum_{i,j=0}^{N-1} \langle (\mathbf{r}_i - \mathbf{r}_j)^2 \rangle, \quad (4.9)$$

where  $N$  is the number of monomers and  $\mathbf{r}_c$  is the center of mass vector

$$\mathbf{r}_c = \frac{1}{N} \sum_{i=0}^{N-1} \mathbf{r}_i. \quad (4.10)$$

To calculate  $r_g$  from vectorized chains, monomers are replaced by vectorization segments. This is a sufficiently good approximation when the segments are short. As lengths are non-uniform, addends in equations 4.9 and 4.10 are weighted by the segment length  $\ell_i$ .

### 4.2.3 Orientation correlation function

Denoting the tangent to a contour as  $\mathbf{t}(\ell)$ , the orientation correlation function is given by the autocorrelation of  $\mathbf{t}$

$$c(\ell) = \frac{1}{L_c - \ell} \int_{\ell'=0}^{L_c - \ell} (\mathbf{t}(\ell' + \ell) - \langle \mathbf{t} \rangle) (\mathbf{t}(\ell') - \langle \mathbf{t} \rangle) d\ell' \quad (4.11)$$

Assuming  $\langle \mathbf{t} \rangle \simeq 0$  it follows

$$c(\ell) = \langle \cos \theta(\ell', \ell' + \ell) \rangle, \quad (4.12)$$

where  $\theta(\ell', \ell' + \ell)$  is the angle between  $\mathbf{t}(\ell')$  and  $\mathbf{t}(\ell' + \ell)$ . To calculate  $c(\ell)$  from vectorized chains the discretization

$$c(\ell) = \langle \cos \theta_{i', i'+i} \rangle \quad (4.13)$$

is used, with  $\theta_{i', i'+i} = \sum_{k=i'}^{i'+i} \theta_k$ . The  $\cos \theta_{i', i'+i}$  values are weighted by a weighting factor

$$w_i = \frac{1}{N-i} \frac{N}{i}. \quad (4.14)$$

The weighting is necessary since chains might be polydisperse. The term  $N - i$  is the number of angles  $\theta_{i', i'+i}$  for a certain  $i$  which are contributed from one chain. Assuming that the segment lengths have (nearly) the same value  $a$  means the number of pieces of length  $\ell = a i$  in the chain is  $\frac{L_c}{\ell} = \frac{N}{i}$ . Therefore weighting with equation 4.14 assures that the total weight of all angles contributed by one chain is proportional to the number of independent segments of length  $\ell$  in the chain.

The averaging in equation 4.13 is done over all chains and over all indices  $i, i'$  per chain where  $i \in [1, N[$ <sup>3</sup>,  $i' \in [0, N - i[$  and the length along the contour  $\ell_{i', i'+i} = \sum_{k=i'}^{i'+i} \ell_k$  is in the bin  $[\ell, \ell + \Delta\ell[$ . The bin-size  $\Delta\ell$  is chosen according to the image resolution, usually between 1 and 10 nm.

Statistical errors are calculated from the set of values  $\theta_{i', i'+i}$  by the method of bootstrapping [289].

---

<sup>3</sup>This notation [...] means that the larger limit is excluded from the interval, i.e. from 1 to  $N$  without  $N$ .

#### 4.2.4 Mean segment-segment distance

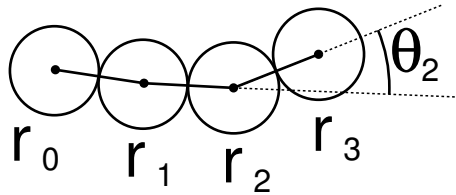
The mean segment-segment distance is calculated similar to what has been described above. The corresponding formula to 4.13 is

$$r^2(\ell) = \langle r_{i',i'+i}^2 \rangle, \quad (4.15)$$

where  $r_{i',i'+i}$  is the spatial distance between points  $i'$  and  $i' + i$ .

### 4.3 Monte Carlo simulation of self avoiding worm-like chains

An off-lattice Monte Carlo simulation is used to calculate chain conformations. The 2D plane is represented as the infinitely large plane which is spanned by  $(x, y)$ , where  $x$  and  $y$  are real numbers. Chains are built from straight segments using a stepwise growth algorithm. To the starting point at  $(0, 0)$  segments of length  $a$  are attached successively until the desired total contour length  $L_c = \Sigma a$  is reached. The orientation  $\Theta_0$  of the first segment is chosen randomly in the interval  $[0, 2\pi[$ . Orientations of following segments are determined by  $\Theta_{i+1} = \Theta_i + \theta_i$ , where the change in orientation  $\theta_i$  is taken from normally distributed random numbers of mean  $\mu = 0$  and variance  $\sigma^2 = \ell/\ell_P$ .



Strictly, the chains are not worm-like chains since they consist of straight segments. The difference to continuous chains affects two relevant properties: (a) the contour length is too small and (b) the segment orientation is not given by the tangent. Both differences are negligible when  $a$  is sufficiently small, i.e.  $a \ll \ell_P$ .

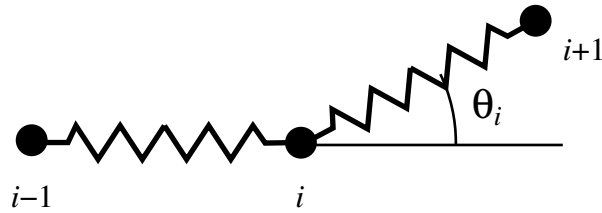
Random numbers in this and all other simulations described in this work are created by the „Mersenne Twister”-generator [298] which is characterized by a very even distribution, a long period and low correlations. It is recommended for numeric simulations [362].

## Simulation of self avoiding chains

A chain is non-self avoiding if it has at least two segments which are crossing. A simple way to create a set of self avoiding chains is to compute chains as described above and remove all chains which are not self-avoiding. This way it is assured that the resulting set of chains is representative.

### 4.4 Simulation of the “undulation” model

The aim of the simulation is to explain the observation of undulating conformations. The polymer chain is modeled as a chain of beads connected by elastic Hookian springs having the force constant  $k_{\text{bond}}$ . Stiffness is introduced by a bending energy term  $E_{\text{bending}} = \frac{1}{2}k_{\text{bending}}\theta_i^2$ , where  $\theta_i$  is the angle between the bond connecting bead  $i - 1$  and  $i$  and the bond between  $i$  and  $i + 1$ .



The beads are attracted towards the surface by the force  $k_{\text{adhesion}} z$  and repelled by the force  $-k_{\text{repulsion}} z$ . This is combined into

$$k_{\text{surface}} = \begin{cases} k_{\text{adhesion}} & z > 0, \\ k_{\text{repulsion}} & z \leq 0. \end{cases} \quad (4.16)$$

The total energy is

$$E = \sum_{i=1}^N \frac{1}{2}k_{\text{surface}}(z_i) z_i^2 + \frac{1}{2}k_{\text{bond}}(a - |\mathbf{x}_i - \mathbf{x}_{i-1}|)^2 + \frac{1}{2}k_{\text{bending}}\theta_i^2 \quad (4.17)$$

For the first and the last bead the interaction terms to the predecessor and successor respectively are set to zero.

Beads which are touching the surface are frozen. The end of the chain pointing away from the surface is fixed to the point  $\mathbf{p}_{\text{funnel}}$ . A sketch of the model is depicted in Fig. 4.8.

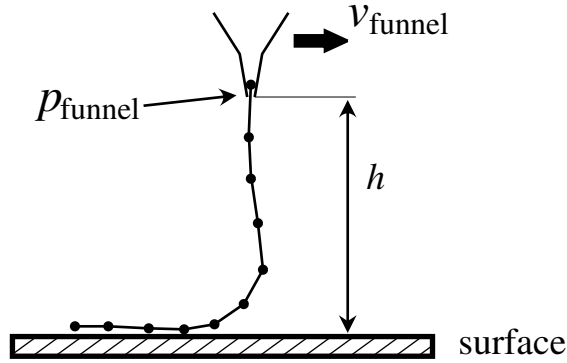


Figure 4.8: Sketch of the simulated model.

The simulation consists of discrete time steps  $\Delta t$ . In each step, the funnel is moved by a lateral distance  $v_{\text{funnel}} \Delta t$  and a new bead is inserted at the funnel. After each step the total energy is minimized. Minimization is done using the vertex algorithm [362].

An important parameter is the ratio of the funnel velocity  $v_{\text{funnel}}$  to the velocity of the beads flowing through the funnel (which is set to 1 here). A ratio greater one would mean that the adsorbed part is stretched and is therefore unphysical. The simulation parameters are listed in table 4.1. The parameters are chosen to roughly mimic the physical reality of an adsorbing polymer chain.

parameter name	value
$a$	1
$k_{\text{bond}}$	1
$k_{\text{repulsion}}$	1
$k_{\text{adhesion}}$	0.02
$k_{\text{bending}}$	4
$v_{\text{funnel}}$	0.8
$h$	10

Table 4.1: Simulation parameters.

## 4.5 Simulation of the “tron” model

The intention behind this simulation is to show the principle mechanism of the formation of spiral conformations. Conformations of adsorbed chains are calculated by a sequential chain growth on a square lattice. At each growth step a segment is attached in the direction  $d$  which is either up, down, left or right. The direction is changed

- when the next field in direction  $d$  is blocked
- randomly with probability 0.25 per step

The new direction is chosen randomly under all possible directions. If no direction is possible because all neighboring fields are occupied the simulation is stopped.

# Chapter 5

## Materials

### 5.1 Substrates

The term substrate denotes a solid body which carries the molecules to be investigated. Possible substrate materials need to be flat on the atomic scale, have a chemically well defined surface and should be easy to clean. These requirements can be best fulfilled with layered materials since cleaving them prior to the adsorption results in a clean and flat surface.

The choice of the substrate depends further on the particular experiment, since the interaction between molecule and substrate determines adhesion and mobility of the adsorbate. Usually a strong adsorption and low mobility is preferred as it allows stable imaging.

In this thesis two substrates are used: mica and highly oriented pyrolytic graphite (HOPG).

#### HOPG

Graphite is a layered material consisting of identical stacked planes (Fig. 5.1). A carbon atom interacts with its neighbors in the same plane much stronger than with those of adjacent planes making graphite crystals cleavable along the sheets. Each atom within a single plane has three nearest neighbors



giving the layers a honeycomb structure. The distance between layers is 3.35 Å, while the distance between neighboring atoms amounts to 1.42 Å.

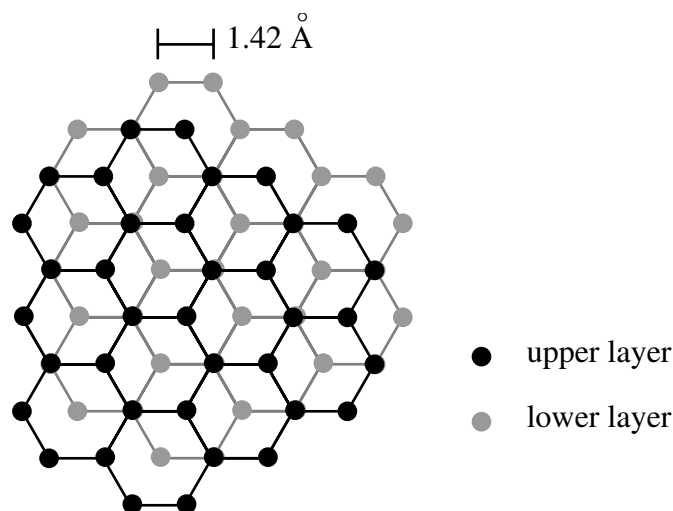


Figure 5.1: Positional relationship between two identical graphene planes A and B. Graphite structures can be described as succession of these planes.

Synthetic highly oriented pyrolytic graphite (HOPG) was obtained from Advanced Ceramics Corporation, Ohio, USA. Samples of two different qualities were used: grade ZYH and ZYB. According to the supplier’s information, the lateral grain size is between 30 to 40 nm for ZYH and “up to 1 μm” for the ZYB.

## Mica

Muscovite mica ( $\text{KAl}_2(\text{AlSi}_3\text{O}_{10})(\text{OH})_2$ ) consists of 10-Å-thick sheets (Fig. 5.2a) of two oppositely oriented layers of  $\text{SiO}_4$  tetrahedra arranged in nearly hexagonal arrays. Three of the oxygen atoms in one tetrahedron are shared with neighbors, forming an extended flat plane. Mica can be easily cleaved along these planes allowing the preparation of perfectly flat surfaces.

The tetrahedra form small single-atom-sized cavities. Due to the substitution of  $\text{Al}^{3+}$  for every fourth  $\text{Si}^{4+}$  atom in the tetrahedra, there is a single excess negative charge per unit cell on the surface of each sheet. In the bulk, these charges are neutralized by  $\text{K}^+$  ions filling the cavities. Cleavage of mica

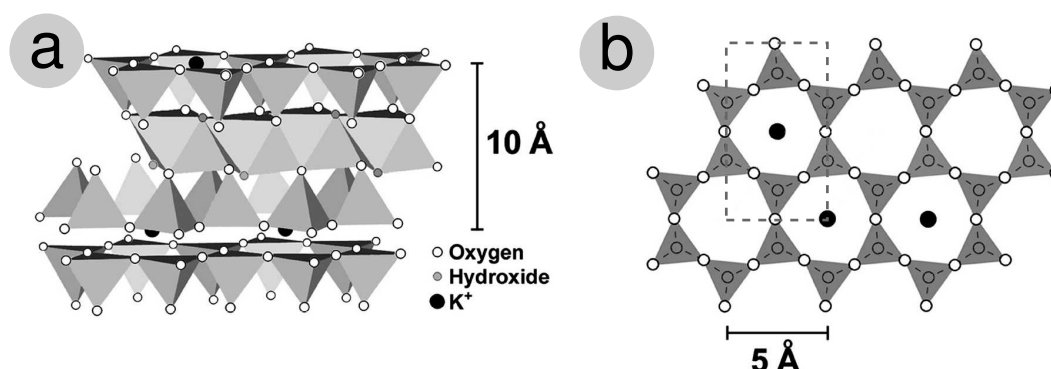


Figure 5.2: Crystallographic structure of mica. (a) side view; (b) top view. Mica can be easily cleaved along the plane of the potassium ions. The resulting surface consists of a hexagonal array of oxygen atoms with regular vacancies which are randomly filled with potassium atoms. The unit cell is characterized by  $a = 5.2 \text{ \AA}$ ,  $b = 9.0 \text{ \AA}$ . Images are taken from reference [96].

produces two surfaces with half of the cavities on each surface occupied by  $\text{K}^+$  atoms (Fig. 5.2b).

In aqueous solution, the basal potassium ions dissociate and the surface is negatively charged. The theoretical surface charge density is taken as one charged site per surface unit cell, i.e. one charge per  $46.8 \text{ \AA}^2$  [330] corresponding to a surface charge density of  $\sigma = 0.34 \text{ Cm}^{-2}$ .

Mica is the most commonly used substrate for SFM imaging and transmission electron microscopy, since it is very good cleavable and cheap. Due to its hydrophilic nature it allows molecule deposition from aqueous solutions, making it an ideal choice for investigations of biological macromolecules.

Muscovite mica is obtained from PLANO (W. Plannet GmbH, Wetzlar, Germany).

## 5.2 Dendronized polymers

Polymers **g2**, **g3** and **g4** were prepared starting from **g1** (Fig. 5.3) protected with trimethylsilylethyl-oxycarbonyl by subsequent steps of deprotection and dendronization. Details of the procedure were reported in [436]. The effi-

ciency of each dendronization step was controlled by UV-markers, stating a total structure perfection of  $97\pm 1\%$  (for **g4**). The length distribution of the parent polymer **g1** was characterized by analytical gel permeation chromatography (GPC). The number averaged molar mass was  $M_n = 308\,000$  (corresponding to 460 repeat units) and the polydispersity  $PD = 1.8$ .

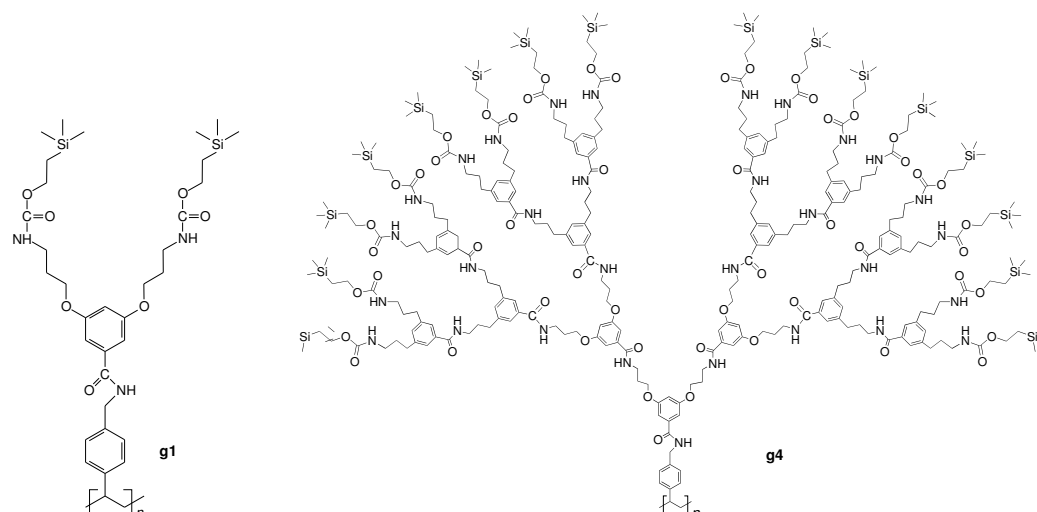


Figure 5.3: Molecular structure of the dendronized polymers **g1** and **g4**.

Variants of the basic molecules **g1** to **g4** are prepared by exchanging the terminal groups (see Fig. 5.4). The unprotected molecules denoted by **u-g1** to **u-g4** carry acidic groups which dissociate ions in aqueous solution leading to a strong charging of the chain. The decoration with dodecyl chains (molecules **a-g1** to **a-g4**) improves the solubility in organic solvents. A side effect is the increased adsorption energy on graphite due to the interaction between the alkyl chains and the substrate. Masses of all monomers are given in table 5.1.

The synthesis of dendronized polymers has been performed by Dr. Lijin Shu in the group of Prof. Dr. A. Dieter Schlüter (Freie Universität Berlin).

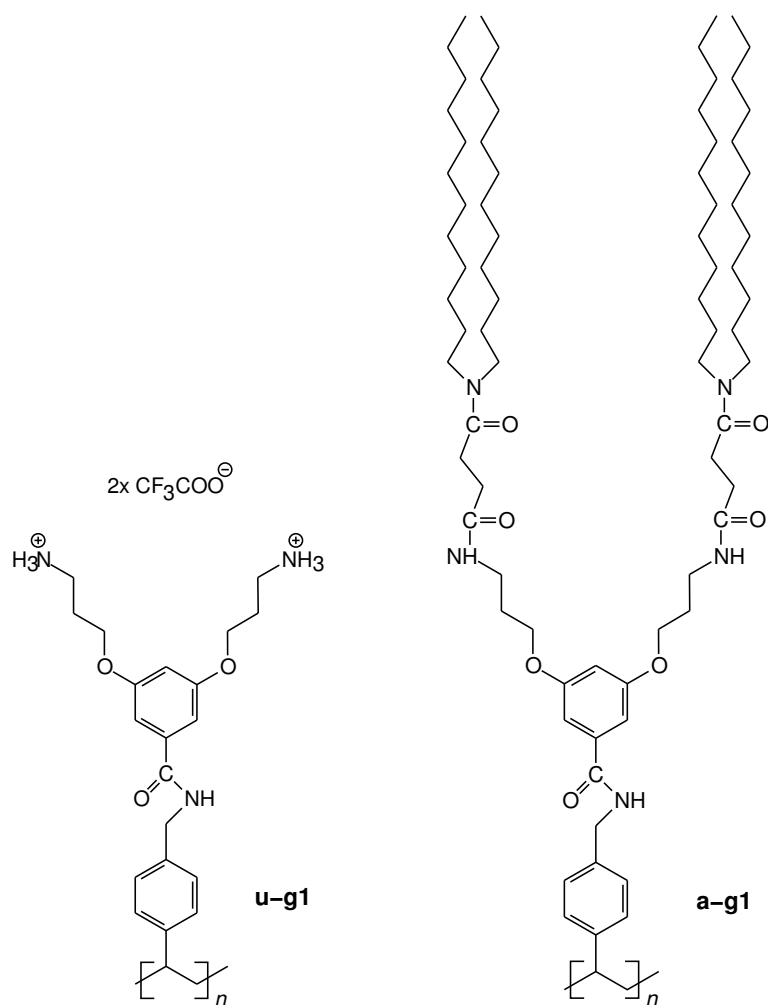


Figure 5.4: Structure variations by exchange of terminal groups.

	$m_0$ [g/mol]	$m_0$ [g/mol] (without counter ions)
<b>g1</b>	671.07	-
<b>g2</b>	1460.27	-
<b>g3</b>	2700.52	-
<b>g4</b>	5811.47	-
counter ion $\text{CF}_3\text{COO}^-$	113.02	-
<b>u-g1</b>	610.59	384.55
<b>u-g2</b>	1339.31	887.23
<b>u-g3</b>	2458.60	1554.44
<b>u-g4</b>	5327.63	3519.31
<b>a-g1</b>	1254.17	-
<b>a-g2</b>	2626.47	-
<b>a-g3</b>	5032.92	-
<b>a-g4</b>	10476.27	-

Table 5.1: Molar masses of all monomer variants.

### 5.3 Poly(isocyanodipeptides)

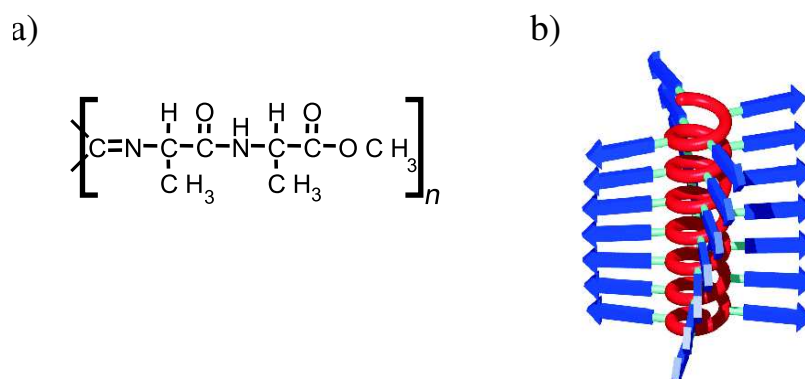


Figure 5.5: (a) Structure of PIC with L-alanine-D-alanine methyl ester side groups. (b) Sketch of the helix which is slightly twisted compared to the ideal  $4_1$ -conformation.

Polymers of isocyanides (PIC) adopt a  $4_1$ -helical conformation (four repeats per turn) when bulky side groups are present [166, 85]. For the PIC with L-alanine-D-alanine methyl ester side groups (Fig. 5.5a) investigated in this thesis the helical backbone is stabilized by hydrogen bonds between amide and carboxyl groups in parallel side chains. Each side chain can be regarded as an individual  $\beta$ -strand, and the overall arrangement of the side chains leads to a helical  $\beta$ -sheet like organization.

Normally the pitch of a polyisocyanide helix is believed to be 4.2 Å. For hydrogen bonding a distance of 4.7 Å between the amide units would be preferred. The helix conformation is therefore expected not to be exactly  $4_1$  but slightly bent allowing a larger distance for hydrogen bonds (Fig. 5.5b). Molecular modeling calculations in combination with NMR studies provided evidence for a helical pitch of 4.6 Å and a rod diameter of 1.58 Å [90]. The helical structure was confirmed by circular dichroism (CD) measurements [90].

The polymerization of PIC was carried out employing either  $\text{Ni}(\text{ClO}_4)_2 \cdot 6\text{H}_2\text{O}$  as catalyst (leading to PIC-Ni) or trifluoroacetic acid as initiator (for PIC-H) ([90]).

PIC-Ni and PIC-H were synthesized in the group of Prof. Dr. Roeland J. M. Nolte (Nijmegen, Netherlands).

## 5.4 DNA

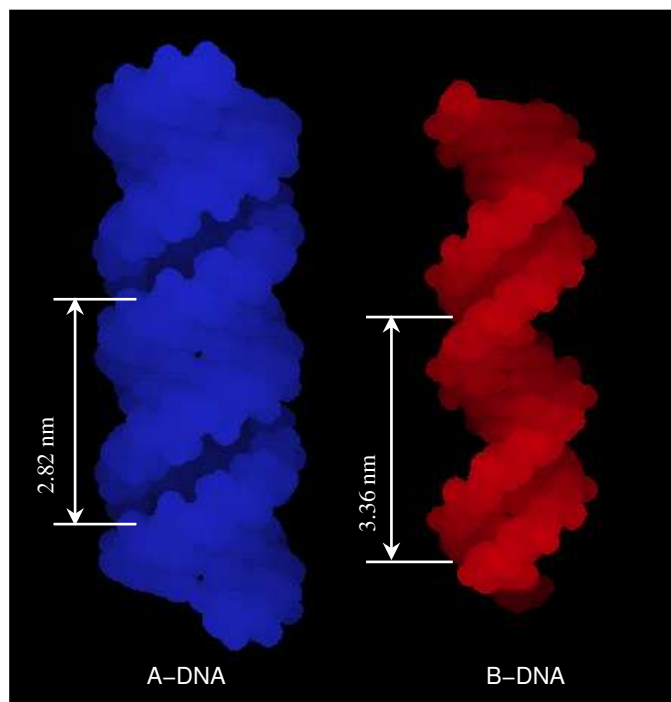


Figure 5.6: DNA helices in the A- and B-form.

Depending on hydration and counter ions DNA can be in different conformations labeled as A, B, C, D and Z. DNA adsorbed onto mica using the conventional preparation method with  $\text{Mg}^{2+}$  ions is in the B-form (see Fig. 5.6) [123]. Evidence for a partial B- to A-form transition was reported by Ref. [378]. The different helices can be distinguished by their pitch and chirality.

helix	A	B	C	D	Z
chirality	r	r	r	r	l
pitch	28.2 Å	33.6 Å	30.7 Å	24 Å	44.5 Å
residues per turn	11	10	9.33	8	12

DNA carries two elementary charges per base pair in solution and therefore belongs to the strongly charged polyelectrolytes.

Several different DNA fragments were used:

- 213 bp
- 562 bp
- 1313 bp
- 2686 bp

The 213 bp fragments were produced by polymer chain reaction, described in [319]. The 2686 bp fragments was linearized from puC19 plasmid DNA using BamHI (New England Biolabs, Frankfurt, Germany) and purified with QIAprep Spin Miniprep Kit (Qiagen, Hilden, Germany). The preparation of the 1313 bp DNA fragments from *E. Coli* is described in [443]. It was donated by Rudi Lurtz (MPI für molekulare Genetik, Berlin). All other fragments were prepared by Stefanie Reich (Institut für Virologie, Charité, Berlin). DNA was stored in a stock solution (5 mM *N*-[2-hydroxyethyl]piperazine-*N'*-[2-ethanesulfonic acid] (HEPES), NaOH at pH 7.5) at concentrations of 10 to 20 ng/ $\mu$ L.



# Chapter 6

## Non-equilibrium: characteristic conformations upon strong adsorption

### 6.1 Introduction

Polymer adsorption onto solid interfaces has great practical importance, as adsorbed polymers can significantly and permanently modify the interfacial properties. Up to now, research was focused on questions concerning thin films (thickness, stability, mobility), the adsorption transition (dependence on chain length) and weak adsorption models (train-loop models) [130]. Technologically more interesting than weak adsorption is the case of strong and irreversible adsorption, i.e. when the monomer sticking energy exceeds  $k_B T$ . Experiments [221, 406] indicate that physical processes in this case are effectively irreversible and chains are trapped in long lasting conformations. Strong adsorption is a common situation. Many polymer species attach through strong hydrogen bonds ( $\varepsilon \simeq 4k_B T$ ) to silicon, glass or metal surfaces in their natural oxidized states [406] while biomolecules such as DNA and proteins adhere to a large variety of materials through hydrogen bonds, bare charge interactions [176] or hydrophobic forces [189]. Despite the importance, strong adsorption is rather poorly understood which might be due to two difficulties: processes are usually far from the thermodynamic equilibrium (theoretical difficulty) and often require the study of single molecules

(experimental difficulty).

With the development of the scanning force microscopy it became possible to image single molecules including polymers at surfaces. Since SFM is increasingly used as a tool for the characterization of polymers there is a growing demand to understand conformations of adsorbed polymers. Polymer chains in the thermal equilibrium can be described statistically by the WLC model for 2D, allowing to measure the persistence length from SFM images [379]. In the case of non-equilibrium an analogous description of conformations is missing. Non-equilibrium conformations further lack a systematic experimental description thus far. Their study is important mainly because of three reasons:

- They are observed in most SFM experiments. Non-equilibrium conformations cannot always be avoided, since the choice of substrate is rather limited. They appear to be more the rule than the exception for molecules other than DNA, as can be seen from a number of studies, reporting about non-WLC conformations [17, 392, 237, 428, 243, 67]. Having a detailed statistical model would allow to characterize molecules from non-equilibrium conformations similarly as the WLC allows the characterization from equilibrium states.
- To avoid misinterpretations. A fundamental problem for the interpretation of observed conformations is to distinguish between conformational deviations from the WLC which are due to the molecular structure and artifacts resulting from a non-equilibrium. Possible reasons for structural deviations might be effects of side group adsorption [237, 428] or helical secondary structures [173, 179].
- To study the dynamics of the process of adsorption. Since trapping prevents the equilibration of chains the conformations preserve the non-equilibrium in which they are adsorbed and thus reflect the process of adsorption. Therefore, conformation analysis allows to study the process of adsorption on a single molecule basis, enabling the direct comparison to molecular dynamics (MD) studies.

In this chapter we study non-equilibrium conformations experimentally and theoretically with the goal of developing a model of strong adsorption which allows the prediction of conformational characteristics.

The chapter is structured as follows. In section 6.2 we give a literature overview of related work concerning strong adsorption and mobility of adsorbed chains. In section 6.3 we develop a detailed model of the strong adsorption process for single chains, which allows predictions of observable conformations. In the experimental part 6.4 we investigate trapped states of two model systems: DNA and dendronized polymers. DNA is selected because it is well characterized and the equilibrium conformations of both dissolved and adsorbed chains are well understood. Dendronized polymers offer the perspective that physical properties develop as a function of the generation number  $g$ , since the number of terminal groups per monomer is  $2^g$ . Therefore by studying dendritic polymers of different generations the side group effects can be systematically varied. If non-WLC conformations would be caused by the molecular structure, they should develop with generation number. The experimental observations are discussed in the framework of the model and against alternative explanations in the discussion section 6.5. The chapter ends with the conclusions 6.6.

## 6.2 Related work

A number of analytical and numerical treatments address the problem of strong polymer adsorption and dynamics [423, 422, 420, 421, 282, 342, 341, 358, 221, 14, 406, 109]. Nevertheless, understanding remains far from the quantitative level which has been achieved for weak adsorption. Details of conformations of single isolated molecules are not investigated in any of these publications. However, the works which are discussed in the following are relevant for the treatment of this problem.

The dynamics of single chain strong adsorption has been studied by Shaffer et al. [422] for poly(methylmethacrylate) (PMMA) chains on an aluminum surface. The authors simulate adsorption using a simplified dynamic model and a potential energy surface obtained from ab-initio electronic structure calculations. They find that the adsorption is governed by a process termed “zipping”, which can be defined as the consecutive sequential adsorption of segments at the contact points (zips), as depicted in the sketch in Fig. 6.1. The physical reason for zipping is the enhanced adsorption rate of an individual segment if one of its nearest neighbors is already adsorbed.

The importance of zipping is confirmed by Ponomarev et al. [358] who used

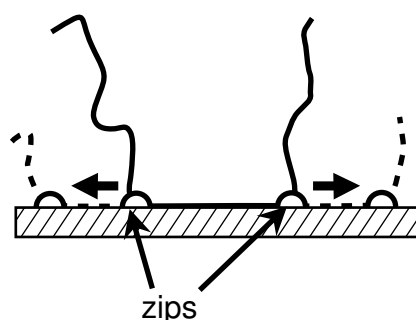


Figure 6.1: Schematic illustration of a zipping process.

lattice MC to study the adsorption kinetics of isolated flexible polymers onto flat surfaces for the case of strong physisorption with a short ranged surface potential. The authors find that the characteristic adsorption time  $t_{\text{ads}}$  is governed by zipping and is well below the rouse time, which is characteristic for chain relaxations in the bulk. The adsorption time scales as  $t_{\text{ads}} \propto N^\alpha$ , with  $\alpha \simeq 1.58$ .

Conformations of adsorbed DNA molecules onto mica surfaces were studied by Rivetti et al. [379] using scanning force microscopy. It was found that molecules could be in two characteristically different states depending on the sample preparation procedure. The states were interpreted as equilibrated and trapped conformations. In the first case chains could be described by the WLC-model. Trapped chains were in a much more compact conformation resembling a projection of the solution conformation. It was assumed that a strong interaction to the surface is the reason for trapping.

Chain mobility is therefore critical for the chain conformations. The mechanism of motion was studied by simulation experiments [313, 48]. It was found that even for large adsorption energies  $\varepsilon$  chain movement can take place. Two basic mechanisms were observed: caterpillar-like motion due to extension in the third dimension and motion at the free boundary of the 2D coil. The first mechanism directly depends on  $\varepsilon$  and leads to a strong decrease of relaxation time  $t$  with  $\varepsilon$  [313, 48]. In contrast to these simulation results, available experimental evidence suggests that the relaxation kinetics of strongly adsorbed polymers are sharply slowed down [221, 406, 109]. The mobility was found to vary strongly with the chain/surface interaction [479] and the detailed adsorption energy landscape [14]. A possible explanation for the discrepancy is the finding that even roughness of the energy surface on the lateral size of atoms can suppress motion [14] since perfectly smooth

potentials were used in the simulations.

## 6.3 Modeling

Unlike in the works listed above, we want to make predictions for conformations of single chains adsorbed from dilute solution onto a sticky surface. As a first step towards this model, we investigate a coarse grained picture of viewing the chain as a random coil, ignoring local conformational details. This allows us to identify three types of adsorption processes which can occur, depending on the polymer and the interaction to the surface. For each type a model is proposed which predicts conformational characteristics of the adsorbed chains.

### 6.3.1 Projection model

In this section we explore the simple projection model of Ref. [379]. It will be shown, that the projection leads to an increase of the density of adsorbed segments on a local scale.

In solution the polymer forms a random coil for which we assume that it can be described by the WLC-model. It has a certain extension parallel and perpendicular to the surface. The longer the chain is with respect to the persistence length, the more the mean shape will be globular.

When this coil is brought close to a surface, surface forces are acting on the coil and cause a deformation. Since the forces are in  $z$ -direction (perpendicular to the surface) the coil is flattened. Deformations in the  $x$ - and  $y$ -directions occur only indirectly through chain rigidity or direct interactions between segments. Rearrangement on the larger scale is the result of the change in conformational entropy by confining the chain into two dimensions. Brownian motion of chain segments is described by the Rouse model and characteristic times for entropic conformation changes are given by the Rouse formula

$$t_p = \frac{\zeta L_c^2}{3\pi^2 k_B T p^2}, \quad (6.1)$$

where  $\zeta$  is the friction coefficient and  $p$  denotes the relaxation mode [168].

The equilibration of chain ends is described by  $t_1$  which is the slowest mode, typically in the range of milliseconds. Local rearrangements correspond to higher mode numbers and are consequently faster.

In the following we assume, that the chain surface interaction is strong and therefore that adsorption times are fast compared to the large scale chain relaxation. Therefore the coil size in the  $x, y$ -plane will be unchanged by the process. Large scale conformational characteristics ( $r_g$ , end-to-end distance  $R$ ) of adsorbed chains can therefore be derived from the geometric projection of the 3D solution conformation onto the surface. This projection description ignores local rearrangements which have to occur as can be seen from a simple argument: The mean length of the projection of a randomly oriented straight segment is shorter than the segment. Using  $a$  as segment length and  $\phi$  for the angle towards the surface the mean projection length is given by  $\langle a_{\text{proj}} \rangle = \frac{2a}{\pi} \int_0^{\pi/2} \cos \phi d\phi = \frac{2a}{\pi} \simeq 0.64a$ . The length of the projected chain is therefore shorter than the contour length. Since the contour length cannot change upon adsorption conformational rearrangements have to take place also in the  $x$  and  $y$ -directions. Since we assumed that large scale rearrangements are not possible, the reduction in length must be realized by local rearrangements. This leads to a local increase of density.

The characteristics of the conformations are investigated by more detailed models based on chain zipping in the following sections.

### 6.3.2 Different regimes of zipping

Depending on the chain length and the shape of the interaction potential between a monomer and the surface, adsorption dynamics can be considerable different. For short chains ( $L_c < \ell_P$ ), the number of active zipping points  $n_{\text{zip}}$  is most likely to be one because zipping starts from the part which first touches the surfaces, and this most likely, will be one of the chain ends. For long chains ( $L_c > \ell_P$ ),  $n_{\text{zip}}$  depends on the zip velocity compared to the center of mass movement of the polymer coil. We therefore have to distinguish between slow and fast zipping by considering the ratio  $t_{\text{CM}}/t_{\text{zip}}$  which is the time needed by a hypothetical single monomer particle at the center of mass to adsorb divided by the time required to zip the whole chain onto the surface (by one zipping point). If  $t_{\text{zip}} \ll t_{\text{CM}}$  the adsorption is accelerated by the zip “sucking” the polymer onto the surface. If zipping is slow ( $t_{\text{zip}} \gg t_{\text{CM}}$ )

and the contour length is sufficiently large, there will be many zipping points at the same time since each loop touching the surface starts two new zips. Zipping can be slow if the surface potential has an activation barrier (e.g. in chemisorption). The center of mass movement on the other hand is fast if surface forces are long ranged. Formulae to estimate  $t_{\text{zip}}$  and  $t_{\text{CM}}$  are given in the chapter 6.7 (appendix).

A further characteristic parameter describes lateral correlations due to interactions of adsorbed segments [325]. The more short ranged the surface forces are, the more sensitive is the zip towards surface inhomogeneities. For the DH-potential the zip effectively interacts with a spot of the surface which is given by a circular disc with a radius of order  $r_{\text{D}}$ . If  $r_{\text{D}}$  is similar to the chain diameter  $d$  or below, already adsorbed segments act as a barrier for the zip.

The ratio  $d/r_{\text{D}}$  and  $n_{\text{zip}}$  are therefore key values for the formed conformations. They divide the parameter space into four quadrants (see Fig. 6.2). For very large  $n_{\text{zip}}$ , zipping has only little influence on the formed conformation. Also self-avoidance is irrelevant, because each zip is started at a different position, so that many chain crossings will occur. Conformations in quadrants 1 and 2 can therefore be described as irregular projections of the solution conformations. Chain conformations in quadrant 3 and 4 are subject of the following two sections.

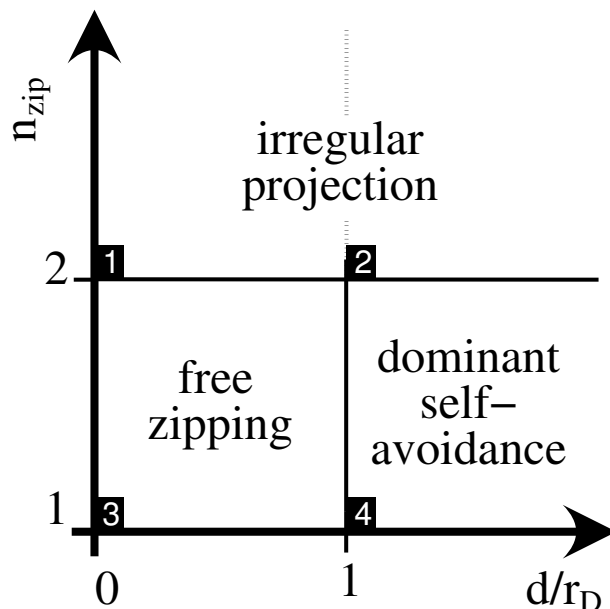


Figure 6.2: Characteristic regions of zipping.

### 6.3.3 Free zipping: undulation model

In this section it is argued that chain adsorption, when it is sufficiently fast, in a natural way leads to undulated conformations on the surface. In order to model the interaction between coil and surface in the vicinity of the surface, the idea of the zip is introduced into the random coil projection picture.

The basic idea of the following model is that the interaction between the zipping point (“zip”) and the coil is decaying with distance  $z$  from the surface. Very close to the surface, zip and coil are strongly connected so that either the zip follows the monomers supplied from solution, or the other way round, the zip is dragging the monomers to the surface. With the distance from the surface, zip and monomers are more and more decoupled. For simplicity, we assume that a distance  $h$  exists, from which on the monomer movement is fully independent from the zip. We then consider the point  $\mathbf{p}$  where the chain first cuts the plane at height  $h$ . The ratio of the velocity  $v_x$  of this point to the rate  $v_z$  of monomers through it result of the chain geometry. This is a direct result from the definition of  $h$ . By assuming a certain polymer model for the part of the coil above the height  $h$  the mean value of this ratio can be calculated. For a random walk, all monomer orientations have equal probability, therefore the  $\langle v_x/v_z \rangle = \frac{2}{\pi} \int_0^{\pi/2} \cos \phi d\phi = \frac{2}{\pi} \simeq 0.64a$ . The following mechanism can be investigated best when  $v_x/v_z$  is constant in time. This simplification does not change the principle result. So, assume that  $v_x/v_z$  is constant in time, what conformations are formed on the surface?

To answer this question, we simulated the adsorption process using a simple bead spring model described in section 4.4. The aim of the simulation is not to provide a realistic detailed model but to give a qualitative picture of the occurring process.

In general, the forces acting on each monomer of an adsorbing chain are resulting from friction, inertia, adhesion and the interaction between neighboring segments, i.e. bending, torsion and stretching. For the simulation inertia forces are ignored since they are rather small due to the low monomer mass. This is a common simplification [168].

Under the simplifying assumption of a constant velocity of  $\mathbf{p}$  the upper part of the chain is irrelevant for the zip movement. The simulation can then be reduced to the part of the chain from the surface to  $\mathbf{p}$ . The point  $\mathbf{p}$  is replaced in the simulation by a movable “funnel” which is moved with



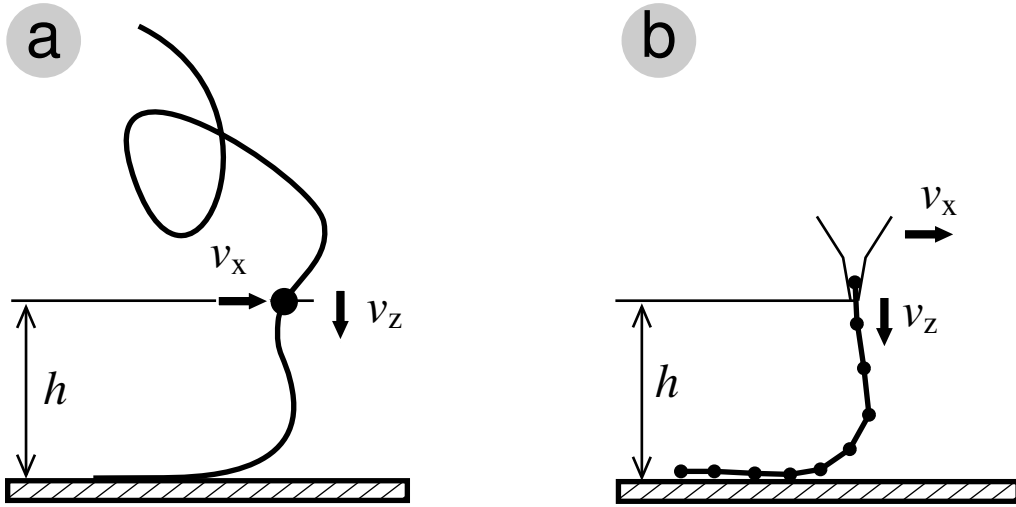


Figure 6.3: Schematic view of a zipping chain (a) and model representation (b) as it was simulated.

constant velocity in  $x$ -direction while monomers are flowing through it toward the surface with velocity  $v_z$ . A schematic sketch of the zipping chain and its model representation are given in Fig. 6.3.

The last and most rigorous simplification concerns the dynamics of single beads. We model the chain at discrete time steps  $t$  and assume that in each time step the chain can be described by a static equilibrium conformation. This can be justified from the shape of the surface potential: since monomers close to the surface feel the strongest interaction forces but only contribute with a small fraction to the total friction force, their rearrangement is virtually instantaneous on the time scale given by the chain movement. We assume the adsorption energy to be large compared to  $k_B T$ . Therefore the influence of entropy can be neglected.

Details of the simulation are given in the methods section (section 4.4). In Fig. 6.4 the first time steps of the simulation are shown. At each time step the funnel is moved by  $v_x/v_z$  and a new bead is inserted at the funnel. For the shown simulation this ratio was chosen smaller one and arbitrarily as 0.8. In the initial situation ( $t = 0$ ) one half of the chain is adsorbed on the surface while the other half is in solution, connecting surface and funnel. In the next step ( $t = 1$ ), the solution part is getting bulged. As can be seen in the topview, this leads to a break of the symmetry along the  $y$ -axis. Consequently the next beads are adsorbed with a shift in  $y$ -direction

( $t = 1, 2$ ). This positive deflection is followed by a negative one ( $t=3,4$ ) and again a positive one ( $t=5,6$ ).

The succession of positive and negative deflections which forms an undulation can be followed best from step 5 to 6. In step 5, the last bead is adsorbed very close to zero deflection. The direction of the next one is given by the direction of the adsorbed part. As it is pointing in the positive  $y$ -direction, the next segment will be adsorbed there. At  $t=7$  the process is repeated in reverse direction.

The appearance of undulations is therefore a consequence of the chain rigidity. To confirm this idea, the same simulation was calculated without bending rigidity, by setting  $k_{\text{bending}}$  to zero. As shown in Fig. 6.5 this leads to a non-regular path compared to the regular undulation of the rigid chain.

It should be noted, that the model is too simple to study quantitatively the changes of undulation with the persistence. The reason is, that the persistence length is not an independent parameter in the model. Changing the parameter  $k_{\text{bending}}$  changes the persistence length, but also influences the value of  $h$ . While it is possible to estimate these dependencies, it may be better to perform a more realistic simulation using Langevin dynamics.

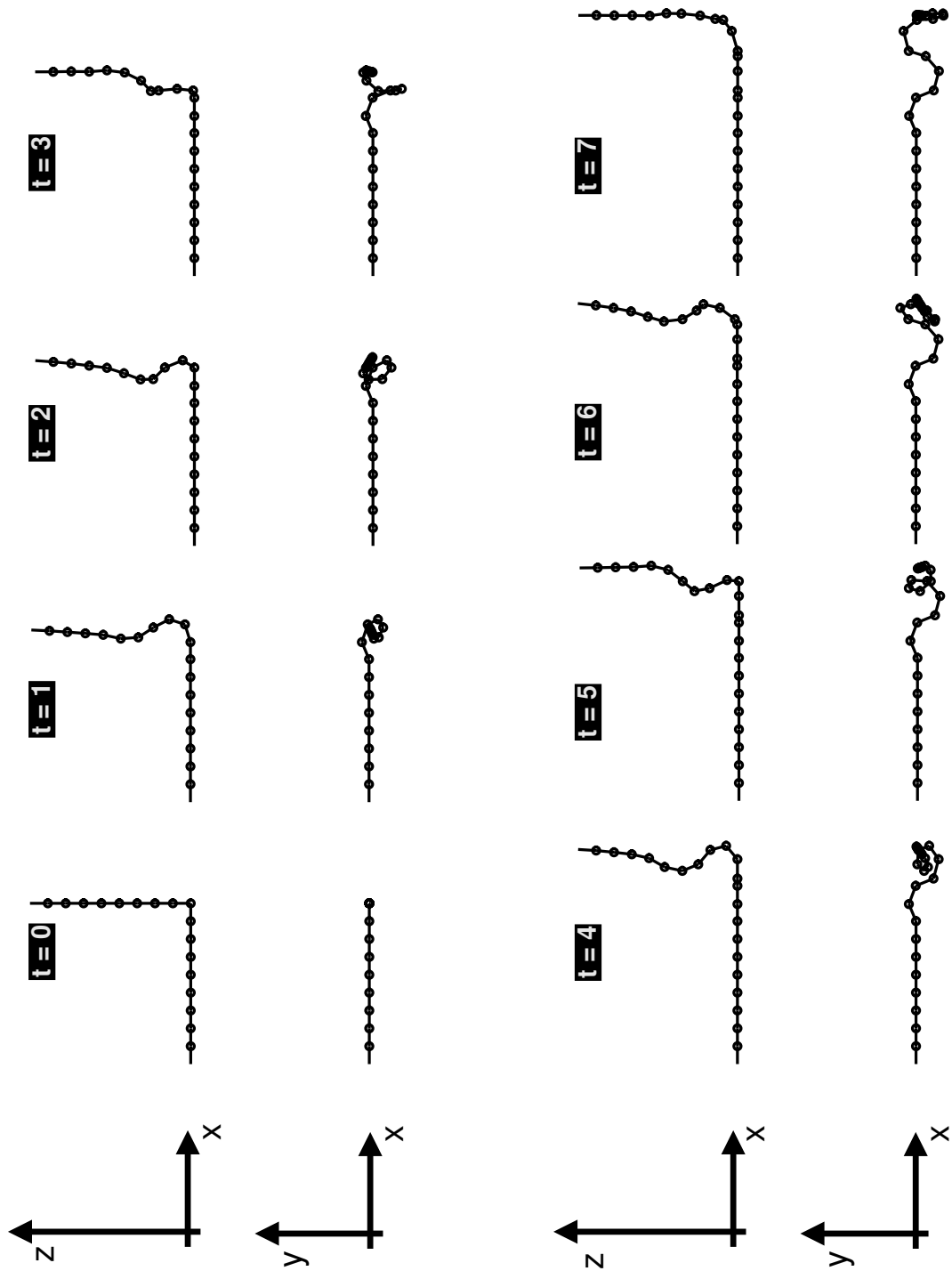


Figure 6.4: Simulation steps of a zipping chain at different time steps. For each step, the chain is displayed as top and side view.

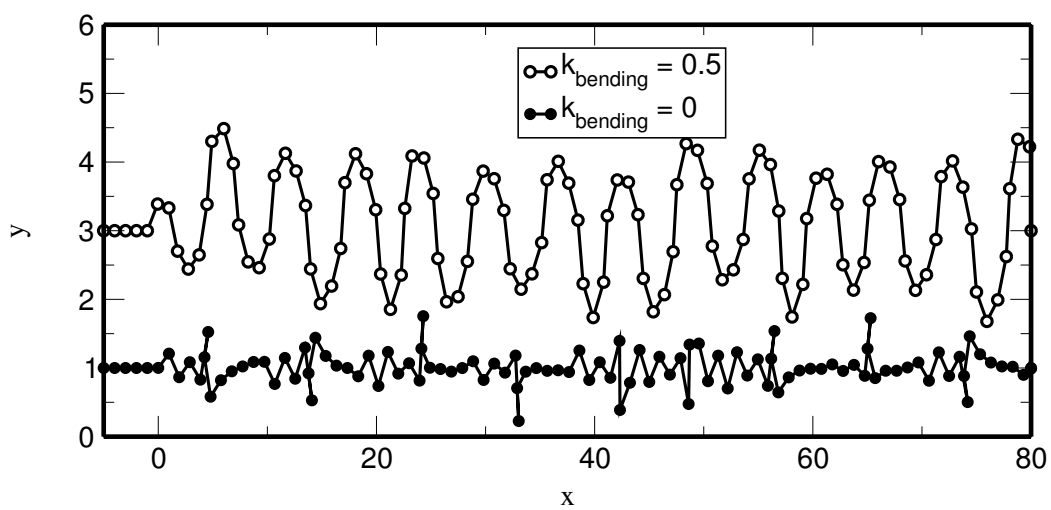


Figure 6.5: Influence of chain rigidity on undulations. With  $k_{\text{bending}} = 0$  the path looks irregular and no undulations appear.

### 6.3.4 Self avoiding zip: “tron process”

In the last section only interactions between neighboring monomers were accounted for. Here, we want to investigate the influence of volume exclusion. We assume that chain crossings in 2D are forbidden.

Under such conditions, the model of the last section remains valid. However, when the chain is long enough, it might happen that the zip meets its own path and from this moment on the zip movement is disturbed by the restriction of not crossing. This situation closely resembles the rules of the early computer game tron, we therefore denote this process a *tron process*. Imagine to look on the surface from the top and that the segments in solution are invisible, so that only the adsorbed parts can be seen. It then would appear as if the zip, while moving on the surface, leaves behind a path, just like a player in tron.

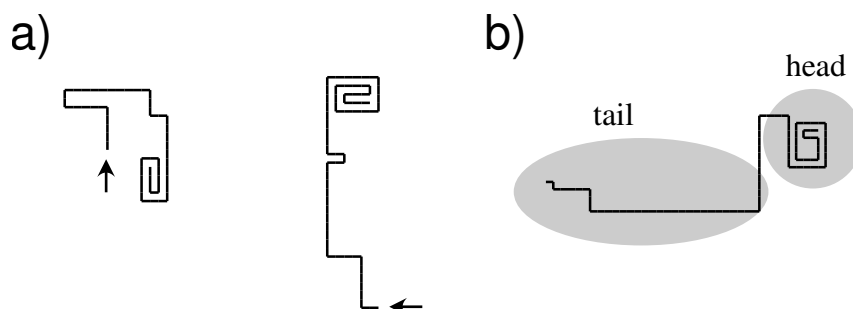


Figure 6.6: a) Tron-conformations created by a random tron player on a square lattice. The starting direction is indicated by arrows. b) Conformations typically consist of a dense often spiral shaped head part and a long tail, which is less dense.

Characteristics of tron conformations are best explained by example. Fig. 6.6 shows conformations which are created by a random tron player on a square lattice. Characteristically they do consist of two parts having a distinctively different density. Regions of high density and spiral shape are formed when the player accidentally meets its own path. Since crossings have to be avoided the player has to change the direction of movement then. Depending on which side is chosen, it may happen that the player is locked in by its own path and forced to move in a spiral.

These characteristics, the spiral shaped head and the tail must also occur for zipping polymer chains where the tron player is replaced by the zip. In the

simple tron simulation, the player cannot leave a spiral and the simulation is stopped, when no possible moves remain. For adsorbing polymers, spirals can be left either if the system accepts a crossing or if the zip changes direction and winds itself out.

## 6.4 Experiment

The aim of this section is to experimentally demonstrate the existence of the above described conformations. Since “unusual” i.e. non-WLC conformations have been observed before and have been explained by other models, it is not sufficient to show that the proposed conformations exist. It is also necessary to show that they cannot be explained by these other models.

Effects which have been proposed to explain undulated or similar conformations are:

1. entropic effects due to the adsorption of side groups [237, 428]
2. strain along the backbone due to drying [366]
3. a helical secondary structure in solution which is flattened upon adsorption [318]

Further, there are effects which can cause deviations from the WLC and therefore have to be considered:

4. volume exclusion
5. interaction to neighbouring chains [294]
6. additional attractive long ranged forces between monomers

In the following, we describe experiments giving undulations and tron-conformations and also other experiments to gain evidence that these conformations are not the result of effects 1 to 6. The structure of this section is as follows. After the procedures part 6.4.1, in 6.4.2 the theoretical conformations of self avoiding WLCs are explored by MC simulation. The generated data will be used

as a reference in the following experiments (avoiding effect (4)). In 6.4.3 the immobility of adsorbed chains is proven experimentally for **u-g2** and **u-g4**. Conformations of dendronized polymers are investigated in 6.4.4 and allow conclusions about the influence of side groups (1) and the density dependence (5). Since DNA is precisely monodisperse, it allows to study the dependence on the contour length which is a test for hypothesis (6). DNA experiments are described in 6.4.5.

### 6.4.1 Experimental procedures

Dendronized polymers (**u-g1** to **u-g4**) were adsorbed by spin coating dilute aqueous solutions (1 ng/ $\mu$ l) onto freshly cleaved mica at 50 rotations/second. Measurements were carried out in air using the tapping mode. Nanomanipulation of **u-g4** was done in deionized water using the liquid cell. Samples from acetone/water solution have been prepared by diluting an aqueous **u-g2** solution (10 ng/ $\mu$ l) 1:9 with acetone and immediately spin coating the solution onto the mica substrate. **u-g2** on a monolayer of dodecanoic acid was prepared by spin coating from aqueous solution. The substrate was prepared by spin coating dodecanoic acid (1 ng/ $\mu$ L) onto freshly cleaved HOPG, followed by 10 minutes of annealing at 35°C. For the coating of mica with poly-(ornithine), a freshly cleaved mica surface was placed onto a 5 $\mu$ L droplet of 0.1 mg/mL poly-L-ornithine solution for 5 min, rinsed three times with deionized water, and then dried under a gentle stream of N<sub>2</sub>. With the same procedure, also DNA molecules were deposited onto poly-L-ornithine-coated mica substrates from the buffer solution (1 ng DNA/ $\mu$ L).

### 6.4.2 Conformations of self avoiding worm-like chains

The worm-like chain model proved to be a good approximation of semi-flexible chains in three dimensions. In 2D the simplification of ignoring volume exclusion can lead to considerable errors. Since chain crossings are forbidden for real polymers their coil size in dilute solution must be larger than for corresponding WLC coils. Therefore, for the discussion of SFM experiments a modified worm-like chain model is used which takes volume exclusion into account. In this section the conformational characteristics of such chains are explored.

Excluded volume interactions are long ranged and therefore difficult to include in an analytical theory. Self avoiding worm-like chains (SAWLC) can on the other hand be simulated relatively easily as described in section 4.3. Simulation parameters are the monomer length, the persistence length and the contour length. When the monomer length is chosen sufficiently small, it becomes irrelevant so that chains can be parameterized by the ratio  $L_c/\ell_P$  of chain- to persistence-length. The values which are relevant for our experiments can be limited to the range 10 to 100. This range can be explored by our Monte Carlo calculations in about two days on a standard personal computer with a Celeron CPU and 1.2 GHz clock rate.

We chose as standard-deviation of the bending angle the value  $\sigma = 0.6$ . For monomers of length 1 nm this value corresponds to a persistence length of 2.8 nm. For comparison also ideal worm-like chains (non-self avoiding) have been simulated. The number of simulated chains is 50000 for chains of 20, 40, 80 and 160 monomers and 10000 for chains of 320 monomers. Due to the strong increase of computation time with chain length, for chains of 640 monomers only 100 chains were simulated. Orientation correlations and segment-segment correlations are calculated as described in section 4.2.

The resulting orientation correlation functions are shown in Fig. 6.7. For the ideal worm-like chains the curve follows an exponential decay as expected from equation 2.2. For the self avoiding chains, the correlation is decaying considerably slower and the difference to the WLC is larger the larger the contour length is. The curves can be characterized by two decays: a strong decay up to a few times the persistence length and a subsequent weaker decay for larger  $\ell$ . The crossover appears at  $\langle \cos \theta \rangle \simeq 0.2$ . Shown in the inset is the persistence length calculated from the slope  $\frac{d}{d\ell} \ln(\langle \cos \theta \rangle)$  as a function of  $\ell$ . The deviations from the true value 2.8 nm is increasing with increasing  $\ell$  and  $L_c$ . The mean segment-segment distances are shown in Fig. 6.8. The deviation from the WLC model are substantial even for short chains and are increasing with chain length. Due to the strong deviation of the SAWLC from the simple WLC for  $L_c \gg \ell_P$ , simulated data are used for comparison with experimental results in the following.



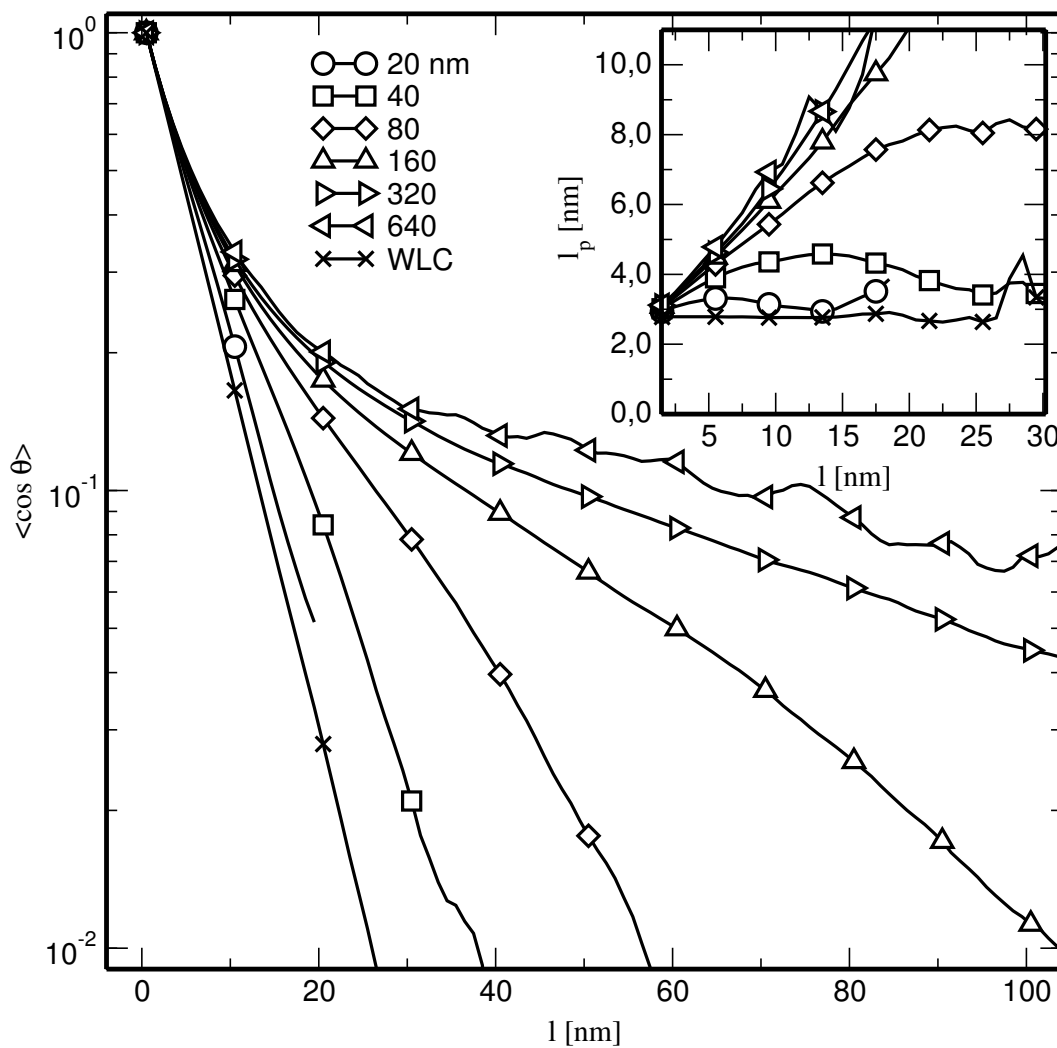


Figure 6.7: Orientation correlation function of the simulated self avoiding chains and for comparison a chain according to the WLC model. Shown in the inset is the persistence length calculated from the derivative  $d \ln(\langle \cos \theta \rangle) / dl$ .

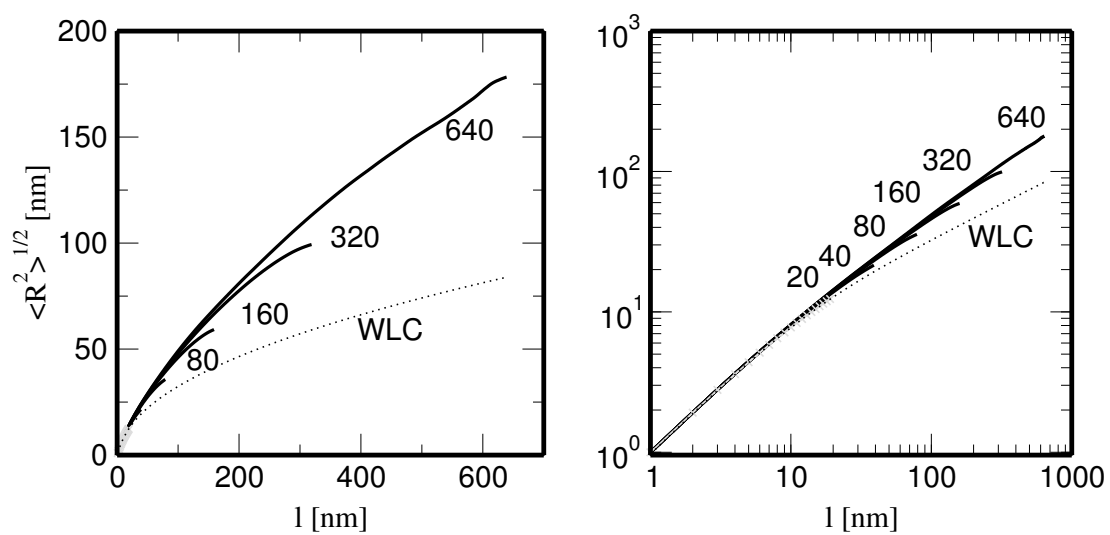


Figure 6.8: Segment-Segment Distances of the simulated chains.

### 6.4.3 Test of lateral mobility of adsorbed chains

Samples of **u-g2** were prepared by spin coating and also by solution casting of **u-g2** on freshly cleaved mica surfaces from aqueous solution of  $1 \text{ ng}/\mu\text{L}$ . From visual inspection, no obvious dependence of conformations on the adsorption time was observed, indicating two possible scenarios: (1) the chains are trapped, or (2) the chains are fully equilibrated. The surface mobility of **u-g2** is investigated in the following two experiments, giving clear evidence for the trapping.

Fig. 6.9 displays images of **u-g2** treated with acetone. In image (a) molecules were coated from a 9:1 acetone water solution. The high proportion of acetone causes molecules to collapse onto the substrate surface. The mica substrate was subsequently covered by a drop of distilled water, allowing the molecules to equilibrate for 5 minutes. After this the sample was dried and imaged. As can be clearly seen in 6.9a, molecules are still in the collapsed conformation. The reverse experiment is a check: **u-g2** was adsorbed from water onto mica in the usual way, then the mica was put into acetone for 5 minutes. Again no relaxation was found, as displayed in image (b).

Further, we directly proved the immobility by pushing (“nanomanipulating”) adsorbed molecules using the SFM tip. Figure 6.10 shows **u-g4** molecules adsorbed onto mica imaged in tapping mode in distilled water. During the time of measurement (20 min), we did not observe any sign of movement. At several positions indicated by arrows molecules are cut. This was done by applying a constant force of  $10 \mu\text{N}$  to the substrate while moving the tip with a velocity of  $20 \text{ nm s}^{-1}$ . If molecules were mobile on the surface they would be moved by the pushing tip [31, 436]. Here however, it was not possible to move molecules, instead they were cut. Even very close (10 nm) to the cuts the contour remains unchanged, indicating that the friction force for moving even a short segment is sufficient to break the covalent bonds of the chain backbone.

Both experiments clearly show that the investigated polyelectrolytes are strongly adsorbed and that lateral motion is inhibited. Relaxation and thermally excited movement can therefore not be observed in the experimental time frame.

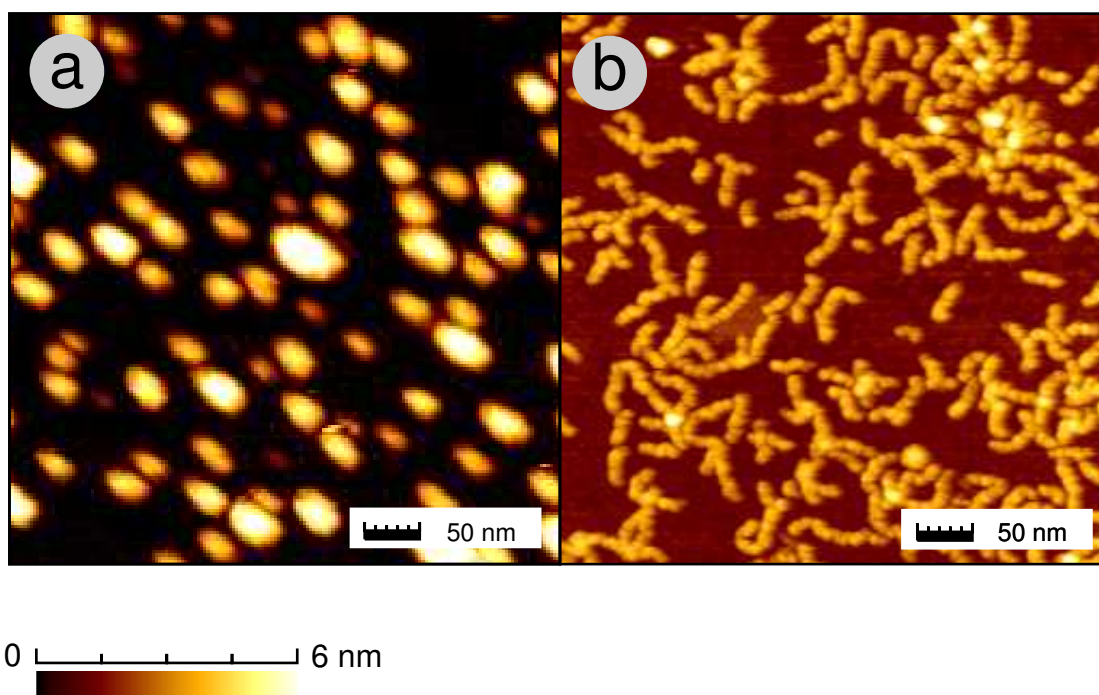


Figure 6.9: (a) **u-g2** adsorbed on mica in a collapsed conformation. The collapse was triggered by mixing acetone to the polymer solution. After adsorption, the sample was left in water for five minutes to allow relaxation. (b) **u-g2** cast from aqueous solution. The sample was left in acetone for five minutes to induce a collapse.

#### 6.4.4 Conformations of charged dendronized polymers

Fig. 6.11 shows a typical SFM image of adsorbed **u-g1**. Single molecules can be clearly resolved. Crossings appear rather seldom. The molecules are lying flat with an apparent height of about 0.5 nm. For comparison, the cylinder width in solution as measured by SANS is 1.3 nm [135] and thus much larger. However, heights of single molecules are commonly underestimated in SFM measurements as discussed in section 3.1.3.

##### Conformation of PG1

For conformation analysis, the chains were vectorized using the automated procedure. Vectorization was performed independently on two sets of data:

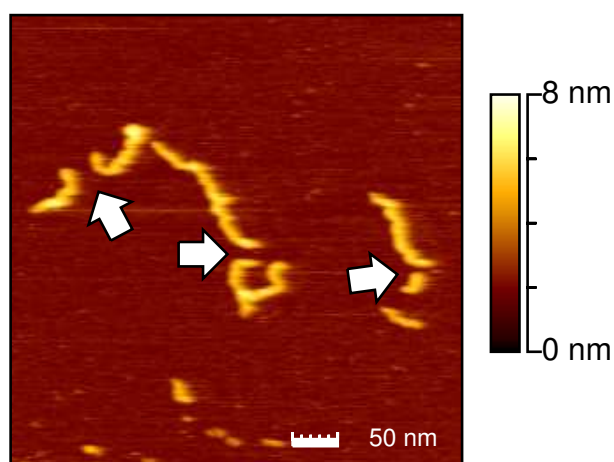


Figure 6.10: **u-g4** imaged in water. The arrows mark positions where the molecules were pushed by the tip.

“free” molecules (or parts of molecules) that are not hindered by neighboring molecules (marked in figure 6.11a), and molecules from high density regions, which are surrounded by neighboring molecules. The sum of the contour lengths of the molecules is  $5.4 \mu\text{m}$  and  $4.5 \mu\text{m}$ , respectively, as observed on 14 SFM images and a total area of  $1.9 \mu\text{m}^2$ . Fig. 6.11b shows a zoom to give an impression of the quality of vectorization.

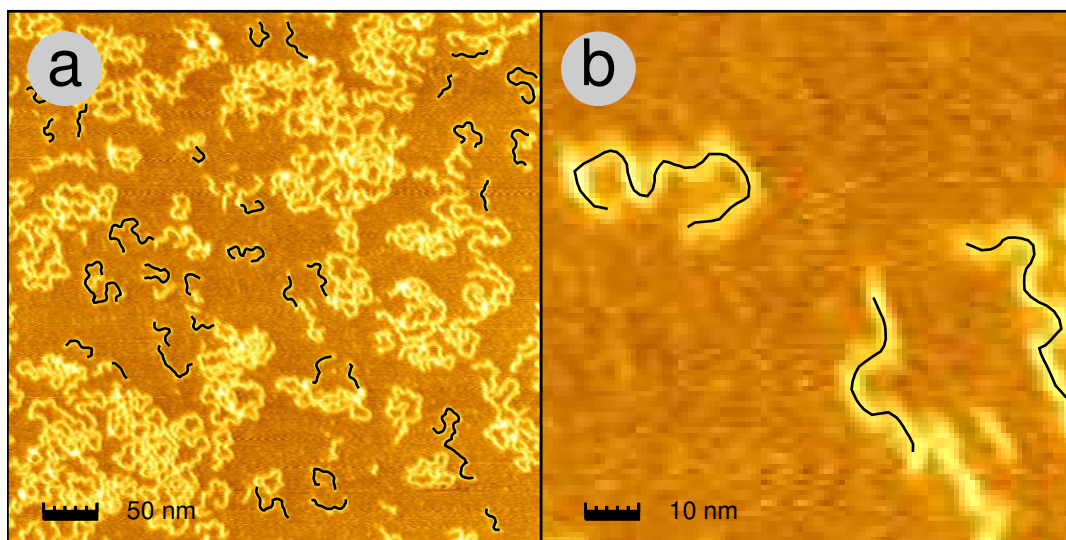


Figure 6.11: (a) Typical SFM image of **u-g1** adsorbed on mica. The black lines display the vectorization for the “low density” set of data. (b) zoom.

Orientation correlation functions of both sets of data are displayed in Fig. 6.12a. Both curves show a steady decrease from 1 to a zero-crossing at  $27.8 \pm 3.4$  nm. Their difference is in the shown range smaller than the statistical errors, therefore we conclude the absence of a dependence on the density. For worm-like chains in two dimensions the orientation correlation function follows  $\langle \cos \theta \rangle = \exp(-\ell/2\ell_P)$ . Fitting the obtained curve in the range of 5 to 15 nm gives a persistence length of  $\ell_P = 5.0 \pm 0.25$  nm. This value has to be handled with care, since the curve clearly does not follow the exponential decay of the WLC for  $\ell \gtrsim 20$  nm. Nevertheless, a similar persistence length was also obtained by SANS and amounts to 3.9 nm [135], which is in fair agreement to our value.

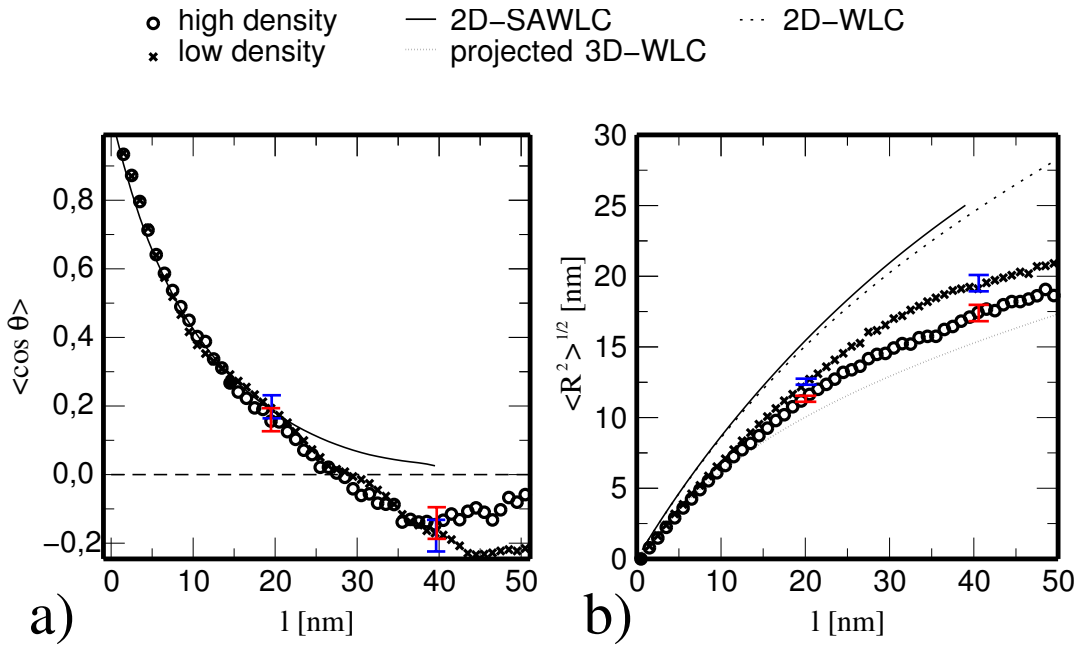


Figure 6.12: a) orientation correlation dependence for **u-g1**. Chains from heigh and low density regions show similar behavior. b) segment-segment correlation for both sets of **u-g1** data compared to the simulation and the projected 3D-WLC.

Also shown in Fig. 6.12a are the resulting curves for simulated self avoiding wormlike chains of  $L_c = 40$  nm and  $\ell_P = 5$  nm. The curve fits to the measured data in the range from 0 to 20 nm. For larger  $l$  the simulated curve decays slower and does not follow the zero crossing. Since we never observed anti-correlations in the simulation, it can be stated even without knowing the exact value for the persistence length that the observed conformations are

clearly and significantly deviating from the equilibrium conformations.

As can be seen from the mean segment-segment distance (Fig. 6.12b), the adsorbed chains are in a more compact conformation compared to the simulation. This is consistent to the observation of orientation anti-correlations: there is an increased probability of back-folding and therefore the overall conformation is more compact than expected for worm-like chains. The mean segment-segment distances are between the predictions of equilibrated SAWLCs and trapped WLCs. In high density regions, the conformations are more compact than in those of low density.

### Comparison of conformations for different generations

Fig. 6.13 exhibits a comparison of all four generations of the unprotected dendronized polymers. The molecules appear thicker with increasing generation. The mean height along the contour is 0.5, 2.0, 2.6 and 4.0 nm. The heights are not constant along the contour but have clear maxima and minima. Fig. 6.14b shows the height structure of a single **u-g2** molecule, following the paths marked with a,b and c in the Fig. 6.14a image. The height above the substrate varies between 1.7 and 3.2 nm. Such variations are typical for all images of higher generations. Also in **u-g1** height variations are seen, but cannot clearly be distinguished from the background unevenness, which causes variations on the same size, i.e. about 0.3 nm. Height variations might be due to an irregular distribution of dendrons.

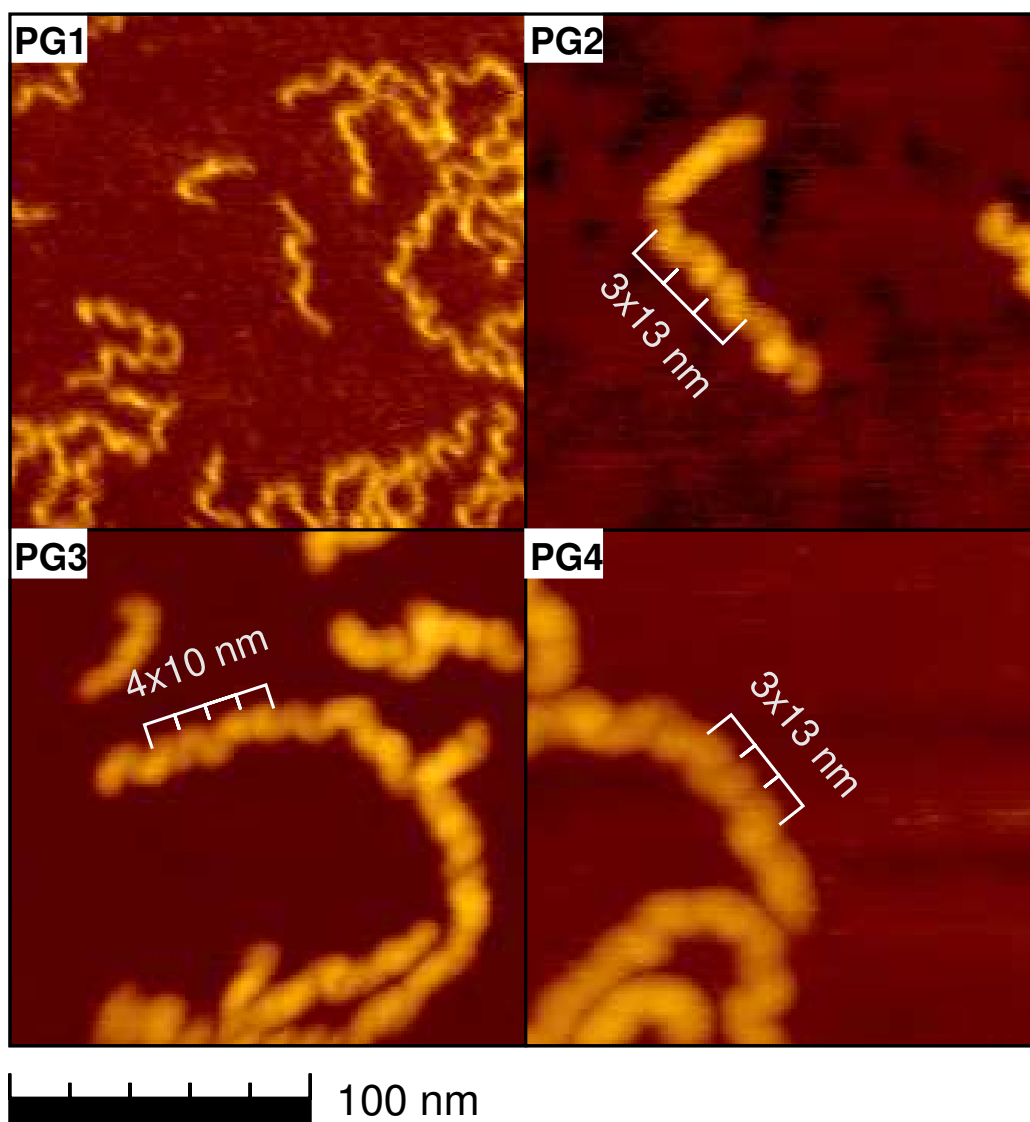


Figure 6.13: Typical SFM images for **u-g1**, **u-g2**, **u-g3** and **u-g4** on mica. All molecules exhibit undulations with a period of  $13 \pm 3$  nm.



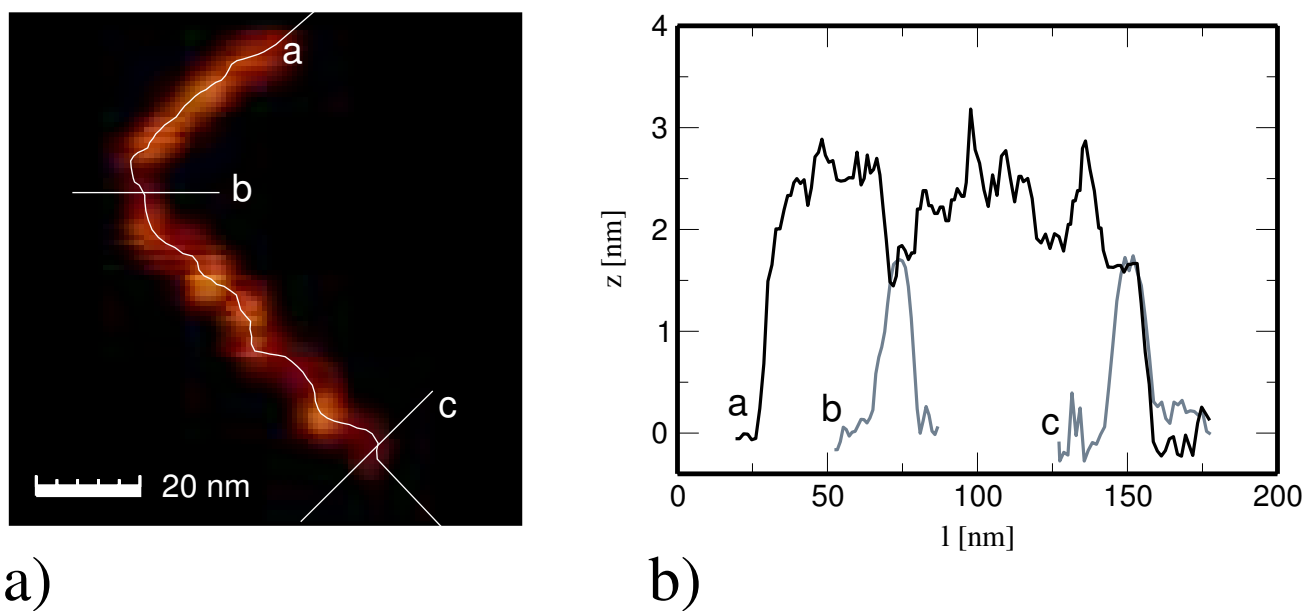


Figure 6.14: Height variations along the contour of a **u-g2** molecule. a) SFM image, b) contour along the paths a, b and c marked in a).

All molecules exhibit a characteristic sinusoidal lateral undulation along the contour. The undulation period is estimated as  $13 \pm 3$  nm for **u-g2**, **u-g3** and **u-g4**. Undulation of **u-g1** is less concise. The chains are stronger coiled than the higher generations and therefore undulations cannot be clearly distinguished from the statistical fluctuations.

Vectorization of higher generation molecules is problematic since the undulations cannot be clearly resolved in all images. Therefore we choose a coarse vectorization, which ignores the fine structure. In Fig. 6.15 the angular correlation functions for all four polymer generations are plotted. The large difference between first and higher generations is partly due to the different way of vectorization which does not allow a direct comparison. Fitting the initial decay from  $\ell = 10$  to 20 nm gives a persistence lengths of  $30.4 \pm 3$  nm,  $18.6 \pm 2$  nm and  $26.6 \pm 2$  nm for **u-g2**, **u-g3**, and **u-g4**. The remarkably high value for **u-g2** was reproduced by two independent samples. Curves for **u-g1**, **u-g3** and **u-g4** show a zero-crossing, indicating a non-equilibrium conformation.

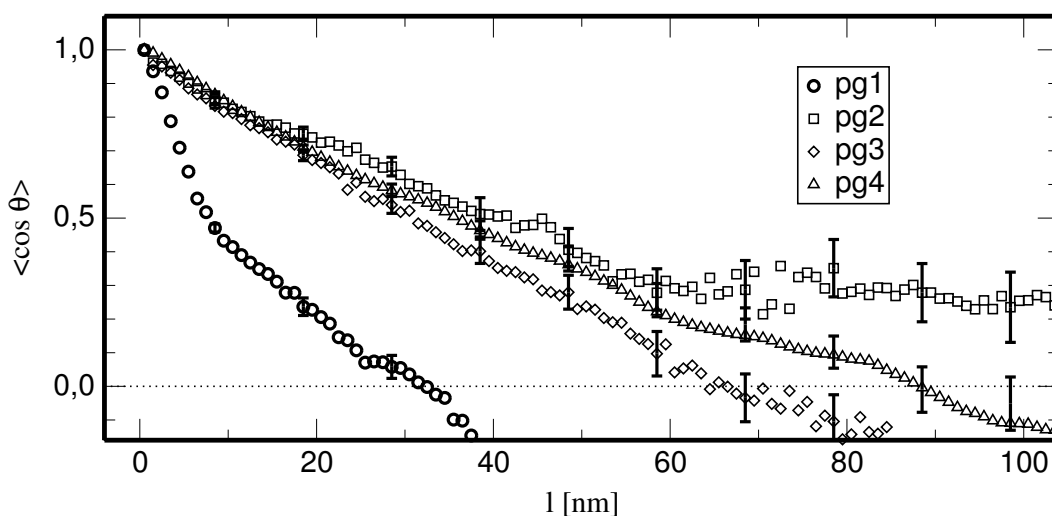


Figure 6.15: Orientation correlation functions of **u-g1**, **u-g2**, **u-g3** and **u-g4**.

The apparent reduction in contour length due to the fine undulation is examined in Figure 6.16 for **u-g2**. Several parts of chains which appear straight on a larger scale are vectorized manually, following the undulations in detail (Fig. 6.16a). The segment-segment distances (Fig. 6.16b) lie on a straight line with a slope of 0.72, corresponding to an apparent length reduction to 72%. This factor is too small to explain the different slopes of **u-g1** compared to the higher generations of the orientation correlation, indicating that the

persistence of **u-g1** is considerably smaller.

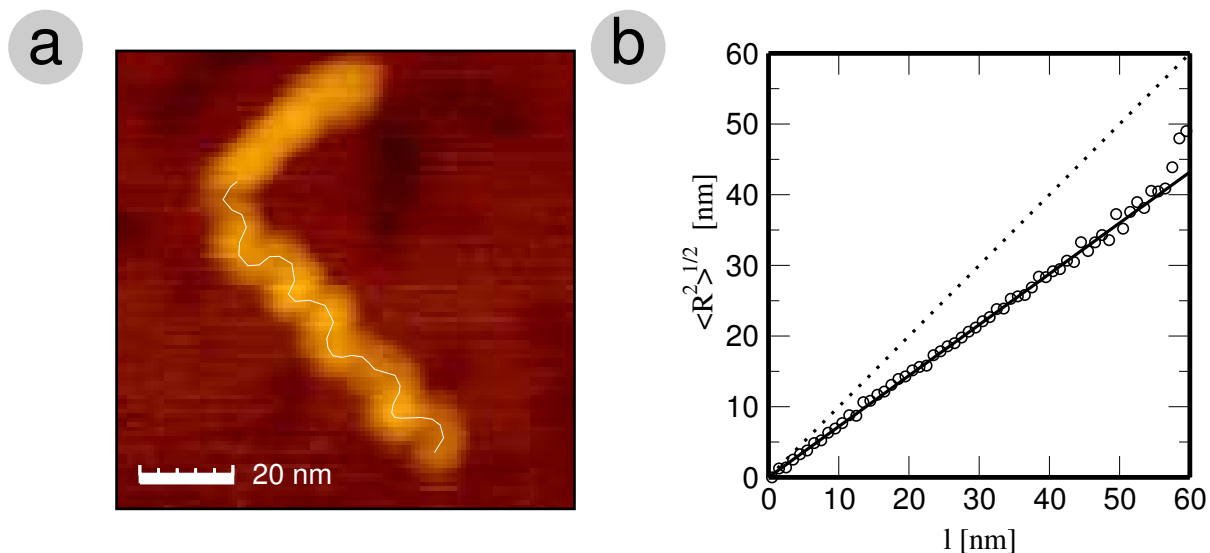


Figure 6.16: Estimation of the length reduction due to undulation. a: One of the segments which were chosen for a detailed vectorization. b: The mean direct distance between points on the chain plotted against the length along the contour. The fit gives a slope of 0.72. This factor describes the reduction in length due to the meandering.

### Conformations on patterned substrates

A way to avoid undulated conformations is to use a substrate where the electrostatic charges are not uniformly distributed but show stripe patterns which act as guides to the adsorbing polymer chain. We choose highly oriented graphite (HOPG) decorated with a monolayer of nonadecanoic acid ( $C_{19}H_{38}O_2$ ). Fatty acids on graphite are known to self assemble into ordered domains consisting of rows of parallel chains. Molecules in every second row are oriented oppositely so that the polar heads form stripes separated by 4.5 nm wide rows of hydrophobic alkyl chains. As shown in [419] the positively charged head-rows act as nanoscopic “rails” for the adsorbing oppositely charged polyelectrolytes.

Fig. 6.17a displays an SFM image of **u-g2** adsorbed onto the patterned substrate. The chains exhibit characteristic bends of  $120^\circ$ , following the

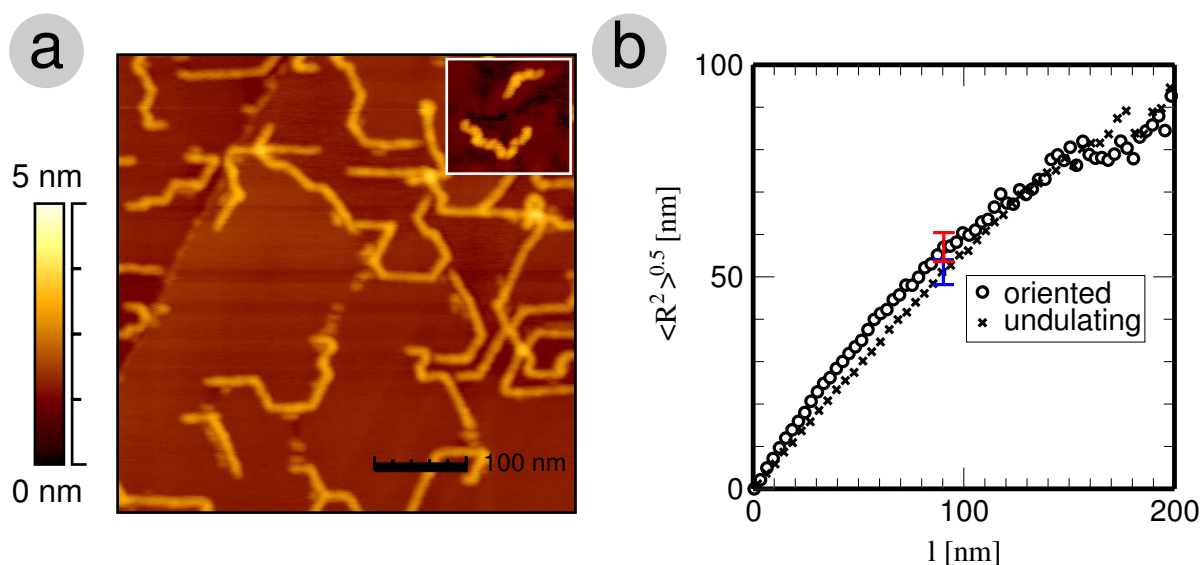


Figure 6.17: (a) **u-g2** adsorbed onto graphite which has been decorated with a monolayer of amphiphiles (nonadecanoic acid). The inset shows **u-g2** molecules adsorbed onto mica for comparison. (b) Segment-segment distance function in comparison to the undulated one. To compensate for the length reduction, the abscissa of the “undulating” curve is multiplied by  $0.72^{-1}$ .

substrate stripe pattern. The sections between the bends are up to 100 nm in length and are perfectly straight, without any undulation. In Fig. 6.17b the segment-segment distances are compared to the ones of crumpled **u-g2**. The abscissa of the “crumpled” data is scaled by  $0.72^{-1}$  to account for the length reduction. Both curves are in good agreement at large values, indicating that the overall coil size is not affected by the change of substrate. For smaller length values (around 100 nm), segment-segment distances for the oriented molecules are larger, which is a result of the straight segments.

In summary, this experiment did show that undulation can be suppressed by the choice of substrate, and that the orienting effect of the substrate similar to the undulation effect changes conformations “locally”, while the overall size is maintained.

### 6.4.5 Trapped conformations of DNA

#### Length dependence

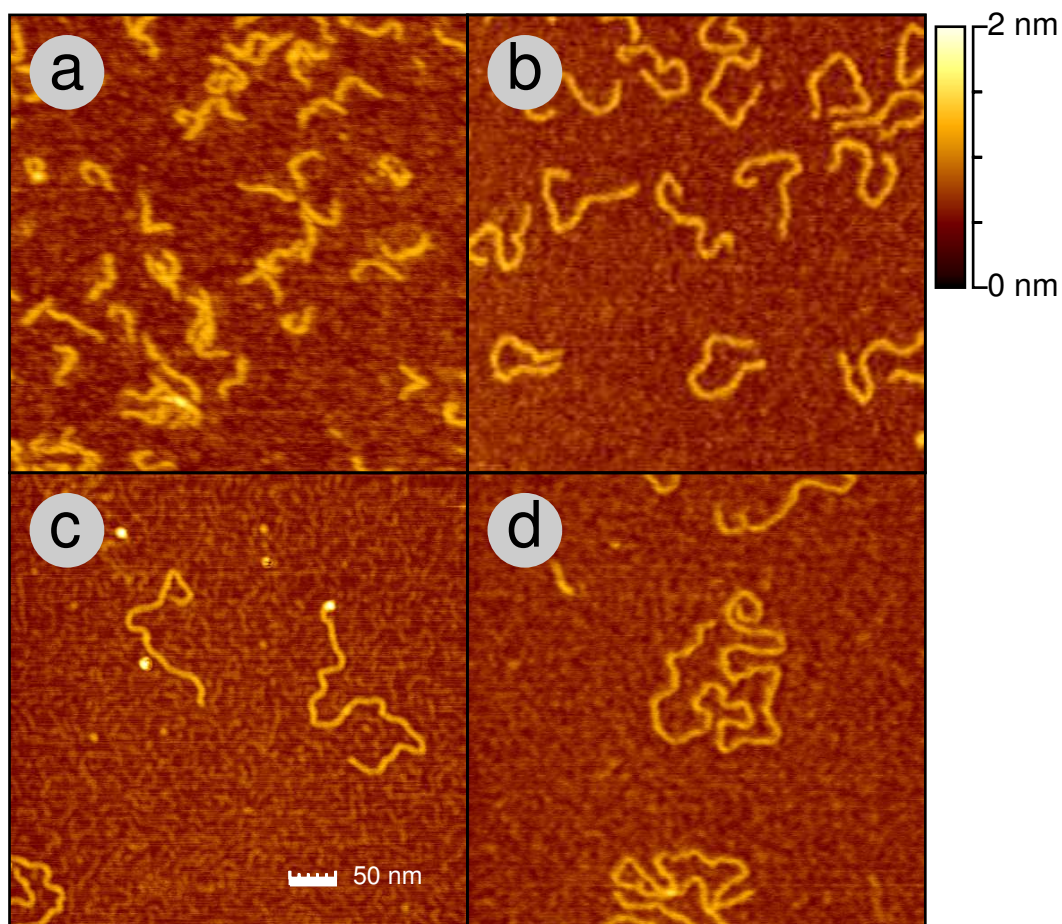


Figure 6.18: DNA fragments of different lengths adsorbed onto PLO. a: 71 nm, b: 187 nm, c: 437 nm, d: 895 nm

In order to investigate the influence of the contour length on the observed conformation, we use DNA fragments of different size: 213 bp, 562 bp, 1313 bp and 2686 bp. Assuming the molecules to be in the *B*-form on the surface, this corresponds to contour lengths of 71, 187, 437 and 895 nm [378, 386].

SFM images of the different segments on PLO coated mica are displayed in Fig. 6.18. The statistical analysis (Fig. 6.19) shows no significant length dependence of the orientation correlation function. All curves show a char-

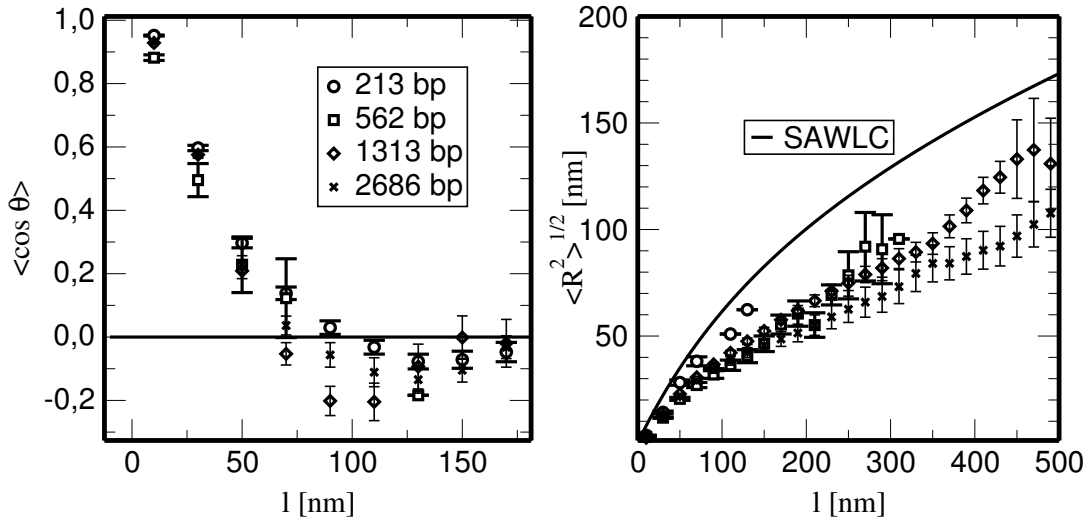


Figure 6.19: Left: orientation correlation function. Right: segment-segment distances of DNA fragments compared to the simulated SAWLC curve (assuming a persistence length of 50 nm).

acteristic zero crossing around 70 nm. For the segment-to-segment correlations, however, there is a deviation for the 213 bp fragments. They appear clearly more stretched, compared to longer chains. This might be caused by the background unevenness, as the length of PLO chains is similar to the DNA. In summary, no simple dependence of the anti-correlations on the chain length are found. In particular, they also appear for short chains indicating that they are not caused by e.g. short ranged attractive interactions between the monomers of a chain.

### Dependence on salt concentration

Adding NaCl to the solution allows to tune the surface chain interaction. With increasing salt concentration the surface potential is getting sharper since the characteristic length of the electrostatic surface potential, the debye length  $r_D$ , depends on the ion concentration as  $r_D \propto c^{-\frac{1}{2}}$  (see Equation 2.31).

Measurements of the 2686 bp fragment in different concentrations of NaCl are displayed in Fig. 6.20, 6.21, 6.22, 6.23. In 1M NaCl the conformations appear strongly influenced by capillary forces upon drying indicating a weak interaction of the polyelectrolyte with the substrate. Polyelectrolyte desorp-

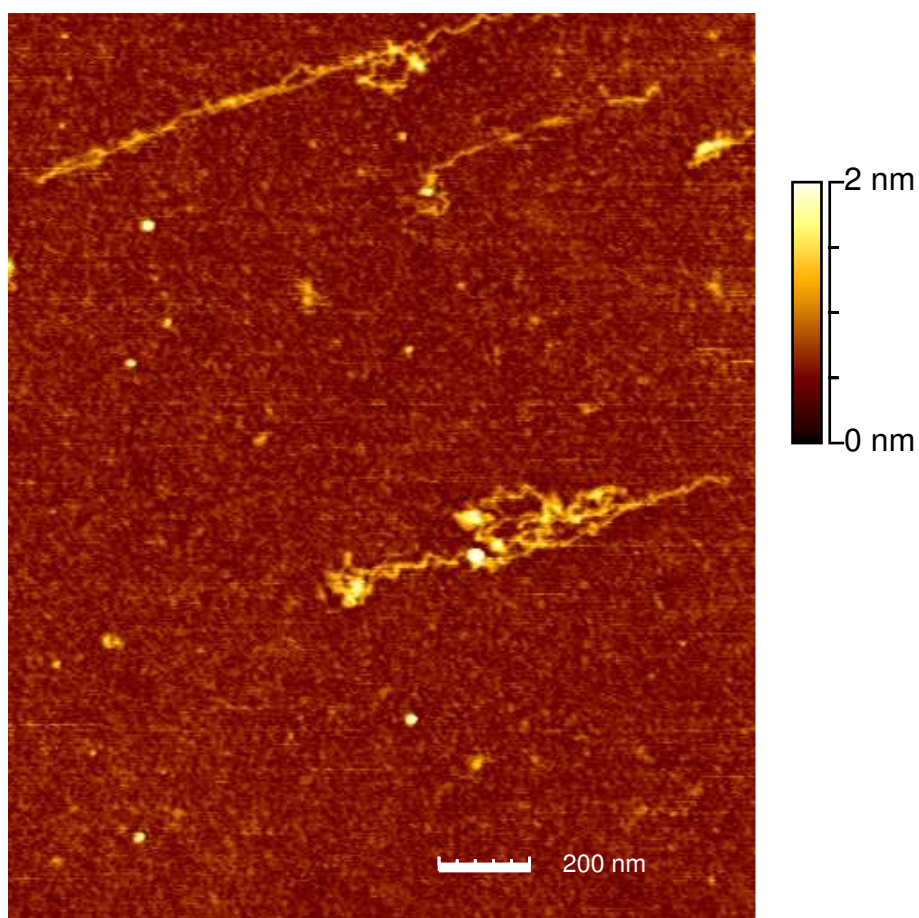


Figure 6.20: DNA adsorbed from 1M NaCl solution on mica. Conformations are strongly affected by viscous drag upon drying, indicating a rather loose adsorption.

tion on mica at high ionic strength is a known phenomenon (see for example [380]) and will not be investigated here, however it gives a limit for the concentrations which can be investigated.

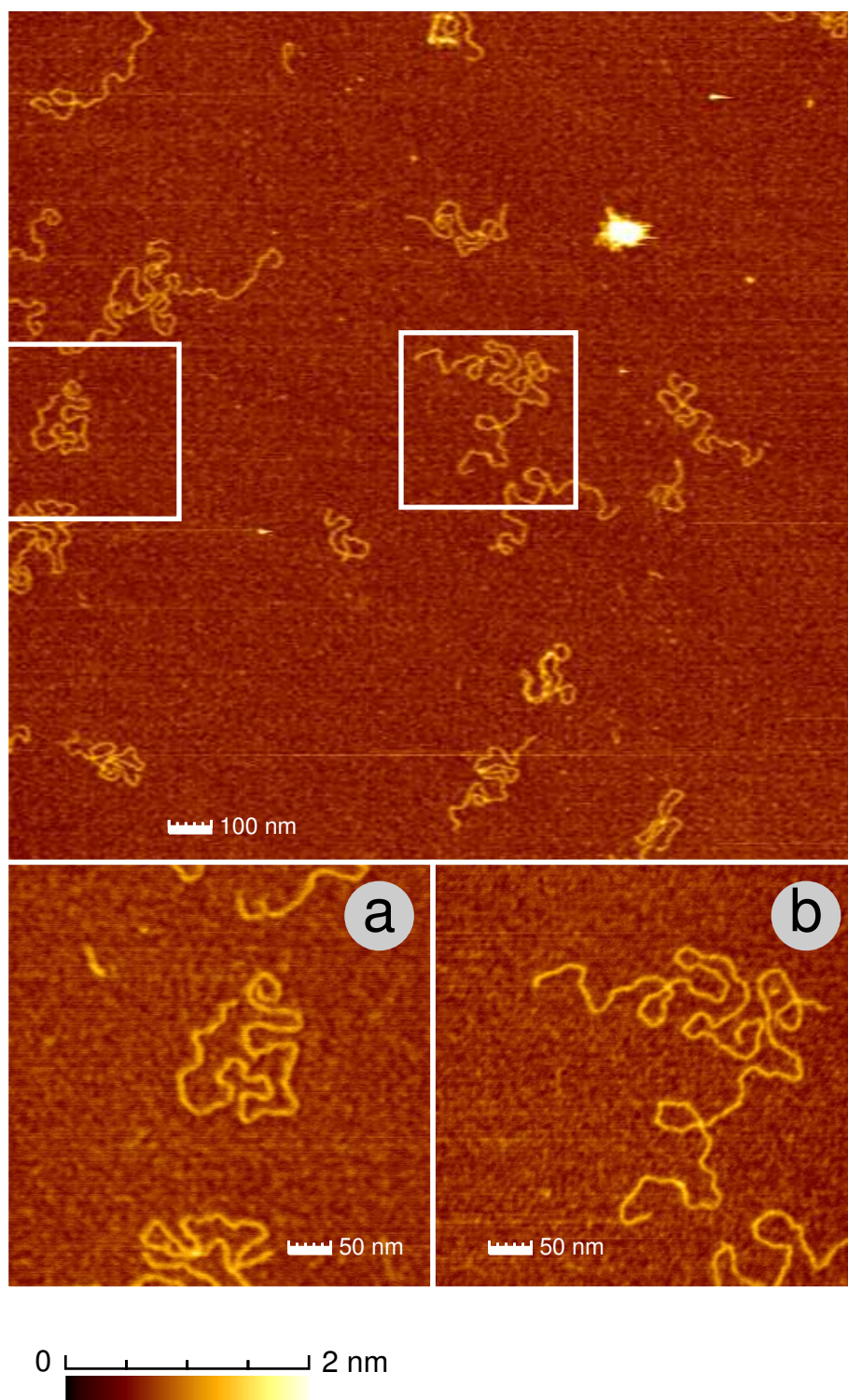


Figure 6.21: Typical DNA conformations on mica without addition of NaCl.



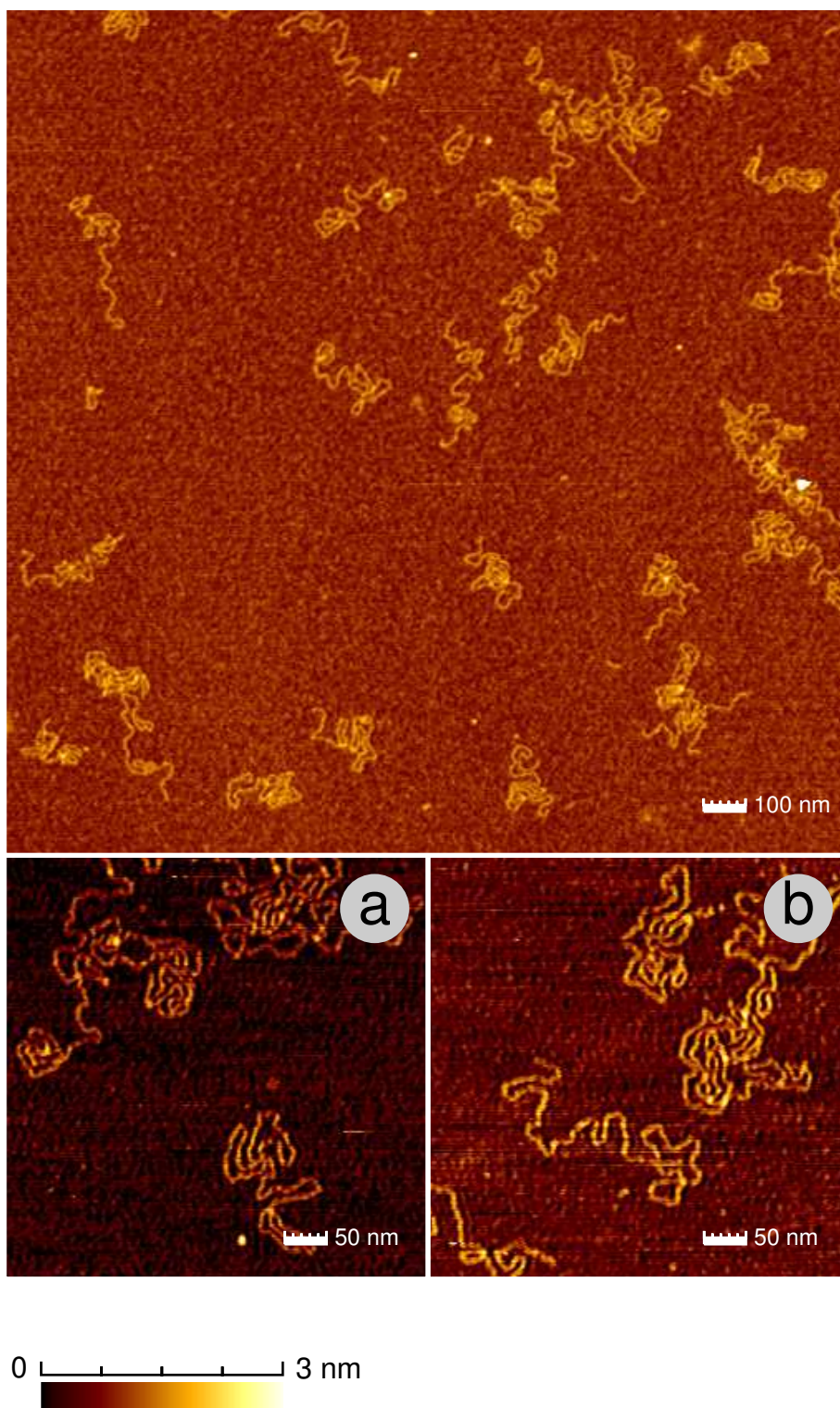


Figure 6.22: Conformations of DNA on mica from 10mM NaCl.

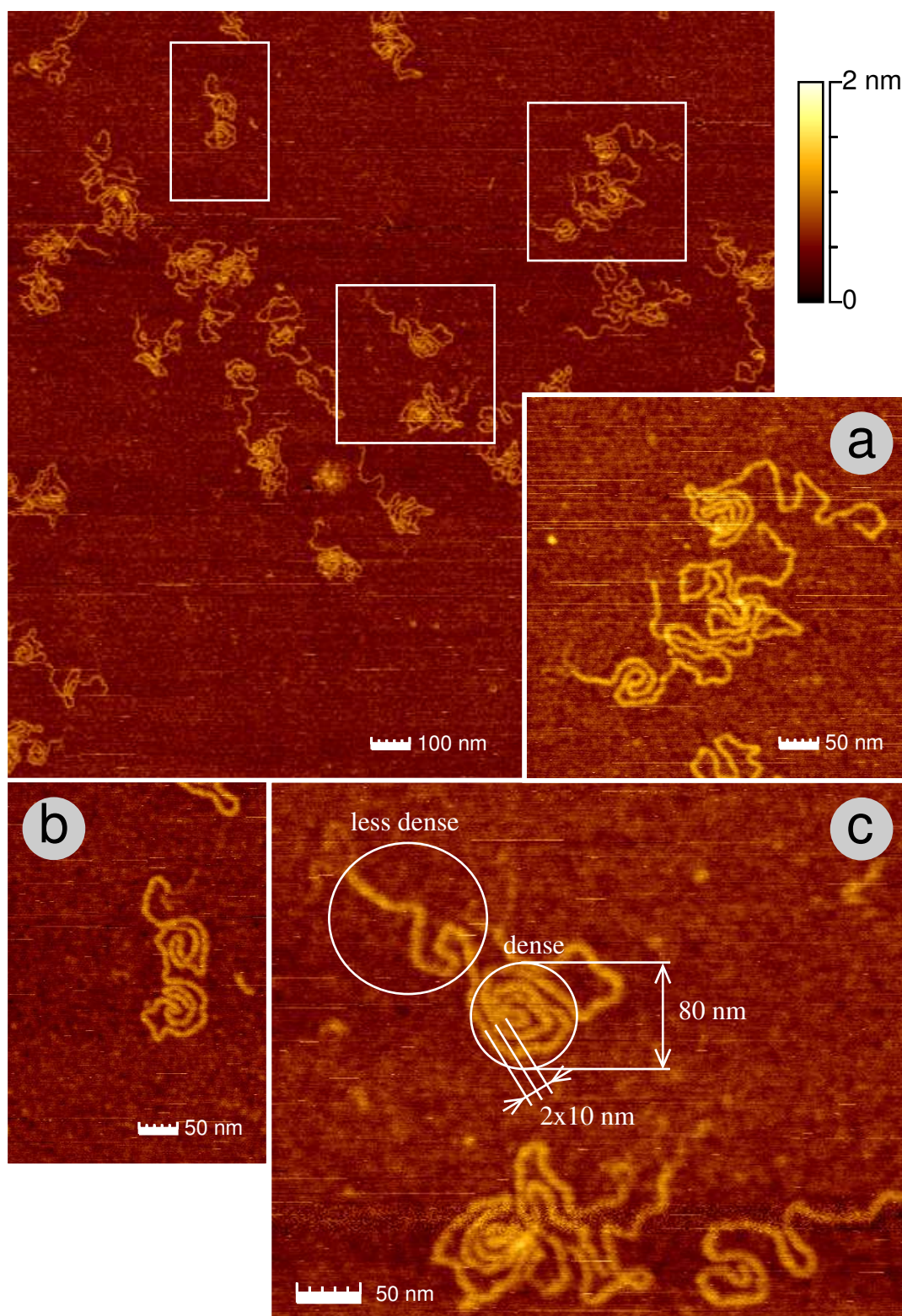


Figure 6.23: Conformations of DNA adsorbed from 100mM NaCl solution onto mica.

In the range of 0 to 100 mM NaCl, conformations become more compact with increasing salt concentration. This is evidenced by the radii of gyration, which amount to  $78.5 \pm 2.9$  nm,  $59.9 \pm 3.3$  nm and  $61.8 \pm 3.7$  nm for 0, 10 and 100 mM respectively. Conformations from 10 and 100 mM solutions consist of two characteristically different types of regions: regions of high density and regions of low density (see Fig. 6.23c). The less densely packed regions consist of strings which are strongly crumpled, similar as the conformations at 0 mM. These regions alternate with spots of high density. In those the typical distances between strands is about 10 nm. Neighboring strands are therefore strongly correlated and lie parallel. For 100 mM these regions are surprisingly regularly shaped, prevailing in spirals.

In Fig. 6.23 it can be seen that spirals are not the exception, but rather the rule. From the 53 investigated molecules, 21 show one or more clearly spiral-shaped sections. Often, spirals have a diameter of about 80 nm and consist of two windings of opposite direction, with about  $360^\circ$  each (Figure 6.23c).

## 6.5 Discussion

### 6.5.1 Overall conformations

All observed conformations have in common that they are too compact on the large scale compared to SAWL-chains. This is in agreement to the projection model indicating that polymers are not equilibrated but trapped instead. This implies (1) that the chains are adsorbed in a fast process  $t_1 \ll t_{\text{ads}}$  and (2) the inhibition of chain relaxation of the whole molecule on the surface.

The observation of negative values for the orientation correlations can be understood as a direct result from the compactness. Anti-correlation of tangent vectors means that there is certain length  $\ell$  where the chain on average bends back. Consequently, a 2D coil showing anti-correlations is more compact than the ideal worm-like chain. The appearance of long ranged orientation anti-correlations is therefore an indication that (1) chains are adsorbed in a fast process with  $t_1 \ll t_{\text{ads}}$  and (2) chain relaxation is inhibited on the surface.

of projection conformations. This is an important result because unlike other

indicators as the end to end distance, it is independent on the persistence length. It can therefore also be applied when  $\ell_P$  is unknown, as in the case of **u-g2**, **u-g3** and **u-g4**.

According to equation 6.1 the rouse time  $t_1$  depends quadratically on the chain length. Short chains do therefore equilibrate considerably faster than long chains. Using the friction coefficient for DNA in water  $\zeta = 7.6 \text{ nNsm}^{-1}$  [304] the equilibration time for the 213 bp fragment amounts to 0.26 ms. This is still more than two orders of magnitude larger than the lower limit for the adsorption time given by  $t_{CM}$ , following from equation 6.3. All DNA chains are therefore adsorbed in a strong non-equilibrium which agrees to the observation of negative orientation correlations.

### 6.5.2 Undulations

Undulations are clearly observed in images of **u-g2**, **u-g3** and **u-g4**. They exhibit periods of  $13 \pm 3 \text{ nm}$ , which appear to be independent of generation number. Undulations are not observed for **u-g1** and in all measurements of DNA. From equation 6.9 (appendix) the condition  $t_{zip} \ll t_{CM}$  is fulfilled for all cases including DNA and **u-g1**. The absence of clear undulations for **u-g1** can be understood from comparing the persistence length to typical values of the undulation period. Due to the small value of  $\ell_P$  the usual statistical bending is on the same length scale as undulations and both contributions cannot clearly be distinguished. The decay length of orientation correlation (5 nm) therefore resembles the persistence length in solution (3.9 nm).

Also for DNA no regular undulations are observed. This might be caused by the high bending rigidity of the DNA double helix. The investigated dendronized polymers on the other hand have a poly(styrene)-backbone which is flexible so that the bending rigidity is small.

### 6.5.3 Lateral self avoidance

Lateral self avoidance can be observed for all investigated systems. It is manifested in the avoidance of chain crossings and the parallel orientation of neighboring strands, which are closer to each other than  $\ell_P$ .

The dependence of the DNA conformation on the ion concentration is in agreement with the proposed tron model. Addition of ions reduces the surface interaction range. In 100 mM NaCl solution,  $r_D$  amounts to 0.96 nm. Since this is clearly below the DNA diameter of 2 nm, tron conformations must arise. Conformations at 100 mM NaCl clearly obey those characteristics: a spiral shaped dense region and one or two less dense tails. Unlike in the simple tron simulation, polymers do not end in the spirals but can leave them. The spirals often consist of two windings with opposite direction. In these conformations the zip changed the direction of movement at the center and moved along the spiral in the opposite direction out.

The resulting sharp turns ( $r \simeq 5$  nm) are energetically favorable compared to the penalty of accepting a crossing. The radii of curvature are well above the minimum curvature which is estimated using equation 6.16 (appendix). For DNA in 0.1 M NaCl solution adsorbing onto mica with an assumed charge density of  $0.34 \text{ Cm}^{-1}$ , the minimum curvature radius amounts to  $r = 0.98$  nm.

#### 6.5.4 Alternative explanations

All non-equilibrium conformations described in this chapter show orientation correlations which deviate from the exponential decay of the WLC model. In the literature a couple of explanations exist, which were proposed to explain observed conformations of adsorbed molecules which were also showing deviations from the WLC behavior.

Excluded volume can cause correlations as argued by Maier and Rädler [294]. They investigated conformations of DNA adsorbed onto a lipid bilayer with fluorescence microscopy. It was observed that the coils are becoming more compact with increasing DNA concentration. Since overlapping of neighboring coils is inhibited in 2D the mean coil size must be reduced for concentrations above the overlap concentration. However, it was shown in Fig. 6.12 that anti-correlations also appear for chains below the overlap concentration. They further appeared also for very short chains (DNA) and did not depend on the concentration (for **u-g1**). In addition, tron conformations and regular undulations can not be explained simply from the excluded volume.

Other explanations were published to explain the unusual conformations of polymers with linear side chains (bottle brushes) which appear similar to the

conformations of **u-g1** to **u-g4** (see [428]). Using a scaling approach, it was shown by O. Borisov (thus far only published in the review [428]) that the adsorption of side chains leads to a contraction of the backbone provided that the solvent is a bad solvent for the side groups. The consequence is strain which can cause a “buckling” of the main chain. A second explanation which is also based on the behavior of large side groups was investigated by I. Potemkin using MD-simulations [360]. If the side groups are distributed randomly (atactic) on both sides of the adsorbed chain, but with a certain preference for one side, then the chain will bend towards one or the other side, depending on the solvent quality.

Against the applicability of both models a couple of arguments can be mentioned. The chain conformations – in both cases – are adopted after adsorption. Therefore a sufficiently high mobility to allow reordering is necessary. As was shown, **u-g1** to **u-g4** are completely immobile after adsorption. It has been further shown, that undulation could be inhibited by using a substrate which is decorated by a monolayer of dodecanoic acid. Since dodecanoic acid is assumed to be mobile on HOPG, the energetic gain for buckling, if there is any, must be rather small. Another argument follows from the similarity of the undulation for **u-g2**, **u-g3** and **u-g4**. For both explanations, the effect should be the stronger the larger the side groups are, but it is not.

Spirals are highly ordered conformations and therefore statistically very unlikely for a random walk. In principle the high density of the spirals could be caused by a long ranged attractive interaction. However, this can not explain the coexistence of distinctively different density regions in one chain. The tron model is a better explanation, as it predicts both and therefore better fits to the experiment.

## 6.6 Conclusions

In this chapter we developed a classification of conformations of strongly physisorbed polymer chains. We presented models describing the influence of zipping and self avoidance. These predictions were verified experimentally by investigating the model systems DNA adsorbed onto PLO and dendronized polymers onto mica. Our models describe a common experimental situation for SFM imaging, since a strong interaction to the substrate is necessary for stable SFM imaging. Further, it is found that the appearance of negative

orientation correlations is a good indication for trapping.

## 6.7 Appendix

### Adsorption times

In this appendix the adsorption time for a polyelectrolyte on a charged surface is calculated for the hypothetical cases of pure zipping and non-zipping. We define the adsorption time as the time between the first contact of the polymer to the surface and the moment when the last segment is adsorbed. In the initial situation the chain is assumed to be in a random conformation. The center of mass is therefore at the height  $r_g$ . For simplicity, we use a purely electrostatic potential.

In order to estimate the adsorption time  $t_{\text{CM}}$  without zipping, we have to imagine that monomers are not connected. We therefore consider the adsorption of a single “monomer particle” of length  $a$  which is positioned at the chain center of mass. The forces acting on this particle are the friction force  $F_{\text{friction}} = \zeta \dot{\mathbf{r}}$ , the force of inertia  $F_{\text{inertia}} = m \ddot{\mathbf{r}}$  and the surface force  $F_{\text{surface}}(z)$ . In ordinary liquids the friction is high so that inertia forces can be neglected for small  $m$ , therefore  $\dot{r} = F_{\text{surface}}(z) \zeta^{-1}$ . Using the Debye-Hückel potential Equation 2.31, the force is

$$F_{\text{surface}}(z) = \frac{2\pi a k_B T \ell_B \sigma}{\lambda e_0} \exp\left(-\frac{z}{r_D}\right).$$

Integrating the inverse velocity leads to the time  $t_{\text{CM}}$ :

$$t_{\text{CM}} = \int_{z=0}^{r_g} \dot{r}^{-1} dz \tag{6.2}$$

$$= \frac{\zeta r_D \lambda e_0}{2\pi a k_B T \ell_B \sigma} \left( \exp\left(\frac{r_g}{r_D}\right) - 1 \right). \tag{6.3}$$

In order to calculate the zipping time, we have to consider the force at the zip in  $x$ -direction. This is given by the gain in energy upon moving a segment of

length  $d\ell$  from the coil to the surface, divided by  $d\ell$ . For the DH-potential this is

$$dU = e_0\lambda^{-1} (\psi(0) - \psi(r_g)) d\ell \quad (6.4)$$

$$\Rightarrow F_x = \frac{d}{d\ell} U \quad (6.5)$$

$$\simeq 2\pi\ell_B r_D \sigma k_B T e_0 \lambda^{-1} \quad (6.6)$$

This force is counter balanced by the friction force acting on the part of the chain which is actually dragged due to the zip motion. We assume that this length is given by the radius of gyration  $r_g$  (equation 2.18) and the friction force is consequently  $F_{\text{friction}} \simeq v_x r_g a^{-1} \zeta$ . The time to zip down the whole chain is then

$$t_{\text{zip}} = \frac{aN}{v_x} \quad (6.7)$$

$$= \frac{\zeta r_g \lambda N e_0}{4\pi\ell_B r_D k_B T \sigma}. \quad (6.8)$$

The zipping time therefore scales as  $t \propto N^\alpha$  with  $\alpha = \nu + 1$ , and  $\nu$  being the scaling exponent. Using  $\nu = 0.588$  for a SAW [107] this is in agreement with the numeric result  $\alpha = 1.58$  observed in Ref. [358]. The ratio  $t_{\text{zip}}/t_{\text{CM}}$  finally is

$$\frac{t_{\text{zip}}}{t_{\text{CM}}} = \frac{r_g N}{r_D \left( \exp\left(\frac{r_g}{r_D}\right) - 1 \right)}. \quad (6.9)$$

Remarkably, it does not depend on the surface charge density, and only indirectly via  $r_g$  on the charge density along the chain.

## Minimum curvature

A limit for the curvature radius of a chain contour formed by zipping is derived here. It is obtained by comparing the zipping force to the force resulting from the chain rigidity. Consider the Gedanken experiment sketched in Figure 6.24, where the zip movement is hindered by a massive barrier. The zip moves towards the barrier until the elastic force  $F_e$  equals the zipping force  $F_x$ . From the analogy of a wormlike-chain to a spring (equation 2.39), the



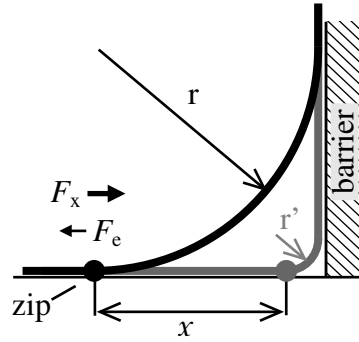


Figure 6.24: Gedanken experiment to obtain an estimate of the minimum radius of curvature.

bending energy is

$$U = \frac{1}{2} k_B T \ell_P \int_0^L r^{-2} d\ell \quad (6.10)$$

$$= \frac{1}{2} k_B T \ell_P r^{-2} L \quad (6.11)$$

$$= \frac{\pi}{4} k_B T \ell_P r^{-1}. \quad (6.12)$$

For the last transformation  $L = \theta r = \frac{\pi}{2} r$  is used. The elastic force follows from the derivative using  $x = r' - r$ :

$$F_e = \frac{d}{dx} U \quad (6.13)$$

$$= -\frac{d}{dr} U \quad (6.14)$$

$$= \frac{\pi}{2} \frac{k_B T \ell_P}{r^2}. \quad (6.15)$$

From  $F_e = F_x$  it follows (using 6.6) the smallest curvature which can be obtained from the DH-potential

$$r = \sqrt{\frac{\ell_P \lambda e_0}{4 \ell_B r_D \sigma}}. \quad (6.16)$$

# Chapter 7

## Equilibrium: Persistence of poly(isocyanodipeptides)

This chapter appeared in similar form as:

P. Samorí, C. Ecker, I. Gössl, P.A.J. de Witte, J.J.L.M. Cornelissen, G.A. Metselaar, M.B.J. Otten, A.E. Rowan, R.J.M. Nolte, and J.P. Rabe:

**High Shape Persistence in Single Polymer Chains Rigidified with Lateral Hydrogen Bonded Networks**

*Macromolecules* 35 (13): 5290-5294 2002.

### 7.1 Introduction

The direct probing of the structural and mechanical properties of isolated polymer chains is one of the major challenges in polymer and material science, since the basic molecular properties can be eventually compared to the macroscopic properties of a material. Scanning probe microscopy techniques make it possible to directly access conformational and mechanical properties of single molecules [156, 514]. For instance, macromolecules can be pulled

with a scanning force microscopy tip [374, 63, 129, 196] or imaged when equilibrated on a surface [379]. In the latter case, the persistence length of the molecule on a surface can be determined and compared to the persistence length in solution. Such studies have revealed that double-stranded DNA (dsDNA) on mica has a persistence length of 53 nm, which is similar to the value measured in solution [379]. Wider, more complex supramolecular bioarchitectures can be even more rigid and have persistence lengths up to a few millimeters. Examples are the tobacco mosaic virus and the microtubuli [157].

The synthesis of shape persistent abiotic polymeric structures with preprogrammed conformations is of great recent interest [322, 338, 129, 196, 389]. Such architectures can be constructed by designing supramolecular polymers, where the repeat units are held together through noncovalent types of forces [410, 169, 251, 188, 163, 145, 373]. Alternatively, conventional polymers, where the repeat units are covalently linked, can be provided with appropriate side-chain functionalities which give additional rigidity to the main chains, e.g., using sterically demanding dendrons [229, 350, 403], or moieties forming hydrogen-bonded networks [101].

Among rodlike conventional polymers, poly(isocyanides) (PIC) (Fig. 7.1) are peculiar since their backbones, when functionalized with sterically demanding side chains, adopt a  $4_1$  helical conformation (four repeats per turn, Figure 7.1b) which accounts for the relatively high stiffness of the polymer [332]. We decided to focus on a PIC bearing L-alanine-D-alanine methyl ester side groups. Solution studies have revealed that the amide moieties in these pendant dipeptides self-associate into four hydrogen-bonded networks which are oriented parallel to the main chain of the polymer (Figure 7.1c) [332]. This effect is expected to play an important role for the stiffness of the overall chain which needs to be quantified.

We describe here a tapping mode-scanning force microscopy (SFM) [459] investigation of long and stiff isolated poly(isocyanodipeptides) chains adsorbed onto the basal surface of mica. The analysis of the SFM data allows us to characterize the stiffness of individual polymer chains by determining their persistence length. We compare the properties of the poly(isocyanodipeptide)s synthesized either with a Ni(II) salt or trifluoroacetic acid as the catalyst.

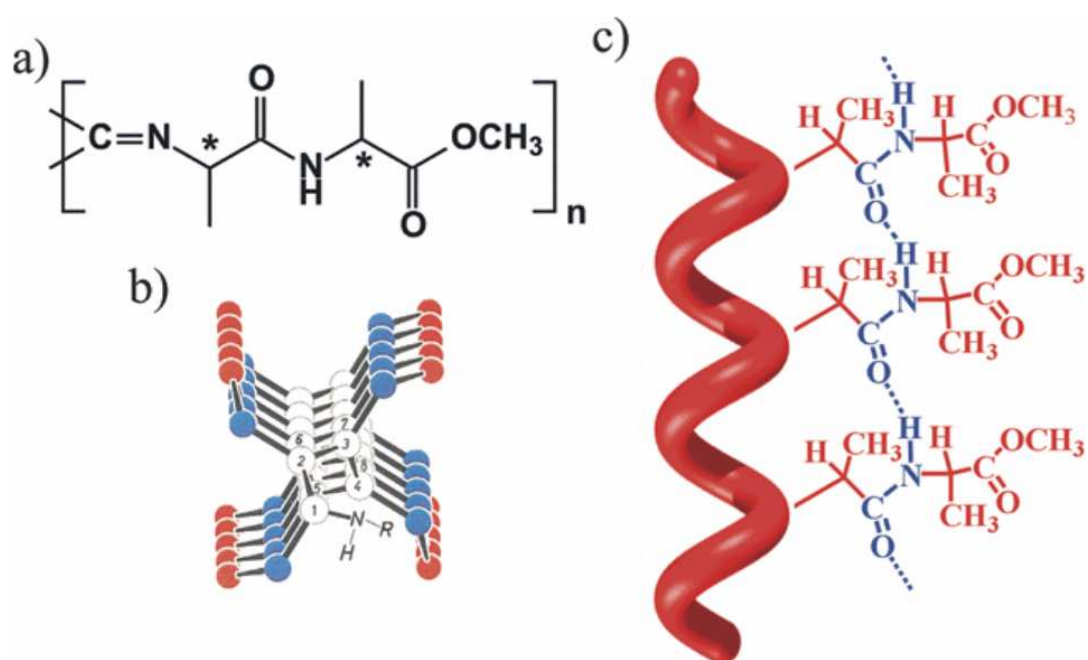


Figure 7.1: a) Structure of poly-isocyano-L-alanine-D-alanine methyl ester; b) Schematic of  $4_1$ -helix ; c) Hydrogen bonding array along polymer backbone.

## 7.2 Experimental procedures

### Sample preparation and SFM imaging

The polymerisation was carried out employing either  $\text{Ni}(\text{ClO}_4)_2 \cdot 6\text{H}_2\text{O}$  as catalyst (leading to PIC-Ni) or trifluoroacetic acid as initiator (for PIC-H). Details of the synthesis of the poly-isocyanodipeptides is described elsewhere [90]. PIC solutions in  $\text{CHCl}_3$  with different concentrations were spin-coated onto freshly cleaved muscovite mica surfaces. The morphologies of the dry thin films were characterized by means of Tapping mode SFM operating at room temperature in an air environment characterized by a relative humidity of 50-70%. Height and phase images were recorded with scan rates of 1-3 lines/s and a resolution of  $512 \times 512$  pixels using microfabricated silicon nanoprobes (length  $125 \mu\text{m}$  and width  $30 \mu\text{m}$ ) with a spring constant between 17 and  $64 \text{ N/m}$ .

### Data processing

The data processing was performed by the manually vectorization procedure described in section 4.2.1. The values for the number average ( $M_n$ ) and mass average ( $M_w$ ) molar mass were determined from the distribution of the contour lengths ( $L_c$ ) calculating the number average and the mass-weighted average, respectively. Since the distribution of  $L_c$  was not Gaussian, the error bars were evaluated for the PIC-Ni with the bootstrapping procedure using 1000 data points on the  $N=212$  data sampled [289]. For PIC-H only a relatively small number of data points was collected; therefore, it was not possible to use the bootstrapping procedure and the error bars were in this case quantified assuming the distribution to be Gaussian. In this case approximately the error bar can be estimated as  $\sqrt{\frac{\sum_1^N ((L_c) - L_c^i)^2}{N-1}}$ , where  $N$  is the number of investigated molecules. For the sake of comparison, for PIC-Ni the error bar was determined both with the bootstrapping and with the assumption of a Gaussian distribution: whilst for the first case it results  $\pm 3 \text{ nm}$ , in the latter one it amounts to  $\pm 5 \text{ nm}$  (calculated using  $N=212$ ).

## 7.3 Results and discussion

### 7.3.1 Single chains visualization with SFM

SFM images of PICs prepared by the acid-catalyzed polymerization reaction (PIC-H) are shown in Figure 7.3. Films prepared from 0.01 g/L solutions (Figure 7.3a) revealed an entangled network of polymer chains coexisting with free-standing single polymer strands. In these two different arrangements the polymer chains exhibited two completely different structures: in the first case topological constraints as a result of the entanglements, marked with the black arrows, caused a tension in the superstructure which did not permit the strands to equilibrate (see also below). In the second case the chains were able to equilibrate locally, as indicated by the white arrows in Figure 7.3, parts a and b (the latter image was taken from a film prepared from a 0.001 g/L solution). As in the case of PIC-Ni, an analysis of the thicknesses of the rods made it possible to identify intersections between two chains and segments consisting of intercoiled or tightly packed chains, besides individual chains on mica with a height of ca. 0.8 nm (Figure 7.3).

Figure 7.2 displays SFM images of isolated PIC chains prepared by a nickel(II)-catalyzed polymerization reaction (PIC-Ni). The chains exhibit cross sections that typically are constant along their whole lengths. The fact that the ends and the middle sections of the chains are equal suggests in particular that they consist of single strands. The apparent thickness of the chains, which amounts to  $0.30 \pm 0.06$  nm, is lower than the diameter of the PIC rod which was calculated to be 1.58 nm [90]. The apparent height reduction is a common phenomenon in SFM experiments of single molecules (see the discussion in section 3.1.3). A careful analysis of the images in Figure 7.2 allowed us to distinguish two different types of features with larger thicknesses: (i) intersections between two chains, as indicated by white arrows and (ii) segments consisting of two chains tightly packed one on the top of each other, as marked with black arrows. In both cases, the thicknesses were approximately 1.6-2.0 times those of the single chains. In the second case, the limits in the spatial resolution of the SFM due to the tip convolution did not permit a distinction between segments consisting of chains that are packed one on top of each other and segments composed of intercoiled strands.

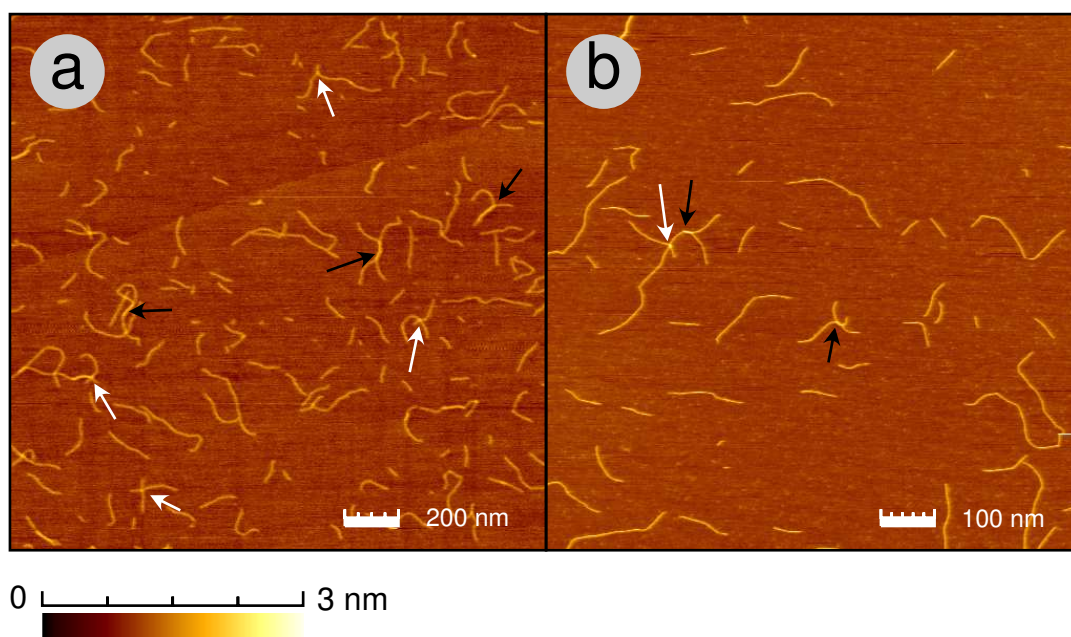


Figure 7.2: SFM images of a PIC-Ni sample. Film prepared from a chloroform solution containing (a) 0.01 and (b) 0.001 g/L of PIC-Ni. White arrows indicate intersections of separate chains and black ones mark segments consisting of intercoiled chains.

### 7.3.2 Contour length

The quantitative determination of the contour lengths ( $L_c$ ) of isolated polymer chains from SFM images 7.2 allows one to quantify the molar mass distribution of a polymer [365]. The distribution of  $L_c$  for the PIC-Ni samples is shown in Figure 7.4. The average contour length was found to be  $\langle L_c \rangle = 70 \pm 3$  nm, which corresponds to a number-average molar mass of  $M_n = 118 \times 10^3$  g/mol. From the distribution the polydispersity was calculated to be  $M_w/M_n = 1.36 \pm 0.04$ , where  $M_w$  is the mass average molar mass. The longest measured polymer chain exhibited a contour length of ca. 220 nm. The polymer synthesized by the acid catalyzed polymerization reaction displayed a higher degree of polymerization. The analysis performed on isolated chains such as the ones in Figure 7.3b, although being limited to only a few tens of strands, revealed the very high value of  $\langle L_c \rangle = 5.3 \pm 1.3$   $\mu\text{m}$ , corresponding to  $M_n = 8.94 \times 10^6$  g/mol, and  $M_w/M_n = 1.35 \pm 0.7$ . In this case the contour length of the longest chain was found to be 12.7  $\mu\text{m}$  !

### 7.3.3 Persistence length

Following the procedure described in section 4.2.1 the persistence lengths for PIC-Ni and PIC-H were determined to be  $\ell_P = 76 \pm 6$  nm and  $\ell_P = 76 \pm 5$  nm, respectively. In the latter case, only chains which were not part of network were selected for the analysis. The agreement of their persistence lengths reflects the identical chemical structure of both polymers.

As a prerequisite for the employed procedure to determine  $\ell_P$  it is important to confirm that chains are adsorbed in a thermodynamic equilibrium conformation. It was found for DNA adsorbed onto mica, that chains could be either in a kinetically trapped 3D-conformation or a conformation that is in a 2D equilibrium. In the former case, the observed structures resemble the projection on the surface of the conformations attained in solution and reflect the history of the approach of the molecules to the surface. In the latter case the molecules are allowed to search among their accessible states in two dimensions before they are captured in a particular 2D-conformation. Only for the latter the WLC can be assumed. Therefore, for our type of investigation it is crucial to be able to differentiate between trapped 3D-conformations and macromolecules equilibrated in quasi 2D. In the present case, this identification was done using two different approaches. In the following part, the data regarding the PIC-Ni samples are presented.

First, according to Ref. [379] the average segment-segment distance  $\langle R \rangle$  of a chain equilibrated in 2D on a surface can be described by

$$\langle R_{2D-EQ}^2 \rangle = 4\ell_P \ell \left( 1 - \frac{2\ell_P}{\ell} \left( 1 - \exp\left(-\frac{\ell}{2\ell_P}\right) \right) \right)$$

whereas for 3D-chains trapped on the surface

$$\langle R_{2D-TRAPPED}^2 \rangle = \frac{4}{3}\ell_P \left( 1 - \frac{\ell_P}{\ell} \left( 1 - \exp\left(-\frac{\ell}{2\ell_P}\right) \right) \right).$$

In Figure 7.5  $\langle R \rangle$  vs.  $\ell$  are plotted for these two functions using the experimentally determined value for  $\ell_P = 76 \pm 6$  nm. A good agreement between the experimental data and the calculated curve representing the equilibrated chains in 2D is observed in the range from  $\ell = 0$  nm to  $\ell = 50$  nm. For higher  $\ell$  values, due to the low number of data points, the evolution of  $\langle R \rangle = f(\ell)$  is characterized by larger fluctuations. Nevertheless, a reasonably good agreement between the theoretical curve for the equilibrated chains in 2D



and the experimental results is still evident. This not only proves that the chains are equilibrated on the surface, but also represents an independent verification of the determined  $\ell_P$ , according to the wormlike chain model.

Alternatively, in Figure 7.6 the orientation correlation function is plotted. A good agreement of the experimental data to  $\exp(-\ell/2\ell_P)$  is obtained, indicating that the conformations can be described by the WLC-model.

The two crosschecks described above provide the evidence that PIC-Ni chains are equilibrated on the surface up to a length scale of about 100 nm. PIC-H are obviously not worm-like, at least on larger scale. The agreement of the persistence lengths however indicates a local equilibration on the length scale which was used for the determination of  $\ell_P$  (about 10 nm). Moreover, it is important to note that none of the samples exhibited a preferential orientation of the adsorbed chains with respect to the 3-fold symmetry of the mica substrate. This determination, which has been accomplished by sampling the orientation of each vectorized segment relative to a fixed coordinate system in the given SFM image, revealed a random distribution of the orientations.

### 7.3.4 Conclusions

We have shown that the recently developed polymers of isocyanodipeptides are extraordinarily stiff macromolecules. To determine the persistence length of synthetic macromolecules, alternatively to the more indirect scattering methods employed in solutions, we have exploited a new versatile method based on SFM visualization of the conformation of isolated macromolecules equilibrated in quasi 2D on a surface. The measured persistence length amounts to  $76 \pm 6$  nm, which is more than 1 order of magnitude larger than the persistence length determined in solutions for a simpler PIC, namely poly( $\alpha$ -phenylethylisocyanide) [166]. This indicates that the hydrogen-bonded networks in the side chains of the polymers stabilize the overall polymer structure in line with previous physicochemical studies [90]. Among single chain synthetic polymers the stiffness of our PICs indeed is very high: it is comparable to the one quantified in solutions for poly( $\gamma$ -benzyl- $\alpha$ ,L-glutamate) for which a persistence lengths of  $\ell_P = 70$  nm was reported [195], and it is higher than other polymers that are considered to be very rigid, e.g., hyperbranched or dendronized polymers that exhibited a  $\ell_P = 50$  nm [350]. Remarkably, our polymer exhibits a persistence length that is even 50% larger than that of dsDNA [379]. Further physicochemical investigations on these extraordinar-

ily stiff macromolecules appear feasible, such as mechano-chemical studies on the elasticity of the chains, which can also be carried out with scanning force spectroscopy [374, 63, 129, 196] or studies using optical tweezers [64].

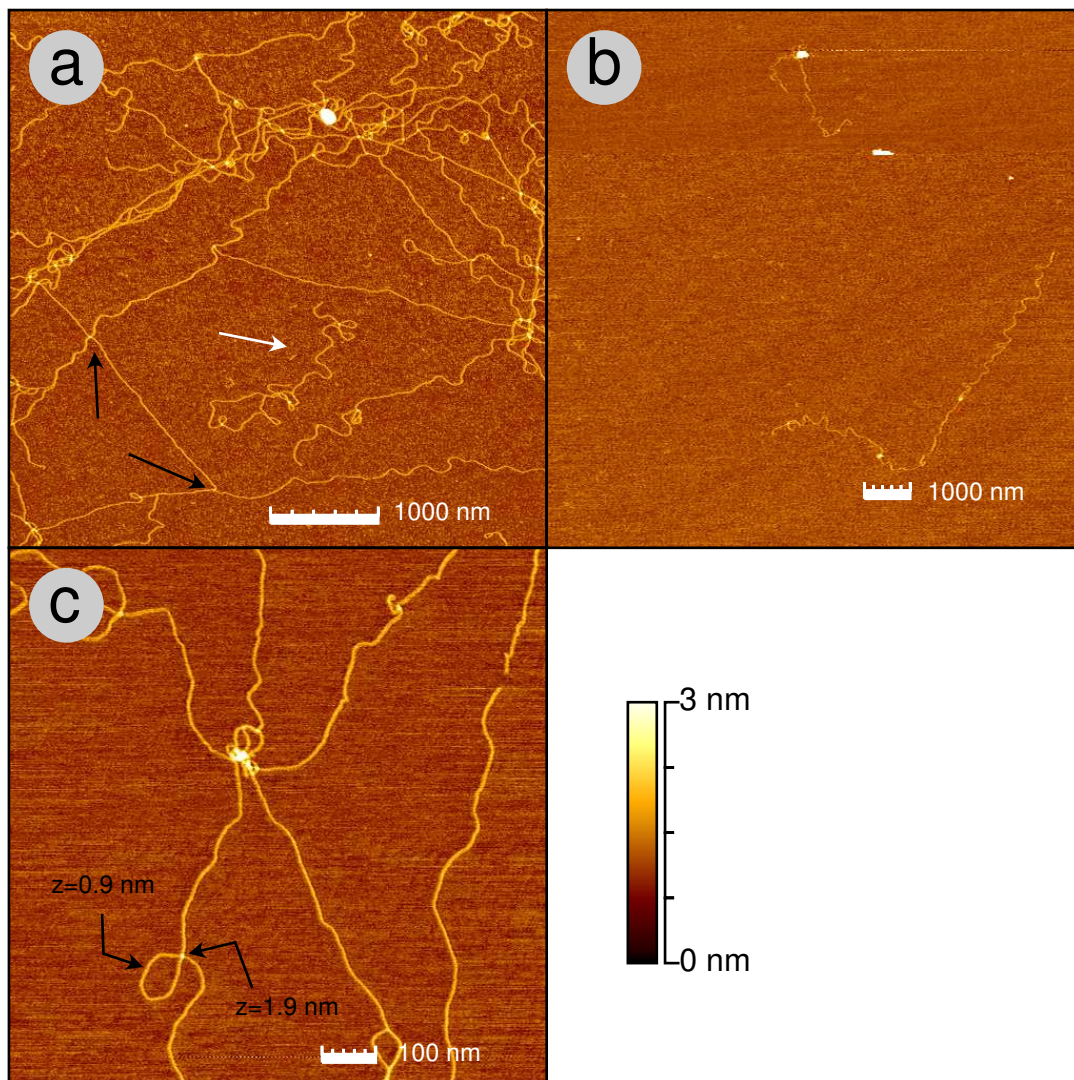


Figure 7.3: SFM images of PIC-H. (a) Sample prepared from an 0.01 g/L polymer solution in  $\text{CHCl}_3$  revealing the coexistence of relaxed chains (indicated by the white arrow) and tightened ones (entanglements at the edges are marked with black arrows). (b, c) Spin-coated films prepared from 0.001 g/L polymer solutions in  $\text{CHCl}_3$  in which isolated chains can be seen. (c) Zoom-in on chain intersections (bottom left) and on wrapped chains (top right). Whereas in the first case the observed thickness is twice that of a single chain, in the latter case this thickness is less than the double value.

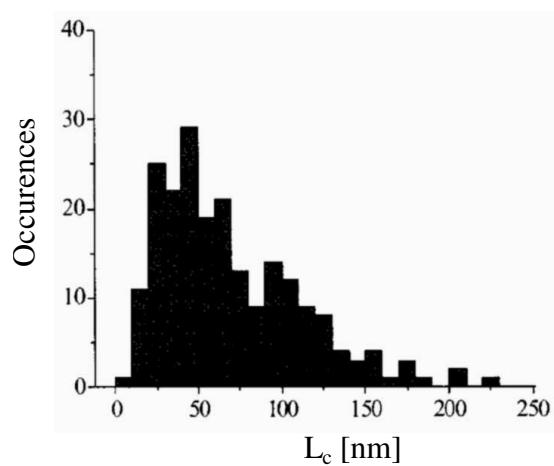


Figure 7.4: Histograms of the distribution of contour lengths obtained from SFM images of PIC-Ni.

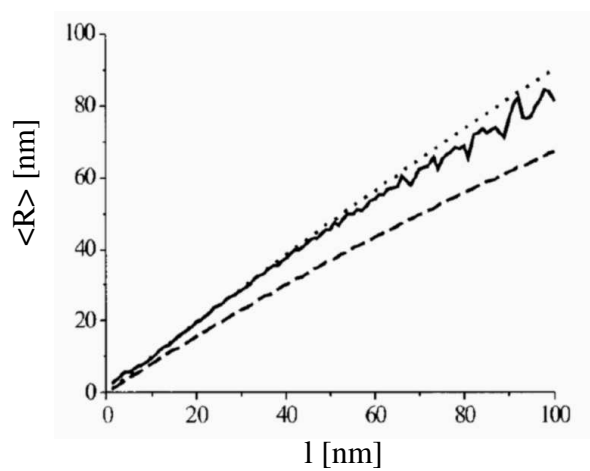


Figure 7.5: Evolution of the segment-segment distance vs. length along the contour. Theoretical function for 2D equilibrated chains (dotted line), 2D trapped chains (dashed line) and experimental results (filled line).

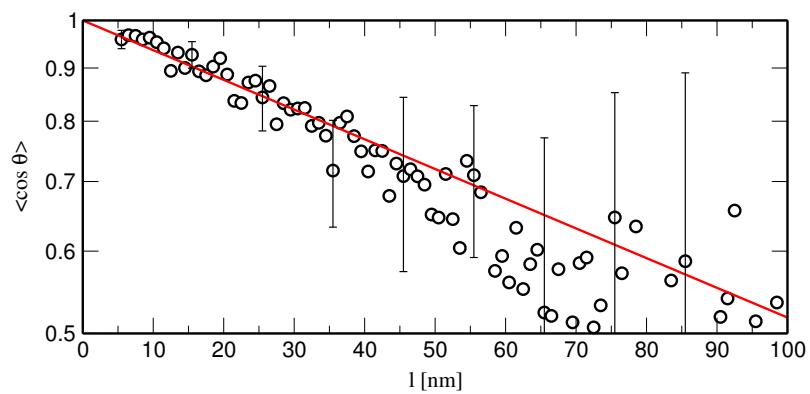


Figure 7.6: Orientation correlation: measurement (circles) and the ideal WLC (line) for  $\ell_p=76$  nm.

# Chapter 8

## Manipulation: Glassy state of single dendronized polymer chains

This chapter appeared in similar form as:

C. Ecker, N. Severin, L.J. Shu, A.D. Schlüter, and J.P. Rabe:

**Glassy state of single dendronized polymer chains**

*Macromolecules* 37 (7): 2484-2489 2004.

### 8.1 Introduction

Dendrimers are regular and highly branched macromolecules with a globular shape. Their large size and surface makes them ideal for applications as containers (e.g. for drug delivery [283]), carriers (e.g. for gene transfection [79]), light-harvestors [3], and building blocks for nanotechnology. Dendronized polymers [403, 515] are a new class of comb polymers whose backbones carry dendrons (dendritic wedges) at each repeat unit (see Fig. 8.1). In opposition

to their great potential for applications [403, 161] are considerable synthetic difficulties. Only recently a successful synthesis of a polystyrene with fourth generation dendrons at every repeat unit was reported [436].

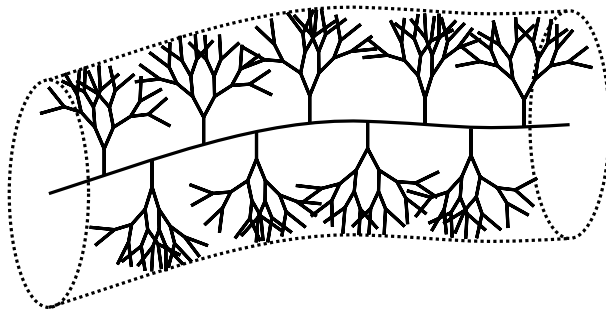


Figure 8.1: Schematic illustration of a fourth generation dendronized polymer.

Thus far only a few experimental studies on dendronized polymers are published using e.g., small angle neutron scattering (SANS) [135, 346] and scanning force microscopy (SFM) [161, 436, 452, 453, 365, 364, 366]. Little is known about the mechanical properties of their single chains. It was found by SANS [135, 346] that dendronized polymers of generation two can be described by the worm-like chain (WLC) model [247] which can be derived from the bending elasticity of a macroscopic rod [258]. Furthermore, the persistence length, which is a measure of chain stiffness in the WLC model, was found to increase with the generation number [135, 346]. Qualitatively similar results were obtained for polymers with linear side chains [504, 262].

The trend of these findings cannot continue to arbitrarily high generation numbers as can be seen from a basic argument: unlike linear side chains, dendrons become more bulky with increasing molar mass. Since the distance between two consecutive dendrons along the polymer backbone is fixed, this leads to a tighter packing of the dendrons and possibly an increased overlap between neighboring dendrons. For high generation numbers chain bending therefore requires rearrangements in the dendritic shell. This links the flexibility of the whole polymer chain directly to the mobility of the dendrons, giving rise to effects such as viscoelasticity and plasticity which go beyond the description of the WLC model.

These effects should be strongly solvent dependent. Despite the debate whether dendrons are back-folded or not [57, 382], theoretical [430], numerical [321, 170, 302] and experimental [476, 448, 98] studies agree that the

size of the dendron is dependent on the solvent quality and becomes smaller in a bad solvent. In a compact configuration, the contact between branches is enhanced and the free volume available for branch movement is reduced and consequently steric effects increased. In the extreme, when dendrons are in the glassy state [456, 302] conformational changes of the polymer chain should be inhibited. Using the most widely accepted definition of the glass transition as a kinetic arrest upon cooling one can describe the single molecule as being in the glassy state. This yet purely hypothetical state would not only be a new and interesting property of a new class of materials, but also might be useful for applications. It would allow to freeze the conformation of a polymer chain just by changing the temperature. For applications it might be interesting to be able to switch between ductile and rigid behavior of single chains.

In this chapter we investigate the mechanical properties of dendronized polymers with the aim of verifying the existence of the glassy state. We use SFM as a tool for imaging and nanomanipulation of individual dendronized polystyrenes of generation one to four adsorbed onto graphite surfaces. We study the influence of temperature and solvent on chain conformation and flexibility.

## 8.2 Experimental procedures

The molecules were deposited by spin coating from dilute THF solutions onto freshly cleaved highly oriented pyrolytic graphite (HOPG) at 50 rps. The surface density of adsorbed molecules was varied from closed films to isolated molecules by varying the concentration of the spin coated solution between 10 mg/l and 100 mg/l. Annealing was carried out both in air and in solution. In the latter case the HOPG sample was removed from the sample puck, put in a closed flask, filled with the solvent, and treated at 60°C.

Scanning Force Microscopy was carried out at room temperature in air, using silicon cantilevers (Olympus) with a resonance frequency of about 300 kHz and a force constant of 42 N/m. All measurements were taken in the tapping mode. Image backgrounds were removed using the first order quantile method described in section 4.1.1. No further image enhancement was applied. Nanomanipulation was performed in the lithography mode, moving the tip with 200 nm/s while applying a force of 1.6  $\mu$ N to the substrate [436].



In order to investigate the orientation of the adsorbed molecules with respect to the substrate crystal axes, the same position was scanned twice, first with molecular resolution in the tapping mode and then with atomic resolution in the contact mode. To find exactly the same position on the sample, images were recorded in the tapping mode while stepwise zooming out to  $80\ \mu\text{m}$  scan size. After replacing the tip by a contact mode cantilever (force constant  $0.4\ \text{N/m}$ , Digital Instruments), it was stepwise zoomed in, using the graphite steps of the previous images as a guide.

## 8.3 Results and discussion

### Conformations of adsorbed molecules as prepared

SFM images of single and clustered molecules of **g1** to **g4** and of **a-g1** to **a-g4** are shown in Fig. 8.2 and 8.3. Some images show artifacts (horizontal stripes, fuzziness) indicating movement of molecules. Stable imaging for **g1** and **g2** was only possible for molecules which are packed in clusters, while isolated molecules could not be resolved. For **g3** and **g4**, on the other hand, the molecules appear quite stable, and diffusion of shorter fragments was observed only occasionally. The alkylated molecules appeared generally more stable compared to their non-alkylated analogues. By scanning a single molecule of **a-g2** several times and varying the time between successive images we found that the molecular motion is much enhanced upon scanning, i. e. it is induced by the hammering of the SFM tip.

Additionally to isolated molecules, we found for most samples regions of dense molecular packing as shown for example in Fig. 8.2d for **g4**. This packing can be attributed to an interplay between attractive (e.g. van der Waals forces and capillary forces upon drying) and repulsive forces (entropy loss of dendrons due to volume exclusion)[246, 276]. Measuring the separation over several molecules in an ordered array (see e.g., the circled area in Fig. 8.2d) allows the precise determination of the width  $w$  of a molecule, while the apparent width of an isolated molecule in an SFM image is broadened by the finite sized tip. Widths and heights as determined by the SFM are given for all molecules in Table 8.1.

In good solvents dendronized polymers are assumed to exhibit a circular cross

molecule	$w$ [nm]	$h$ [nm]	molecule	$w$ [nm]	$h$ [nm]
<b>g1</b>	$3.0\pm 0.3$	$0.74\pm 0.1$	<b>a-g1</b>	$6.1\pm 0.3$	$1.2\pm 0.2$
<b>g2</b>	$3.8\pm 0.5$	$1.8\pm 0.1$	<b>a-g2</b>	$6.8\pm 0.3$	$2.0\pm 0.2$
<b>g3</b>	$7.4\pm 0.6$	$2.1\pm 0.2$	<b>a-g3</b>	$8.2\pm 0.3$	$2.5\pm 0.2$
<b>g4</b>	$7.3\pm 0.6$	$2.4\pm 0.2$	<b>a-g4</b>	$8.8\pm 0.3$	$4.7\pm 0.3$

Table 8.1: Measured widths  $w$  and apparent heights  $h$  for all investigated molecules.

section which was measured by SANS for **g1** and **g2** in methanol to be 3.8 nm and 4.9 nm, respectively [135]. These values are slightly larger than the widths obtained here, indicating that the dendrons at the surface may be not fully stretched out.

M. Mansfield [296] performed MD simulations of dendrimers at attracting surfaces. It was found that low generation dendrimers flatten at the interface in order to maximize the contact area. First generation dendronized polymers can thus be expected to be in a flattened conformation. The local shape of **g4**, on the other hand, should be nearly cylindrical following from a simple geometrical argument: Assuming that each repeat unit fills a cylindrical slice where the thickness is given by the length of the repeat unit, and assuming a reasonable density of  $\rho \simeq 1 \text{ g ml}^{-1}$ , one obtains a diameter of 8.2 nm. This value is in fair agreement to the width determined from ordered structures. In other words, **g4** and in a similar manner **a-g4** rather tightly fill the accessible space and therefore cannot be flattened much.

Heights of single molecules are usually underestimated in SFM measurements, possibly due to different deformation of substrate and molecule by the tip as discussed in section 3.1.3. Interestingly, heights are not constant along the contour of a single molecule as is shown later for a **g4** molecule. Typical height variations for **g4** are about 0.4 nm on a length of 20 nm.

We rule out chemical imperfections like missing dendrons as explanation, since each step in the synthesis was quantified by UV-markers, stating a chemical perfection of 97 % for **g4** [436]. Instead, height variations might be explained by an irregular distribution of dendrons around the backbone.

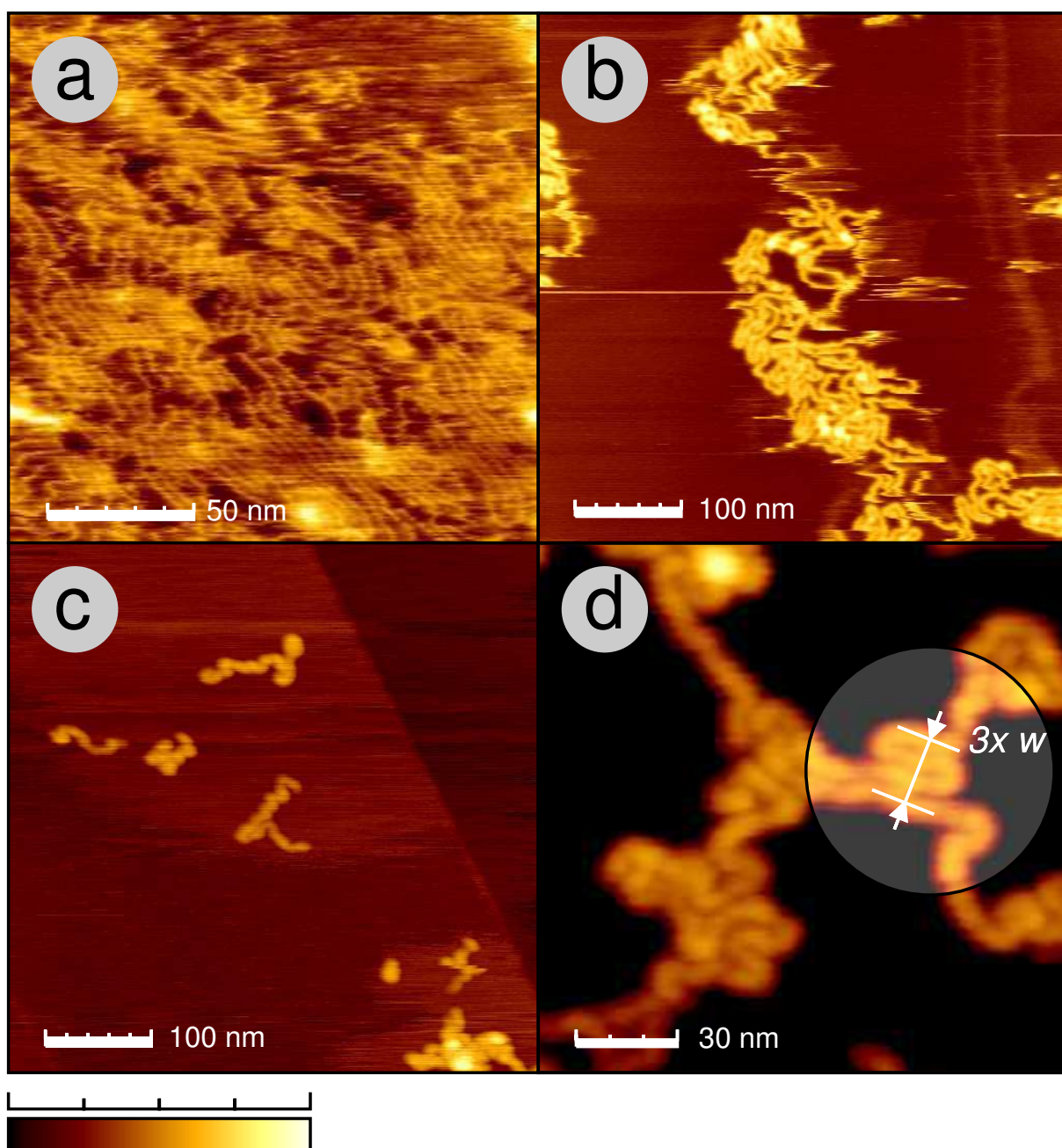


Figure 8.2: Typical SFM images of **g1** (a), **g2** (b), **g3** (c), and **g4** (d) on HOPG. The  $z$ -range is 2 nm, 4 nm, 6 nm, and 8 nm, respectively. Since **g1** and **g2** are rather mobile on the substrate the images show artifacts caused by movement of molecules. In this case stable imaging was only possible for aggregated chains. Molecular widths are determined by measuring the separation over several molecules as shown in the circle in (d).

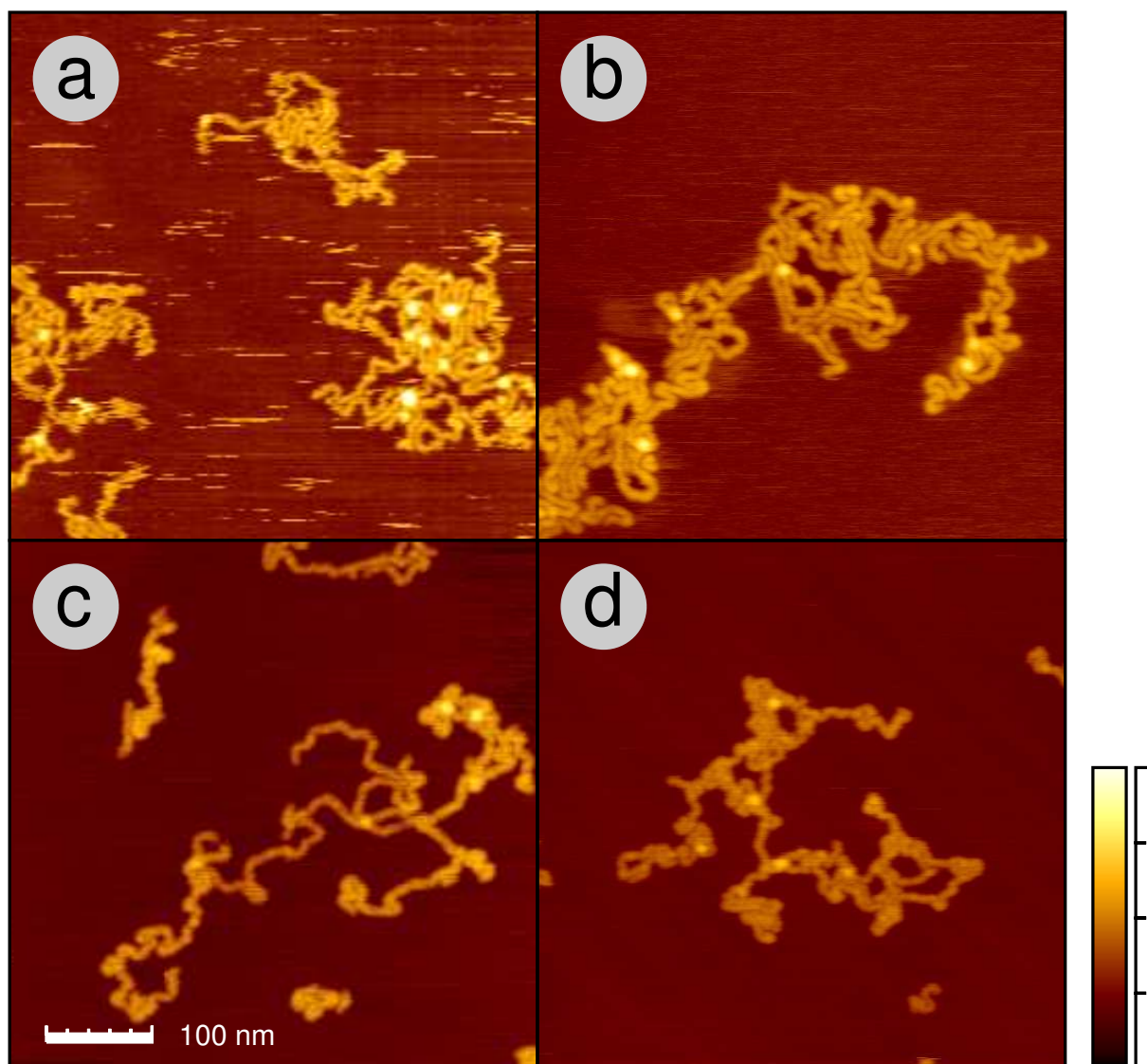


Figure 8.3: SFM images,(a) to (d), of alkyated samples **a-g1** to **a-g4** on HOPG. The  $z$ -range is 4 nm, 6 nm, 8 nm, and 10 nm for **a-g1** to **a-g4**, respectively.

## Annealing

Dendronized polymers spin coated onto HOPG were annealed in THF at 60°C for 30 minutes. As the SFM images show, molecules are not washed off by the treatment, but changed their conformation. Fig. 8.4a displays an image of **a-g4** after annealing. The molecules are aligned parallel to the substrate and bent at characteristic angles of 60° and 120° in order to follow the 3-fold symmetry of the substrate. The same annealing procedure was applied to **a-g4** samples in air, water and in THF at room temperature but no ordering was observed. However, **a-g1** could be oriented by heating in air (see figure 8.4b). For the non-alkylated molecules (**g1** to **g4**) we did not observe any orientation effect.

The inset of Fig. 8.4b displays an image of the graphite lattice taken at the same position. The polymers are oriented perpendicular (with an uncertainty of  $\pm 2^\circ$ ) to the graphite zigzag axis. The observed backbone orientations are, therefore, consistent with the alkyl chains following the zigzag axis of the graphite substrate as sketched in Fig. 8.4c. The observed backbone orientation differs by 30° from the one assumed in Ref. [426] for a related polymer.

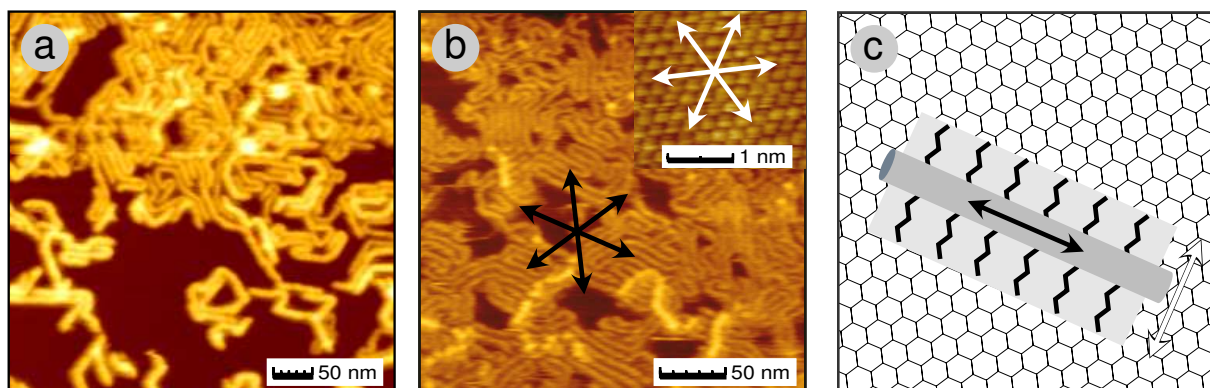


Figure 8.4: Orientation of chains and underlying graphite lattice. (a) oriented **a-g4**. (b) oriented **a-g1** and graphite lattice measured at the same positions. The black and white rosettes are rotated by 90° showing that the polymers are oriented perpendicular to the zigzag axes. (c) schematic view of the orientation of the dendronized polymer backbone (grey) and the orientation of those alkyl side chains directly in contact with the surface.

Ordering of alkanes along the zigzag axis is known from STM studies [371]

and the alignment of polymers with alkylated side groups has been observed before [366, 393]. The driving force for the molecular orientation is, therefore, assumed to be the specific interaction of alkyl chains and the graphite surface. The observed irreversibility can be understood if the chains in air are trapped in their conformation on the time scale of the measurement. Besides this trapped state in air at room temperature, also a state must exist, which allows full chain relaxation within 30 minutes.

In principle the trapping can be caused either by the interaction to the substrate or be inherent to the molecules. Since the interaction and also the chain thickness is different between **a-g1** and **a-g4**, it is not possible to distinguish between both influences from only this experiment.

## Manipulation of single molecules

The mechanical properties of macroscopic materials are commonly characterized by bending, stretching, shear, or compression experiments. Similar experiments can be performed by applying forces to single molecules using the tip of an SFM [436, 31]. In Fig. 8.5 a molecule of **a-g4** is shown before and after it is manipulated by moving the tip along the marked path in the left image. Interestingly, the molecule moved as a whole and the

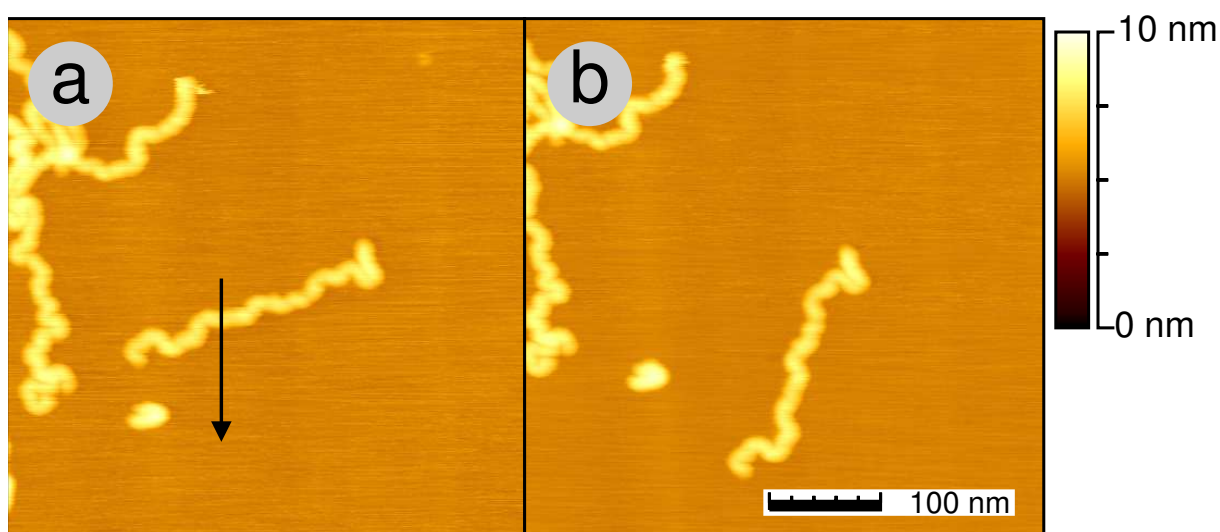


Figure 8.5: Nanomanipulation of a single **a-g4** molecule from (a) to (b). The manipulation path is marked by the arrow. The lateral shape of the contour is clearly preserved.

molecular shape was preserved, except for one kink near the right hand terminus. This experiment shows that it is not the immobility on the substrate causing the shape persistence. If the molecule would be trapped because of strong frictional forces to the substrate the chain would have been deformed upon manipulation because the pushing tip and the opposed frictional forces. Hence the trapping is an inherent property of the polymer chain.

Besides this shape persistence in 2D upon applying lateral forces, a persistence of the height structure can also be observed. In Fig. 8.7 a series of images is presented describing the manipulation of a **g4** molecule. Unlike the alkylated analogue it gets deformed. The molecule unfolds its hairpin “a” in Fig. 8.7 and changes its shape upon manipulation, similarly to a macroscopic wire. Only the hairpin “b” at the molecules’ “head” does not open. In

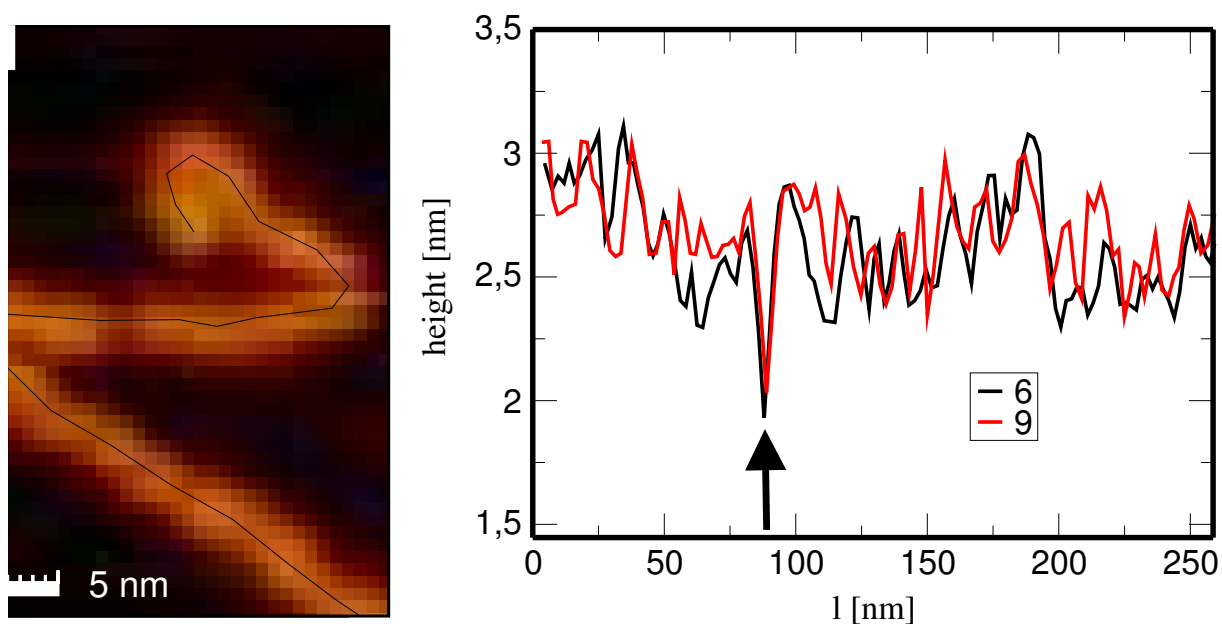


Figure 8.6: Height along the contour for the manipulated **g4** molecule, for images 6 and 9 from the sequence. Left: zoom of image 9 showing the line at which the height was recorded. The arrow marks a characteristic nick which can be found in all the images of this molecule. Right: height structure for images 6 and 9. The height scale starts from 0 at the substrate surface. Besides some noise, both curves show a clear correlation of characteristic features. The arrow gives the position of the nick.

Fig. 8.6 the height along the molecular backbone starting from the “head” is plotted for images 6 and 9 of the manipulation sequence. Despite the background noise, there is a clear correlation of characteristic features. The most distinctive feature observed in all these molecules’ images is a characteristic nick which is marked with an arrow. Since dendrons are only connected at the backbone, in a liquid state they would be free to float and change conformation. The preservation of height features indicates that the dendron shell around the backbone is not liquid-like. Thus also for **g4** a shape persistence can be stated, though laterally less distinct compared to **a-g4**.

Figure 8.8 displays a manipulation sequence of an **a-g3** macromolecule from an oriented sample. During the manipulation the molecule is stretched, bent, and finally compressed. Once manipulated the chain segments loose their alignment with respect to the substrate axes. During the experiment no relaxation back to an oriented state was observed. Image 3 was recorded twice



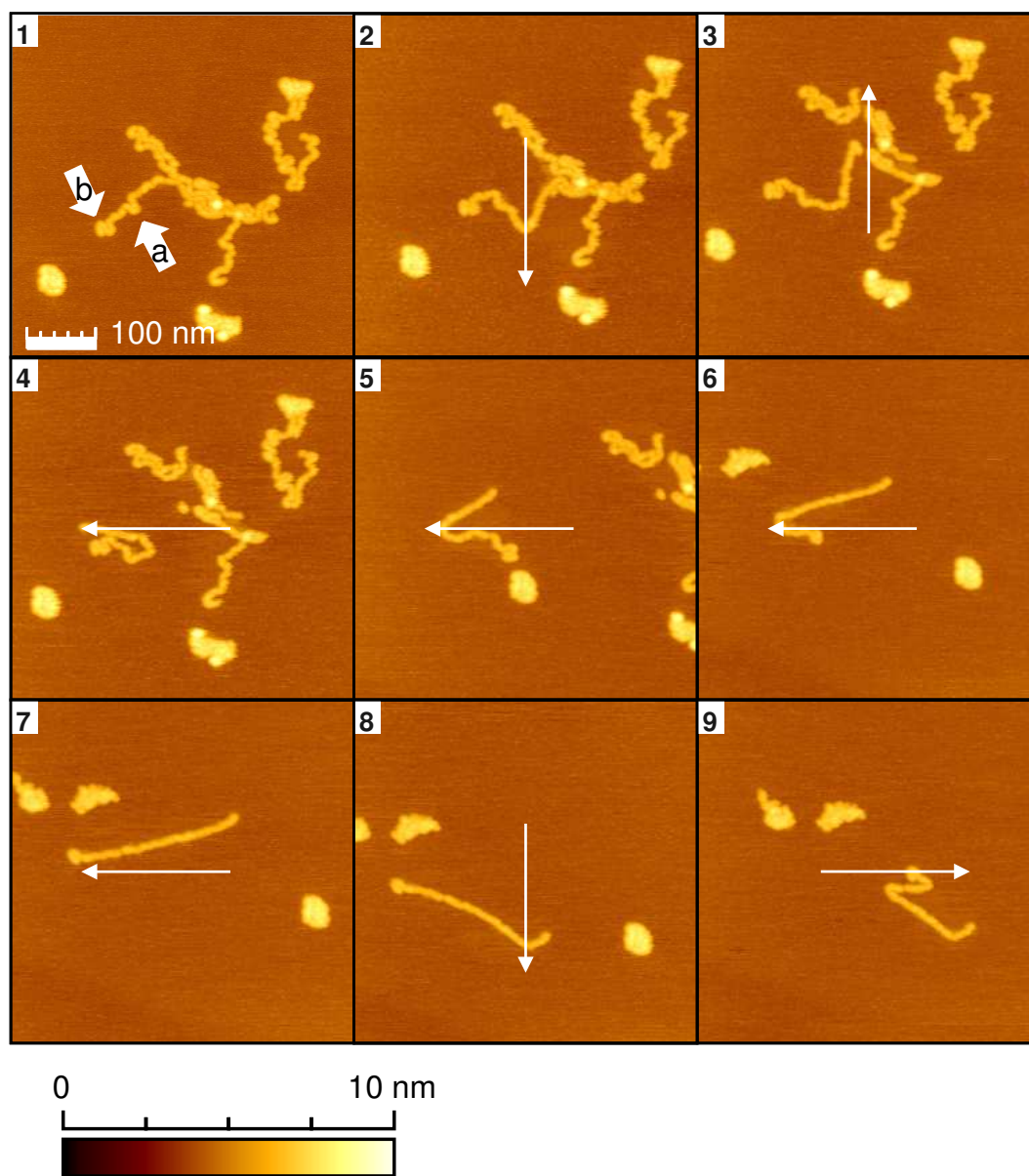


Figure 8.7: Manipulation sequence of a **g4** molecule. From 1 to 2 the hairpin (a) opens, whereas the “head” (b) does not change upon manipulation all the way from 1 to 9.

with a time lag of 30 minutes without any notable change in the conformation.

The analysis of the positions of kinks displayed in Fig. 8.9 gives an interest-

ing hint on the origin of the shape persistence. The segment orientation  $\Theta$  relative to the horizontal is measured and plotted. The kinks appear to be at the same positions in both images, marked with letters a to f. At positions a and d the sign of the curvature  $\frac{d\Theta(\ell)}{d\ell}$  changed sign. The appearance of kinks at the same positions is unlikely to be an accidental coincidence, but is rather attributed to weak locations. The simplest explanation would be, that the molecule is thinner at these positions and therefore less rigid. However, there is no correlation between the height structure and the kink positions. Another explanation is that the weak positions are formed during drying and cooling.

The presented manipulation experiments show, that there is an inherent rigidity of at least **a-g3** and **a-g4** against lateral deformation. This result is in agreement with the idea of a glassy state of the dendrons which leads via the steric hindrance of neighboring dendrons to a freezing of the whole chain. From our experiments it is not possible to exclude alternative explanations as for example the crystallization of terminal alkyl chains. Both explanations do lead to a shape persistence and additionally allow the interpretation of weak positions as inhomogeneities in the dendritic hull which are frozen in. However, the glassy state model is also consistent with the horizontal shape persistence observed for the non-alkylated molecules **g3** and **g4**.

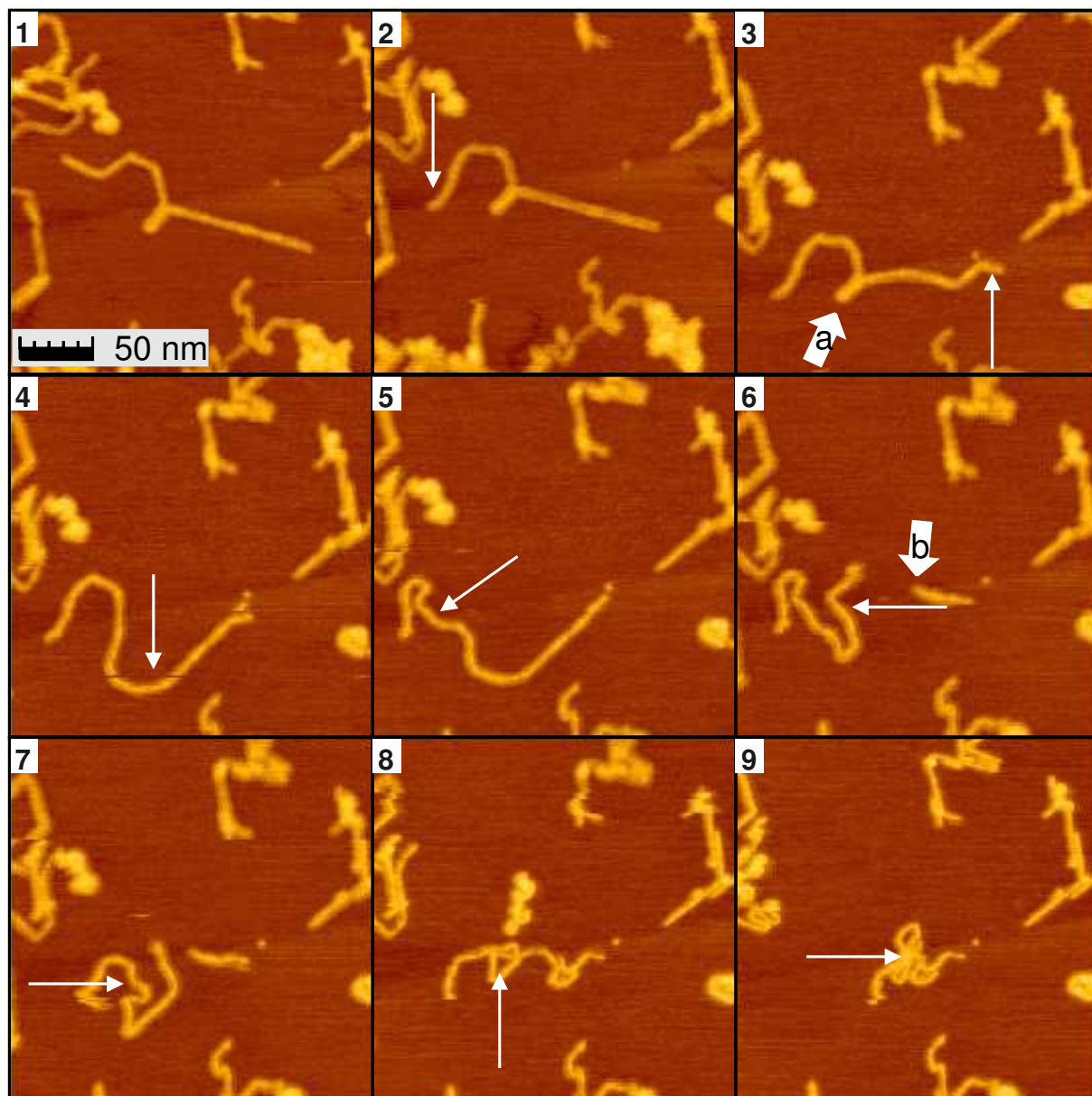


Figure 8.8: Manipulation sequence of an oriented **a-g3** molecule. The sample was annealed in THF as described in the text. Interesting is the opening of the hairpin (3 to 4, mark a) and the cutting (5 to 6, mark b). Image 3 was recorded twice with a time lag of 30 minutes, without a notable change of conformation.

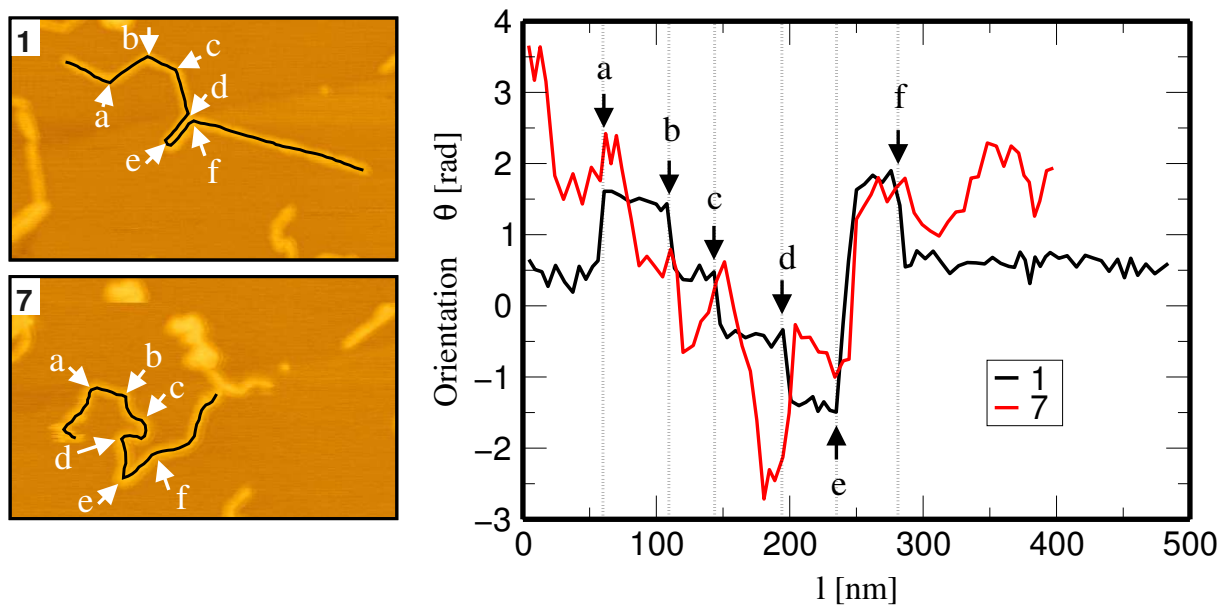


Figure 8.9: Orientation as a function of position along the contour for the manipulated **a-g3** molecule.  $\Theta$  is the angle between the tangent in point  $\ell$  to the horizontal. In both images the kinks are at the same positions, marked with a to f. At positions a and d the sign of the curvature changed sign.

## 8.4 Summary and Conclusion

In summary, we presented experiments demonstrating that there is a shape persistence of dendronized polymer chains and further experiments to clarify the physical origin. Particularly, we probed the shape persistence effect directly by nanomanipulating single polymer chains adsorbed onto graphite substrates at room temperature and in air. We found for all chains of higher generation (3 and 4) that there is a shape persistence. The effect appeared clearer for molecules which are decorated with alkyl chains, but was also observable for the non-alkylated chains. We showed by annealing experiments that the shape persistence further depends on the number of branching generations and on the solvent quality. We interpret the shape persistence as a single molecule glass state which is caused by the glassification of dendrons.

We believe that the switchable single polymer glass state is an interesting new property and might be useful for single molecule experiments as well as for applications. For example we have been able to image the surface of a thick layer of **a-g4** with sub molecular resolution, allowing to identify the conformation of the single chains. The glassy state might be also useful when dendronized polymer chains are used as building blocks in nanotechnology applications, since it allows to give single molecules a defined and stable shape.

# Bibliography

- [1] N. I. Abu-Lail and T. A. Camesano. Elasticity of pseudomonas putida kt2442 surface polymers probed with single-molecule force microscopy. *Langmuir*, 18:4071–4081, 2002.
- [2] D. B. Adolf, A. V. Lyulin, and G. R. Davies. Computer simulation of dendrimers and hyperbranched polymers. *Abstr. Pap. Am. Chem. Soc.*, 222:264–PMSE, 2001.
- [3] A. Adronov and J. M. J. Fréchet. Light-harvesting dendrimers. *Chem. Commun.*, pages 1701–1710, 2000.
- [4] A. Adronov, S. L. Gilat, J. M. J. Fréchet, K. Ohta, F. V. R. Neuwahl, and G. R. Fleming. Light harvesting and energy transfer in laser-dye-labeled poly(aryl ether) dendrimers. *J. Am. Chem. Soc.*, 122:1175–1185, 2000.
- [5] T. R. Albrecht, P. Grütter, D. Horne, and D. Rugar. Frequency modulation detection using high-q cantilevers for enhanced force microscope sensitivity. *J. Appl. Phys.*, 69(2):668–673, 1991.
- [6] D. B. Amabilino, E. Ramos, J. L. Serrano, T. Sierra, and J. Veciana. Long-range chiral induction in chemical systems with helical organization. promesogenic monomers in the formation of poly(isocyanide)s and in the organization of liquid crystals. *J. Am. Chem. Soc.*, 120:9126–9134, 1998.
- [7] B. Anczykowski, J. P. Cleveland, D. Kruger, V. Elings, and H. Fuchs. Analysis of the interaction mechanisms in dynamic mode sfm by means of experimental data and computer simulation. *Appl. Phys. A-Mater. Sci. Process.*, 66:S885–S889, 1998.
- [8] D. Andelman and J. F. Joanny. Polyelectrolyte adsorption. *C. R. Acad. Sci. Ser. IV-Phys. Astrophys.*, 1:1153–1162, 2000.

- [9] D. Appelhans, H. Komber, D. Voigt, L. Haussler, and B. I. Voit. Synthesis and characterization of poly(ether amide) dendrimers containing different core molecules. *Macromolecules*, 33:9494–9503, 2000.
- [10] G. Ariel and D. Andelman. Persistence length of a strongly charged rodlike polyelectrolyte in the presence of salt. *Phys. Rev. E*, 67:art. no.–011805, 2003.
- [11] J. B. Avalos, J. F. Joanny, A. Johner, and A. N. Semenov. Equilibrium interaction between adsorbed polymer layers. *Europhys. Lett.*, 35:97–102, 1996.
- [12] J. B. Avalos, A. Johner, and J. F. Joanny. Bridging by adsorbed polymers between 2 surfaces. *J. Chem. Phys.*, 101:9181–9194, 1994.
- [13] J. Rädler B. Maier. Conformation of single DNA molecules confined to two dimensions. *Phys. Rev. Lett.*, 82(9):1911–1914, 1999.
- [14] S. C. Bae, F. Xie, S. Jeon, and S. Granick. Single isolated macromolecules at surfaces. *Curr. Opin. Solid State Mat. Sci.*, 5:327–332, 2001.
- [15] M. Ballauff. Structure of dendrimers in dilute solution. *Top. Curr. Chem.*, 212:177–194, 2001.
- [16] E. Balnois, S. Stoll, K. J. Wilkinson, J. Buffle, M. Rinaudo, and M. Milas. Conformations of succinoglycan as observed by atomic force microscopy. *Macromolecules*, 33:7440–7447, 2000.
- [17] E. Balnois, S. Stoll, K.J. Wilkinson, J. Buffle, M. Rinaudo, and M. Milas. Conformations of succinoglycan as observed by atomic force microscopy. *Macromolecules*, 33:7440–7447, 2000.
- [18] E. Balnois and K. J. Wilkinson. Sample preparation techniques for the observation of environmental biopolymers by atomic force microscopy. *Colloid Surf. A-Physicochem. Eng. Asp.*, 207:229–242, 2002.
- [19] L. Balogh, D. A. Tomalia, and G. L. Hagnauer. A revolution of nanoscale proportions. *Chem. Innov.*, 30:19–26, 2000.
- [20] V. Balzani, P. Ceroni, S. Gestermann, M. Gorka, C. Kauffmann, and F. Vogtle. Fluorescent guests hosted in fluorescent dendrimers. *Tetrahedron*, 58:629–637, 2002.

- [21] G. Bar, R. Brandsch, M. Bruch, L. Delineau, and M. H. Whangbo. Examination of the relationship between phase shift and energy dissipation in tapping mode atomic force microscopy by frequency-sweep and force-probe measurements. *Surf. Sci.*, 444:L11–L16, 2000.
- [22] G. Bar, L. Delineau, R. Brandsch, M. Bruch, and M. H. Whangbo. Importance of the indentation depth in tapping-mode atomic force microscopy study of compliant materials. *Appl. Phys. Lett.*, 75:4198–4200, 1999.
- [23] G. Bar, L. Delineau, R. Brandsch, and M. H. Whangbo. Tapping mode atomic force microscopy study of elastomers: Dynamics of tip-sample interaction. *Abstr. Pap. Am. Chem. Soc.*, 220:278–POLY, 2000.
- [24] L. Barbieri, P. Valbonesi, F. Righi, G. Zuccheri, F. Monti, P. Gorini, B. Samorí, and F. Stirpe. Polynucleotide : adenosine glycosidase is the sole activity of ribosome-inactivating proteins on DNA. *J. Biochem. (Tokyo)*, 128:883–889, 2000.
- [25] S. Bardon, M. P. Valignat, A. M. Cazabat, W. Stocker, and J. P. Rabe. Study of liquid crystal prewetting films by atomic force microscopy in tapping mode. *Langmuir*, 14:2916–2924, 1998.
- [26] C. Barentin and J. F. Joanny. Surface pressure of adsorbed polymer layers. effect of sticking chain ends. *Langmuir*, 15:1802–1811, 1999.
- [27] C. Barentin, P. Müller, and J. F. Joanny. Polymer brushes formed by end-capped poly(ethylene oxide) (peo) at the air-water interface. *Macromolecules*, 31:2198–2211, 1998.
- [28] C. Barentin, P. Müller, C. Ybert, J. F. Joanny, and J. M. di Meglio. Shear viscosity of polymer and surfactant monolayers. *Eur. Phys. J. E*, 2:153–159, 2000.
- [29] C. Barentin, C. Ybert, J. M. di Meglio, and J. F. Joanny. Surface shear viscosity of gibbs and langmuir monolayers. *J. Fluid Mech.*, 397:331–349, 1999.
- [30] M. Barna, T. Merghoub, J. A. Costoya, D. Ruggero, M. Branford, A. Bergia, B. Samorí, and P. P. Pandolfi. Plzf mediates transcriptional repression of *hoxd* gene expression through chromatin remodeling. *Dev. Cell*, 3:499–510, 2002.



- [31] J. Barner. *Dissertation (in preparation)*. PhD thesis, Humboldt-Universität zu Berlin, 2004.
- [32] J. L. Barrat and J. F. Joanny. Interacting rigid polyelectrolytes. *J. Phys. II*, 4:1089–1102, 1994.
- [33] J. L. Barrat and J. F. Joanny. Theory of polyelectrolyte solutions. *Advan Chem Physics*, 94:1–66, 1996.
- [34] J. Baschnagel, A. Johner, and J. F. Joanny. Adsorption of a bidisperse polymer mixture onto a flat wall. *Phys. Rev. E*, 55:3072–3086, 1997.
- [35] J. Baschnagel, A. Johner, and J. F. Joanny. Adsorption kinetics of a bidisperse polymer solution. *Eur. Phys. J. B*, 6:45–55, 1998.
- [36] J. Baschnagel, C. Mischler, and K. Binder. Dynamics of confined polymer melts: Recent monte carlo simulation results. *J. Phys. IV*, 10:9–14, 2000.
- [37] B. J. Bauer, A. Topp, D. A. Tomalia, and E. J. Amis. Effect of solvent quality on the molecular dimensions of pamam dendrimers. *Abstr. Pap. Am. Chem. Soc.*, 216:139–PMSE, 1998.
- [38] C. Baur, A. Bugacov, B.E. Koel, A. Madhukar, N. Montoya, T. R. Ramachandran, A.A.G. Requicha, R. Resch, and P. Will. Nanoparticle manipulation by mechanical pushing: underlying phenomena and real-time monitoring. *Nanotechnology*, 9:360–364, 1998.
- [39] N. Becker, E. Oroudjev, S. Mutz, J. P. Cleveland, P. K. Hansma, C. Y. Hayashi, D. E. Makarov, and H. G. Hansma. Molecular nanosprings in spider capture-silk threads. *Nat. Mater.*, 2:278–283, 2003.
- [40] O. P. Behrend, L. Odoni, J. L. Loubet, and N. A. Burnham. Phase imaging: Deep or superficial? *Appl. Phys. Lett.*, 75:2551–2553, 1999.
- [41] O. P. Behrend, F. Oulevey, D. Gourdon, E. Dupas, A. J. Kulik, G. Gremaud, and N. A. Burnham. Intermittent contact: tapping or hammering? *Appl. Phys. A-Mater. Sci. Process.*, 66:S219–S221, 1998.
- [42] H. Benoit, J. E. Joanny, B. Hammouda, and M. Kosmas. Large-angle neutron-scattering by polymer networks. *Abstr. Pap. Am. Chem. Soc.*, 208:375–PMSE, 1994.

- [43] J. Berg and G. A. D. Briggs. Nonlinear dynamics of intermittent-contact mode atomic force microscopy. *Phys. Rev. B*, 55:14899–14908, 1997.
- [44] T. A. Betley, J. A. Hessler, A. Mecke, M. M. B. Holl, B. G. Orr, S. Uppuluri, D. A. Tomalia, and J. R. Baker. Tapping mode atomic force microscopy investigation of poly(amidoamine) core-shell tecto(dendrimers) using carbon nanoprobcs. *Langmuir*, 18:3127–3133, 2002.
- [45] T. A. Betley, M. M. B. Holl, B. G. Orr, D. R. Swanson, D. A. Tomalia, and J. R. Baker. Tapping mode atomic force microscopy investigation of poly(amidoamine) dendrimers: Effects of substrate and ph on dendrimer deformation. *Langmuir*, 17:2768–2773, 2001.
- [46] H. Bielefeldt and F. J. Giessibl. A simplified but intuitive analytical model for intermittent-contact-mode force microscopy based on Hertzian mechanics. *Surf. Science*, 440:L863–L867, 1999.
- [47] K. Binder, J. Baschnagel, and W. Paul. Glass transition of polymer melts: test of theoretical concepts by computer simulation. *Prog. Polym. Sci.*, 28:115–172, 2003.
- [48] K. Binder, A. Milchev, and J. Baschnagel. Simulation studies on the dynamics of polymers at interfaces. *Annu. Rev. Mater. Sci.*, 26:107–134, 1996.
- [49] G. Binnig, C. F. Quate, and Ch. Gerber. Atomic force microscope. *Phys. Rev. Lett.*, 56(9):930–933, 1986.
- [50] G. Binnig, H. Rohrer, Ch. Gerber, and E. Weibel. Surface studies by scanning tunneling microscopy. *Phys. Rev. Lett.*, 49(1):57–61, 1982.
- [51] V. Blobel and E. Lohrmann. *Statistische und numerische Methoden der Datenanalyse*. B. G. Teubner, Stuttgart, 1998.
- [52] Z. S. Bo, J. P. Rabe, and A. D. Schlüter. A poly(para-phenylene) with hydrophobic and hydrophilic dendrons: Prototype of an amphiphilic cylinder with the potential to segregate lengthwise. *Angew. Chem.-Int. Edit.*, 38:2370–2372, 1999.
- [53] Z. S. Bo, C. M. Zhang, N. Severin, J. P. Rabe, and A. D. Schlüter. Synthesis of amphiphilic poly(p-phenylene)s with pendant dendrons and linear chains. *Macromolecules*, 33:2688–2694, 2000.

- [54] Zhishan Bo, Jürgen P. Rabe, and A. Dieter Schlüter. *Angew. Chem. Int. Ed.*, 38:2370–2372, 1999.
- [55] D. T. Bong, T. D. Clark, J. R. Granja, and M. R. Ghadiri. Self-assembling organic nanotubes. *Angew. Chem.-Int. Edit.*, 40:988–1011, 2001.
- [56] O. V. Borisov, F. Hakem, T. A. Vilgis, J. F. Joanny, and A. Johner. Adsorption of hydrophobic polyelectrolytes onto oppositely charged surfaces. *Eur. Phys. J. E*, 6:37–47, 2001.
- [57] A.W. Bosman, H.M. Janssen, and E.W. Meijer. About dendrimers: structure, physical properties and applications. *Chem. Rev.*, 99:1665–1688, 1999.
- [58] C. Böttcher, H. Stark, and M. van Heel. Stacked bilayer helices: A new structural organisation of amphiphilic molecules. *Ultramicroscopy*, 62:133–139, 1996.
- [59] N. A. Burnham. Instabilities in dynamic force curves. *Abstr. Pap. Am. Chem. Soc.*, 224:060–COLL, 2002.
- [60] N. A. Burnham, S. P. Baker, and H. M. Pollock. Model for mechanical properties nanoprobe. *J. Mater. Res.*, 15:2006–2014, 2000.
- [61] N. A. Burnham, O. P. Behrend, F. Oulevey, G. Gremaud, P. J. Gallo, D. Gourdon, E. Dupas, A. J. Kulik, H. M. Pollock, and G. A. D. Briggs. How does a tip tap? *Nanotechnology*, 8:67–75, 1997.
- [62] S. V. Bushin, N. V. Girbasova, E. V. Belyaeva, M. A. Bezrukova, L. N. Andreeva, and A. Y. Bilibin. Hydrodynamic, optical, and conformational properties of acrylic polymers bearing side dendrons. *Polym. Sci. Ser. A*, 44:632–639, 2002.
- [63] C. Bustamante, J. C. Macosko, and G. J. L. Wuite. Grabbing the cat by the tail: Manipulating molecules one by one. *Nat. Rev. Mol. Cell Biol.*, 1:130–136, 2000.
- [64] C. Bustamante, S. B. Smith, J. Liphardt, and D. Smith. Single-molecule studies of DNA mechanics. *Curr. Opin. Struct. Biol.*, 10:279–285, 2000.
- [65] C. Bustamante, G. Zuccheri, S. H. Leuba, G. L. Yang, and B. Samorí. Visualization and analysis of chromatin by scanning force microscopy. *Methods*, 12:73–83, 1997.

- [66] Y. Bustanji and B. Samorí. The mechanical properties of human angiotensin can be modulated by means of its disulfide bonds: A single-molecule forcespectroscopy study. *Angew. Chem.-Int. Edit.*, 41:1546–1548, 2002.
- [67] T. A. Camesano and K. J. Wilkinson. Single molecule study of xanthan conformation using atomic force microscopy. *Biomacromolecules*, 2:1184–1191, 2001.
- [68] J. L. Casson, H. L. Wang, J. B. Roberts, A. N. Parikh, J. M. Robinson, and M. S. Johal. Kinetics and interpenetration of ionically self-assembled dendrimer and pazo multilayers. *J. Phys. Chem. B*, 106:1697–1702, 2002.
- [69] M. Castelnovo and J. F. Joanny. Formation of polyelectrolyte multilayers. *Langmuir*, 16:7524–7532, 2000.
- [70] M. Castelnovo and J. F. Joanny. Complexation between oppositely charged polyelectrolytes: Beyond the random phase approximation. *Eur. Phys. J. E*, 6:377–386, 2001.
- [71] M. Castelnovo and J. F. Joanny. Phase diagram of diblock polyampholyte solutions. *Macromolecules*, 35:4531–4538, 2002.
- [72] M. Castelnovo, P. Sens, and J. F. Joanny. Charge distribution on annealed polyelectrolytes. *Eur. Phys. J. E*, 1:115–125, 2000.
- [73] T. Charitat and J. F. Joanny. Solid-like friction of a polymer chain. *Eur. Phys. J. E*, 3:369–376, 2000.
- [74] X. Chatellier and J. F. Joanny. Adsorption of polyelectrolyte solutions on surfaces: A debyehuckel theory. *J. Phys. II*, 6:1669–1686, 1996.
- [75] X. Chatellier and J. F. Joanny. Pull-off of a polyelectrolyte chain from an oppositely charged surface. *Phys. Rev. E*, 57:6923–6935, 1998.
- [76] X. Chatellier and J. F. Joanny. Adsorption of a gaussian random copolymer chain at an interface. *Eur. Phys. J. E*, 1:9–25, 2000.
- [77] X. Chatellier, T. J. Senden, J. F. Joanny, and J. M. di Meglio. Detachment of a single polyelectrolyte chain adsorbed on a charged surface. *Europhys. Lett.*, 41:303–308, 1998.

- [78] J. Chen, R. K. Workman, D. Sarid, and R. Hoper. Numerical simulations of a scanning force microscope with a large-amplitude vibrating cantilever. *Nanotechnology*, 5:199–204, 1994.
- [79] W. Chen, N. J. Turro, and D. A. Tomalia. Using ethidium bromide to probe the interactions between DNA and dendrimers. *Langmuir*, 16:15–19, 2000.
- [80] X. Chen, C. J. Roberts, J. Zhang, M. C. Davies, and S. J. B. Tendler. Phase contrast and attraction-repulsion transition in tapping mode atomic force microscopy. *Surf. Sci.*, 519:L593–L598, 2002.
- [81] L. A. J. Chrisstoffels, A. Adronov, and J. M. J. Fréchet. Surface-confined light harvesting, energy transfer, and amplification of fluorescence emission in chromophore-labeled self-assembled monolayers. *Angew. Chem.-Int. Edit.*, 39:2163–+, 2000.
- [82] F. Clement, T. Charitat, A. Johner, and J. F. Joanny. Self-assembled layers under flow: Stabilization by chain end exchange. *Europhys. Lett.*, 54:65–71, 2001.
- [83] F. Clement and J. F. Joanny. Curvature elasticity of an adsorbed polymer layer. *J. Phys. II*, 7:973–980, 1997.
- [84] F. Clement, A. Johner, J. F. Joanny, and A. N. Semenov. Stress relaxation in telechelic gels. 1. sticker extraction. *Macromolecules*, 33:6148–6158, 2000.
- [85] M. Clericuzio, G. Alagona, C. Ghio, and P. Salvadori. Theoretical investigations on the structure of poly(iminomethylenes) with aliphatic side chains. conformational studies and comparison with experimental spectroscopic data. *J. Am. Chem. Soc.*, 119:1059–1071, 1997.
- [86] J. P. Cleveland, B. Anczykowski, A. E. Schmid, and V. B. Elings. Energy dissipation in tapping-mode atomic force microscopy. *Appl. Phys. Lett.*, 72:2613–2615, 1998.
- [87] C. C. Co, P. Cotts, S. Burauer, R. de Vries, and E. W. Kaler. Microemulsion polymerization. 3. molecular weight and particle size distributions. *Macromolecules*, 34:3245–3254, 2001.
- [88] M. Conti, G. Donati, G. Cianciolo, S. Stefoni, and B. Samorí. Force spectroscopy study of the adhesion of plasma proteins to the surface of a dialysis membrane: Role of the nanoscale surface hydrophobicity and topography. *J. Biomed. Mater. Res.*, 61:370–379, 2002.

- [89] M. Conti, G. Falini, and B. Samorí. How strong is the coordination bond between a histidine tag and ni-nitrilotriacetate? an experiment of mechanochemistry on single molecules. *Angew. Chem.-Int. Edit.*, 39:215–+, 2000.
- [90] J. J. L. M. Cornelissen, J. J. J. M. Donners, R. de Gelder, W. S. Graswinckel, G. A. Metselaar, A. E. Rowan, N. A. J. M. Sommerdijk, and R. J. M. Nolte. Beta-helical polymers from isocyanopeptides. *Science*, 293:676–680, 2001.
- [91] J. J. L. M. Cornelissen, A. E. Rowan, R. J. M. Nolte, and N. A. J. M. Sommerdijk. Chiral architectures from macromolecular building blocks. *Chem. Rev.*, 101:4039–4070, 2001.
- [92] J. J. L. M. Cornelissen, N. A. J. M. Sommerdijk, and R. J. M. Nolte. Determination of the helical sense in alanine based polyisocyanides. *Macromol. Chem. Phys.*, 203:1625–1630, 2002.
- [93] F. S. Csajka, R. R. Netz, C. Seidel, and J. F. Joanny. Collapse of polyelectrolyte brushes: Scaling theory and simulations. *Eur. Phys. J. E*, 4:505–513, 2001.
- [94] G. L. Cui, Y. Xu, M. Z. Liu, T. Ji, Y. M. Chen, and Y. F. Li. Highly ordered assemblies of dendritic molecules bearing multihydrophilic head groups. *Macromol. Rapid Commun.*, 20:71–76, 1999.
- [95] S. X. Cui, C. J. Liu, and X. Zhang. Simple method to isolate single polymer chains for the direct measurement of the desorption force. *Nano Lett.*, 3:245–248, 2003.
- [96] D.M. Czajkowski and Z. Shao. Inhibition of protein adsorption to muscovite mica by monovalent ions. *J. Microscopy*, 211(1):1–7, 2003.
- [97] Michel Daune. *Molekulare Biophysik*. Vieweg, 1997.
- [98] S. De Backer, Y. Prinzie, W. Verheijen, M. Smet, K. Desmedt, W. Dehaen, and F. C. De Schryver. Solvent dependence of the hydrodynamical volume of dendrimers with a rubicene core. *J. Phys. Chem. A*, 102:5451–5455, 1998.
- [99] V. M. De Cupere and P. G. Rouxhet. Surface crystallization of poly(ethylene terephthalate) studied by atomic force microscopy. *Polymer*, 43:5571–5576, 2002.

- [100] P.-G. De Gennes. *Scaling concepts in polymer science*. Cornell University Press, 1979.
- [101] D. A. P. Delnoye, R. P. Sijbesma, J. A. J. M. Vekemans, and E. W. Meijer. Pi-conjugated oligomers and polymers with a self-assembled ladder-like structure. *J. Am. Chem. Soc.*, 118:8717–8718, 1996.
- [102] Digital Instruments, Inc., 112 Robin Hill Road, Santa Barbara, California 93117, USA. *MultiMode Scanning Probe Microscope Instruction Manual*, 4.31ce edition.
- [103] R. Djalali, S. Y. Li, and M. Schmidt. Amphipolar core-shell cylindrical brushes as templates for the formation of gold clusters and nanowires. *Macromolecules*, 35:4282–4288, 2002.
- [104] A. V. Dobrynin, M. Rubinstein, and J. F. Joanny. Adsorption of a polyampholyte chain on a charged surface. *Macromolecules*, 30:4332–4341, 1997.
- [105] A. V. Dobrynin, M. Rubinstein, and J. F. Joanny. Polyampholyte solutions between charged surfaces: Debye-huckel theory. *J. Chem. Phys.*, 109:9172–9176, 1998.
- [106] A. V. Dobrynin, M. Rubinstein, and S. Obukhov. *Macromolecules*, 29:2674–2979, 1996.
- [107] M. Doi. *Introduction to polymer physics*. Clarendon Press, Oxford, 1995.
- [108] J. J. J. M. Donners, R. J. M. Nolte, and N. A. J. M. Sommerdijk. A shape-persistent polymeric crystallization template for caco3. *J. Am. Chem. Soc.*, 124:9700–9701, 2002.
- [109] J. F. Douglas, H. M. Schneider, P. Frantz, R. Lipman, and Granick S. The origin and characterization of conformational heterogeneity in adsorbed polymer layers. *J. Phys. Cond. Mat.*, 9(37):7699–7718, 1997.
- [110] C. J. Durning, B. O’Shaughnessy, U. Sawhney, D. Nguyen, J. Majewski, and G. S. Smith. Adsorption of poly(methyl methacrylate) melts on quartz. *Macromolecules*, 32:6772–6781, 1999.
- [111] G. Duve, O. Fuchs, and H. Overbeck. *Lösungsmittel Hoechst*. Hoechst Aktiengesellschaft, 1976. 6. Auflage.
- [112] G. Ebert. *Biopolymere*. Teubner, Stuttgart, 1993.

- [113] C. Ecker, M. Baenitz, K. Luders, E. S. Otabe, T. Matsushita, H. R. Khan, and E. V. Antipov. Orientation dependence of irreversible magnetic properties in Hg-based superconducting ceramics. *Physica B*, 284:905–906, 2000.
- [114] C. Ecker, N. Severin, L. J. Shu, A. D. Schlüter, and J. P. Rabe. Glassy state of single dendronized polymer chains. *Macromolecules*, 37:2484–2489, 2004.
- [115] C. J. Ellison, S. D. Kim, D. B. Hall, and J. M. Torkelson. Confinement and processing effects on glass transition temperature and physical aging in ultrathin polymer films: Novel fluorescence measurements. *Eur. Phys. J. E*, 8:155–166, 2002.
- [116] R. Esfand and D. A. Tomalia. Poly(amidoamine) (pamam) dendrimers: from biomimicry to drug delivery and biomedical applications. *Drug Discov. Today*, 6:427–436, 2001.
- [117] W. Essafi, F. Lufama, and C. E. Williams. *J. Phys. II*, 5:1269, 1275, 1995.
- [118] P. G. Khalatur et al. Unusual conformation of molecular cylindrical brushes strongly adsorbed on a flat solid surface. *Eur. Phys. J. E*, 1(1):99–103, 2000.
- [119] R. Everaers, A. Johner, and J. F. Joanny. Complexation and precipitation in polyampholyte solutions. *Europhys. Lett.*, 37:275–280, 1997.
- [120] G. Evmenenko, B. J. Bauer, R. Kleppinger, B. Forier, W. Dehaen, E. J. Amis, N. Mischenko, and H. Reynaers. The influence of molecular architecture and solvent type on the size and structure of poly(benzyl ether) dendrimers by SANS. *Macromol. Chem. Phys.*, 202:891–899, 2001.
- [121] S. C. Fain, K.A. Berry, M.G. Bush, B.Pittenger, and R.N. Louie. Measuring average tip-sample forces in intermittent-contact (tapping) force microscopy in air. *Appl. Phys. Lett.*, 76(7):930–932, 2000.
- [122] Y. Fang and J. H. Hoh. Early intermediates in spermidine-induced DNA condensation on the surface of mica. *J. Am. Chem. Soc.*, 120:8903–8909, 1998.
- [123] Y. Fang, T. S. Spisz, and J.H. Hoh. Ethanol-induced structural transitions of DNA on mica. *Nucleic Acid Research*, 27(8):1943–1949, 1999.



- [124] R. Festag. How big is a molecule? *Macromol. Chem. Phys.*, 198:3317–3318, 1997.
- [125] R. Festag, S. D. Alexandratos, K. D. Cook, D. C. Joy, B. Annis, and B. Wunderlich. Single- and few-chain polystyrene particles by electrospray. *Macromolecules*, 30:6238–6242, 1997.
- [126] G. H. Findenegg and M. Liphard. Adsorption from solution of large alkane and related molecules onto graphitized carbon. *Carbon*, 25:119–128, 1987.
- [127] H. Fischer and H. Kaul. *Mathematik für Physiker*. B. G. Teubner, Stuttgart, 1990.
- [128] K. Fischer and M. Schmidt. Solvent-induced length variation of cylindrical brushes. *Macromol. Rapid Commun.*, 22:787–791, 2001.
- [129] T. E. Fisher, P. E. Marszalek, and J. M. Fernandez. Stretching single molecules into novel conformations using the atomic force microscope. *Nat. Struct. Biol.*, 7:719–724, 2000.
- [130] G.J. Fleer, M.A. Cohen Stuart, J.M.H.M. Scheutjens, T. Cosgrove, and B. Vincent. *Polymers at Interfaces*. Kluwer Academic Publishers, Dordrecht, 1993.
- [131] E. Flikkema, A. Subbotin, and G. ten Brinke. Ring comb copolymer brushes. *J. Chem. Phys.*, 113:7646–7651, 2000.
- [132] E. Flikkema and G. ten Brinke. Influence of rigid side chain attraction on stiffness and conformations of comb copolymer brushes strongly adsorbed on a flat surface. *Macromol. Theory Simul.*, 11:777–784, 2002.
- [133] J. G. Forbes, A. J. Jin, and K. Wang. Atomic force microscope study of the effect of the immobilization substrate on the structure and force-extension curves of a multimeric protein. *Langmuir*, 17:3067–3075, 2001.
- [134] J. A. Forrest and J. Mattsson. Reductions of the glass transition temperature in thin polymer films: Probing the length scale of cooperative dynamics. *Phys. Rev. E*, 61:R53–R56, 2000.
- [135] S. Förster, I. Neubert, A. D. Schlüter, and P. Lindner. How dendrons stiffen polymer chains: A SANS study. *Macromolecules*, 32:4043–4049, 1999.

- [136] S. Förster and M. Schmidt. In *Adv. Poly. Sci.*, volume 120. Springer Verlag, Berlin, Heidelberg, 1995.
- [137] C. Frontali, E. Dore, A. Ferrauto, and E. Gratton. An absolute method for the determination of the persistence length of native DNA from electron micrographs. *Biopolymers*, 18:1353–1373, 1979.
- [138] G. Fuchs, K. A. Nenkov, A. Attenberger, K. Lüders, M. Baenitz, C. Ecker, K. Kajikawa, E. V. Antipov, and H. R. Khan. A uniform description of irreversibility lines for various high-T-c superconductors. *Physica C*, 355:299–306, 2001.
- [139] K. Fukao and Y. Miyamoto. Glass transitions and dynamics in thin polymer films: Dielectric relaxation of thin films of polystyrene. *Phys. Rev. E*, 61:1743–1754, 2000.
- [140] K. Fukao, S. B. Uno, Y. Miyamoto, A. Hoshino, and H. Miyaji. Relaxation dynamics in thin supported polymer films. *J. Non-Cryst. Solids*, 307:517–523, 2002.
- [141] R. Garcia, J. Tamayo, M. Calleja, and F. Garcia. Phase contrast in tapping-mode scanning force microscopy. *Appl. Phys. A-Mater. Sci. Process.*, 66:S309–S312, 1998.
- [142] R. Garcia, J. Tamayo, and A. San Paulo. Phase contrast and surface energy hysteresis in tapping mode scanning force microscopy. *Surf. Interface Anal.*, 27:312–316, 1999.
- [143] M. Gerle, M. Fischer, K. Schmidt, S. Roos, A.H.E. Müller, S.S. Sheiko, S.A. Prokhorova, and M. Möller. Main chain conformation and anomalous elution behaviour of cylindrical brushes by GPC/MALLS, light scattering and SFM. *Macromolecules*, 32:2629–2737, 1999.
- [144] A. Gesquiere, M. M. Abdel-Mottaleb, S. De Feyter, F. C. De Schryver, M. Sieffert, K. Müllen, A. Calderone, R. Lazzaroni, and J. L. Bredas. Dynamics in physisorbed monolayers of 5-alkoxy-isophthalic acid derivatives at the liquid/solid interface investigated by scanning tunneling microscopy. *Chem.-Eur. J.*, 6:3739–3746, 2000.
- [145] A. Gesquiere, M. M. S. Abdel-Mottaleb, S. De Feyter, F. C. De Schryver, F. Schoonbeek, J. van Esch, R. M. Kellogg, B. L. Feringa, A. Calderone, R. Lazzaroni, and J. L. Bredas. Molecular organization of bis-urea substituted thiophene derivatives at the liquid/solid interface

- studied by scanning tunneling microscopy. *Langmuir*, 16:10385–10391, 2000.
- [146] T. Gibtner, F. Hampel, J. P. Gisselbrecht, and A. Hirsch. End-cap stabilized oligoynes: Model compounds for the linear sp carbon allotrope carbyne. *Chem.-Eur. J.*, 8:408–432, 2002.
- [147] F. J. Giessibl. A direct method to calculate tip-sample forces from frequency shifts in frequency-modulation atomic force microscopy. *Appl. Phys. Lett.*, 78:123–125, 2001.
- [148] F. J. Giessibl. Advances in atomic force microscopy. *Rev. Modern Phys.*, 75:949–983, 2003.
- [149] F. J. Giessibl. Low-temperature AFM provides Hot paper. *Trac-trends In Analytical Chem.*, 22:IX–IX, 2003.
- [150] F. J. Giessibl, H. Bielefeldt, S. Hembacher, and J. Mannhart. Imaging of atomic orbitals with the Atomic Force Microscope - experiments and simulations. *Annalen Der Physik*, 10:887–910, 2001.
- [151] F. J. Giessibl, S. Hembacher, H. Bielefeldt, and J. Mannhart. Subatomic features on the silicon (111)-(7x7) surface observed by atomic force microscopy. *Science*, 289:422–425, 2000.
- [152] F. J. Giessibl, S. Hembacher, H. Bielefeldt, and J. Mannhart. Subatomic features on the silicon (111)-(7x7) surface observed by atomic force microscopy. *Science*, 289:422–425, 2000.
- [153] F. J. Giessibl, S. Hembacher, M. Herz, C. Schiller, and J. Mannhart. Stability considerations and implementation of cantilevers allowing dynamic force microscopy with optimal resolution: the qPlus sensor. *Nanotechnology*, 15:S79–S86, 2004.
- [154] F. J. Giessibl, M. Herz, and J. Mannhart. Friction traced to the single atom. *Proc. National Acad. Sciences United States Am.*, 99:12006–12010, 2002.
- [155] S. L. Gilat, A. Adronov, and J. M. J. Fréchet. Light harvesting and energy transfer in novel convergently constructed dendrimers. *Angew. Chem.-Int. Edit.*, 38:1422–1427, 1999.
- [156] J. K. Gimzewski and C. Joachim. Nanoscale science of single molecules using local probes. *Science*, 283:1683–1688, 1999.

- [157] F. Gittes, B. Mickey, J. Nettleton, and J. Howard. Flexural rigidity of microtubules and actin filaments measured from thermal fluctuations in shape. *Journal of Cell Biology*, pages 923–934, 1993.
- [158] T. Glauser, C. M. Stancik, M. Möller, S. Voytek, A. P. Gast, and J. L. Hedrick. Dendritic-linear miktoarm star polymers from orthogonal protected initiators. *Macromolecules*, 35:5774–5781, 2002.
- [159] P. Gleyzes, P.K. Kuo, and A.C. Boccaro. Bistable behavior of a vibrating tip near a solid-surface. *Appl. Phys. Lett.*, 58(25):2989, 2991 1991.
- [160] N. Godbert and M. R. Bryce. Molecular saddles - part 8: Highly-charged organic nanoparticles: redox-active dendrimers incorporating 9,10bis(1,3-dithiol-2-ylidene)-9,10-dihydroanthracene units. *J. Mater. Chem.*, 12:27–36, 2002.
- [161] I. Gössl, L. Shu, A.D. Schlüter, and J.P. Rabe. Molecular structure of single DNA complexes with positively charged dendronized polymers. *J. Am. Chem. Soc.*, 124:6860–6865, 2002.
- [162] I. Gossel, L. J. Shu, A. D. Schlüter, and J. P. Rabe. Molecular structure of single DNA complexes with positively charged dendronized polymers. *J. Am. Chem. Soc.*, 124:6860–6865, 2002.
- [163] G. Gottarelli, S. Masiero, E. Mezzina, S. Pieraccini, J. P. Rabe, P. Samorí, and G. P. Spada. The self-assembly of lipophilic guanosine derivatives in solution and on solid surfaces. *Chem.-Eur. J.*, 6:3242–3248, 2000.
- [164] S. Granick, A. Mukhopadhyah, S. Jeon, S. C. Bae, and J. Turner. Watching molecules under confinement and during sliding. *Abstr. Pap. Am. Chem. Soc.*, 223:245–PHYS, 2002.
- [165] S. K. Grayson and J. M. J. Fréchet. Convergent dendrons and dendrimers: from synthesis to applications. *Chem. Rev.*, 101:3819–3867, 2001.
- [166] M. M. Green, R. A. Gross, F. C. Schilling, K. Zero, and C. Crosby. Macromolecular stereochemistry: effect of pendant group structure on the conformational properties of polyisocyanides. *Macromolecules*, 21(6):1839–1846, 1988.

- [167] G. S. Grest, M. D. Lacasse, and M. Murat. Molecular-dynamics simulations of polymer surfaces and interfaces. *MRS Bull.*, 22:27–31, 1997.
- [168] A.Y. Grosberg and A.R. Khokhlov. *Statistical Physics of Macromolecules*. AIP Press, 1994.
- [169] S. W. Guo, L. Konopny, R. Popovitz-Biro, H. Cohen, H. Porteanu, E. Lifshitz, and M. Lahav. Thioalkanoates as site-directing nucleating centers for the preparation of patterns of CdS nanoparticles within 3-D crystals and LB films of Cd alkanoates. *J. Am. Chem. Soc.*, 121:9589–9598, 1999.
- [170] A. Gurtovenko, Y. Gotlib, and A. Blumen. Rouse dynamics of polymer networks bearing dendritic wedges. *Macromolecules*, 35:7481–7491, 2002.
- [171] B.-Y. Ha and D. Thirumalai. Persistence length of flexible polyelectrolyte chains. *JACS*, 110(15):2533–2541, 1999.
- [172] F. Hakem, A. Johner, and J. F. Joanny. Polymeric salts: Static and dynamic debye-huckel theory. *Macromolecules*, 31:8305–8311, 1998.
- [173] H. G. Hansma. Polysaccharide helices in the atomic-force microscope. *Biophys. J.*, 68:3–4, 1995.
- [174] H. G. Hansma. Surface biology of DNA by atomic force microscopy. *Annu. Rev. Phys. Chem.*, 52:71–92, 2001.
- [175] H. G. Hansma, K. J. Kim, D. E. Laney, R. A. Garcia, M. Argaman, M. J. Allen, and S. M. Parsons. Properties of biomolecules measured from atomic force microscope images: A review. *J. Struct. Biol.*, 119:99–108, 1997.
- [176] H. G. Hansma and D. E. Laney. DNA binding to mica correlates with cationic radius: Assay by atomic force microscopy. *Biophys. J.*, 70:1933–1939, 1996.
- [177] H. G. Hansma, L. I. Pietrasanta, I. D. Auerbach, C. Sorenson, R. Golan, and P. A. Holden. Probing biopolymers with the atomic force microscope: A review. *J. Biomater. Sci.-Polym. Ed.*, 11:675–683, 2000.
- [178] H. G. Hansma, L. I. Pietrasanta, R. Golan, J. C. Sitko, M. B. Viani, G. T. Paloczi, B. L. Smith, D. Thrower, and P. K. Hansma. Recent highlights from atomic force microscopy of DNA. *J. Biomol. Struct. Dyn.*, pages 271–275, 2000.

- [179] H.G. Hansma, D.E. Laney, M. Bezanilla, R.L. Sinsheimer, and P.K. Hansma. Applications for atomic-force microscopy of DNA. *Biophys. J.*, 68(5):1672–1677, 1995.
- [180] L. Hartmann, W. Gorbatschow, J. Hauwede, and F. Kremer. Molecular dynamics in thin films of isotactic poly(methyl methacrylate). *Eur. Phys. J. E*, 8:145–154, 2002.
- [181] S. Hembacher, F. J. Giessibl, and J. Mannhart. Evaluation of a force sensor based on a quartz tuning fork for operation at low temperatures and ultrahigh vacuum. *Appl. Surf. Science*, 188:445–449, 2002.
- [182] S. Hembacher, F. J. Giessibl, J. Mannhart, and C. F. Quate. Revealing the hidden atom in graphite by low-temperature atomic force microscopy. *Proc. National Acad. Sciences United States Am.*, 100:12539–12542, 2003.
- [183] S. Herminghaus, K. Jacobs, and R. Seemann. The glass transition of thin polymer films: some questions, and a possible answer. *Eur. Phys. J. E*, 5:531–538, 2001.
- [184] A. C. Hernandez and K. A. Fichthorn. Monte Carlo study of the static and dynamic behaviors of polymer chains near an adsorbent surface. *Int. J. Hydrog. Energy*, 26:1307–1313, 2001.
- [185] M. Herz, F. J. Giessibl, and J. Mannhart. Probing the shape of atoms in real space. *Phys. Rev. B*, 68, 2003.
- [186] Bernhard Herzog. <http://sketch.sourceforge.org>, 2002.
- [187] A. Hierlemann, J. K. Campbell, L. A. Baker, R. M. Crooks, and A. J. Ricco. Structural distortion of dendrimers on gold surfaces: A tapping-mode AFM investigation. *J. Am. Chem. Soc.*, 120(21):5323–5324, 1998.
- [188] J. H. K. K. Hirschberg, L. Brunsveld, A. Ramzi, J. A. J. M. Vekemans, R. P. Sijbesma, and E. W. Meijer. Helical self-assembled polymers from cooperative stacking of hydrogen-bonded pairs. *Nature*, 407:167–170, 2000.
- [189] V. Hlady and J. Buijs. Protein adsorption on solid surfaces. *Curr. Opin. Biotechnol.*, 7(1):72–77, 1996.
- [190] S. Hoger, K. Bonrad, S. Rosselli, A. D. Ramminger, T. Wagner, B. Silier, S. Wiegand, W. Haussler, G. Lieser, and V. Scheumann.

- Shape-persistent macrocycles: Building blocks for complex organic and polymeric architectures. *Macromol. Symp.*, 177:185–191, 2002.
- [191] T. Hugel, M. Grosholz, H. Clausen-Schaumann, A. Pfau, H. Gaub, and M. Seitz. Elasticity of single polyelectrolyte chains and their desorption from solid supports studied by AFM based single molecule force spectroscopy. *Macromolecules*, 34:1039–1047, 2001.
- [192] T. Hugel and M. Seitz. The study of molecular interactions by AFM force spectroscopy. *Macromol. Rapid Commun.*, 22:989–1016, 2001.
- [193] J. P. Hunt and D. Sarid. Kinetics of lossy grazing impact oscillators. *Appl. Phys. Lett.*, 72:2969–2971, 1998.
- [194] J. N. Israelachvili. *Intermolecular and Surface Forces*. Academic Press Ltd., 2nd ed. edition, 1985.
- [195] T. Jamil and P.S. Russo. Dynamic light scattering from a semiflexible polymer at very low concentrations. *J. Chem. Phys.*, 97:2777–2782, 1992.
- [196] A. Janshoff, M. Neitzert, Y. Oberdorfer, and H. Fuchs. Force spectroscopy of molecular systems - single molecule spectroscopy of polymers and biomolecules. *Angew. Chem.-Int. Edit.*, 39:3213–3237, 2000.
- [197] S. Jeon, S. C. Bae, and S. Granick. Local chain dynamics of adsorbed polystyrene studied by timeresolved fluorescence anisotropy. *Macromolecules*, 34:8401–8404, 2001.
- [198] X. L. Ji, J. Oh, A. K. Dunker, and K. W. Hipps. Effects of relative humidity and applied force on atomic force microscopy images of the filamentous phage fd. *Ultramicroscopy*, 72:165–176, 1998.
- [199] X. Q. Jiang, K. Tanaka, A. Sakai, A. Takahara, and T. Kajiyama. Surface relaxation behavior of proton- and perfluoroalkylterminated poly(2-vinylpyridine) films. *Polymer*, 42:8959–8964, 2001.
- [200] X. Q. Jiang, C. Z. Yang, K. Tanaka, A. Takahara, and T. Kajiyama. Effect of chain end group on surface glass transition temperature of thin polymer film. *Phys. Lett. A*, 281:363–367, 2001.
- [201] C. Joachim and J. K. Gimzewski. Single molecular rotor at the nanoscale. *Struct Bond*, 99:1–18, 2001.

- [202] C. Joachim, J. K. Gimzewski, and A. Aviram. Electronics using hybrid-molecular and mono-molecular devices. *Nature*, 408:541–548, 2000.
- [203] J. F. Joanny. Adsorption of a polyampholyte chain. *J. Phys. II*, 4:1281–1288, 1994.
- [204] J. F. Joanny. Liquid crystals - nematic emulsions. *Science*, 275:1751–1752, 1997.
- [205] J. F. Joanny. Polyelectrolyte adsorption and charge inversion. *Eur. Phys. J. B*, 9:117–122, 1999.
- [206] J. F. Joanny. Electrostatic interactions in charged polymer solutions. *J. Phys. IV*, 10:39–43, 2000.
- [207] J. F. Joanny. Special issue on polyelectrolytes. *Eur. Phys. J. E*, 5:3–3, 2001.
- [208] J. F. Joanny. Polymers at interfaces. *Interface Sci.*, 11:157–158, 2003.
- [209] J. F. Joanny and H. Benoit. Some remarks on the scattering by compressible polymer solutions and blends. *Macromolecules*, 30:3704–3707, 1997.
- [210] J. F. Joanny, H. Benoit, and W. H. Stockmayer. Does compressibility affect the results obtained by small angle neutron scattering? *Macromol. Symp.*, 121:95–96, 1997.
- [211] J. F. Joanny and M. Castelnovo. Theoretical study of polyelectrolyte-multilayer formation. *Abstr. Pap. Am. Chem. Soc.*, 219:56–COLL, 2000.
- [212] J. F. Joanny, M. Castelnovo, and R. Netz. Adsorption of charged polymers. *J. Phys.-Condes. Matter*, 12:A1–A7, 2000.
- [213] J. F. Joanny and A. Johner. Adsorption of polymers with various architectures: Mean field theory. *J. Phys. II*, 6:511–527, 1996.
- [214] J. F. Joanny, A. Johner, and M. Rubinstein. Loop statistics in adsorbed polymer-solutions. *Colloid Surf. A-Physicochem. Eng. Asp.*, 86:133–136, 1994.
- [215] J. F. Joanny, A. Johner, and T. A. Vilgis. Gels at interfaces. *Eur. Phys. J. E*, 6:201–209, 2001.



- [216] A. Johner, H. Benoit, and J. F. Joanny. Structure factor of a self-avoiding polymer-chain at high momentum-transfer. *Macromol. Theory Simul.*, 4:45–51, 1995.
- [217] A. Johner, J. BouetAvalos, C. C. vanderLinden, A. N. Semenov, and J. F. Joanny. Adsorption of neutral polymers: Interpretation of the numerical self-consistent field results. *Macromolecules*, 29:3629–3638, 1996.
- [218] A. Johner and J. F. Joanny. Probing chain ends in adsorbed polymer layers. *Macromol. Theory Simul.*, 6:479–505, 1997.
- [219] A. Johner, J. F. Joanny, S. D. Orrite, and J. B. Avalos. Gelation and phase separation in colloid-polymer mixtures. *Europhys. Lett.*, 56:549–555, 2001.
- [220] A. Johner, T. A. Vilgis, and J. F. Joanny. Polyelectrolyte gel elasticity in poor solvent. *Macromol. Symp.*, 146:223–226, 1999.
- [221] H. E. Johnson and S. Granick. New mechanism of nonequilibrium polymer adsorption. *Science*, 266:966–968, 1992.
- [222] J. L. Jones, C. M. Marques, and J. F. Joanny. Shear-induced micellization of diblock copolymers. *Macromolecules*, 28:136–142, 1995.
- [223] R. L. Jones, S. K. Kumar, D. L. Ho, R. M. Briber, and T. P. Russell. Chain conformation in ultrathin polymer films using small-angle neutron scattering. *Macromolecules*, 34:559–567, 2001.
- [224] T. A. Jung, R. R. Schlitter, J. K. Gimzewski, H. Tang, and C. Joachim. Controlled room-temperature positioning of individual molecules: molecular flexure and motion. *Science*, 271:181–184, 1996.
- [225] T. Kajiyama, K. Tanaka, N. Satomi, and A. Takahara. Surface relaxation process of monodisperse polystyrene film based on lateral force microscopic measurements. *Macromolecules*, 31:5150–5151, 1998.
- [226] T. Kajiyama, K. Tanaka, and A. Takahara. Surface molecular motion of the monodisperse polystyrene films. *Macromolecules*, 30:280–285, 1997.
- [227] T. Kaneko, M. Asano, K. Yamamoto, and T. Aoki. Polymerization of phenylacetylene-based monodendrons and structure of the corresponding polydendrons. *Polym. J.*, 33:879–890, 2001.

- [228] T. Kaneko, T. Horie, T. Aoki, and E. Oikawa. Polymerization of a monodendron with phenylacetylene repeating unit. *Kobunshi Ronbunshu*, 57:672–677, 2000.
- [229] B. Karakaya, W. Claussen, K. Gessler, W. Saenger, and A. D. Schlüter. Toward dendrimers with cylindrical shape in solution. *J. Am. Chem. Soc.*, 119:3296–3301, 1997.
- [230] B. Karakaya, W. Claussen, A. Schafer, A. Lehmann, and A. D. Schlüter. Full coverage of a hydroxy-substituted poly(para-phenylene) with first- and second-generation dendritic wedges having isocyanate focal points. *Acta Polym.*, 47:79–84, 1996.
- [231] K. Karatasos, D. B. Adolf, and G. R. Davies. Statics and dynamics of model dendrimers as studied by molecular dynamics simulations. *J. Chem. Phys.*, 115:5310–5318, 2001.
- [232] D. Kawaguchi, K. Tanaka, T. Kajiyama, A. Takahara, and S. Tasaki. Mobility gradient in surface region of monodisperse polystyrene films. *Macromolecules*, 36:1235–1240, 2003.
- [233] D. Kawaguchi, K. Tanaka, A. Takahara, and T. Kajiyama. Surface mobile layer of polystyrene film below bulk glass transition temperature. *Macromolecules*, 34:6164–6166, 2001.
- [234] J. L. Keddie and R. A. L. Jones. Glass-transition behavior in ultra-thin polystyrene films. *Isr. J. Chem.*, 35:21–26, 1995.
- [235] J. L. Keddie, R. A. L. Jones, and R. A. Cory. Interface and surface effects on the glass-transition temperature in thin polymer-films. *Faraday Discuss.*, pages 219–230, 1994.
- [236] T. Kerle, Z. Q. Lin, H. C. Kim, and T. P. Russell. Mobility of polymers at the air/polymer interface. *Macromolecules*, 34:3484–3492, 2001.
- [237] P. G. Khalatur, A. R. Khokhlov, S. A. Prokhorova, S. S. Sheiko, M. Möller, P. Reineker, D. G. Shirvanyanz, and N. Starovoitova. Unusual conformation of molecular cylindrical brushes strongly adsorbed on a flat solid surface. *Eur. Phys. J. E*, 1:99–103, 2000.
- [238] H. R. Khan, K. Luders, K. Kajikawa, M. Baenitz, and C. Ecker. Irreversibility fields of polycrystalline  $\text{Hg}(1-x)\text{PbxBa}_2\text{Ca}_2\text{Cu}_3\text{O}_y$  superconductors. *Physica C*, 341:683–684, 2000.

- [239] A. R. Khoklov. On the collapse of weakly charged polyelectrolytes. *J. Phys. A*, 13(3):979, 1980.
- [240] A. R. Khoklov. *J. Chem. Phys.*, 89:231, 1982.
- [241] J. Kim and M. Swager. Control of conformational and interpolymer effects in conjugated polymers (vol 411, pg 1030, 2001). *Nature*, 413:548–548, 2001.
- [242] J. H. Kim, J. S. Jang, and W. C. Zin. Thickness dependence of the melting temperature of thin polymer films. *Macromol. Rapid Commun.*, 22:386–389, 2001.
- [243] A. Kiriy, G. Gorodyska, S. Minko, W. Jaeger, P. Stepanek, and M. Stamm. Cascade of coil-globule conformational transitions of single flexible polyelectrolyte molecules in poor solvent. *J. Am. Chem. Soc.*, 124:13454–13462, 2002.
- [244] L. I. Klushin, A. M. Skvortsov, and F. A. M. Leermakers. Exactly solvable model with stable and metastable states for a polymer chain near an adsorbing surface. *Phys. Rev. E*, 66:art. no.–036114, 2002.
- [245] T. Komatsu, E. Tsuchida, C. Böttcher, D. Donner, C. Messerschmidt, U. Siggel, W. Stocker, J. P. Rabe, and J. H. Fuhrhop. Solid vesicle membrane made of meso-tetrakis[(bixinylamino)-ophenyl]porphyrins. *J. Am. Chem. Soc.*, 119:11660–11665, 1997.
- [246] P. A. Kralchevsky and K. Nagayama. Capillary forces between colloidal particles. *Langmuir*, 10:23–36, 1994.
- [247] O. Kratky and G. Porod. Röntgenuntersuchung aufgelöster Fadenmoleküle. *Recueil*, 68:1106–1122, 1949.
- [248] A. Kros, R. J. M. Nolte, and N. A. J. M. Sommerdijk. Conducting polymers with confined dimensions: Track-etch membranes for amperometric biosensor applications. *Adv. Mater.*, 14:1779–1782, 2002.
- [249] D. Kruger, B. Anczykowski, and H. Fuchs. Physical properties of dynamic force microscopies in contact and noncontact operation. *Ann. Phys.-Leip.*, 6:341–363, 1997.
- [250] D. G. Kurth, P. Lehmann, and C. Lesser. Engineering the surface chemical properties of semiconductor nanoparticles: surfactant-encapsulated cdte-clusters. *Chem. Commun.*, pages 949–950, 2000.

- [251] D. G. Kurth, P. Lehmann, and M. Schütte. A route to hierarchical materials based on complexes of metallosupramolecular polyelectrolytes and amphiphiles. *Proc. Natl. Acad. Sci. U. S. A.*, 97:5704–5707, 2000.
- [252] D. G. Kurth, P. Lehmann, D. Volkmer, H. Colfen, M. J. Koop, A. Müller, and A. Du Chesne. Surfactant-encapsulated clusters (secs): (doda)(20)(nh4)[h3mo57v6(no)(6)o-183(h2o)(18)], a case study. *Chem.-Eur. J.*, 6:385–393, 2000.
- [253] D. G. Kurth, P. Lehmann, D. Volkmer, A. Müller, and D. Schwahn. Biologically inspired polyoxometalate-surfactant composite materials. investigations on the structures of discrete, surfactant-encapsulated clusters, monolayers, and langmuirblodgett films of (doda)(40)(nh4)(2)[(h2o)(n)subset of mo132o372(ch3co2)(30)(h2o)(72)]. *J. Chem. Soc.-Dalton Trans.*, pages 3989–3998, 2000.
- [254] E. Laarz, A. Meurk, J. A. Yanez, and L. Bergstrom. Silicon nitride colloidal probe measurements: Interparticle forces and the role of surface-segment interactions in poly(acrylic acid) adsorption from aqueous solution. *J. Am. Ceram. Soc.*, 84:1675–1682, 2001.
- [255] M. T. R. Laguna, J. Gallego, F. Mendicuti, E. Saiz, and M. P. Tarazona. Solution properties of poly(n-vinylcarbazole) and its copolymers with methyl methacrylate. *Macromolecules*, 35:7782–7790, 2002.
- [256] P. Y. Lai. Apparent glassy dynamics of an adsorbed polymer chain in the bond-fluctuation model. *Macromol. Theory Simul.*, 5:255–268, 1996.
- [257] Pik-Yin Lai. Statics and dynamics of a polymer chain adsorbed on a surface: Monte Carlo simulation using the bond-fluctuation model. *Phys. Rev. E*, 49(6):5420, 5430 1994.
- [258] L. D. Landau and E. M. Lifshitz. *Theory of Elasticity*. Pergamon Press, 1986.
- [259] J. Langowski and U. Giesen. Configurational and dynamic properties of different length superhelical DNAs measured by dynamic light scattering. *Biophys. Chem.*, 34:4–18, 1989.
- [260] M. Laus, K. Sparnacci, B. Ensoli, S. Butto, A. Caputo, I. Mantovani, G. Zuccheri, B. Samorí, and L. Tondelli. Complex associates of plasmid DNA and a novel class of block copolymers with peg and cationic

- segments as new vectors for gene delivery. *J. Biomater. Sci.-Polym. Ed.*, 12:209–228, 2001.
- [261] P. N. Lavrenko. Apparent polymer homology of lactosylated polyamidoamine dendrimers (comments on "sedimentation, translational diffusion, and viscosity of lactosylated polyamidoamine dendrimers" by pavlov gm, korneeva ev, roy r, michailova na, ortega pc, perez ma). *Colloid Polym. Sci.*, 279:200–202, 2001.
- [262] S. Lecommandoux, F. Checot, R. Borsali, M. Schappacher, A. Deffieux, A. Brulet, and J. P. Cotton. Effect of dense grafting on the backbone conformation of bottlebrush polymers: Determination of the persistence length in solution. *Macromolecules*, 35(23):8878–8881, 2002.
- [263] S. Lecommandoux, F. Checot, R. Borsali, M. Schappacher, A. Deffieux, A. Brulet, and J. P. Cotton. Effect of dense grafting on the backbone conformation of bottlebrush polymers: Determination of the persistence length in solution. *Macromolecules*, 35:8878–8881, 2002.
- [264] S. I. Lee, S. W. Howell, A. Raman, and R. Reifengerger. Nonlinear dynamics of microcantilevers in tapping mode atomic force microscopy: A comparison between theory and experiment. *Phys. Rev. B*, 66:art. no.–115409, 2002.
- [265] P. Lehmann, D. G. Kurth, G. Brezesinski, and C. Symietz. Structural analysis of a metallosupramolecular polyelectrolyteamphiphile complex at the air/water interface. *Chem.-Eur. J.*, 7:1646–1651, 2001.
- [266] S. H. Leuba, C. Bustamante, J. Zlatanova, and K. van Holde. Contributions of linker histones and histone h3 to chromatin structure: Scanning force microscopy studies on trypsinized fibers. *Biophys. J.*, 74:2823–2829, 1998.
- [267] S. H. Leuba, G. L. Yang, C. Robert, B. Samorí, K. Vanholde, J. Zlatanova, and C. Bustamante. 3-dimensional structure of extended chromatin fibers as revealed by tapping-mode scanning force microscopy. *Proc. Natl. Acad. Sci. U. S. A.*, 91:11621–11625, 1994.
- [268] H. Li, M. Rief, F. Oesterhelt, and H. E. Gaub. Force spectroscopy on single xanthan molecules. *Appl. Phys. A-Mater. Sci. Process.*, 68:407–410, 1999.

- [269] H. B. Li, B. B. Liu, X. Zhang, C. X. Gao, J. C. Shen, and G. T. Zou. Single-molecule force spectroscopy on poly(acrylic acid) by afm. *Langmuir*, 15:2120–2124, 1999.
- [270] H. B. Li, M. Rief, F. Oesterhelt, and H. E. Gaub. Single-molecule force spectroscopy on xanthan by AFM. *Adv. Mater.*, 10:316–319, 1998.
- [271] H. B. Li, M. Rief, F. Oesterhelt, H. E. Gaub, X. Zhang, and J. C. Shen. Single-molecule force spectroscopy on polysaccharides by AFM - nanomechanical fingerprint of alpha-(1,4)-linked polysaccharides. *Chem. Phys. Lett.*, 305:197–201, 1999.
- [272] J. Li, L. T. Piehler, D. Qin, J. R. Baker, D. A. Tomalia, and D. J. Meier. Visualization and characterization of poly(amidoamine) dendrimers by atomic force microscopy. *Langmuir*, 16:5613–5616, 2000.
- [273] J. Li, D. Qin, J. R. Baker, and D. A. Tomalia. Characterization of poly(amidoamine) dendrimer packing by atomic force microscopy. *Abstr. Pap. Am. Chem. Soc.*, 220:212–POLY, 2000.
- [274] J. Li, D. J. Qin, J. R. Baker, and D. A. Tomalia. The characterization of high generation poly(amidoamine) g9 dendrimers by atomic force microscopy (AFM). *Macromol. Symp.*, 167:257–269, 2001.
- [275] J. Li, D. R. Swanson, D. Qin, H. M. Brothers, L. T. Piehler, D. Tomalia, and D. J. Meier. Characterizations of core-shell tecto-(dendrimer) molecules by tapping mode atomic force microscopy. *Langmuir*, 15:7347–7350, 1999.
- [276] C. N. Likos, S. Rosenfeldt, N. Dingenouts, M. Ballauff, P. Lindner, N. Werner, and F. Vogtle. Gaussian effective interaction between flexible dendrimers of fourth generation: A theoretical and experimental study. *J. Chem. Phys.*, 117:1869–1877, 2002.
- [277] C. N. Likos, M. Schmidt, H. Lowen, M. Ballauff, D. Potschke, and P. Lindner. Soft interaction between dissolved flexible dendrimers: Theory and experiment. *Macromolecules*, 34:2914–2920, 2001.
- [278] E. K. Lin, R. Kolb, S. K. Satija, and W. L. Wu. Reduced polymer mobility near the polymer solid interface as measured by neutron reflectivity. *Macromolecules*, 32:3753–3757, 1999.
- [279] J. Liphardt, S. Dumont, S. B. Smith, I. Tinoco, and C. Bustamante. Equilibrium information from nonequilibrium measurements in an experimental test of Jarzynski’s equality. *Science*, 296:1832–1835, 2002.

- [280] J. Liphardt, B. Onoa, S. B. Smith, I. Tinoco, and C. Bustamante. Reversible unfolding of single rna molecules by mechanical force. *Science*, 292:733–737, 2001.
- [281] D. J. Liu, S. De Feyter, P. C. M. Grim, T. Vosch, D. Grebel-Koehler, U. M. Wiesler, A. J. Berresheim, K. Müllen, and F. C. De Schryver. Self-assembled polyphenylene dendrimer nanofibers on highly oriented pyrolytic graphite studied by atomic force microscopy. *Langmuir*, 18:8223–8230, 2002.
- [282] H. Liu and A. Chakrabarti. Molecular dynamics study of adsorption and spreading of a polymer chain onto a flat surface. *Polymer*, 40:7285–7293, 1999.
- [283] M. J. Liu and J. M. J. Fréchet. Designing dendrimers for drug delivery. *Pharm. Sci. Technol. Today*, 2:393–401, 1999.
- [284] Y. Liu, T. P. Russell, M. G. Samant, J. Stohr, H. R. Brown, A. Cossy-Favre, and J. Diaz. Surface relaxations in polymers. *Macromolecules*, 30:7768–7771, 1997.
- [285] A. I. Livshits, A. L. Shluger, and A. L. Rohl. Contrast mechanism in non-contact sfm imaging of ionic surfaces. *Appl. Surf. Sci.*, 140:327–332, 1999.
- [286] S. Loi, H. J. Butt, C. Hampel, R. Bauer, U. M. Wiesler, and K. Müllen. Two-dimensional structure of self-assembled alkyl-substituted polyphenylene dendrimers on graphite. *Langmuir*, 18:2398–2405, 2002.
- [287] B. Loppinet, G. Gebel, and C. E. Williams. *J. Phys. Chem. B*, 101:1884–1892, 1997.
- [288] M. Ludwig, M. Rief, L. Schmidt, H. Li, F. Oesterhelt, M. Gautel, and H. E. Gaub. Afm, a tool for single-molecule experiments. *Appl. Phys. A-Mater. Sci. Process.*, 68:173–176, 1999.
- [289] C. E. Lunneborg. *Data analysis by resampling: Concepts and applications*. Brooks-Cole, Pacific Grove - CA, Pacific Grove - CA, 1999.
- [290] R. Lüthi, E. Meyer, H. Haefke, L. Howald, W. Gutmannsbauer, and H.-J. Güntherodt. Sled-type motion on the nanometer-scale - determination of dissipation and cohesive energies of c-60. *Science*, 266:1979–1980, 1994.

- [291] A. Lyulin, B. Dünweg, O. Borisov, and A. Dariinski. *Macromolecules*, 32:3264–3278, 1999.
- [292] A. V. Lyulin, D. Adolf, and G. R. Davies. Computer simulations of hyperbranched polymers in shear flows (vol 34, pg 3783, 2001). *Macromolecules*, 34:8818–8818, 2001.
- [293] A. V. Lyulin, G. R. Davies, and D. B. Adolf. Location of terminal groups of dendrimers: Brownian dynamics simulation. *Macromolecules*, 33:6899–6900, 2000.
- [294] B. Maier and J. Rädler. Conformation and self-diffusion of single DNA molecules confined in two dimensions. *Phys. Rev. Lett.*, 82(9):1911–1914, 1999.
- [295] G.S. Manning. Counterion condensation theory constructed from different models. *Phys. A*, 231:236–253, 1996.
- [296] M. Mansfield. Surface adsorption of model dendrimers. *Polymer*, 37(17):3835–3841, 1996.
- [297] J. L. Masson and P. F. Green. Viscosity of entangled polystyrene thin film melts: Film thickness dependence. *Phys. Rev. E*, 65:art. no.–031806, 2002.
- [298] M. Matsumoto and T. Nishimura. Mersenne twister: A 623-dimensionally equidistributed uniform pseudorandom number generator. *ACM Transactions on Modeling and Computer Simulation*, 8(1):3–30, 1998.
- [299] M. A. Mazo, E. B. Gusarova, and N. K. Balabaev. A molecular dynamics simulation of intermolecular interaction between dendrimers. *Russ. J. Phys. Chem.*, 74:1804–1808, 2000.
- [300] M. A. Mazo, N. S. Perov, E. B. Gusarova, P. A. Zhilin, and N. K. Balabaev. The influence of the chemical structure of terminal fragments on the spatial-dynamic organization of dendrimers. *Russ. J. Phys. Chem.*, 74:S52–S58, 2000.
- [301] M. A. Mazo, S. S. Sheiko, P. A. Zhilin, E. B. Gusarova, and N. K. Balabaev. Molecular dynamics simulation of dendrimer intramolecular mobility. *Izv. Akad. Nauk Ser. Fiz.*, 62:1098–1102, 1998.



- [302] M. A. Mazo, P. A. Zhilin, E. B. Gusarova, S. S. Sheiko, and N. K. Balabaev. Computer simulation of intramolecular mobility of dendrimers. *J. Mol. Liquids*, 82:105–116, 1999.
- [303] M. A. Mazo, P. A. Zhilin, E. B. Gusarova, S. S. Sheiko, and N. K. Balabaev. Computer simulation of intramolecular mobility of dendrimers. *J. Mol. Liq.*, 82:105–116, 1999.
- [304] J.-C. Meiners and S.R. Quake. Femtonewton force spectroscopy of single extended DNA molecules. *Phys. Rev. Lett.*, 84(21):5014–5017, 2000.
- [305] A. B. Mel'nikov, G. E. Polushina, E. A. Antonov, E. I. Ryumtsev, and A. V. Lezov. Hydrodynamic and electrooptical properties of dendron modified polystyrene molecules in toluene. *Polym. Sci. Ser. A*, 42:760–764, 2000.
- [306] S. M. Mel'nikov, M.O. Khan, B. Lindman, and B. Jönsson. Phase behaviour of single DNA in mixed solvents. *J. Am. Chem. Soc.*, 121:1130–1136, 1999.
- [307] J. M. Mendez-Alcaraz, A. Johner, and J. F. Joanny. Density profiles and interaction between irreversibly adsorbed polymer layers. *Macromolecules*, 31:8297–8304, 1998.
- [308] Christoph Merkel. *Benetzung von Festkörper/Gas-Grenzflächen durch aliphatische Moleküle*. PhD thesis, Uni Potsdam, 1997.
- [309] A. Michel, D. Goritz, and S. Kreitmeier. Molecular dynamics simulation study - localization and multifold effects in a single polymer chain on a surface. *Kautsch. Gummi Kunstst.*, 55:447–453, 2002.
- [310] A. Michel and S. Kreitmeier. Adsorption of a single polymer chain on a surface: A molecular dynamics simulation study. *J. Polym. Sci. Pt. B-Polym. Phys.*, 39:2333–2339, 2001.
- [311] U. Micka and K. Kremer. *Langmuir*, 15:4033–4044, 1999.
- [312] Uwe Micka and K. Kremer. *Europhys. Lett.*, 49(2):189–195, 2000.
- [313] A. Milchev and K. Binder. Static and dynamic properties of adsorbed chains at surfaces: Monte Carlo simulation of a bead-spring model. *Macromolecules*, 29:343–354, 1996.

- [314] S. Minko, A. Kiriya, G. Gorodyska, and M. Stamm. Single flexible hydrophobic polyelectrolyte molecules adsorbed on solid substrate: Transition between a stretched chain, necklace-like conformation and a globule. *J. Am. Chem. Soc.*, 124:3218–3219, 2002.
- [315] O. Mondain-Monval, A. Espert, P. Omarjee, J. Bibette, F. Leal-Calderon, J. Philip, and J. F. Joanny. Polymer-induced repulsive forces: Exponential scaling. *Phys. Rev. Lett.*, 80:1778–1781, 1998.
- [316] H. Morawatz. Polymers with necklace configuration ? comments on a paper by Dobrynin et al. *Macromolecules*, 31:5170–5170, 1998.
- [317] F. Moreno-Herrero, P.J. de Pablo, J. Colchero, J. Gómez-Herrero, and A.M. Baró. The role of shear forces in scanning force microscopy: a comparison between the jumping mode and tapping mode. *Surface science*, 453:152–158, 2000.
- [318] J. Mou, D. M. Czajkowsky, Y. Zhang, and Z. Shao. High-resolution atomic-force microscopy of DNA : the pitch of the double helix. *FEBS Lett.*, 371:279–282, 1995.
- [319] M. Mücke, S. Reich, E. Müncke-Buchner, M. Reuter, and D. H. Krüger. DNA cleavage by type III restriction-modification enzyme EcoP15I is independent of spacer distance between two head to head oriented recognition sites. *J. Mol. Biol.*, 312(4):687–698, 2001.
- [320] T. Müller, D. G. Yablou, R. Karchner, D. Knapp, M. H. Kleinman, H. B. Fang, C. J. Durning, D. A. Tomalia, N. J. Turro, and G. W. Flynn. AFM studies of high-generation pamam dendrimers at the liquid/solid interface. *Langmuir*, 18:7452–7455, 2002.
- [321] M. Murat and G. S. Grest. Molecular dynamics of dendrimer molecules in solvents of varying quality. *Macromolecules*, 29(4):1278–1285, 1996.
- [322] M. Muthukumar, C.K. Ober, and E.L. Thomas. Competing interactions and levels of ordering in self-organizing polymeric materials. *Science*, 277(5330):1225–1232, 1997.
- [323] I. Muzzalupo, C. Nigro, G. Zuccheri, B. Samorí, C. Quagliariello, and M. Buttinelli. Deposition on mica and scanning force microscopy imaging of DNA-molecules whose original b-structure is retained. *J. Vac. Sci. Technol. A-Vac. Surf. Films*, 13:1752–1754, 1995.

- [324] F. Nagami, G. Zuccheri, B. Samorí, and R. Kuroda. Time-lapse imaging of conformational changes in supercoiled DNA by scanning force microscopy. *Anal. Biochem.*, 300:170–176, 2002.
- [325] R. Netz. Neutral and charged polymers at interfaces. preprint: cond-mat/0203364 v2, 2003.
- [326] R. R. Netz and J. F. Joanny. Complexation behavior of polyampholytes and charged objects. *Macromolecules*, 31:5123–5141, 1998.
- [327] R. R. Netz and J. F. Joanny. Adsorption of semiflexible polyelectrolytes on charged planar surfaces: Charge compensation, charge reversal, and multilayer formation. *Macromolecules*, 32:9013–9025, 1999.
- [328] I. Neubert, E. Amoulong-Kirstein, A.-D. Schlüter, and H. Dautzenberg. Polymerization of styrenes with dendritic fragments of the first, second, and third generation. *Macromol. Chem. Phys.*, 17:517–527., 1996.
- [329] B.R.A. Neves, D.N. Leonard, M.E. Salmon, P.E. Russell, and E.B. Troughton Jr. Observation of topography inversion in atomic force microscopy of self-assembled monolayers. *Nanotechnology*, 10:399–404, 1999.
- [330] S. Nishimura, P.J. Scales, H. Takeyama, K. Tsunematsu, and T.W. Healy. Cationic modification of mica: An electrokinetic study. *Langmuir*, 11:291–295, 1995.
- [331] R. J. M. Nolte. PhD thesis, University of Utrecht, 1973.
- [332] R. J. M. Nolte. Helical poly(isocyanides). *Chem. Soc. Rev*, 23(1):11–19, 1994.
- [333] S. J. Van Noort, K. O. Van der Werf, B. G. de Groth, N. F. Van Hulst, and J. Greve. Height anomalies in tapping mode atomic force microscopy in air caused by adhesion. *Ultramicroscopy*, 69:117–127, 1997.
- [334] R. Klein N.V. Brilliantov, D.V. Kuznetsov. Chain collapse and counterion condensation in dilute polyelectrolyte solutions. *Phys. Rev. Lett.*, 81(7):1433–1436, 1998.
- [335] I. A. Nyrkova, A. N. Semenov, and J. F. Joanny. Highly anisotropic rigidity of "ribbon-like" polymers .2. nematic phases in systems between two and three dimensions. *J. Phys. II*, 7:825–846, 1997.

- [336] I. A. Nyrkova, A. N. Semenov, J. F. Joanny, and A. R. Khokhlov. Highly anisotropic rigidity of "ribbon-like" polymers .1. chain conformation in dilute solutions. *J. Phys. II*, 6:1411–1428, 1996.
- [337] C. K. Ober. Polymer science - shape persistence of synthetic polymers. *Science*, 288:448–449, 2000.
- [338] C. K. Ober. Self-assembly – persistence pays off. *Science*, 296:859, 2002.
- [339] T. Odijk. Polyelectrolytes near the rod limit. *J. Polym. Sci., Polym. Phys. Ed.* 15:477, 1977.
- [340] C. Ortiz and G. Hadziioannou. Entropic elasticity of single polymer chains of poly(methacrylic acid) measured by atomic force microscopy. *Macromolecules*, 32:780–787, 1999.
- [341] B. O’Shaughnessy and D. Vavylonis. Irreversibility and polymer adsorption. *Phys. Rev. Lett.*, 50(5):art. no. –056103, 2003.
- [342] B. O’Shaughnessy and D. Vavylonis. Irreversible adsorption from dilute polymer solutions. preprint: cond-mat/0301206 v1, 2003.
- [343] M. B. J. Otten. Shape persistence of proton polymerized polyisocyanides on surfaces. Master’s thesis, Humboldt Universität, Berlin, 2002.
- [344] M. B. J. Otten, C. Ecker, G. A. Metselaar, A. E. Rowan, R. J. M. Nolte, P. Samorí, and J. P. Rabe. Alignment of extremely long single polymer chains by exploiting hydrodynamic flow. *Chemphyschem*, 5:128–130, 2004.
- [345] M. B. J. Otten, C. Ecker, G. A. Metselaar, E.A. Rowan, R.J.M. Nolte, J.P. Rabe, and P. Samorí. Conformation of extremely stiff synthetic polymer chains across different length scales: a SFM study. in preparation, 2003.
- [346] N. Ouali, S. Mery, A. Skoulios, and L. Noirez. Backbone stretching of wormlike carbosilane dendrimers. *Macromolecules*, 33:6185–6193, 2000.
- [347] A. Ozerin. Nano-scaled ordering in highly branched regular polymer structures. *Macromol. Symp.*, 174:93–102, 2001.
- [348] F. Ozon, J. M. di Meglio, and J. F. Joanny. Adsorption of polyampholytes on charged surfaces. *Eur. Phys. J. E*, 8:321–330, 2002.

- [349] G. M. Pavlov, E. V. Korneeva, and E. W. Meijer. Molecular characteristics of poly(propylene imine) dendrimers as studied with translational diffusion and viscometry. *Colloid Polym. Sci.*, 280:416–423, 2002.
- [350] V. Percec, C. H. Ahn, W. D. Cho, A. M. Jamieson, J. Kim, T. Le-man, M. Schmidt, M. Gerle, M. Möller, S. A. Prokhorova, S. S. Sheiko, S. Z. D. Cheng, A. Zhang, G. Ungar, and D. J. P. Yeardley. Visualizable cylindrical macromolecules with controlled stiffness from backbones containing libraries of selfassembling dendritic side groups. *J. Am. Chem. Soc.*, 120:8619–8631, 1998.
- [351] V. Percec, W. D. Cho, G. Ungar, and D. J. P. Yeardley. Synthesis and structural analysis of two constitutional isomeric libraries of ab(2)-based monodendrons and supramolecular dendrimers. *J. Am. Chem. Soc.*, 123:1302–1315, 2001.
- [352] V. Percec, M. N. Holerca, S. N. Magonov, D. J. P. Yeardley, G. Ungar, H. Duan, and S. D. Hudson. Poly(oxazolines)s with tapered minidendritic side groups. the simplest cylindrical models to investigate the formation of two-dimensional and three-dimensional order by direct visualization. *Biomacromolecules*, 2:706–728, 2001.
- [353] Virgil Percec, C.-H. Ahn, G. Ungar, D.J.P. Yeardley, M.Möller, and S.S. Sheiko. Controlling polymer shape through the self-assembly of dendritic side-groups. *Nature*, 391:161–164, 1998.
- [354] J. P. Pickering and G. J. Vancso. Apparent contrast reversal in tapping mode atomic force microscope images on films of polystyrene-b-polyisoprene-b-polystyrene. *Polym. Bull.*, 40:549–554, 1998.
- [355] G. Pistolis and A. Malliaris. Study of poly(propylene imine) dendrimers in water, by exciplex formation. *Langmuir*, 18:246–251, 2002.
- [356] S. Podzimek, T. Vlcek, and C. Johann. Characterization of branched polymers by size exclusion chromatography coupled with multiangle light scattering detector. i. size exclusion chromatography elution behavior of branched polymers. *J. Appl. Polym. Sci.*, 81:1588–1594, 2001.
- [357] E. Polushkin, G. O. R. A. van Ekenstein, M. Knaapila, J. Ruokolainen, M. Torkkeli, R. Serimaa, W. Bras, I. Dolbnya, O. Ikkala, and G. ten Brinke. Intermediate segregation type chain length dependence of the long period of lamellar microdomain structures of supramolecular comb-coil diblocks. *Macromolecules*, 34:4917–4922, 2001.

- [358] A. L. Ponomarev, T. D. Sewell, and C. J. Durning. Adsorption of isolated, flexible polymers onto a strongly attracting substrate. *Macromolecules*, 33:2662–2669, 2000.
- [359] A. L. Ponomarev, T. D. Sewell, and C. J. Durning. Surface diffusion and relaxation of partially adsorbed polymers. *J. Polym. Sci. Pt. B-Polym. Phys.*, 38:1146–1154, 2000.
- [360] I.I. Potemkin, A.R. Khokhlov, and P. Reineker. Stiffness and conformations of molecular bottle-brushes strongly adsorbed on a flat surface. *Eur. Phys. J. E*, 4:93–101, 2001.
- [361] D. Potschke, P. Hickl, M. Ballauff, P. O. Astrand, and J. S. Pederesen. Analysis of the conformation of worm-like chains by small-angle scattering: Monte-carlo simulations in comparison to analytical theory. *Macromol. Theory Simul.*, 9:345–353, 2000.
- [362] W. H. Press, S. A. Teukolsky, W. T. Vetterling, and B. P. Flannery. *Numerical Recipes in C*. Cambridge University Press, Cambridge, 1999.
- [363] V. V. Prokhorov and K. Nitta. Afm investigation of polyolefines nanoobjects. *Phys. Low-Dimens. Struct.*, 3-4:141–149, 2001.
- [364] S. A. Prokhorova, S. S. Sheiko, C.-H. Ahn, V. Percec, and M. Möller. Molecular conformations of monodendron-jacketed polymers by scanning force microscopy. *Macromolecules*, 32:2653–2660, 1999.
- [365] S. A. Prokhorova, S. S. Sheiko, M. Möller, C.-H. Ahn, and V. Percec. Molecular imaging of monodendron jacketed linear polymers by scanning force microscopy. *Macromol. Rapid Commun.*, 19:359–366, 1998.
- [366] S. A. Prokhorova, S. S. Sheiko, A. Mourran, R. Azumi, U. Beginn, G. Zipp, C. H. Ahn, M. N. Holerca, V. Percec, and M. Möller. Epitaxial adsorption of monodendron-jacketed linear polymers on highly oriented pyrolytic graphite. *Langmuir*, 16:6862–6867, 2000.
- [367] T. J. Prosa, B. J. Bauer, A. Topp, E. J. Amis, and R. Scherrenberg. Size changes and interpenetration within concentrated dendrimer solutions. *Abstr. Pap. Am. Chem. Soc.*, 216:136–PMSE, 1998.
- [368] Y. Pu, M. H. Rafailovich, J. Sokolov, D. Gersappe, T. Peterson, W. L. Wu, and S. A. Schwarz. Mobility of polymer chains confined at a free surface. *Phys. Rev. Lett.*, 8720:art. no.–206101, 2001.

- [369] X. Y. Qiu, L. Huang, G. B. Luo, X. S. Zhao, Y. Yu, X. F. Shen, and B. Shi. Synthesis of multibranched fullerene polymer and studies of its thin film. *Chem. J. Chin. Univ.-Chin.*, 22:1031–1035, 2001.
- [370] J. P. Rabe. Self-assembly of single macromolecules at surfaces. *Curr. Opin. Colloid Interface Sci.*, 3:27–31, 1998.
- [371] J. P. Rabe and S. Buchholz. Commensurability and mobility in two-dimensional molecular patterns on graphite. *Science*, 253:242–427, 1991.
- [372] A. Ramzi, R. Scherrenberg, J. Joosten, P. Lemstra, and K. Mortensen. Structure-property relations in dendritic polyelectrolyte solutions at different ionic strength. *Macromolecules*, 35:827–833, 2002.
- [373] F. M. Raymo, M. D. Bartberger, K. N. Houk, and J. F. Stoddart. The magnitude of [C-H $\cdots$ O] hydrogen bonding in molecular and supramolecular assemblies. *J. Am. Chem. Soc.*, 123:9264–9267, 2001.
- [374] M. Rief, M. Gautel, F. Oesterhelt, J. M. Fernandez, and H. E. Gaub. Reversible unfolding of individual titin immunoglobulin domains by AFM. *Science*, 276:1109–1112, 1997.
- [375] M. Rief, F. Oesterhelt, B. Heymann, and H. E. Gaub. Single molecule force spectroscopy on polysaccharides by atomic force microscopy. *Science*, 275:1295–1297, 1997.
- [376] I. B. Rietveld and D. Bedeaux. Self-diffusion of poly(propylene imine) dendrimers in methanol. *Macromolecules*, 33:7912–7917, 2000.
- [377] I. B. Rietveld, D. Bedeaux, and J. A. M. Smit. Osmotic compressibility of poly(propylene imine) dendrimers in deuterated methanol. *J. Colloid Interface Sci.*, 232:317–325, 2000.
- [378] C. Rivetti and S. Codeluppi. Accurate length determination of DNA molecules visualized by atomic force microscopy: evidence for a partial B- to A-form transition on mica. *Ultramicroscopy*, 87:55–66, 2001.
- [379] C. Rivetti, M. Guthold, and C. Bustamante. Microscopy of DNA deposited on mica: Equilibration versus kinetic trapping studied by polymer chain analysis. *J. Mol. Biol.*, 264:919–932, 1996.
- [380] O. J. Rojas, M. Ernstsson, R. D. Neuman, and P. E. Claesson. Effect of polyelectrolyte charge density on the adsorption and desorption behaviour on mica. *Langmuir*, 18:1604–1612, 2002.

- [381] Jean-Francois Joanny Roland R. Netz. Adsorption of semiflexible polymers on charged planar surfaces. *Macromolecules*, 32:9013–9025, 1999.
- [382] S. Rosenfeldt, N. Dingenouts, M. Ballauff, N. Werner, F. Vogtle, and P. Lindner. Distribution of end groups within a dendritic structure: A SANS study including contrast variation. *Macromolecules*, 35:8098–8105, 2002.
- [383] A. N. Round, M. Berry, T. J. McMaster, S. Stoll, D. Gowers, A. P. Corfield, and M. J. Miles. Heterogeneity and persistence length in human ocular mucins. *Biophys. J.*, 83:1661–1670, 2002.
- [384] M. Rubinstein, R. H. Colby, A. V. Dobrynin, and J. F. Joanny. Elastic modulus and equilibrium swelling of polyelectrolyte gels. *Macromolecules*, 29:398–406, 1996.
- [385] M. Saariaho, A. Subbotin, I. Szleifer, O. Ikkala, and G. ten Brinke. Effect of side chain rigidity on the elasticity of comb copolymer cylindrical brushes: A Monte Carlo simulation study. *Macromolecules*, 32:4439–4443, 1999.
- [386] W. Saenger. *Principles of nucleic acid structure*. Springer, New York, 1984.
- [387] A. Sakai, K. Tanaka, T. Kajiyama, and A. Takahara. Thermal molecular motion at surface of atactic polypropylene films. *Polymer*, 43:5109–5115, 2002.
- [388] B. Samorí. Stretching, tearing, and dissecting single molecules of DNA. *Angew. Chem.-Int. Edit.*, 37:2198–2200, 1998.
- [389] B. Samorí. Stretching single molecules along unbinding and unfolding pathways with the scanning force microscope. *Chem.-Eur. J.*, 6:4249–4255, 2000.
- [390] B. Samorí, I. Muzzalupo, and G. Zuccheri. Deposition of supercoiled DNA on mica for scanning force microscopy. *Scanning Microscopy*, 10(4):953–962, 1996.
- [391] B. Samorí, C. Nigro, A. Gordano, I. Muzzalupo, and C. Quagliariello. Trapping and imaging molecular dynamics by combining scanning force microscopy with topology. *Angew. Chem.-Int. Edit. Engl.*, 35:529–530, 1996.



- [392] P. Samorí, C. Ecker, I. Gössl, P. A. J. de Witte, J. J. L. M. Cornelissen, G. A. Metselaar, M. B. J. Otten, A. E. Rowan, R. J. M. Nolte, and J. P. Rabe. High shape persistence in single polymer chains rigidified with lateral hydrogen bonded networks. *Macromolecules*, 35:5290–5294, 2002.
- [393] P. Samorí, N. Severin, K. Müllen, and Rabe J. P. Macromolecular fractionation of rod-like polymers at atomically flat solid-liquid interfaces. *Adv. Mat.*, 12:579–582, 2000.
- [394] B. Sampaolese, A. Bergia, A. Scipioni, G. Zuccheri, M. Savino, B. Samorí, and P. De Santis. Recognition of the DNA sequence by an inorganic crystal surface. *Proc. Natl. Acad. Sci. U. S. A.*, 99:13566–13570, 2002.
- [395] D. Sarid. *Scanning probe microscopy with Mathematica*. Wiley, 1997.
- [396] D. Sarid, J. P. Hunt, R. K. Workman, X. Yao, and C. A. Peterson. The role of adhesion in tapping-mode atomic force microscopy. *Appl. Phys. A-Mater. Sci. Process.*, 66:S283–S286, 1998.
- [397] D. Sarid, T. G. Ruskell, R. K. Workman, and D. Chen. Driven nonlinear atomic force microscopy cantilevers: From noncontact to tapping modes of operation. *J. Vac. Sci. Technol. B*, 14:864–867, 1996.
- [398] F. A. Schabert and Jürgen P. Rabe. Vertical dimension of hydrated biological samples in tapping mode scanning force microscopy. *Biophys. J.*, 70:1514–1520, 1996.
- [399] R. Scherrenberg, B. Coussens, P. van Vliet, G. Edouard, J. Brackman, E. de Brabander, and K. Mortensen. The molecular characteristics of poly(propyleneimine) dendrimers as studied with small-angle neutron scattering, viscosimetry, and molecular dynamics. *Macromolecules*, 31:456–461, 1998.
- [400] A. D. Schlüter, W. Claussen, E. Amoulongkirstein, and B. Karakaya. Polymers with dendritic wedges in the side-chain. *Abstr. Pap. Am. Chem. Soc.*, 210:120–PMSE, 1995.
- [401] A. D. Schlüter, W. Claussen, B. Karakaya, and W. Lamer. Dendritic structures with polyfunctional cores. *Acc Symp Ser*, 624:145–155, 1996.
- [402] A. D. Schlüter, B. Karakaya, and W. Claussen. Toward macrocylinders: Complete coverage of rigid-rod polymers with dendritic fragments. *Abstr. Pap. Am. Chem. Soc.*, 211:224–POLY, 1996.

- [403] A. D. Schlüter and J. P. Rabe. Dendronized polymers: synthesis, characterization, assembly at interfaces, and manipulation. *Angew. Chem. Int. Ed.*, 39:864–883, 2000.
- [404] A. D. Schlüter and J. P. Rabe. Dendronized polymers: Synthesis, characterization, assembly at interfaces, and manipulation. *Angew. Chem.-Int. Edit.*, 39:864–883, 2000.
- [405] V. Schlüter, C. Rabe, M. Meyer, R. Koshy, and W. H. Caselmann. Intracellular accumulation of middle hepatitis b surface protein activates gene transcription. *Dig. Dis.*, 19:352–363, 2001.
- [406] H. M. Schneider, P. Frantz, and S. Granick. The bimodal energy landscape when polymers adsorb. *Langmuir*, 12:994–996, 1996.
- [407] B. L. Schürmann, U. Niebergall, C. Severin, C. Burger, W. Stocker, and J. P. Rabe. Polyethylene (pehd)/polypropylene (ipp) blends: mechanical properties, structure and morphology. *Polymer*, 39:5283–5291, 1998.
- [408] A. Scipioni, C. Anselmi, G. Zuccheri, B. Samorí, and P. De Santis. Sequence-dependent DNA curvature and flexibility from scanning force microscopy images. *Biophys. J.*, 83:2408–2418, 2002.
- [409] J. V. Selinger, M. S. Spector, and J. M. Schnur. Theory of self-assembled tubules and helical ribbons. *J. Phys. Chem. B*, 105:7157–7169, 2001.
- [410] A. Semenov, J. P. Spatz, M. Möller, J. M. Lehn, B. Sell, D. Schubert, C. H. Weidl, and U. S. Schubert. Controlled arrangement of supramolecular metal coordination arrays on surfaces. *Angew. Chem.-Int. Edit.*, 38:2547–2550, 1999.
- [411] A. N. Semenov, J. BonetAvalos, A. Johner, and J. F. Joanny. Adsorption of polymer solutions onto a flat surface. *Macromolecules*, 29:2179–2196, 1996.
- [412] A. N. Semenov and J. F. Joanny. Kinetics of adsorption of linear homopolymers onto flat surfaces - rouse dynamics. *J. Phys. II*, 5:859–876, 1995.
- [413] A. N. Semenov and J. F. Joanny. Formation of hairpins and band broadening in gel electrophoresis of DNA. *Phys. Rev. E*, 55:789–799, 1997.

- [414] A. N. Semenov, J. F. Joanny, A. Johner, and J. BonetAvalos. Interaction between two adsorbing plates: The effect of polymer chain ends. *Macromolecules*, 30:1479–1489, 1997.
- [415] A. N. Semenov, J. F. Joanny, and A. R. Khokhlov. Associating polymers - equilibrium and linear viscoelasticity. *Macromolecules*, 28:1066–1075, 1995.
- [416] P. Sens and J. F. Joanny. Counterion release and electrostatic adsorption. *Phys. Rev. Lett.*, 84:4862–4865, 2000.
- [417] P. Sens, C. M. Marques, and J. F. Joanny. Viscoelasticity of adsorbed polymer layers. *Macromolecules*, 27:3812–3820, 1994.
- [418] P. Sens, C. M. Marques, and J. F. Joanny. Mixed micelles in a bidisperse solution of diblock copolymers. *Macromolecules*, 29:4880–4890, 1996.
- [419] N. Severin, J. Barner, A.A. Kalachev, and J.P. Rabe. Manipulation and overstretching genes on solid substrates. *Nano Letters*, 4(4):577–579, 2004.
- [420] J. S. Shaffer. Computer-simulation of homopolymer and copolymer adsorption dynamics. *Macromolecules*, 27:2987–2995, 1994.
- [421] J. S. Shaffer. Monte-carlo simulations of random copolymers near solid-surfaces. *Macromolecules*, 28:7447–7453, 1995.
- [422] J. S. Shaffer and A. K. Chakraborty. Dynamics of poly(methyl methacrylate) chains adsorbed on aluminium surfaces. *Macromolecules*, 26:1120–1136, 1993.
- [423] J.S. Shaffer and P.M. Adriani. On the existence of non-equilibrium, glass-like structures at strongly interacting polymer/solid interfaces. *Macromolecules*, 24:5226–5229, 1991.
- [424] S. S. Sheiko, A. I. Buzin, A. M. Muzafarov, E. A. Rebrov, and E. V. Getmanova. Spreading of carbosilane dendrimers at the air/water interface. *Langmuir*, 14:7468–7474, 1998.
- [425] S. S. Sheiko, M. Gerle, K. Fischer, M. Schmidt, and M. Möller. Worm-like polystyrene brushes in thin films. *Langmuir*, 13:5368–5372, 1997.

- [426] S. S. Sheiko and M. Möller. Hyperbranched macromolecules: Soft particles with adjustable shape and persistent motion capability. *Top. Curr. Chem.*, 212:137–175, 2001.
- [427] S. S. Sheiko and M. Möller. Hyperbranched macromolecules: Soft particles with adjustable shape and persistent motion capability. *Top. Cur. Chem.*, 212(212):137–175, 2001.
- [428] S. S. Sheiko and M. Möller. Visualization of macromolecules— a first step to manipulation and controlled response. *Chem. Rev.*, 101:4099–4123, 2001.
- [429] S.S. Sheiko, S.A. Prokhorova, K.L. Beers, K. Matyjaszewski, I.I. Potemkin, A.R. Khokhlov, and M. Möller. Single molecule rod-globule phase transition for brush molecules at a flat interface. *Macromolecules*, 34:8354, 2001.
- [430] Y. J. Sheng, S. Y. Jiang, and H. K. Tsao. Radial size of a starburst dendrimer in solvents of varying quality. *Macromolecules*, 35:7865–7868, 2002.
- [431] P. F. Sheridan, D. B. Adolf, A. V. Lyulin, I. Neelov, and G. R. Davies. Computer simulations of hyperbranched polymers: The influence of the wiener index on the intrinsic viscosity and radius of gyration. *J. Chem. Phys.*, 117:7802–7812, 2002.
- [432] H. S. Shin, Y. M. Jung, T. Y. Oh, T. Y. Chang, S. B. Kim, D. H. Lee, and I. Noda. Glass transition temperature and conformational changes of poly(methyl methacrylate) thin films determined by a twodimensional map representation of temperature-dependent reflection-absorption ftir spectra. *Langmuir*, 18:5953–5958, 2002.
- [433] D. G. Shirvanyanz, A. S. Pavlov, P. G. Khalatur, and A. R. Khokhlov. Self-organization of comblike copolymers with endfunctionalized side chains: A cellular-automaton-based simulation. *J. Chem. Phys.*, 112:11069–11079, 2000.
- [434] L. Shu, A. Schäfer, and A.-D. Schlüter. Dendronized polymers: Increasing of dendron generation by the attach-to approach. *Macromolecules*, 33:4321–4328, 2000.
- [435] L. J. Shu, A. D. Schlüter, J. Barner, and J. P. Rabe. Synthesis of a fourth generation dendronized polystyrene and sfm manipulation

- of cylindrical nanoobjects on surfaces. *Abstr. Pap. Am. Chem. Soc.*, 221:408–PMSE, 2001.
- [436] L. J. Shu, A. D. Schlüter, C. Ecker, N. Severin, and J. P. Rabe. Extremely long dendronized polymers: Synthesis, quantification of structure perfection, individualization, and SFM manipulation. *Angew. Chem.-Int. Ed.*, 40:4666, 2001.
- [437] L. J. Shu, A. D. Schlüter, C. Ecker, N. Severin, and J. P. Rabe. Extremely long dendronized polymers: Synthesis, quantification of structure perfection, individualization, and SFM manipulation. *Angew. Chem.-Int. Edit.*, 40:4666–+, 2001.
- [438] A. Sidorenko, X. W. Zhai, S. Peleshanko, A. Greco, V. V. Shevchenko, and V. V. Tsukruk. Hyperbranched polyesters on solid surfaces. *Langmuir*, 17:5924–5931, 2001.
- [439] R. P. Sijbesma, F. H. Beijer, L. Brunsveld, B. J. B. Folmer, J. H. K. K. Hirschberg, R. F. M. Lange, J. K. L. Lowe, and E. W. Meijer. Reversible polymers formed from self-complementary monomers using quadruple hydrogen bonding. *Science*, 278:1601–1604, 1997.
- [440] G. Siligardi, B. Samorí, S. Melandri, M. Visconti, and A. F. Drake. Correlations between biological-activities and conformational properties for human, salmon, eel, porcine calcitonins and elcatonin elucidated by cd spectroscopy. *Eur. J. Biochem.*, 221:1117–1125, 1994.
- [441] T. Sintes, K. Sumithra, and E. Straube. Adsorption of semiflexible polymers on flat, homogenous surfaces. *Macromolecules*, 34(5):1352–1357, 2001.
- [442] E. Sivaniah, J. Genzer, G. H. Fredrickson, E. J. Kramer, M. Xiang, X. Li, C. Ober, and S. Magonov. Periodic surface topology of three-arm semifluorinated alkane monodendron diblock copolymers. *Langmuir*, 17:4342–4346, 2001.
- [443] K. Skarstad, G. Lueder, R. Lurz, C. Speck, and W. Messer. The escherichia coli SeqA protein binds specifically and co-operatively to two sites in hemimethylated and fully methylated oriC. *Molecular Microbiologist*, 36(6):1319–1326, 2000.
- [444] J. Skolnick and M. Fixman. Electrostatic persistence length of a worm-like polyelectrolyte. *Macromolecules*, 10:944–948, 1977.

- [445] R. Solimani, F. Bayon, I. Domini, P. G. Pifferi, P. E. Todesco, G. Marconi, and B. Samorí. Flavonoid-DNA interaction studied with flow linear dichroism technique. *J. Agric. Food Chem.*, 43:876–882, 1995.
- [446] J. P. Spatz, S. Sheiko, and M. Möller. Substrate induced lateral microphase separation by self-ordering of a diblock copolymer. *Adv. Mat.*, 8:513–517, 1996.
- [447] M. Stark, C. Möller, D. J. Müller, and R. Guckenberger. From images to interactions: High-resolution phase imaging in tapping-mode atomic force microscopy. *Biophys. J.*, 80:3009–3018, 2001.
- [448] S. Stechemesser and W. Eimer. Solvent-dependent swelling of poly(amido amine) starburst dendrimers. *Macromolecules*, 30:2204–2206, 1997.
- [449] R. Stepanyan, A. Subbotin, and G. ten Brinke. Strongly adsorbed comb copolymers with rigid side chains. *Phys. Rev. E*, 6306:art. no.–061805, 2001.
- [450] R. Stepanyan, A. Subbotin, and G. ten Brinke. Comb copolymer brush with chemically different side chains. *Macromolecules*, 35:5640–5648, 2002.
- [451] W. Stocker, J. Beckmann, R. Stadler, and J. P. Rabe. Surface reconstruction of the lamellar morphology in abctriblock copolymers. *Abstr. Pap. Am. Chem. Soc.*, 212:410–POLY, 1996.
- [452] W. Stocker, B. Karakaya, B. L. Schürmann, J. P. Rabe, and A. D. Schlüter. Ordered dendritic nanorods with a poly(p-phenylene) backbone. *J. Am. Chem. Soc.*, 120:7691–7695, 1998.
- [453] W. Stocker, B. L. Schürmann, J. P. Rabe, S. Förster, P. Lindner, I. Neubert, and A. D. Schlüter. A dendritic nanocylinder: Shape control through implementation of steric strain. *Adv. Mater.*, 10:793–797, 1998.
- [454] S. Stoll, K. Starchev, J. Wilkinson, P. Chodanowski, E. Balnois, X. J. Leng, and J. Buffle. The study of environmental biopolymers by mathematical modeling and single molecule detection techniques (vol 55, pg 190, 2001). *Chimia*, 55:466–466, 2001.
- [455] Lubert Stryer. *Biochemistry*. W.H. Freeman, New York, 1995.

- [456] H Stutz. The glass temperature of dendritic polymers. *J. Polym. Sci. Pt. B-Polym. Phys.*, 33(3):333–340, 1995.
- [457] A. Subbotin, M. Saariaho, O. Ikkala, and G. ten Brinke. Elasticity of comb copolymer cylindrical brushes. *Macromolecules*, 33:3447–3452, 2000.
- [458] S. A. Sukhishvili, Y. Chen, J. D. Müller, E. Gratton, K. S. Schweizer, and S. Granick. Surface diffusion of poly(ethylene glycol). *Macromolecules*, 35:1776–1784, 2002.
- [459] H. Takano, J. R. Kenseth, S. S. Wong, J. C. O’Brien, and M. D. Porter. Chemical and biochemical analysis using scanning force microscopy. *Chem. Rev.*, 99:2845, 1999.
- [460] J. Tamayo and R. Garcia. Deformation, contact time, and phase-contrast in tapping mode scanning force microscopy. *Langmuir*, 12:4430–4435, 1996.
- [461] J. Tamayo and R. Garcia. Effects of elastic and inelastic interactions on phase contrast images in tapping-mode scanning force microscopy. *Appl. Phys. Lett.*, 71:2394–2396, 1997.
- [462] K. Tanaka, S. Dai, T. Kajiyama, K. Aoi, and M. Okada. Aggregation states and molecular motion in amphiphilic poly(amido amine) dendrimer monolayers on solid substrates. *Langmuir*, 19:1196–1202, 2003.
- [463] K. Tanaka, X. Q. Jiang, K. Nakamura, A. Takahara, T. Kajiyama, T. Ishizone, A. Hirao, and S. Nakahama. Effect of chain end chemistry on surface molecular motion of polystyrene films. *Macromolecules*, 31:5148–5149, 1998.
- [464] K. Tanaka, A. Takahara, and T. Kajiyama. Film thickness dependence of the surface structure of immiscible polystyrene/poly(methyl methacrylate) blends. *Macromolecules*, 29:3232–3239, 1996.
- [465] K. Tanaka, A. Takahara, and T. Kajiyama. Effect of polydispersity on surface molecular motion of polystyrene films. *Macromolecules*, 30:6626–6632, 1997.
- [466] R. S. Tate, D. S. Fryer, S. Pasqualini, M. F. Montague, J. J. de Pablo, and P. F. Nealey. Extraordinary elevation of the glass transition temperature of thin polymer films grafted to silicon oxide substrates. *J. Chem. Phys.*, 115:9982–9990, 2001.

- [467] D. A. Tomalia. Dendrimer molecules. *Sci.Am.*, 272:62–66, 1995.
- [468] D. A. Tomalia. Architecturally driven properties based on the dendritic state. *High Perform. Polym.*, 13:S1–S10, 2001.
- [469] D. A. Tomalia and J. M. J. Fréchet. Discovery of dendrimers and dendritic polymers: A brief historical perspective. *J. Polym. Sci. Pol. Chem.*, 40:2719–2728, 2002.
- [470] D. A. Tomalia and D. A. Kaplan.
- [471] D. A. Tomalia, A. M. Naylor, and W. A. Goddard. Starburst dendrimers - molecular-level control of size, shape, surface-chemistry, topology, and flexibility from atoms to macroscopic matter. *Angew. Chem.-Int. Edit. Engl.*, 29:138–175, 1990.
- [472] D. A. Tomalia and D. R. Swanson. Dendrimers as macromolecular modules for the synthesis of new nanoscale structures: Megamers. *Abstr. Pap. Am. Chem. Soc.*, 221:9–PMSE, 2001.
- [473] D. A. Tomalia, S. Uppuluri, D. R. Swanson, and J. Li. Dendrimers as reactive modules for the synthesis of new structure-controlled, higher-complexity megamers. *Pure Appl. Chem.*, 72:2343–2358, 2000.
- [474] D. A. Tomalia, Z. G. Wang, and M. Tirrell. Experimental self-assembly: the many facets of self-assembly. *Curr. Opin. Colloid Interface Sci.*, 4:3–5, 1999.
- [475] A. Topp, B. J. Bauer, J. W. Klimash, R. Spindler, D. A. Tomalia, and E. J. Amis. Probing the location of the terminal groups of dendrimers in dilute solution. *Macromolecules*, 32:7226–7231, 1999.
- [476] A. Topp, B. J. Bauer, T. J. Prosa, R. Scherrenberg, and E. J. Amis. Size change of dendrimers in concentrated solution. *Macromolecules*, 32:8923–8931, 1999.
- [477] A. Topp, B. J. Bauer, D. A. Tomalia, and E. J. Amis. Effect of solvent quality on the molecular dimensions of pamam dendrimers. *Macromolecules*, 32:7232–7237, 1999.
- [478] K. C. Tseng, N. J. Turro, and C. J. Durning. Molecular mobility in polymer thin films. *Phys. Rev. E*, 61:1800–1811, 2000.



- [479] O. K. C. Tsui, T. P. Russell, and C. J. Hawker. Effect of interfacial interactions on the glass transition of polymer thin films. *Macromolecules*, 34:5535–5539, 2001.
- [480] N. V. Tsvetkov, V. O. Ivanova, I. V. Ksenofontov, N. V. Girbasova, and A. Y. Bilibin. Large-scale reorientation of cylindrical dendrimers in electric fields. *Polym. Sci. Ser. A*, 45:142–148, 2003.
- [481] D. C. Tully and J. M. J. Fréchet. Dendrimers at surfaces and interfaces: chemistry and applications. *Chem. Commun.*, pages 1229–1239, 2001.
- [482] M. S. Turner, A. Johner, and J. F. Joanny. Wetting behavior of thin diblock films. *J. Phys. I*, 5:917–932, 1995.
- [483] M. S. Turner, M. Maaloum, D. Ausserre, J. F. Joanny, and M. Kunz. Edge dislocations in copolymer lamellar films. *J. Phys. II*, 4:689–702, 1994.
- [484] Magnus Ullner, B. Jönsson, C. Peterson, O. Sommelius, and B. Söderberg. The electrostatic persistence length calculated from Monte Carlo, variational and perturbation methods. *J. Chem. Phys.*, 107:1279–1287, 1997.
- [485] Magnus Ullner and Clifford E. Woodward. Orientational correlation function and persistence lengths of flexible polyelectrolytes. *Macromolecules*, 35(4):1437–1445, 2002.
- [486] H. J. van Manen, F. C. J. M. van Veggel, and D. N. Reinhoudt. Non-covalent synthesis of metallodendrimers. *Top. Curr. Chem.*, 217:121–162, 2001.
- [487] F. Varnik, J. Baschnagel, and K. Binder. Reduction of the glass transition temperature in polymer films: A molecular-dynamics study. *Phys. Rev. E*, 65:art. no.–021507, 2002.
- [488] V. V. Vasilevskaya, A. A. Klochkov, P. G. Khalatur, A. R. Khokhlov, and G. ten Brinke. Microphase separation within a comb copolymer with attractive side chains: A computer simulation study. *Macromol. Theory Simul.*, 10:389–394, 2001.
- [489] S. Vetter, S. Koch, and A. D. Schlüter. Synthesis and polymerization of functionalized dendritic macromonomers. *J. Polym. Sci. Pol. Chem.*, 39:1940–1954, 2001.

- [490] T. A. Vilgis, A. Johner, and J. F. Joanny. Compression of finite size polymer brushes. *PCCP Phys. Chem. Chem. Phys.*, 1:2077–2081, 1999.
- [491] T. A. Vilgis, A. Johner, and J. F. Joanny. Polyelectrolyte gels in poor solvent: Elastic moduli. *Eur. Phys. J. E*, 3:237–244, 2000.
- [492] J. S. Villarrubia. Algorithms for scanned probe microscope image simulation, surface reconstruction, and tip estimation. *J. Res. NIST 102 (4): 425-454 JUL-AUG 1997*, 102(4):425–454, 1997.
- [493] P. Viville, A. Deffieux, M. Schappacher, J. L. Bredas, and R. Lazzaroni. Surface organization of single hyperbranched polymer molecules, as studied by atomic force microscopy. *Mater. Sci. Eng. C-Biomimetic Supramol. Syst.*, 15:311–314, 2001.
- [494] P. Viville, A. Deffieux, M. Schappacher, P. Leclere, J. L. Bredas, and R. Lazzaroni. Surface organization of hyperbranched polymer molecules, as studied by atomic force microscopy. *Macromol. Symp.*, 167:243–256, 2001.
- [495] A. Vix, B. Sapich, J. Stumpe, W. Stocker, and J. P. Rabe. Interfacial ordering and photo-orientation of a liquid crystalline main chain polymer. *Abstr. Pap. Am. Chem. Soc.*, 216:426–POLY, 1998.
- [496] A. Vix, W. Stocker, M. Stamm, G. Wilbert, R. Zentel, and J. P. Rabe. Chain folding in liquid-crystalline main-chain polymers with a smectic phase. *Macromolecules*, 31:9154–9159, 1998.
- [497] A. B. E. Vix, P. Müller-Buschbaum, W. Stocker, M. Stamm, and J. P. Rabe. Crossover between dewetting and stabilization of ultrathin liquid crystalline polymer films. *Langmuir*, 16:10456–10462, 2000.
- [498] D. Vlassopoulos, G. Fytas, B. Loppinet, F. Isel, P. Lutz, and H. Benoit. Polymacromonomers: Structure and dynamics in nondilute solutions, melts, and mixtures. *Macromolecules*, 33:5960–5969, 2000.
- [499] D. Vlassopoulos, G. Fytas, T. Pakula, and J. Roovers. Multiarm star polymers dynamics. *J. Phys.-Condes. Matter*, 13:R855–R876, 2001.
- [500] E. J. Wallace, D. M. A. Buzza, and D. J. Read. Monte carlo simulation scheme for dendrimers satisfying detailed balance. *Macromolecules*, 34:7140–7146, 2001.

- [501] W. N. Wang, J. Y. Lin, and D. C. Schwartz. Scanning force microscopy of DNA molecules elongated by convective fluid flow in an evaporating droplet. *Biophys. J.*, 75:513–520, 1998.
- [502] Roland Wiesendanger. *Scanning Probe Microscopy and Spectroscopy*. Cambridge university press, 1994.
- [503] Roland Wiesendanger. *The Image Processing Handbook*. CRC Press, 3rd ed. edition, 1998.
- [504] M. Wintermantel, M. Gerle, K. Fischer, M. Schmidt, I. Wataoka, H. Urakawa, K. Kajiwara, and Y. Tsukahara. Molecular bottlebrushes. *Macromolecules*, 29:978–983, 1996.
- [505] M. Wintermantel, M. Schmidt, Y. Tsukahara, K. Kajiwara, and S. Kohjiya. Rodlike combs. *Macromol. Rapid Commun.*, 15:279–284, 1994.
- [506] Denis Wirtz. Direct measurement of the transport properties of a single DNA molecule. *Phys. Rev. Lett.*, 75(12):2436–2439, 1995.
- [507] J. Wittmer, A. Johner, and J. F. Joanny. Some dynamic properties of grafted polymer layers. *Colloid Surf. A-Physicochem. Eng. Asp.*, 86:85–89, 1994.
- [508] J. Wittmer, A. Johner, and J. F. Joanny. Precipitation of polyelectrolytes in the presence of multivalent salts. *J. Phys. II*, 5:635–654, 1995.
- [509] J. Wittmer, A. Johner, J. F. Joanny, and K. Binder. Chain desorption from a semidilute polymer brush - a montecarlo simulation. *J. Chem. Phys.*, 101:4379–4390, 1994.
- [510] F. C. Xie, H. F. Zhang, F. K. Lee, B. Y. Du, O. K. C. Tsui, Y. Yokoe, K. Tanaka, A. Takahara, T. Kajiyama, and T. B. He. Effect of low surface energy chain ends on the glass transition temperature of polymer thin films. *Macromolecules*, 35:1491–1492, 2002.
- [511] Q. B. Xue, K. Z. Yang, L. T. Cai, H. G. Liu, X. Chen, Q. Z. Zhang, and Z. H. Liu. Atomic force microscope observation of langmuir film of side chain liquid crystalline polysiloxane. *Acta Chim. Sin.*, 58:1374–1379, 2000.
- [512] S. Yamamoto, Y. Tsujii, and T. Fukuda. Glass transition temperatures of high-density poly(methyl methacrylate) brushes. *Macromolecules*, 35:6077–6079, 2002.

- [513] G. Yang, J. P. Vesenka, and C. J. Bustamante. Effects of tip-sample forces and humidity on the imaging of DNA with a scanning force microscope. *Scanning*, 18:344–350, 1996.
- [514] A. Yazdani and C. M. Lieber. Up close and personal to atoms. *Nature*, 401:227–230, 1999.
- [515] A. Zhang, L. Shu, Z. Bo, and A. D. Schlüter. Dendronized polymers: Recent progress in synthesis. *Macromol. Chem. Phys.*, 204(2):328–339, 2003.
- [516] A. F. Zhang, S. Vetter, and A. D. Schlüter. On the improved accessibility of dendronized macromonomers with peripheral protected amine groups. *Macromol. Chem. Phys.*, 202:3301–3315, 2001.
- [517] W. K. Zhang, S. X. Cui, Y. Fu, and X. Zhang. Desorption force of poly(4-vinylpyridine) layer assemblies from amino groups modified substrates. *J. Phys. Chem. B*, 106:12705–12708, 2002.
- [518] V. P. Zhdanov and B. Kasemo. Monte Carlo simulation of diffusion of adsorbed proteins. *Proteins*, 39:76–81, 2000.
- [519] H. Zhou, H. K. Kim, F. G. Shi, B. Zhao, and J. Yota. Thickness dependent glass transition temperature of pecvd low-k dielectric thin films: effect of deposition methods. *Microelectron. J.*, 33:221–227, 2002.
- [520] P. W. Zhu and D. H. Napper. The effect of molecular weight on the dynamics of adsorbed poly(n-isopropylacrylamide) at particle surfaces in water. *Macromol. Chem. Phys.*, 200:698–705, 1999.
- [521] Wei Zhuang. SFM investigation of Ni catalyzed polyisocyanids in controlled environments. Master’s thesis, Humboldt Universität, Berlin, 2002.
- [522] E.B. Zhulina, O.V. Borisov, and V.A. Pryamitsyn. The theory of sterical stabilization of colloid dispersions by grafted. *J. Coll. & Interface Sci.*, 137(2):495, 1990.
- [523] L. Zitzler, S. Herminghaus, and F. Mugele. Capillary forces in tapping mode atomic force microscopy. *Phys. Rev. B*, 66:art. no.–155436, 2002.
- [524] G. Zuccheri, A. Bergia, G. Gallinella, M. Musiani, and B. Samorí. Scanning force microscopy study on a single-stranded DNA : The genome of parvovirus b19. *Chembiochem*, 2:199–204, 2001.

- [525] G. Zuccheri, R. T. Dame, M. Aquila, I. Muzzalupo, and B. Samorí. Conformational fluctuations of supercoiled DNA molecules observed in real time with a scanning force microscope. *Appl. Phys. A-Mater. Sci. Process.*, 66:S585–S589, 1998.
- [526] G. Zuccheri, G. A. Ranieri, C. Nigro, and B. Samorí. Writhing number of supercoiled DNA from its scanning force microscopy imaging. *J. Vac. Sci. Technol. B*, 13:158–160, 1995.
- [527] G. Zuccheri and B. Samorí. Scanning force microscopy studies on the structure and dynamics of single DNA molecules. *Method Cell Biol*, 68:357–395, 2002.
- [528] G. Zuccheri, A. Sciponi, V. Cavaliere, G. Gargiulo, P. De Santis, and B. Samorí. Mapping the intrinsic curvature and flexibility along the DNA chain (vol 98, pg 3074, 2001). *Proc. Natl. Acad. Sci. U. S. A.*, 98:5368–5368, 2001.

# Lebenslauf

---

## Christof Gereon Ecker

---

\* 10. Juli 1972 in Rheinberg

### Schulbildung

08/79–07/83	Grundschule in Nidderau
08/83–07/89	St. Lioba Gymnasium in Bad Nauheim
08/89–07/92	Technisches Gymnasium Ludwig-Geissler-Schule in Hanau

### Hochschulausbildung

10/92–07/95	Physik/Diplomstudiengang an der Eberhard Karls Universität Tübingen Abschluss: Vordiplom
08/95–04/96	Physics/BSc an der University of Sussex in Brighton, Großbritannien
04/96–07/99	Physik/Diplomstudiengang an der Freien Universität Berlin Beifachstudium der Betriebswirtschaft Abschluss: Diplom in Physik Diplomarbeit: <i>Irreversible magnetische Eigenschaften von Hg-1223- und Hg,Pb-1223 Kupraten</i> Gastaufenthalt an der Kyuchu University in Fukuoka, Japan
seit 07/99	Promotion an der Humboldt-Universität zu Berlin in der Arbeitsgruppe von Prof. J. P. Rabe über die Konformationen von adsorbierten Polymerketten

# Selbständigkeitserklärung

Hiermit erkläre ich, die vorliegende Arbeit selbständig und ohne unerlaubte Hilfe angefertigt zu haben und nur die angegebene Literatur und Hilfsmittel verwendet zu haben. Ich habe mich anderwärts nicht um einen Doktorgrad beworben und besitze einen entsprechenden Doktorgrad nicht. Ich erkläre die Kenntnisnahme der dem Verfahren zugrunde liegenden Promotionsordnung der Mathematisch-Naturwissenschaftlichen Fakultät I der Humboldt-Universität zu Berlin.

Christof Ecker  
27. September 2004